ANNUAL REPORTS ON NMR SPECTROSCOPY

Volume 21

ACADEMIC PRESS

ANNUAL REPORTS ON

NMR SPECTROSCOPY

This Page Intentionally Left Blank

ANNUAL REPORTS ON
NMR SPECTROSCOPY

Edited by

G. A. WEBB

Department of Chemistry, University of Surrey, Guildford, Surrey, England

VOLUME 21

ACADEMIC PRESS

Harcourt Brace Jovanovich, Publishers

London • San Diego • New York
Berkeley • Boston • Sydney • Tokyo • Toronto

ACADEMIC PRESS LIMITED
24/28 Oval Road,
LONDON NW1 7DX

U.S. Edition Published by

ACADEMIC PRESS INC.
San Diego, CA 92101

British Library Cataloguing in Publication Data
Annual reports on NMR Spectroscopy, Vol. 21
1. Nuclear magnetic resonance spectroscopy
—periodicals
QD96.N8.
ISBN 0-12-505321-5
ISSN 0066-4103

Typeset by Colset Pte Ltd, Singapore
Printed in Great Britain by St Edmundsbury Press, Bury St Edmunds, Suffolk

List of Contributors

Isao Ando, *Department of Polymer Chemistry, Tokyo Institute of Technology, Ookayama, Meguro-ku, Tokyo 152, Japan.*

P.S. Belton, *AFRC Institute of Food Research, Colney Lane, Norwich NR4 7UA, UK.*

Robert T.C. Brownlee, *Department of Chemistry, La Trobe University, Bundoora, Victoria, Australia 3083.*

D.B. Chesnut, *Department of Chemistry, Duke University, Durham, North Carolina, USA.*

David J. Craik, *School of Pharmaceutical Chemistry, Victorian College of Pharmacy Ltd, 381 Royal Parade, Parkville, Victoria, Australia 3052.*

B.P. Hills, *AFRC Institute of Food Research, Colney Lane, Norwich NR4 7UA, UK.*

Hazime Saitô, *Biophysics Division, National Cancer Center Research Institute, Tsukiji 5-chome, Chuo-ku, Tokyo 104, Japan.*

David L. Turner, *Department of Chemistry, University of Southampton, Highfield, Southampton SO9 5NH, UK.*

This Page Intentionally Left Blank

Preface

The continuing expansion of interest in NMR spectroscopy, and its many applications in the various areas of the biological and physical sciences, has led to a change in editorial policy for *Annual Reports on NMR Spectroscopy*. Many of the previous twenty volumes in this series have consisted of a small number of lengthy and specifically comprehensive accounts of chosen areas of NMR interest. Commencing with this volume the aim is to produce a larger number of relatively short but timely and authoritative reviews. These will concentrate on those areas of NMR where recent progress and developments are of special interest. However, this will not be carried out at the expense of accounts on well established areas of activity where interest is perhaps more widespread. The main aim in these reports will continue to be the reflection of the many NMR developments occurring in the primary scientific literature.

The present volume consists of reports on graphics-aided NMR, NMR studies of membrane transport, recent *ab initio* calculations of nuclear shieldings, recent developments in multiple pulse NMR and progress in the NMR determination of the structures of biological and synthetic macromolecules.

I am very grateful to all of the authors concerned for careful manuscript preparation and for their prompt delivery.

G. A. WEBB

This Page Intentionally Left Blank

Contents

Some Recent *Ab Initio* Calculations of the NMR Chemical Shift

D. B. CHESNUT

NMR Studies of Membrane Transport

B. P. HILLS and P. S. BELTON

Recent Developments of Multiple Pulse NMR

DAVID L. TURNER

High-Resolution Solid-State NMR Studies of Synthetic and Biological Macromolecules

HAZIME SAITÔ and ISAO ANDO

Graphics-aided NMR

DAVID J. CRAIK and ROBERT T. C. BROWNLEE

School of Pharmaceutical Chemistry,
Victorian College of Pharmacy Ltd,
381 Royal Parade, Parkville,
Victoria, Australia 3052
and
Department of Chemistry,
La Trobe University,
Bundoora, Victoria,
Australia 3083

I. INTRODUCTION

The days are long gone when obtaining a high-resolution NMR spectrum involved an operator spending up to several hours coercing a magnet into a state of homogeneity and then quickly photographing a transient trace on an oscilloscope screen. Improvements in magnet technology and radio frequency (RF) electronics in the last two decades have resulted in

ANNUAL REPORTS ON NMR SPECTROSCOPY
VOLUME 21 ISBN 0-12-505321-5

tremendous improvements in stability and sensitivity on the one hand but, equally, improvements in the ways in which we visualize and present spectra have also contributed significantly to the current explosion of applications of NMR spectroscopy. While advances in the latter area of NMR technology are often taken for granted, being overshadowed by magnet or RF hardware advances, or by the development of elegant new pulse sequences, the exciting developments in NMR of the past decade would probably not have taken place so rapidly without concurrent advances in graphics representations. The thought of wrestling with a 2D NMR spectrum on a 12 cm × 10 cm monochrome oscilloscope display would not appeal to most spectroscopists. It is appropriate, therefore, to examine some of the developments that have taken place in the graphics field as applied to NMR, and to speculate about what needs to be done in the future.

The title "graphics-aided NMR" could cover a multitude of areas and it is useful to define briefly at the outset the areas to be covered (and more particularly, those not to be covered) by this review. We aim to examine aspects of graphics related to the measurement, processing, presentation and interpretation of *high-resolution* NMR spectra. This specifically excludes the large field of imaging. Although there are some areas of overlap in the graphics requirements and, indeed, some high-resolution 2D NMR processing packages include imaging applications, in general the requirements of imaging graphics are different from those of high-resolution NMR studies. The topic of graphics in imaging work is regularly addressed in the medical, radioligand and imaging journals. We also emphasize the word *graphics* in the title, and while graphics advances have been closely related to advances in computers, we have tried to avoid a heavy emphasis on purely *computational* applications. The only computational advances discussed here are those involving graphics-related applications. A number of other articles and reviews[1-5] have concentrated more on computational aspects of NMR.

Graphics requires a combination of hardware and software, and these are discussed in Sections II and III respectively. Since software and applications on NMR spectrometers are very closely related, these are examined together. With the increasing trend of doing a large amount of data manipulation on off-line systems, it is also necessary to discuss means of transferring data to such systems (Section IV) and describing applications on them (Section V). Section VI is a brief summary and conclusion.

II. GRAPHICS HARDWARE

As a result of chemists' needs to display increasing quantities of information, all of the spectrometer companies have developed more sophisticated hard-

ware and software to output spectral data onto high-resolution colour terminals on the spectrometer. This trend follows that in other branches of science where the impact of real-time graphics has been dramatic in the last few years because of increased computing power and reduced unit costs. There has also been an increasing trend over recent years to do a considerable amount of NMR data processing on off-line computers. The graphics generally available on such systems are often somewhat more powerful than those on the spectrometer itself, and so spectrometer-based and off-line systems are discussed separately below.

As noted in the Introduction, our emphasis is on *graphics* hardware and we shall not examine in detail other aspects of computing hardware. It should briefly be mentioned, however, that advances in many of these other areas of computing hardware have also greatly aided the development of NMR spectroscopy over recent years. For example, the availability of sophisticated pulse programmers and fast, high-capacity disc storage has facilitated the rapid expansion of 2D NMR.[6] The increased availability of large computer memories has also been shown to be important in some ultrahigh-resolution applications.[7,8]

A. Graphics hardware on NMR spectrometers

The primary graphics device for data acquisition and processing is a real-time display screen. As recently as eight years ago, the primary display device on many NMR spectrometers was an oscilloscope screen. Although this is formally an analogue device, and hence it is difficult to quantify screen resolution, effective resolution is determined by the size of the phosphor dot in relation to the screen size. A typical working resolution is approximately 240 × 200 for a 12 cm × 10 cm screen. The limitations of this small screen size have been overcome on modern systems, which incorporate much larger display screens with a high inherent resolution. This is indicated in Table 1, which lists typical graphics display devices used on current NMR spectrometers. The ubiquitous availability of colour on modern graphics devices is another major advantage relative to early display devices. Colour is an extremely important processing aid, even in 1D NMR spectroscopy where, for example, the spectrum, integral and chemical-shift scales can be clearly identified by displaying them in different colours. For the processing of 2D NMR data, colour is mandatory.

Graphics devices used in current spectrometers are based on raster technology (see Section II.B). Generally, spectrometer manufacturers have opted to utilize standard RGB (red–green–blue) video monitors (available from companies like NEC, Hitachi and Mitsubishi), but have driven these monitors by graphics display processor hardware of their own design. Recently there has been a trend to replace the monitor/processor

TABLE 1

Typical colour graphic display devices on current high-resolution NMR spectrometers.

Manufacturer	Description	Screen size (cm × cm)	Screen resolution
Bruker	Display processor and high-resolution monitor	24 × 17	512 × 256
GE[a]	Display processor and high-resolution monitor	24 × 19	640 × 480
Jeol	Tektronix terminal	24 × 19	640 × 480
Varian[a]	Display processor and high-resolution monitor	28 × 20	576 × 433

[a]At the time of writing, GE and Varian are beginning to deliver spectrometer systems incorporating Sun workstations as the graphics display device. These have a screen resolution of 1152 × 900 pixels.

combination with commercial workstations (e.g. the Sun 3 series system) as the on-line spectrometer graphics device.

To gain maximum benefit from powerful display facilities, it is necessary to have a flexible and convenient means of manipulating the displayed information. A number of devices have been used to facilitate user interaction, including keyboard, control knobs, light pen, touch pad, joystick, joydisc, and mouse, or a combination of these. The keyboard remains the favoured device for the entry of numerical data or filenames. On modern systems, programmable function keys are often used to reduce typing for frequently executed operations. Control knobs are widely used for functions requiring analogue-type manipulation, e.g. movement of cursors, expansion, phasing, etc. Light pens provide very close cueing of hand and spectrum, but can produce fatigue in long processing sessions. Devices such as joydiscs (e.g. on Tektronix terminals) and mice (e.g. on Sun workstations) are becoming more commonly used in NMR processing.

Some kind of hard copy device is also an integral part of any NMR spectrometer. These have evolved from chart recorders to accurate analogue plotters to multipen digital plotters. The latter are common on most modern systems, and while they provide excellent quality high-resolution line plots, they are still relatively slow, especially for two-dimensional contour or stacked plots. It is likely that such plotters will be replaced by laser printers in the future, although at present digital plotters have the advantage of multicolour display at moderate cost. Most digital plotters used on current NMR spectrometers are produced by the Hewlett-Packard, Watanabe or Zeta companies, and utilize either single flat-bed sheets, fan-fold paper, or paper rolls.

Continuous feed systems have the advantage of not requiring operator intervention for multiple plots and are hence suitable for automated systems, but have the disadvantage of higher paper costs. Autofeed single-sheet plotters are also available, but these are more expensive than plotters requiring manual paper change.

Alphanumeric printouts (of spectral and processing parameters, etc.) are normally done on an inexpensive dot matrix printer. Since it is generally not necessary to produce extensive listings of data for NMR applications, printers with a capacity of around 100 characters per second are adequate. Many such printers have been developed for the personal-computing (PC) market and are commonly available for less than $US300.

A high-quality plot and parameter printout is not necessarily required for every spectrum measured, and as an alternative it is sometimes useful to be able to obtain a rapid screen-dump of displayed spectral and alphanumeric data. Such crude copies of spectra can be used for documentation purposes (e.g. in laboratory notebooks) and slower, high-resolution plots can be obtained only for those spectra requiring detailed analysis, or to be used for publication. This rapid screen-dump function can be carried out on many dot matrix printers or on low-cost, ink jet-type devices.

B. Graphics devices on off-line systems

Many chemists have entered the field of computer graphics in recent years through three-dimensional molecular-graphics programs. These programs build, energy-minimize, manipulate, and display molecules in real time, and use a large range of high-resolution terminals as graphics output devices. The two major hardware approaches used in the field of computer-aided molecular design thus far are calligraphic (vector-based) and raster-graphics systems. The relative merits of the two technologies have been reviewed elsewhere,[9,10] but for completeness the important features are summarized below.

In calligraphic or vector devices a display processor generates voltages which are applied to the X and Y plates of a cathode ray tube (CRT) to draw point-to-point vectors. Since the phosphor light dissipates quickly, vectors must be continuously redrawn (preferably at about 30 lines s^{-1}) by access to a refresh buffer which contains the plotting commands. The actual length of time required to refresh the screen depends on the number of vectors to be drawn, but on modern systems typically several thousand vectors may be displayed before picture flicker becomes apparent. Colour pictures are generated using high-resolution shadow mask CRTs or, less commonly, using beam penetration (where a variable-energy beam is used to excite one of several phosphor layers with different spectral responses). In the past

calligraphic devices such as those marketed by Evans & Sutherland have represented the high-cost, high-performance end of the graphics market.

Raster-graphics systems have traditionally been cheaper, being based on well-established television technology. In these systems the picture is made up of many horizontal lines, each consisting of a number of points or pixels. The whole screen is refreshed at a constant rate independent of the complexity of the picture. Raster devices have the advantage of being able to more readily represent solid areas than calligraphic systems, but have the disadvantage of generally lower resolution, which can manifest itself as "stepping" of non-horizontal or non-vertical lines.

Although there has been considerable debate between the proponents of raster and calligraphic systems with regard to which is better for molecular-modelling applications, in the NMR field the raster system has been widely adopted. Some of the more popular examples of such devices, such as the Tektronix terminals and Sun workstations, are ideally suited to NMR graphics applications, and major software packages are already available or under development by independent software companies. It is expected that there will be a considerable growth in NMR software for a full range of systems in the near future.

Spectrometer manufacturers themselves have also recognized the need for off-line processing, and have provided packages for this purpose. Some manufacturers have opted to develop software for the commonly available hardware systems, such as the Sun workstation (e.g. Varian and GE), while others have developed their own hardware as well (e.g. X-32 workstation from Bruker). Jeol have addressed the problem of off-line processing by utilizing a multi-user, multitasking computer (DEC 11/73) as part of the spectrometer, thus allowing multiple graphics terminals, plotters, etc. to be used for processing. A totally separate 11/73 computer could also be utilized for off-line processing.

Examples of some of the types of graphics devices currently utilized for off-line processing of NMR data are given in Table 2. These and other devices are regularly reviewed in the graphics literature.[11] All are colour devices. Approximate screen resolution is noted for each system to allow comparison with typical NMR data sizes, but it should be noted also that the effective resolution of such systems depends not only on the physical characteristics of the screen, but also on the size of the associated graphics memory and the screen-refresh time. It can be seen that in all the systems listed in the table there is insuffcient horizontal resolution for all points within a 1D NMR spectrum (typically 16 k or 32 k) to be simultaneously displayed. This is not a difficulty, as all operations requiring fine data-point resolution are carried out using expanded subspectral regions. For 2D NMR, the screen resolution more closely approaches the data matrix size (typically 1 k × 1 k).

TABLE 2

Representative graphics display devices for off-line NMR processing.

Device	Approx. resolution	Application
DEC PDP 11/73/Tektronix terminal 4205	640 × 480	(a)
Silicon Graphics workstation	1024 × 768	(b)
Sun workstation	1152 × 900	(b, c, d)
VAX or μVAX computer/serial terminal		(b)
Tektronix 4105	480 × 360	(b)
Tektronix 4107	640 × 480	(b)
Tektronix 4207	640 × 480	(b)
VAXstation workstations	1024 × 1024	(b)
X-32 workstation	704 × 528	(e)

(a) Jeol data processing.
(b) processing using independent software such as FTNMR or NMR1/NMR2 (see Table 4).
(c) GE data processing.
(d) Varian data processing.
(e) Bruker data processing.

III. GRAPHICS SOFTWARE/APPLICATIONS ON NMR SPECTROMETERS

As noted in the introduction, we shall examine graphics applications in the measurement, processing, presentation and interpretation of NMR spectra. The first of these areas includes the use of graphics to set up the spectrometer (e.g. tune probes, shim, enter parameters), as well as to monitor actual data acquisition. In the area of processing and presentation we include all data reduction and processing steps necessary to derive fundamental NMR parameters such as chemical shifts, intensities, etc. as well as physical presentation of the data. Interpretation includes the extraction of chemically useful data from spectra. These aspects are discussed in the following sections.

A. Graphics for control of spectrometer function and data measurement

The increasing computerization of NMR spectrometers over the last 15 years has meant that many of the routine functions associated with spectrometer control are now no longer represented by dial settings on the console, but are visualized on a graphics display. Some of the impacts of these changes are discussed below.

1. Probe tuning

Although not required for every sample, for optimum results on crucial samples, or after a probe change, it is usual to tune the probe. There are a number of ways in which this can be done,[12] but most commercial spectrometers incorporate a method based on observation of reflected power. The basic aim is the minimization of reflected power by adjustment of tuning and matching capacitors on the probe. Often the process is monitored by a single meter, and for gross changes in probe tuning (as occurs when changing nuclei in a multinuclear probe) it may sometimes be difficult to find the optimum setting of the two variable capacitors. One way of overcoming this problem has been to use a sweep generator and reflectance bridge in the circuit shown in Fig. 1 to tune probes off line. In this arrangement the oscilloscope displays the frequency response of the probe, with the resonance condition being indicated by a peak on the screen. The degree of tuning and matching can be judged respectively by the frequency position of the peak and its match to a nominal 50 Ω line on the oscilloscope. Such a procedure is in widespread use in NMR laboratories, but has the disadvantage of requiring the purchase of specialist hardware (sweep generator, reflectance bridge and X–Y oscilloscope). Since the spectrometer itself contains all the components necessary for such a procedure, it should be possible to incorporate this as an inbuilt feature of commercial spectrometers. This has been done by at least one manufacturer (Bruker) by providing software and hardware to sweep the frequencies on spectrometer synthesizer. The graphics display device on the spectrometer is used to display the probe frequency response.

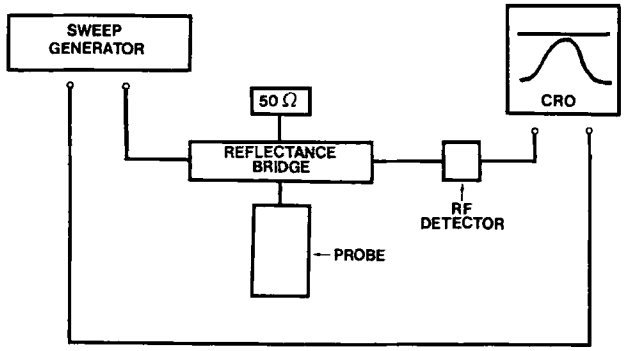

FIG. 1. Schematic arrangement for probe tuning. The sweep generator applies a selected range of frequencies to the reflectance bridge and transmitted power is RF-detected and displayed on the vertical axis of a CRO. The sweep generator time-base is used as the horizontal axis. The probe is opposed to a 50 Ω dummy load across the bridge and the CRO then displays the frequency response of the probe. Resonance is indicated by matching to a 50 Ω line on the CRO. In commercial sweep generators (e.g. Wavetek 1062) the RF detector is in-built.

In the near future, it is likely that some degree of automatic probe tuning will be incorporated into spectrometers. This will be of particular value for systems equipped with automatic sample changers designed for unattended operation.

2. *Shimming/locking*

Ten years ago, the process of shimming involved adjusting an array of ten or more potentiometers to maximize ringing and exponential decay in a swept deuterium lock signal or FID, or to maximize a DC lock level represented by a meter or by a trace on an oscilloscope screen. Potentiometer settings were religiously recorded in the spectrometer log book to facilitate their re-entry after probe changes, or for samples in different lock solvents. The computerization of the lock system now means that manual recording of shim values is no longer necessary as shim files can be stored on disc and readily loaded after a probe or sample change. Moreover, fine or even coarse adjustments of shimming can be made by automatic computerized optimization. Simplex algorithms are often used for this purpose. While such innovations are more computational than graphical, the graphics display device is utilized to display groups of shims to be optimized, or to monitor the progress of the autoshimming process.

The main area in which graphics has been of value in the shimming process is ergonomic. Shimming is often a tedious process, and the provision of large, high-resolution, multicolour displays significantly reduces user-fatigue associated with manual shimming. Different manufacturers have opted for different graphic representations of the lock signal, but all are considerable improvements over monochrome CRO-based displays. Even with the advent of automated shimming and locking, a user-friendly lock display is still extremely important, as most proficient users are able to shim significantly faster than currently available automated systems. Autoshim and autolock systems generally have maximum benefit for totally unattended spectrometer operation, incorporating an automatic sample changer.

Another important application where autoshim systems may find increasing use is for very fine homogeneity work. While many users are able to shim spectrometers rapidly to a state of "good" shimming, extracting the last few tenths of a Hz resolution or obtaining ultimate lineshape specifications is much more time-consuming. Most autoshim systems are much better at optimizing a minimum in the field profile than they are at finding the global minimum, and so the combination of an operator finding the best valley and then allowing the autoshim system to optimize it seems to be a commonly applied protocol. One application where such a procedure is useful is in water suppression work, where if the method of presaturation is

used it is essential to have excellent shimming. This application has become increasingly important in recent years with more studies of proteins in H_2O being carried out.

3. *Setting up NMR experiments*

On spectrometers in use in the 1970s, multipulse or two-dimensional experiments required considerable user effort to set up. A large number of parameters needed to be entered and the software available at the time did little prompting, i.e. users generally either relied on their memory or had a handwritten check-list of parameters that needed to be set. On modern spectrometers, convenient lists of appropriately grouped 1D or 2D parameters may be displayed. These usually contain default parameters that would at least allow the experiment to run, if required, without further user intervention. The software then prompts the user for parameters to be modified for an optimal experiment. On some systems the graphics device is used to display pulse sequences in schematic form to assist users in deciding on appropriate parameters for pulse lengths, delays, etc. A simple example of the type of display available on one commercial spectrometer is shown in Fig. 2.

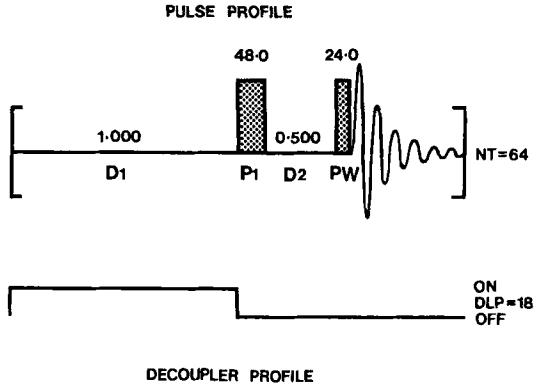

FIG. 2. Representation of graphics display available on Varian VXR spectrometers for setting up simple two-pulse experiments. For convenience, the pulse timing sequence displayed on the graphics screen is not to scale; thus delays (e.g. D1, D2) are shown in seconds, while pulse lengths (P1 = 48.0 and PW = 24.0) are in microseconds. The scheme also shows the number of scans per FID (NT = 64) and the decoupler profile and power setting (DLP = 18 refers to 18 dB of attenuation on the low power range of the decoupler).

4. Monitoring the progress of experiments

Early data systems allowed only rudimentary monitoring of experiments with, for example, only the number of scans completed being displayed. Later systems allowed processing of partially completed acquisitions to be done in a second area of memory. With the increasing use of 2D NMR, it is important to be able to monitor the progress of long experiments to guard against the possibility of a failed run due to incorrect parameter entry or sample-related problems. Most modern systems allow the user access to information such as number of FIDs completed, lock-level, temperature, spinning rate, etc. Individual slices of 2D experiments may be readily extracted during an acquisition and examined. Parts of a 2D matrix can be transformed once a reasonable number of FIDs have been acquired. Experiments can thus be stopped when sufficient resolution has been obtained in the F1 dimension.

B. Graphics for Processing of NMR Data

Software for the processing of NMR data is a very important aspect of the NMR spectrometer. With the increasing array of new NMR techniques and the increasing desire of a range of chemists to exploit these techniques, a user-friendly interface for the processing of data has become essential. Most major scientific software packages are either command-driven or menu-driven. In the former, the user is required to remember a number of mnemonics to execute desired functions, while in the latter, at every stage of operation the user is presented with a list (menu) of commands appropriate at that particular time. Both systems are represented in commercial software packages, although the command-driven structure is more common. It is often supplemented with computerized "help" menus which can be readily called up if the user forgets or is unaware of commands available.

Some companies have opted to take the "help" menu system one stage further, and have incorporated the spectrometer manual in the computer. Once users learn to overcome the barrier to reading sections of the manual on the graphics display, this represents a powerful innovation. Until now, documentation produced by the spectrometer manufacturers has in general not been as up-to-date as users would like. Part of the reason for this is that hard-copy manuals are time-consuming and expensive to produce, and so regular updates tend not to be forthcoming. Incorporation of manuals in the computer potentially allows updates to be distributed (as on floppy disc) more regularly and less expensively. Such an innovation would not have been possible without large, high-resolution graphics display screens.

1. Routine 1D processing

FIDs are normally displayed, as they are acquired, on a raster-graphics display such as those indicated in Table 1. After storage on disc, the data are usually multiplied by an appropriate window function and then Fourier transformed. Some systems allow the user to display graphically a window function superimposed on the FID prior to transformation, and to adjust interactively the function for optimal results. After Fourier transformation, the standard range of manipulations that might then be applied include phasing, expansion of selected regions (usually done by two control knobs, one for lateral shifts and one for expansion), assignment of a reference peak to a particular chemical shift (again done with a knob-controlled cursor), integration, peak picking (i.e. having the computer identify maxima in the spectrum and producing a list of chemical shifts of these maxima). The latter operation is usually preceded by the operator using the graphics display to assign an appropriate threshold level below which peaks (or noise) will not be picked. An example of the type of hard copy produced is shown in Fig. 3. This mode of display, in which peak frequencies are marked on spectra, is much more convenient than the older method where lists of chemical shifts were produced separately from the spectra.

In all the operations noted above it is important that the graphics display device is able to represent the data in a form similar to that to be produced on the hard-copy device. For example, it is annoying to discover only after a hard-copy plot has commenced that the peak-picking threshold was incorrectly set, and that every noise spike in the spectrum is identified as a peak and marked on the spectrum in a very time-consuming plotting process. It is

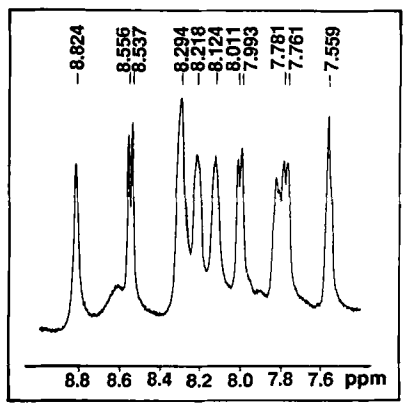

FIG. 3. Part of the 1D spectrum of the decapeptide angiotensin I showing computer-generated peak picking.

preferable if the peak-picked spectrum can be rapidly drawn on the graphics display device and thereby checked prior to committing it to hard copy. Similar comments apply to insets of subspectral regions. It is very convenient to be able to use the graphics screen to position subspectra of selected regions above the main spectrum, and then issue one command to plot the spectrum and insets as they appear on the screen.

Another extremely useful application of interactive graphics display devices is the dual (or multiple) display mode. If two or more spectra have been acquired with some perturbation applied between them (e.g. NOE difference, kinetic studies or concentration studies), then it is very convenient to be able to display both spectra simultaneously and to manipulate them (e.g. expand, offset, superimpose, add, subtract) on the graphics display interactively to discern differences. The use of colour is important in superimposition applications where, for example, if a red and a green spectrum are superimposed, the identical parts of the spectrum appear in yellow and difference regions appear in red or green. Direct subtraction of spectra on the graphics display also aids in discerning regions of difference.

Software and graphics display which allows subtraction/addition of a proportion of one spectrum from another is also very useful. This has applications, for example, in subtracting peaks from one component from a multicomponent mixture, or in the processing of DEPT spectra.[13,14] In the latter case it is usual, if complete spectral editing is required, to acquire three spectra where the final ^1H pulse is the sequence is 45°, 90° and 135°, respectively. For normalization of intensity, the 90° spectrum is acquired with twice as many scans as the other two and, in theory, provides a pure CH subspectrum. The CH_2 subspectrum is obtained by subtracting the 45° spectrum from the 135° spectrum, while the CH_3 subspectrum results from subtraction of 0.7 times the 90° spectrum from the sum of the 45° and 135° spectra. In practice, pulse imperfections mean that it is useful to be able to add/subtract interactively other proportions of spectra to obtain pure subspectra.

2. *Two-dimensional processing*

(a) Display methods for 2D data. Representation of a 2D NMR spectrum on conventional graphics devices is more complicated than for 1D spectra because in principle three dimensions are involved: one intensity variable and two frequency variables. One way of representing these variables is by the use of so-called "stacked plots" which are obtained by plotting successive rows of the transformed data matrix with small horizontal and vertical offsets. For clarity, a "whitewash" routine is usually incorporated to omit plotting of components behind earlier peaks in the matrix. Although such plots are aesthetically pleasing (Fig. 4), they require considerable time to produce, and

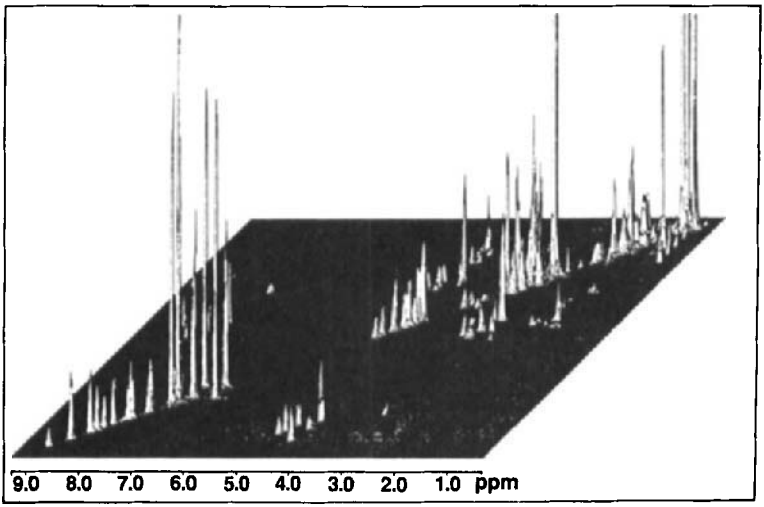

FIG. 4. Stacked plot representation of a 2D COSY spectrum of angiotensin I (Asp-Arg-Val-Tyr-Ile-His-Pro-Phe-His-Leu).

are of minimal value for data analysis. The contour plot representation in which lines join points of equal intensity is much more useful and is the standard presentation mode (Fig. 5). It is often used in conjunction with projections in each frequency dimension or with selected cross-sections through particular frequencies in either dimension, depending on the type of 2D experiment involved. For example, in 2D *J*-resolved spectroscopy, a cross-section through the chemical shift axis at a specific chemical shift yields the multiplet that corresponds to that chemical shift (Fig. 6). Good interactive graphics software is important for the extraction of cross-sections. This is normally done by displaying a contour plot on the screen and positioning a cursor (using either control knobs, joystick or mouse) on the row or column to be sectioned. On issue of the appropriate command the cross-section is displayed and can be interactively expanded, peak-picked, integrated or plotted as required.

The relative merits of the various display possibilities for 2D data are summarized in Table 3. As contour plots are the most widely used representation, further comment is required. It is important to note that while hard-copy contour plots can be produced significantly faster than stacked plots, the output of a complex contour plot is still a time-consuming process and may take up to an hour to produce on a high-resolution digital plotter. It is therefore very important to have available good interactive graphics software for screen display devices so that manipulations such as adjustment of

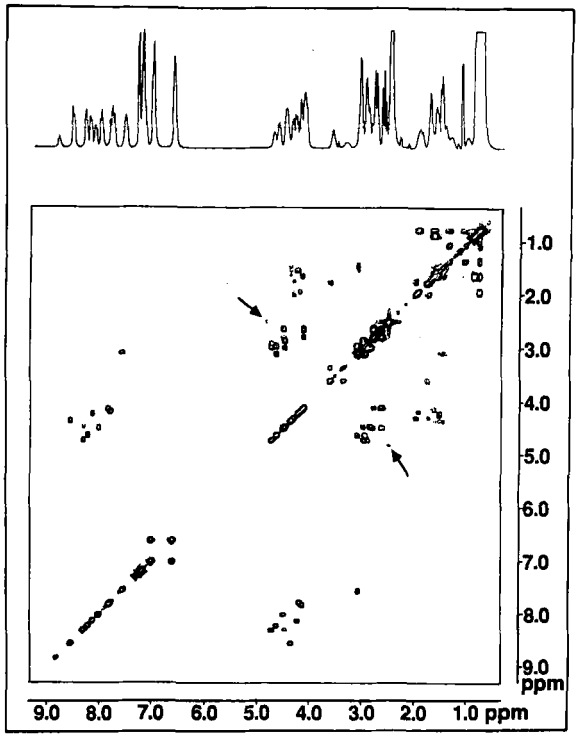

FIG. 5. Contour plot of a 2D COSY spectrum of angiotensin I. A projection is shown above the contour map. The spectrum has been symmetrized. The arrowed peaks are symmetrization artifacts (see Section III.B.2(d)).

contour levels or expansions can be conveniently and rapidly done prior to committing the plot to a hard-copy device. For speed of presentation, most commercial spectrometer packages use colour density plots for the initial representation of 2D data on a graphics display. Every point (or every few points where screen resolution is low) in the 2D matrix is represented as a pixel with a colour-coded intensity. No calculation is done to join points of equal intensity and so display is fairly rapid. On some systems a colour scale is displayed to one side of the density plot to indicate relative intensities of each colour.

The number and spacing of effective contours displayed varies from system to system, but as a default it is usual to colour-code contours in an exponential manner, e.g. if the lowest level to be displayed has an arbitrary intensity, I, then successive contours would have intensities $2I$, $4I$, $8I$, . . ., etc. On many graphics devices 16 colours can be displayed simultaneously

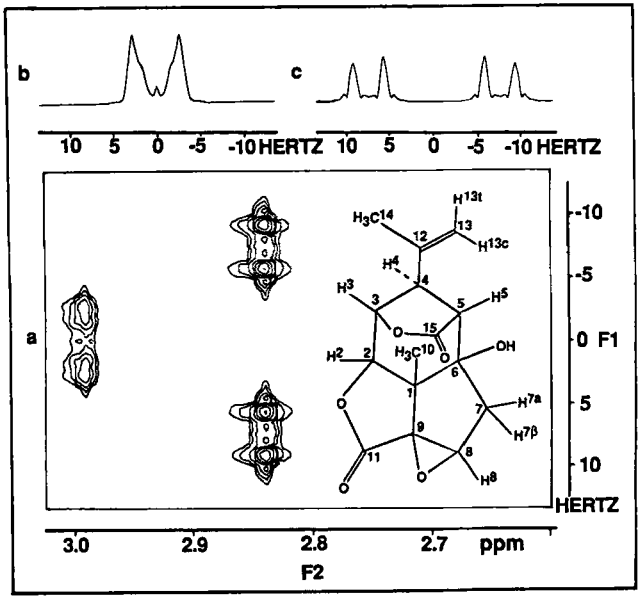

FIG. 6. (a) Contour plot of part of the 2D *J*-resolved spectrum of picrotoxinin showing selected cross-sections, (b) at 3.0 ppm and (c) at 2.84 ppm. The spectrum has been tilted and symmetrized about the line F1 = 0. Assignments are given in ref. 15.

TABLE 3

Relative merits of 2D display methods.

Method	Advantages	Disadvantages
Stacked plot	Good perception of relative intensities Aesthetically pleasing	Difficult to measure spectral parameters Hidden peaks Time-consuming
Contour plots	Easy to extract spectral parameters Faster than stacked plots	Information between contours and below lowest contour may be lost
Cross-sections	Selected parameters readily extracted (frequencies, amplitudes, lineshapes)	Only give partial information
Projections	Helps relate 2D spectrum to 1D spectrum	Low digital resolution

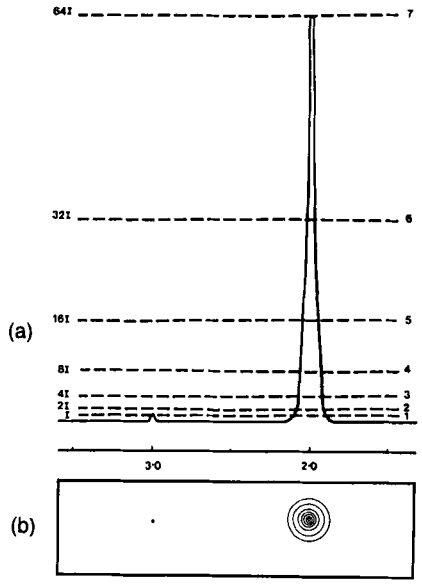

FIG. 7. (a) Simulated cross-section of a row of a 2D matrix containing two peaks having an intensity ratio of 64:1 (peaks are at 2.0 ppm and 3.0 ppm). Contour levels based on power of 2 spacing are shown. In the contour representation (b), both peaks are readily detected.

and this allows a dynamic range of more than 32 000 to be covered. Figure 7 shows that even if only seven contour levels are available, spectra with dynamics ranges of 64:1 may be readily represented by the contour method based on exponential spacing.

It may take from a few seconds to more than a minute to display such a colour density map on a graphics screen, depending on the size of the data matrix. This can be speeded up considerably on systems equipped with an array processor. Expansions are normally made by first defining a square or rectangular sub-area by means of knob-driven cursors, and then issuing an expansion command. Expansions are displayed significantly faster than full 2D matrices, but the limitations of the density mode representation become much more apparent, i.e. if the expanded region contains only a few hundred by a few hundred data points, the "blocks" of colour for each point become visible. It is often difficult for the eye to interpolate instinctively between colour blocks to identify true contours, particularly in regions containing overlapped peaks or in phase-sensitive representations (Section III.B.2(c)). Most systems do allow users to draw true multicontour line plots on graphics display devices, but in general these take considerably longer to display than the colour density plots. A true contour plot display may only be necessary if

the user wants to see exactly what form the plot will take on a hard-copy device, or if a high-resolution interactive display is required, for example to experiment with window functions to try to resolve overlapping peaks.

Once an appropriate area for plotting has been defined using the colour density display on a graphics display device, the plot command does the internal calculations necessary for a true contour plot to be produced on the digital plotter. Multipen, multicolour digital plotters are generally used to assist in the display of different contour levels and again, the default level spacing is usually in powers of 2. The plotting software allows the user to enter the number of levels to be plotted and their spacing. The accuracy of modern digital plotters is such that if the user wishes to plot more than the maximum allowed number of contours, this can be done by over-plotting the

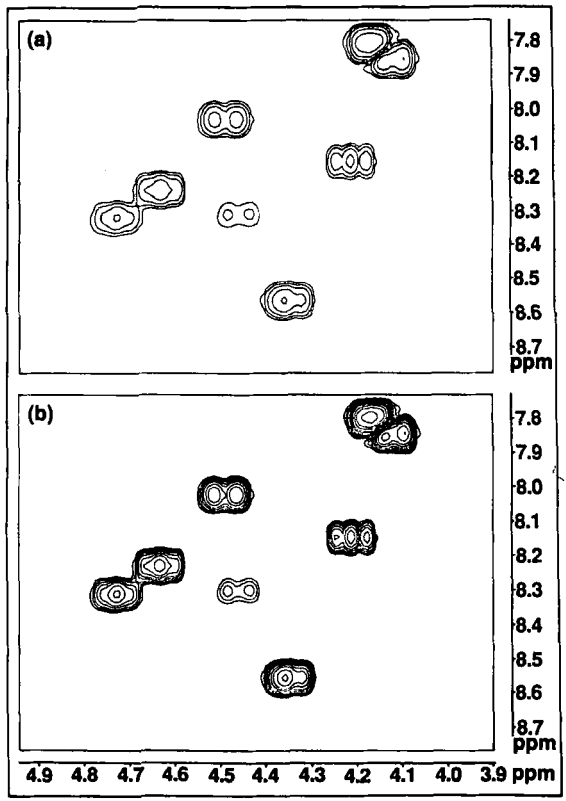

FIG. 8. Plot of the region containing the αH–NH correlations of the COSY spectrum of angiotensin I using (a) default contour-level spacing, and (b) an additional four levels interspersed between default levels. Extra resolution is apparent in the latter case.

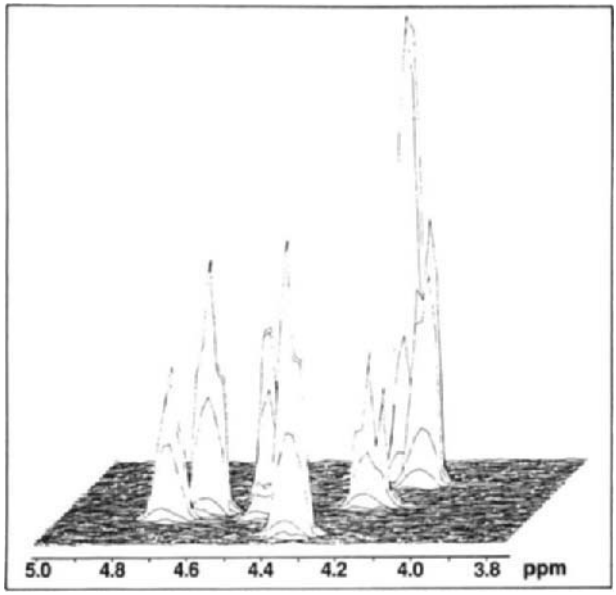

FIG. 9. Stacked plot of the same spectral region shown in Fig. 8.

original plot after making a change in contour levels. It is useful to point out that the aesthetics, and sometimes information content, of contour plots can be significantly improved by plotting more than the standard default contour levels offered by the software. This is illustrated in Fig. 8 for an expanded region of the COSY spectrum of angiotensin I. A comparison with Fig. 9, which is a stacked plot of the same region, shows the advantage of a clearer interpretation of the contour plot mode relative to stacked plots, even for relatively uncomplicated spectral regions.

(b) Processing of 2D data. The sorts of function normally applied in 1D data processing are also necessary in 2D NMR, but are made slightly more complex by the presence of a second dimension. For example, peak-picking routines in 2D matrices generate coordinate pairs rather than scalar chemical shifts. Such routines are only just becoming available on spectrometer software packages but have been incorporated into off-line packages for a number of years. Integration of cross-peak is complicated by the fact that a *volume* integration is required. Such a procedure might be applied, for example, to determine relative sizes of cross-peaks in 2D NOESY spectra used to generate interproton distances. Usually the contour plot is displayed on the graphics screen and cursors are used to define the integration limits,

i.e. the area on the contour map containing the peak to be integrated. Again, such a facility has only just become available in spectrometer processing packages.

Some of the other functions required for the processing of 2D data require more detailed comment and so are discussed separately in other sections. For example, the selection of expansions, cross-sections or projections is discussed in Section II.B.2(a) and symmetrization is examined in Section III.B.2(d).

(c) Phase-sensitive 2D data. In two-dimensional NMR experiments where the detected signal is phase modulated by the process occurring during the evolution period, complicated lineshapes are observed. These are said to be phase twisted (Fig. 10) and it is generally not possible to correct them by simple phase-correction routines. It has been usual in the past to avoid this mixed absorption/dispersion lineshape mode by calculating absolute value spectra. However, this has the disadvantage of yielding broader 2D peaks, especially near the base. Figure 11 shows the effect of absolute value presentation in the 1D case. Similar effects apply for the 2D case, where a four-pointed star lineshape is observed in contour form. The broadening and tailing in two dimensions results in lower resolution for an absolute magnitude spectrum compared with a pure absorption spectrum. In the former case lines of low intensity may be obscured by tailing from higher-intensity peaks. In order to compensate for the loss of resolution in absolute value spectra, it is usual to process the 2D matrix using quite severe resolution-enhancement window functions. These can result in a substantial decrease in signal-to-noise ratio. An additional disadvantage of the absolute value mode is that positive and negative cross-peaks cannot be distinguished, since the absolute value is always positive.

A number of methods have now been developed for the generation of pure-absorption 2D spectra.[16,17] Despite the slightly more complicated data handling required, the gains in both resolution and sensitivity that can be achieved in phase-sensitive 2D experiments have meant that a significant and ever-increasing fraction of experiments are now being carried out in this mode.

As for 1D data, the ability to phase 2D spectra depends critically on the availability of good graphics software and hardware to allow the user to interactively adjust the phase. In 2D NMR, initial phase correction is usually done by extracting appropriate rows or columns from the transformed data matrix, phasing these individually, and then applying the derived phase constants to the whole 2D matrix.

Since for the display of phase-sensitive 2D spectra, positive and negative peaks need to be represented, and since to take full advantage of the extra

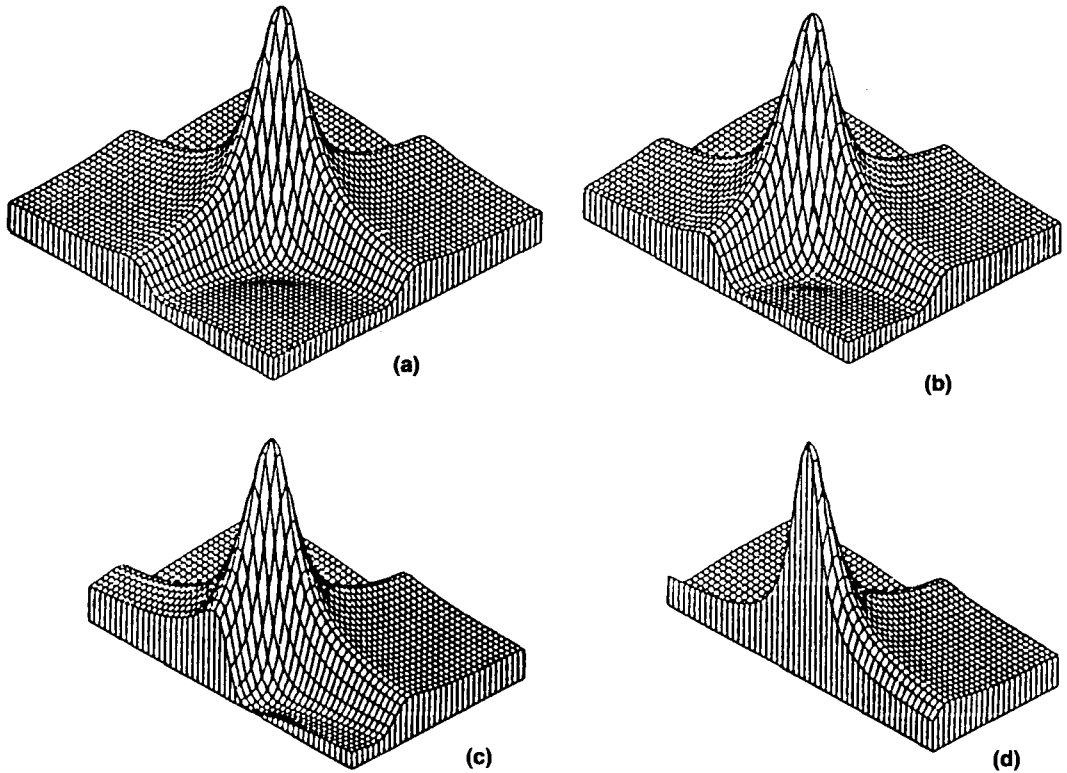

FIG. 10. Computer simulations of the "phase twist" lineshape obtained in many 2D NMR experiments. A slice through this lineshape far from resonance (a) shows a dispersion-mode lineshape. As slices are taken closer to resonance, (b) and (c), mixed-mode lineshape is obtained, while a slice (d) taken at exact resonance yields a pure absorption-mode lineshape.[70]

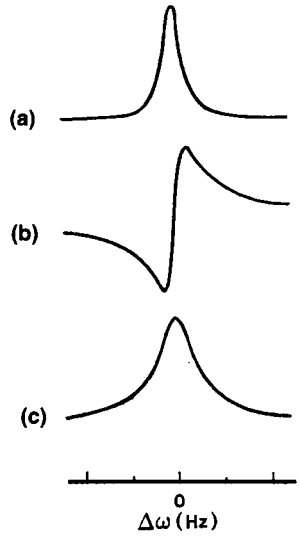

FIG. 11. (a) Absorption mode, (b) dispersion mode and (c) absolute value lineshapes associated with a single resonance in 1D NMR. Note the significant broadening near the baseline of the absolute value mode relative to pure absorption lineshape.

resolution available, it is desirable to use increased points in the data matrix, additional demands are made on graphics display devices. Most systems allow separate display of either positive contour levels, negative contour levels, or both. When positive and negative levels are displayed simultaneously, the number of colours available for display of either is halved, and hence there may potentially be difficulties in dynamic ranges if only a limited number of colours are available. Where 16 colours can be displayed simultaneously, and hence eight may be used for positive and eight for negative levels, this is not usually a problem.

Most hard-copy plotting routines also allow separate plotting of positive, negative or both levels, it being usual to use just two coloured pens — one for positive contours and one for negative contours — when both are plotted simultaneously. When the plot is eventually to be reproduced for a journal where only black lines on a white background are allowed, then negative contours can be distinguished by plotting them as dashed lines, or with extra contours.

(d) Artifacts in 2D. 2D spectra are subject to a number of instrument-related artifacts.[18] Many of these can be minimized by phase cycling during data acquisition, but inevitably some appear in the transformed 2D spectra. One well-known artifact is so-called t_1 noise,[19] which is a band of noise

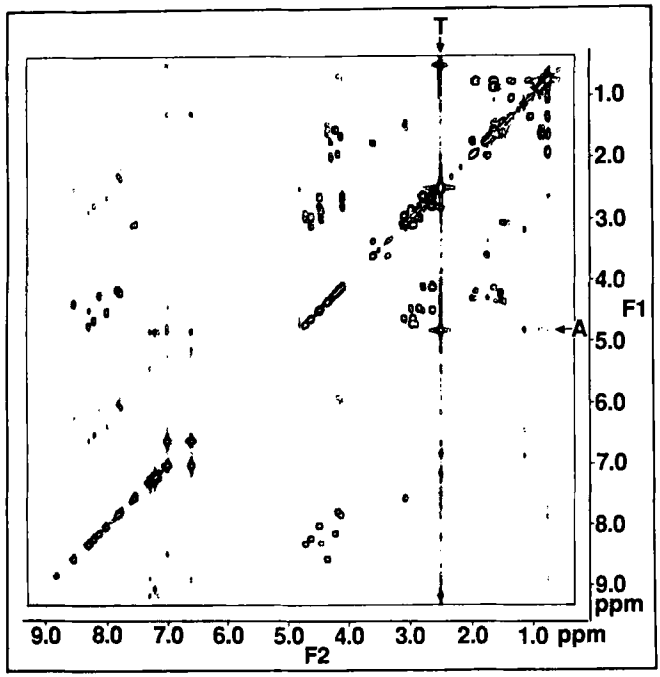

FIG. 12. Non-symmetrized COSY of angiotensin I. Note the artifacts (arrowed) in the form of t_1 noise (T) and axial peaks (A). Figure 5 is the symmetrized version of the same data set.

running parallel to the F1 axis, and usually associated with larger spectral peaks. Because of the symmetric nature of COSY- or NOESY-type spectra, and because the t_1 noise is not symmetrical, it can be reduced by the technique of symmetrization.[20,21] The improvement in appearance that may be obtained can be seen by comparing the symmetrized COSY spectrum of angiotensin I (Fig. 5) with the original, unsymmetrized data (Fig. 12). This comparison also shows that weak artifacts along F1 = 0 (so-called axial peaks) are also removed by symmetrization. Caution must be exercised when using symmetrization, however, as the chance occurrence of symmetric noise peaks may lead to the false impression of their being real peaks, as indicated by arrows in Fig. 5. Symmetrized spectra should also not be used for quantitative interpretations, as peak intensity distortions occur. Finally, it should be noted that other types of 2D spectra (e.g. *J*-resolved, 2D INADEQUATE) exhibit symmetry (albeit of a different type to COSY spectra), and artifacts can also be removed from these spectra by appropriate symmetrization routines.

3. Non-routine processing

The number of spectral data reduction and manipulation techniques available is steadily increasing. For non-routine processing applications the decision whether the processing should be done on an off-line system or on-line requires a trade-off between factors such as the extra computing power and time available on off-line systems as opposed to the inconvenience of having to transfer data to such systems. For processes such as baseline correction, curve-fitting and T_1 or T_2 analysis, the balance is generally on the side of on-line processing, and all commercial spectrometer software packages contain routines for performing these functions. Spectral simulation is carried out frequently on both on- and off-line systems.

(a) Baseline correction. There are several ways in which baseline correction may be carried out. Most spectrometer processing packages incorporate some degree of automatic baseline correction (to eliminate simple DC offsets) as part of the Fourier transform process. More complicated defects can be corrected interactively on a graphics display screen by using knob-controlled "guidelines" of various orders (zero order = DC offset, first order = baseline slant, second order = quadratic curvature, etc.). The user interactively fits the graphic "guideline" onto the displayed spectrum to identify the true baseline and then issues a command for the computer to adjust the data to this baseline. Alternatively, for very complex baseline disorders, some systems allow the user to define a large number of "true" baseline points in the data (using a cursor) and then carry out an appropriate correction.

(b) Curve fitting. Curve fitting can also be carried out conveniently on modern systems using interactive graphics displays. This procedure can be used either to best define the parameters (i.e. frequency, intensity, linewidth) of a single Lorentzian or Gaussian line, or to deconvolute a peak from other overlapping peaks. In the former case the graphics display is used to define or expand the region near the peak of interest and then the calculation routine is commenced. The fitted line is then superimposed over the raw data and the parameters of the peak are displayed. This procedure is often used to obtain linewidth measurements as it is somewhat more precise than the alternative technique of using cursors to measure the frequency difference at half peak height.

(c) T_1 and T_2 calculations. T_1 and T_2 calculations are also generally incorporated as part of the standard spectrometer package. Early systems utilized a semilogarithmic analysis, but most packages now incorporate the more accurate two- or three-parameter exponential fitting procedure.[22-24] Again,

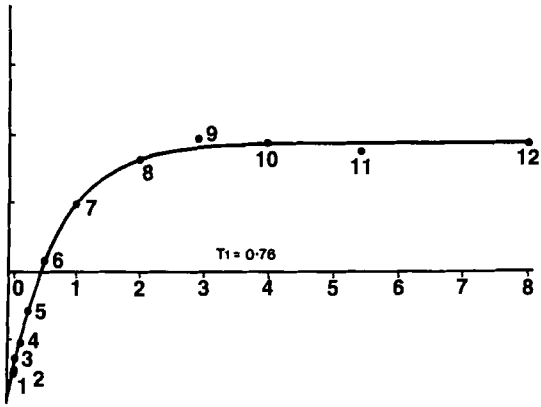

FIG. 13. Typical display of T_1 data to which a three-parameter exponential has been fitted. By presenting this display on the graphics screen, the user is able to assess the fit rapidly and delete spurious points if required.

the availability of interactive graphics displays has greatly facilitated this process. Typically a cursor is used to define the peaks to be analysed in the "infinity" spectrum and then a data-reduction routine is initiated to determine automatically intensities of these peaks for each τ value. T_1 or T_2 is then calculated. The fitted curve and raw intensity data are displayed on the graphics screen (Fig. 13), giving the user the opportunity to remove spurious points and recalculate if necessary. The information can be plotted on a hard-copy device if a permanent record is required.

(d) Spectral simulation. For complex spectra the first stage of NMR processing leads to a set of line frequencies and intensities, but these may not directly correspond to chemical shifts or coupling constants. Spectral simulation programs are designed to derive these "pure" NMR parameters from second-order spectra. As such spectral analysis was central to the early development of NMR, particularly of proton NMR, and because it is a computationally extensive task, programs were originally developed for main-frame, off-line computers (Section IV.B).[25-29] However, the availability of more powerful on-line computers, and the need for rapid and convenient analysis of second-order spectra during acquisition or soon afterwards, has resulted in simulation packages being incorporated as an integral part of the spectrometer software.

The procedure used in spectral simulation is to compare a theoretically calculated spectrum, based on assumed chemical shifts and coupling constants, with the experimental spectrum. The chemical shifts and coupling constants are then adjusted to obtain the best fit. Initially, the spectrum is

calculated by defining the number of spins involved (usually a maximum of seven) and guessed chemical shifts, coupling constants and line-broadening function. This calculated spectrum is then matched with the observed spectrum. In early programs the observed and calculated spectral lines were identified and matched line by line, using numerical sequence numbers. This is a tedious process, but is made considerably easier with newer programs linked to a graphics output. The experimental spectrum can readily be displayed simultaneously with the theoretical spectrum and dual cursors used to assign theoretical and observed transitions. The chemical shift and coupling constant parameters may then be optimized to give the best fit with the experimental data, and the real and calculated spectra plotted under identical conditions of expansion and amplitude to enable a precise comparison to be made.

4. Automated processing

With the advent of automatic sample changers, there has been increased development of software to allow for unattended spectrometer operation. By definition user interaction is absent in such systems, and so graphics features are not incorporated in such packages, except for initiating an automated experiment.

C. Graphics for interpretation of spectra

So far we have discussed graphics aspects of *measurement*, *presentation* and *processing* of spectra. We have defined *processing* as including all of the data reduction steps necessary to obtain fundamental NMR parameters such as chemical shifts, coupling constants, NOEs, T_1s, etc. from spectra. The next step in the analysis of spectra is that of *interpretation*, which is regarded as the use of the fundamental NMR parameters to obtain chemical information. This might include, for example, applying chemical shifts to deduce primary structural information, or coupling constants to yield molecular connectivities or conformations. NOEs can be used to provide distance information, which in turn can be used to generate 3D structures, while T_1s or other relaxation parameters can yield information on molecular dynamics. These sorts of interpretive applications often require extensive or specialist computation and have usually been done on off-line systems in the past. They will therefore be more fully discussed in Section V. A prerequisite of all these applications is, however, assignment of spectral peaks to atomic sites, and this is briefly discussed below.

The use of graphics to aid in the assignment of organic systems has been fairly limited. The first step in the assignment process is often to make some

of the more obvious assignments on the basis of chemical shift. This is usually done by reference to tables in standard texts or shift compilations (e.g. refs 30, 31), but with the addition of modems to commercial spectrometers, it is now possible to link into computerized databases. This latter approach is still not in widespread use, but is more common for ^{13}C NMR[32-34] than for ^{1}H NMR.[35]

For ^{1}H NMR, connectivity information may be established via selective decoupling, in which case the dual-display mode of irradiated and control spectra on the graphics unit is more rapid and convenient than making such comparisons on hard-copy spectra. In most cases, however, COSY-type 2D experiments have superseded selective decoupling as an aid to making connectivities. A useful graphic innovation that is now offered by a number of the spectrometer processing packages is automatic peak picking and drawing of connectivity lines from cross-peaks back to the diagonal. This is illustrated in Fig. 14.

This graphics representation is potentially more accurate and less time-consuming than the alternative method of making such connections using pen and paper. However, its utility depends on the reliability of the computer in identifying cross-peaks, and is limited to moderately simple systems at present. Further development of a convenient user interface to allow removal of spurious connectivities, or addition of connectivities missed by the computer, is required. Another area that needs to be addressed is the distinction between overlapping two-spin systems and multiple-spin systems. Thus, while a definite connection between two spins is established by horizontal and vertical lines linking their diagonal peaks via a common cross-peak, the appearance of additional cross-peaks on the vertical or horizontal lines could indicate either the presence of additional coupled spins within the same spin system, or fortuitous overlap with a separate spin system. In practice, the spectroscopist attempts to distinguish these possibilities on the basis of the known structure, but in principle such a distinction can also be made by consideration of cross-peak fine structure. Initial efforts are, indeed, being made in computer-aided pattern recognition of cross-peak fine structure in phase-sensitive 2D-correlated spectra.[36,37] With further development, this approach promises to be extremely valuable in the automated identification of spin systems and spectral assignment, but is at present limited to small molecules.

The potential for automated, or at least semi-automated assignment is greatest in molecular systems containing regular repeating units. Proteins and nucleic acids fall into this category, and it is in just these cases that the need for computational and graphics-based aids are greatest due to the large number of spectral peaks present. Again, much of the developmental work so far has been done on off-line systems, so this area is discussed in Section V.B.

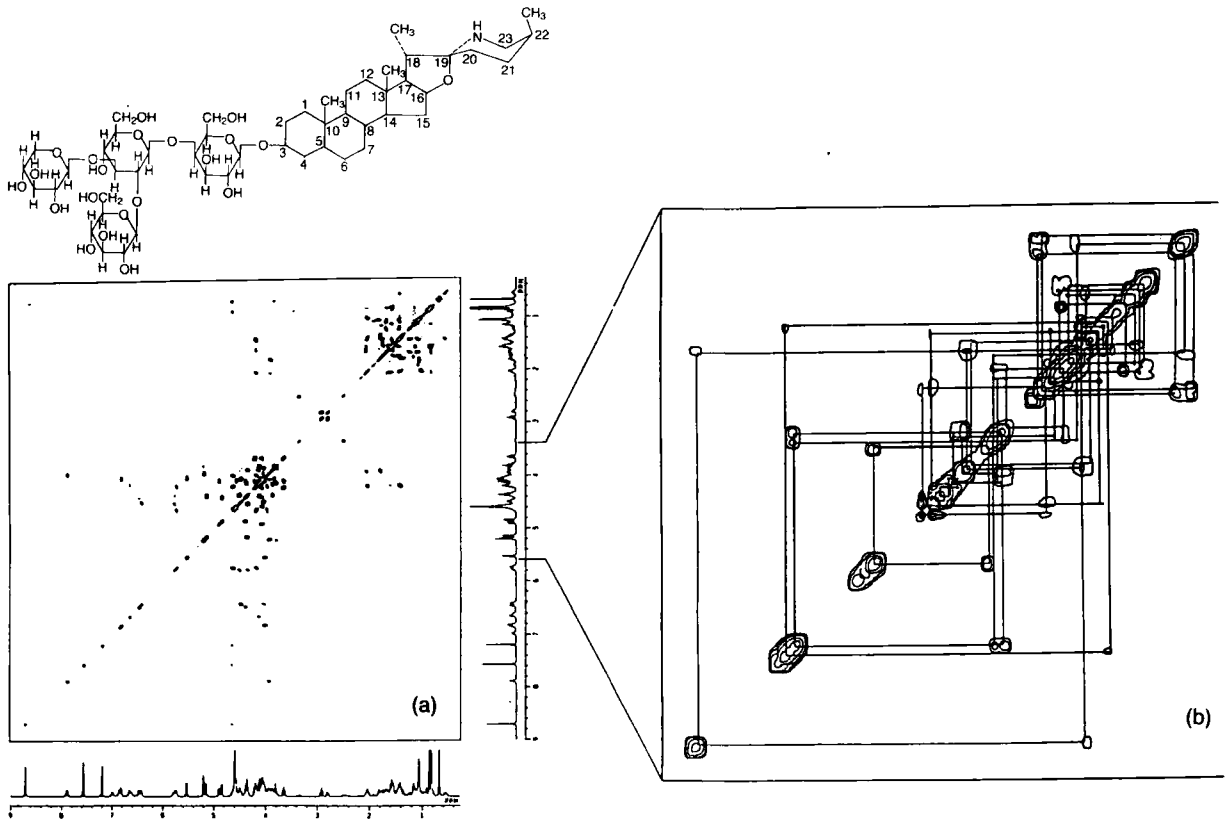

FIG. 14. (a) 2D COSY spectrum of tomatine, with (b) expanded region showing computer-generated connectivities. Spectrum from Jeol Software Application Note 1988.

IV. TRANSFER OF DATA TO OFF-LINE SYSTEMS

The need to transfer NMR data from the NMR computer and process it on a small mainframe or workstation arises from the general limitations of the NMR computer and the general availability of laboratory computers such as the DEC MicroVAX and Sun workstations. In addition, there are a number of specific factors which make off-line processing desirable:

(a) the NMR computer may be so dedicated to collecting data that there is neither sufficient time nor access to the system to process all the data collected;
(b) the power of the dedicated NMR computer may be limited in terms of the speed or the software available;
(c) the cost of software, mass storage and peripheral devices may be uneconomical when compared to those costs on a commercial computer system;
(d) there is often a need to incorporate NMR results or spectra into data-bases or word-processing packages that are more readily available on laboratory computers.

The major instrument companies have responded to this need by providing versatile independent workstations (e.g. X-32, Bruker; Sun workstation, Varian, GE; or the Jeol system which operates on DEC computers) for the processing of NMR data. Data transfer between systems may be achieved either by direct means, i.e. via a hard-wired connection or modem, or by indirect means, i.e. on magnetic media such as floppy disc or magnetic tape.

A. Hardware and software for direct data transfer

Direct transfer of data from the NMR computer to an off-line workstation requires both a physical connection between the two computers and an appropriate communication program that runs on both computers.

The most efficient method of data transfer is via an Ethernet connection, requiring special hardware and cables, and an Ethernet protocol. Transfer rate is fast ($\approx 10^5$ bytes per second) but the system is relatively expensive. Ethernet protocol is supported by all manufacturers, and in theory allows data to be transferred to any computer system; however, it is considerably more sophisticated and expensive than is required for data transfer between just two computers. Because of this expense, the spectrometer companies also use simpler, high-speed data-transfer methods. These include MAGnet for Varian and LIGHTNET for Bruker; Jeol, on the other hand, use the DECNET transfer protocols developed by DEC, which can operate at high speed with the appropriate hardware.

A considerably less expensive procedure is to use the serial RS232 interface ports available on the spectrometers to transfer data. These serial lines operate at 9.6 or 19.2 kbaud ($\approx$900 or 1800 bytes per second), and hence are significantly slower than the networks considered above. In addition, the programs which allow data transfer usually have considerable overheads, further slowing transfer rates. All the spectrometer companies have such specialist programs for transferring data via serial lines between their computers. The widely available and more general program Kermit (available through Columbia University) is designed to transfer files between a wide range of mainframe and personal computers. Kermit versions must be obtained for both computers involved in the transfer process. At present in the NMR field Kermit versions are available for Aspect (Bruker) and DEC (Jeol) computers.

B. Data transfer using magnetic media

Where there is no direct link between the NMR computer and off-line workstation, floppy discs or magnetic tape may be used, although in general they are less convenient than direct transfer. The use of floppy discs is generally confined to the transfer of files and software between similar computer systems, since each manufacturer has opted for different protocols. The limited capacity of floppy discs means that they are cumbersome for the transfer of large 2D data sets, multiple discs being required. On the other hand, industry standard half-inch magnetic tape can be used by a wide range of computer systems, has high capacity, and is therefore useful for storage and transfer of large 2D files.

V. OFF-LINE PROCESSING

The three areas in which the use of graphics has been described are measurement, processing/presentation and interpretation of spectral data. The measurement or data-acquisition function is absent from off-line systems, and their main application is in the last two areas. It is worth noting, however, that off-line systems can have some role as teaching aids in the "measurement" aspect of spectrometer operation. PC-based simulation programs have been developed for this purpose and these and other PC-based applications are discussed in Section V.F. The main discussion under the heading of off-line systems will, however, be on processing (Section V.A) and interpretation (Sections V.B–V.E) on powerful minicomputers or workstations.

A. Major processing packages

Processing programs for off-line systems incorporate all of the features available with on-line systems, but also extend the range of tasks which can be carried out. The greater processing power of off-line systems arises from larger memories, greater access to mass storage devices, and interfaces to other programs such as molecular modelling or molecular dynamics.

The two major sources of such off-line processing packages are the spectrometer companies themselves and independent software developers. The latter category includes commercial companies as well as academic institutions that have developed in-house processing software. Up to this point the spectrometer companies have developed packages which are largely designed to process data originally acquired on their own brand of spectrometer. On the other hand, the independent software companies have included transfer and conversion programs which allow their processing packages to accept data from several brands of spectrometer.

Generally, the off-line packages developed by spectrometer companies are fairly similar in structure and command format to their own on-line packages, but take advantage of more powerful off-line hardware to speed up processing, particularly for two-dimensional data. As far as packages developed by independent companies are concerned, the two in most widespread use at present are FTNMR, developed by Dennis Hare and marketed through MR Resources Inc. (Table 4), and NMR1/NMR2, developed by George Levy through New Methods Research Inc. (Table 4).

FTNMR runs on DEC VAX and Sun Systems and supports a range of terminals. It is a complete 1D and 2D NMR processing package, including data transfer, storage and comprehensive manipulation functions from the free-induction decay through to plotting. Initial versions of the program were

TABLE 4

Off-line NMR processing packages.

Program	Description	Source
FTNMR	Processing of 1D and 2D data on minicomputers or workstations	M. R. Resources[a]
NMR1/NMR2	Processing and analysis of 1D/2D and imaging data on minicomputers or workstations	New Methods Research Inc.[b]
Various	Spectrometer manufacturers' software adapted to off-line computers	Bruker, GE, Jeol, Varian

[a]M. R. Resources Inc., 262 Lakeshore Drive, Ashburnham, MA 01430, USA.
[b]New Methods Research Inc., 719 East Genesee Street, Syracuse, NY 13210, USA.

command-driven, requiring the user to learn its commands, as applies to many of the on-line systems developed by spectrometer manufacturers. New "macro" capabilities effectively allow menus for commonly repeated tasks to be built, making the program more convenient for novice or occasional users. This program also includes many of the advanced processing features described in Section III.B.3, such as 2D peak picking and volume integration.

The NMR1/NMR2 package is an extensive data-reduction system for NMR spectroscopy and imaging. NMR1 is designed primarily for the processing and analysis of 1D NMR data, while NMR2 is applied for 2D NMR spectra as well as images. Both systems are modular FORTRAN 77 programs designed to be utilized on general purpose virtual memory computers. These include microVAX and VAX computers, several UNIX-based minicomputers, and workstations such as Sun or VAXstation systems. While the programs are designed to take full advantage of high-speed, direct memory access (DMA) graphics, they also support a range of serial graphic devices. These include, for example, the Tektronix 4100 and 4200 series terminals. The programs are menu driven, and hence provide the user with a list of options (a menu) appropriate for the studies in hand.

A number of other programs for the interpretation of NMR data have been written or are under development. Many of these do not perform general data-processing functions but were written for specialist applications to assist in the use of NMR data to obtain chemical information. These are discussed in the following sections.

B. Resonance assignments in proteins

NMR is increasingly being used as a tool to determine the three-dimensional structure of proteins in solution. As a prerequisite to structure determination, it is necessary to make a large number of specific resonance assignments. Such a procedure is very time-consuming and a considerable effort is currently being made to automate the process.

There are two general areas where computer graphics is useful: (a) as a predictive aid in the assignment process, and (b) as a "book-keeping" aid to keep track of assignments once they have been made. While the latter consideration may at first appear trivial, it is important to stress that at any intermediate point in a major assignment process for, say, a protein, the ability to illustrate conveniently those assignments already made allows one to focus more readily on those cross-peaks not yet assigned. Such an "accounting" role is, of course, easily implemented on computers, and it is a fairly straightforward procedure to link this to a suitable graphics output (e.g. by the use of horizontal or vertical lines connecting assigned spin

systems or amino acids). This feature is built into the ANALYS2D package under development by Brown.[38]

The use of computers and graphics systems for direct predictive uses in 2D NMR is still in its early stages, but will no doubt expand rapidly in the next few years. Two major approaches that are currently being developed are: (1) the identification of spin systems by the overall pattern of cross-peaks in a 2D spectrum; and (2) the further identification of spin systems (and hence amino acids in a protein) by examination of the fine structure of individual cross-peaks. Before discussing these further it is useful to review briefly the steps required in a resonance assignment of a peptide or protein. The sequential assignment method[39] consists of the following steps:

(1) Identification of the spin systems of non-liable protons in individual amino-acid residues in D_2O solutions of the native protein.
(2) Completion of spin-system assignments for non-liable protons by experiments in H_2O.
(3) Connection of sequential amino-acid spin systems.
(4) Comparison of unique peptide segment assignments with the primary protein sequence determined by an independent method.

Full details are given in the authoritative book by Wuthrich[40] on NMR of proteins and nucleic acids. Steps 1 and 2 are usually carried out using the J connectivity information available from COSY-type spectra, while NOESY spectra are used to obtain the sequential connections noted in Step 3. These are usually made using the so-called $d_{\alpha N}$ connections (Fig. 15) between the NH proton of one residue and the α proton of the preceding residue. d_{NN} or $d_{\beta N}$ connections may also be used for this purpose. In a manual assignment process, the allocation of peaks to a particular type of amino-acid is usually

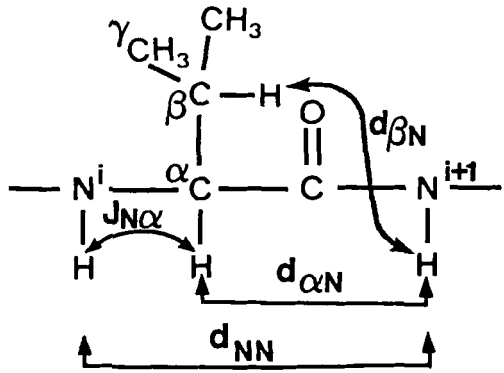

FIG. 15. A segment of a polypeptide showing the labelling scheme commonly used to describe connectivities.

carried out by identification of spin-connectivity patterns in the COSY spectrum. For example, Fig. 16 shows the theoretically expected patterns for valine and arginine, and illustrates the location of these patterns in a 2D COSY spectrum of a peptide (angiotensin I) containing these residues.

The automatic identification of such spin systems within a complex 2D spectrum is not a trivial problem. Some of the difficulties which may occur are:

(1) not all amino-acids have unique COSY patterns;[40] e.g. Cys, Ser, Asp, Asn, Phe, Tyr, His and Trp have similar patterns in the aliphatic spectral region;
(2) the pattern for one particular amino-acid type may change in different proteins, e.g. while threonine has a unique pattern when its α and β protons are chemically shifted, it has a similar pattern to alanine when they are degenerate;
(3) peak overlap from several different amino-acids may mask identification of characteristic COSY patterns from the individual amino-acids;
(4) not all expected cross-peaks may be visible. Since cross-peak intensity depends on the size of the coupling constant involved, and this may change from one protein to another, a given amino-acid may lead to different patterns in different proteins;
(5) artifactual peaks may occur.

Despite these difficulties, a number of groups are actively pursuing automated analysis of 2D spectra. Figure 17 shows a flow chart of the approach used by Neidig *et al.*[41] Note that in addition to a library of cross-peak patterns, this method incorporates expected ranges of chemical shifts for individual protons. A recent survey[42] of ranges of ^{1}H chemical shifts in proteins may be useful in this regard.

Once as many amino-acid types as possible have been identified, the next step is to make sequential assignments by reference to NOESY data. A convenient way of illustrating sequential connectivities is by COSY–NOESY maps,[43] in which the upper left triangle of a NOESY spectrum is combined with the lower right triangle of a COSY spectrum recorded under the same conditions. An example is shown in Fig. 18. In the past, such maps have been produced by modifications of plot routines or by cutting and pasting spectra together, but in the future a greater use of direct graphics display of these or similar representations will considerably facilitate assignment of 2D spectra. In particular, the ability of the computer to keep track of chemical shifts and assignments accurately allows considerable flexibility in on-screen spectral interpretation. For example, in the ANALYS2D package,[38] the user interactively identifies cross-peaks within a spin system (amino-acid) on a COSY

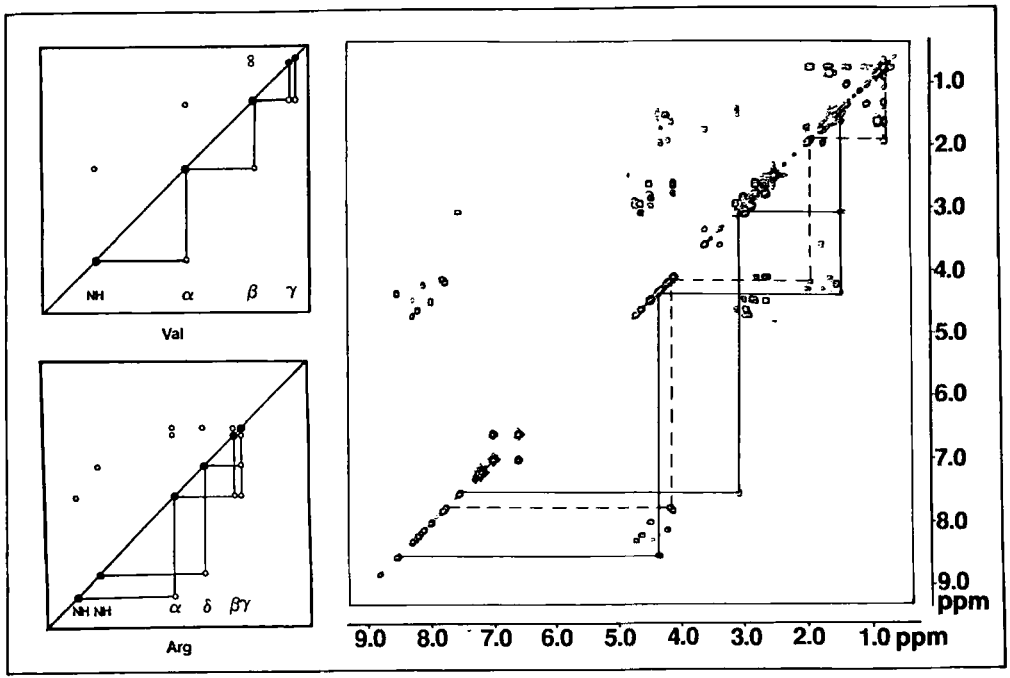

FIG. 16. Theoretical representation of the connectivity patterns for valine and arginine, and the actual patterns seen in angiotensin I. The observed patterns differ slightly from the expected patterns (based on random-coil shifts) because in angiotensin I the two γ-methyl groups for valine (dashed lines) have degenerate shifts, as do the β-methylene protons of arginine (solid lines).

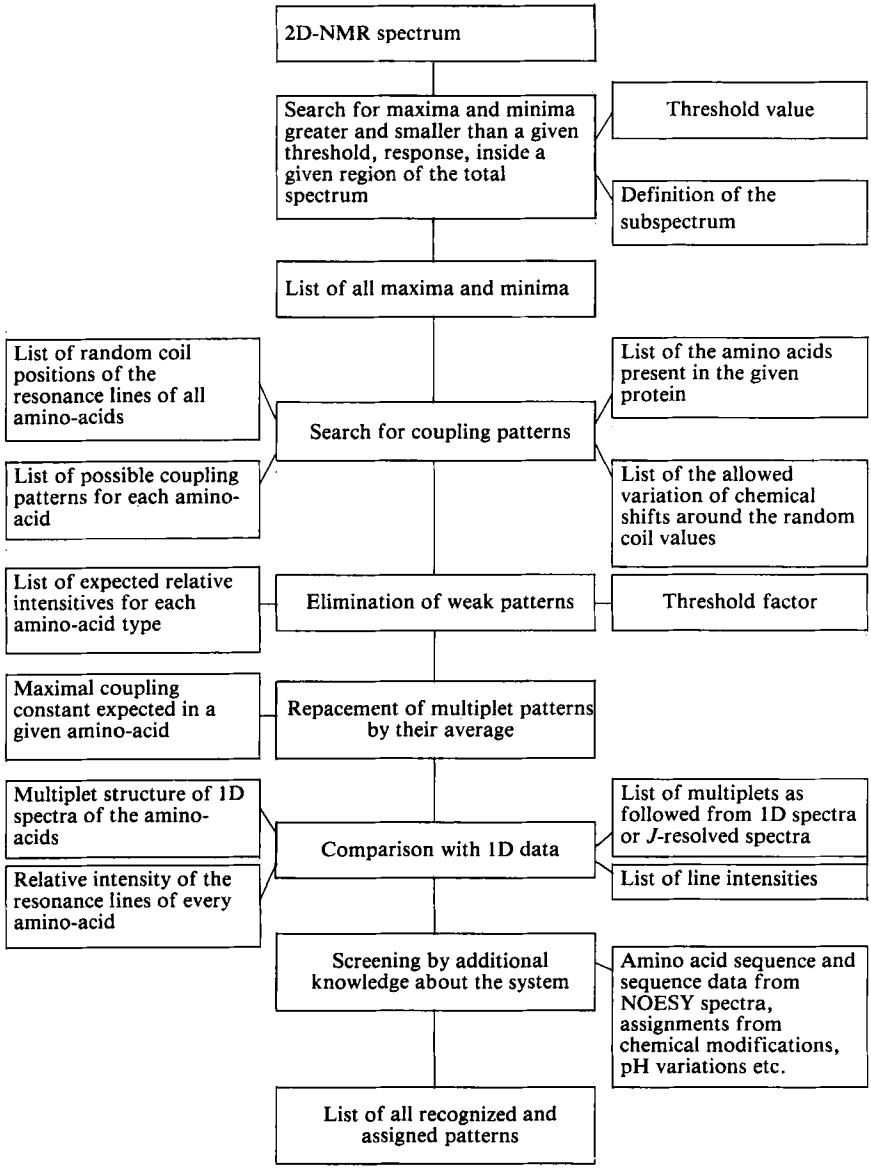

FIG. 17. Flow chart of program NOPP[41] for computer-aided evaluation of two-dimensional NMR spectra of proteins.

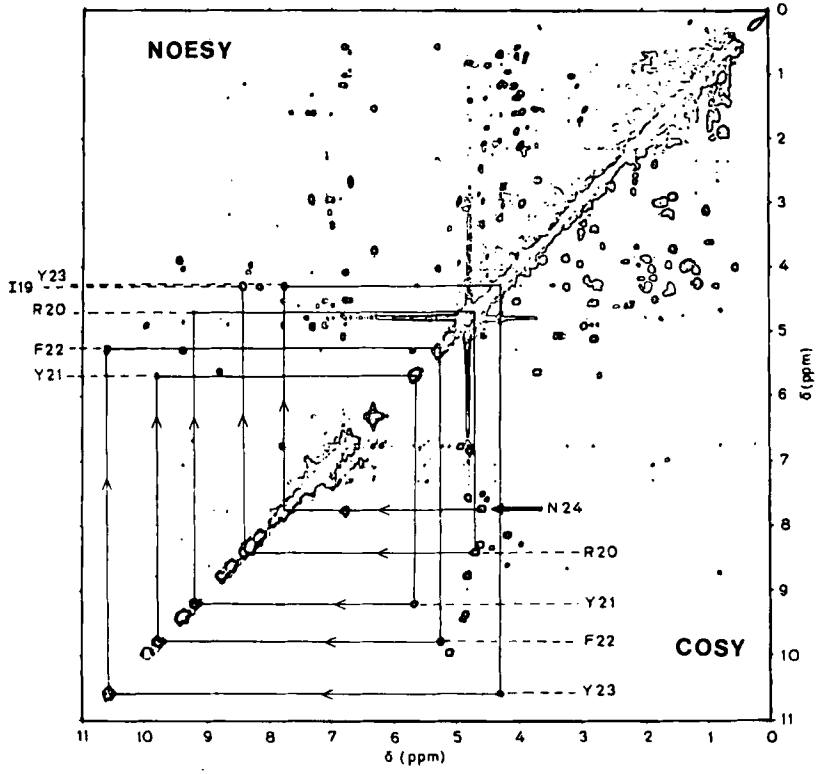

FIG. 18. COSY–NOESY connectivity diagram for ^{1}H NMR sequential assignments in a peptide segment. The sample is a freshly prepared D_2O solution of BPTI, and hence only NOESY connections for slowly exchanging protons are detected. Single letter amino-acid codes and the connectivity pathway for six sequential residues in the polypeptide are indicated. Adapted from ref. 43.

spectrum, stores this information, and is then able to superimpose selected amino-acid-type assignments on the NOESY spectrum to assist in making sequential assignments.

A further advance has been made recently with the development of a program[44] to assist in the semi-automatic sequential resonance assignment of protein ^{1}H NMR spectra. For a number of reasons[40] there is always the possibility of ambiguity occurring in a sequential assignment process, and the program by Billeter *et al.*[44] deals with this by considering *all* possible assignments that are consistent with currently available data. As new information is added, inconsistent assignments are eliminated. Input consists of the peptide or protein sequence, a set of spin systems derived from 2D spectra, and a list

of NOEs. Simple letter codes are used to create a number of data matrices on which the program operates. Elements of these matrices indicate the reliability of spin-system assignments and NOE connectivities. The program is split into an automatic and an interactive part. The former uses the above matrices to generate all possible assignments, while the latter displays information on possible assignments as required and accepts new input as it becomes available. The program is not yet linked to a computer graphics output, but such an interface should considerably enhance its operation.

Further enhancement could also be obtained by linking the program to peak-picking or pattern-recognition algorithms. It was noted earlier that a second level of application of computer graphics to automated analysis is in the recognition of patterns within cross-peaks. In recent times it has become more usual to record phase-sensitive double-quantum filtered COSY (PS-DQ COSY)[17] spectra at high digital resolution rather than normal COSY[45] spectra. The greater resolution and improved lineshapes of the DQ COSY cross-peaks allow additional information on the spin system to be derived. The theoretical basis for the prediction of cross-peak fine structures was originally described by Aue *et al.*,[45] and has been further examined by a number of other groups. Most recently, Widmer and Wuthrich[46] have provided an atlas of cross-peak fine structures for the principal spin systems seen in protein and polydeoxynucleotide NMR which takes into account variations due to changes in chemical shift, scalar couplings, and different processing and acquisition parameters. It is expected that the introduction of this sort of information into automated analysis systems in the future will significantly enhance their effectiveness.

Finally, it was noted earlier that spectral overlap presents a major impediment to automated assignment procedures. Chemical means of minimizing overlap include variations in pH, temperature, salt concentration, etc., while spectroscopic methods include the use of F1 decoupling,[47,48] double-quantum spectroscopy,[49] or RELAYED-COSY[50] experiments. In amino-acid spin-system assignments using COSY, the tracing of connections from β-protons to NHs of the same residue is halted if there is overlap of α-protons from two residues. The RELAYED-COSY technique provides additional cross-peaks between NH protons and β-protons which can be used to confirm NH assignments.[51] Since normal COSY cross-peaks occur in the RELAYED experiments, the latter are usually interpreted in conjunction with the COSY spectrum so that RELAYED peaks can be unambiguously identified. Clearly such a comparison can readily be made using computer graphics, and it is expected that software for achieving this will be readily available in the near future.

C. 3D structure determination/refinement

The determination of a fairly complete set of spectral assignments is the first step in the use of NMR to derive the three-dimensional structure of a macromolecule in solution. In order to determine the structure of a small protein or piece of DNA, the NMR experiment should then provide a large number of intramolecular NOE interactions between known hydrogens in the structure. Such NOE interactions denote pairs of hydrogens closer than 5 Å apart, and can be used to define the 3D structure with reasonable precision, provided a sufficient number of such interactions are known. The procedures that have been used to convert this NOE information into a molecular geometry are DISGEO,[52-54] based on the distance-geometry method developed by Crippen,[55,56] and the DISMAN procedure, developed by Braun and Go.[57]

In the simplest case, the distance between three atoms can be used to define their relative Cartesian coordinates with certainty. For a molecule with a number of defined distances (or distance constraints) and a large number of atoms, the problem is considerably more complex, and there are usually a number of structures consistent with the distance constraints, as well as unresolved inconsistencies in these constraints. The distance-geometry programs use input data concerning the distance constraints, bond lengths, angles, and van der Waals' radii of the atoms, and generate a range of molecular structures consistent with this information.

In the initial uses of this method, the presence of an NOE was used to indicate hydrogens closer than 5 Å and a structure consistent with this set of constraints was generated. More recently, however, attempts have been made to quantify NOE intensities using internal calibration into distance ranges (e.g. 2.0–2.5 Å, 2.5–3.0 Å, 3.0–4.0 Å) and generate a range of structures consistent with these more precise distance constraints.[40] The results of distance-geometry calculations are often represented as a series of overlapping stick structures (Fig. 19). This contrasts with X-ray crystallography, where a single structure is derived from the diffraction data.

The structures derived from the distance-geometry methods may be further refined to provide structures which are in lower energy conformations by the use of molecular mechanics or molecular dynamics methods. Both the AMBER program from the San Francisco group, and the GROMOS programs of Groningen may be used to perform this energy minimization directly or in conjunction with NOE distance constraints.[59] Both programs will handle extremely large molecules but are computationally expensive. They are primarily designed to operate on VAX computers under VMS, but other versions are available. Table 5 lists sources of these and other programs useful for 3D structure determination.

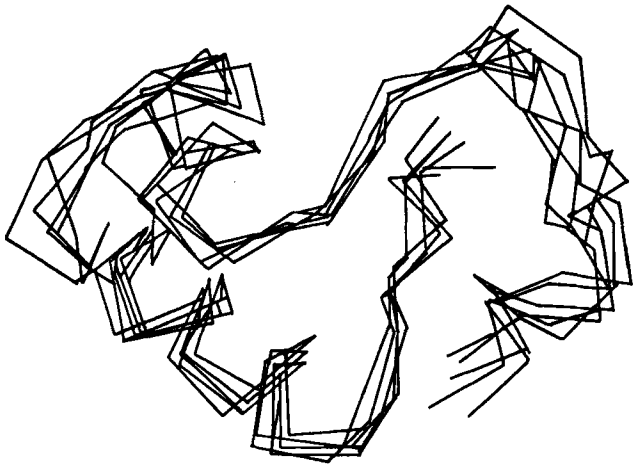

FIG. 19. Typical representation of multiple consistent structures for a polypeptide (in this case crambin) generated by input of NOE data into distance-geometry or restrained molecular dynamics programs. For ease of comparison the structures are usually represented by lines joining Cα atoms. Adapted from ref. 58.

TABLE 5

Programs for structure determination/refinement.

Program	Description	Source
DISGEO	Distance-geometry method	QCPE 507
DISMAN	Distance-geometry method	(a)
AMBER	Molecular mechanics/molecular dynamics	(b)
GROMOS	Molecular mechanics/molecular dynamics	(c)
CHARMM	Molecular modelling/molecular dynamics	(d)
D-SPACE	3D structure determination	(e)

(a) Ref. 57.
(b) Professor P. A. Kollman, School of Pharmacy, Department of Pharmaceutical Chemistry, University of California, San Francisco, CA 94143, USA.
(c) Professor W. F. van Gunsteren, Bromos BV, Laboratory of Physical Chemistry, Mijenborgh 16, 9747 AG Groningen, The Netherlands.
(d) Polygen Corporation, 200 Fifth Avenue, Waltham, MA 02254, USA.
(e) M. R. Resources Inc., 262 Lakeshore Drive, Ashburnham, MA 01430, USA.

D. Molecular modelling/molecular design

Determination of 3D structures of proteins in solution opens up a range of applications in chemistry and biology. These include relating structure to

function, molecular design, and studies of protein–ligand interactions. For all these applications it is essential to have good interactive graphics to allow molecules to be built and manipulated in real time. A large number of programs are now available to help the chemist with this task, and a representative selection of some of the more widely used programs is given in Table 6.

Applications of computer graphics in molecular design have been extensively reviewed elsewhere,[9,10,60–65] and the only further comment that will be made here is that NMR is becoming more important in providing the basic information that allows structures to be determined and used in graphics modelling.

E. QCPE programs

A wide range of NMR-related programs of value to the NMR chemist are available through the Quantum Chemistry Program Exchange (Table 7).

TABLE 6

Graphics modelling programs.

Program	Description	Source/reference
SYBYL/MENDYL	Small-molecule and macromolecular modelling	Tripos Associates[a]
MIDAS	Molecular Interactive Display and Simulation	University of California[b]
MMS	Molecular Modelling System	University of California[b]
CHEM-X	3D molecular graphics	Chemical Design[c]
HYDRA	3D macromolecular graphics	University of York[d]
QUANTA	3D molecular graphics	Polygen Corp.[e]
X-PLOR	Macromolecular structure refinement	Polygen Corp.[e]
MACROMODEL	Small-molecule and macromolecular modelling	Columbia University[f]
CRYSX	Small-molecule superimposition and conformational analysis	Victorian College of Pharmacy Ltd[g]

[a]Tripos Associates, Inc., 6548 Clayton Road, St Louis, MO 63117, USA.

[b]Professor Robert Langridge, Computer Graphics Laboratory, Department of Physical Chemistry, School of Pharmacy, University of California, San Francisco, CA 94143, USA.

[c]Chemical Design Ltd, Unit 12, 7 West Way, Oxford OX2 0JB, UK.

[d]Dr R.E. Hubbard, Department of Chemistry, University of York, Heslington, York YO1 5DD, UK.

[e]Polygen Corporation, 200 Fifth Avenue, Waltham, MA 02254, USA.

[f]Dr C. Still, Box 663, Havemeyer Hall, Department of Chemistry, Columbia University, New York, NY 10027, USA.

[g]School of Pharmaceutical Chemistry, Victorian College of Pharmacy Ltd, 381 Royal Parade, Parkville, Victoria 3052, Australia.

Many of the programs discussed do not have direct screen graphics output, but produce output such as lineshape, chemical shift, coupling constant or relaxation time information that may be directly compared with data produced by the spectrometer. The programs in Table 7 may be divided into several distinct groups described below.

1. Spectral simulation

A number of programs are available to help in the analysis of high-resolution NMR spectra. The programs LAOCN-5 and LAOCOR are based on the

TABLE 7

NMR programs available through QCPE[a].

Program	Description	No.
DISGEO	DIStance-GEOmetry program	QCPE 507
ISHTAR	Interactive System to Help the Theoretical Approach to Relaxation	QCPE 499
MOLDYN	A generalized program for the evaluation of MOLecular DYNamics models using NMR spin-relaxation data	QCPE 489
LAOCN-5	Analysis of isotropic NMR spectra of spin-½ systems	QCPE 458
NMR	Interactive simulation of NMR spectra (PASCAL)	QCPE 456
LAOCOR	Modified LAOCOON (NMR simulation)	QCPE 440
DOKI77/DOKI78	NMR spectra simulation	QCPE 519
DAISY	Simulation and automated analysis of HR-NMR spectra	QCPE 518
DSYMPLOT	Program for the simulation of NMR spectra in isotropic and anisotropic phases using chemical equivalences in a general way	QCPE 470
DAVINS	Direct Analysis of Very Intricate NMR Spectra	QCPE 378
DNMR4	Calculations of chemically exchanging spectra	QCPE 466
DNMR3H	A modified version of DNMR 3 (NMR of chemically exchanging spectra)	QCPE 450
PSEUROT	Computer-assisted PSEUdoROTational analysis of five-membered rings by means of vicinal proton spin–spin coupling constants	QCPE 463
3JHH	NMR vincinal coupling constants	QCPE 461
SCP-FERMI	Self-Consistent Perturbation calculation of the Fermi-contact nuclear spin coupling constant	QCPE 457
NMRCIN-80	Semi-empirical program to calculate NMR shielding constants	QCPE 441

[a]Quantum Chemistry Program Exchange, Chemistry Department, Indiana University, Bloomington, IN 47401, USA.

LAOCOON program (QCPE 111) written by Bothner-By and Castellano, and have been modified to provide simplified input and more attractive output. As has been described earlier, the general procedure with LAOCOON is for the user to define the spin system and suggest chemical shifts and coupling constants. The program then calculates the NMR spectrum, which may be compared with the actual spectrum and used to refine the suggested chemical shifts and coupling constants. These versions can handle up to eight different nuclei, and more if magnetic equivalence is present.

A second group of programs designed for spectral analysis, written by Professor Hagele and his group, is intended to automate the process of NMR spectral analysis to the greatest possible extent. Further information on this package is available in a recent book by Hagele *et al.*[29]

2. *Chemical exchange*

When the rate of magnetic-site exchange is such that NMR peaks are broadened, linewidth can give information about the rate of the exchange processes. For coupled systems, the linewidth analysis is quite complex and programs based on DNMR3, written by D.A. Klerer and G. Binsch, are available through QCPE. These are DNMR4 and DNMR3H.

DNMR4 is designed to decrease the CPU time and memory requirements of the original program, and to reduce the numerical instability (underflow and overflow errors). DNMR3H also attempts to correct these errors, inherent in the original program, but also allows the calculation of exchanging spin systems which include heteronuclei.

3. *Coupling constant and chemical shift calculations*

Molecular conformation and geometry have been determined for many years using the Karplus equation which relates the proton–proton vicinal coupling constant to a torsional angle. The program 3JHH calculates vicinal coupling constants from the molecular geometry, using a Karplus-type equation suggested by Haasnoot and co-workers,[66] and hence can be used to determine a structure or mixture of structures consistent with measured coupling constants. The program PSEUROT operates in a similar way, but is restricted to five-membered rings, and calculates the best fit of conformations to experimental vicinal couplings.

Finally, two programs that calculate the coupling constant (SCF-FERMI) and chemical-shielding constant (σ) from first principles are included. Both use the CNDO/INDO levels of approximation.

4. Relaxation

Two programs are available for the evaluation of relaxation data in terms of the geometry of the molecule in question and its rotational motion (ISHTAR and MOLDYN). The program MOLDYN[67] is a generalized package which calculates T_1, T_2 (and hence linewidth) and NOE for dipolar relaxation in homonuclear or heteronuclear spin systems. The program incorporates a wide range of models for both overall and internal motions. While the program is largely computational, it allows crude graphic displays of, for example, plots of T_1 versus correlation times. ISHTAR is likewise an interactive program which yields quantitative information about molecular geometry and anisotropic rotational motion from dipole–dipole and quadrupolar relaxation within the framework of the diffusional model.

5. Distance-geometry

The distance-geometry method is used to calculate macromolecular structures from hydrogen–hydrogen distance measurements obtained by two-dimensional NOE spectroscopy, and was described above. The method is relatively time-consuming: a system containing approximately 300 atoms requires about four hours of VAX 11/780 CPU time. The QCPE program[53] requires a VAX with a PASCAL compiler. Input and output from the program is in the form of atomic coordinates in the Protein Data Bank format which may be generated and viewed using a number of molecular graphics programs (e.g. CHEM-X).

F. PC-based applications

In many personal computer systems, it is relatively easy to write graphics software and to output results to a plotter, so these systems are ideally suited to NMR applications. Until recently, the lack of computing speed and memory has restricted the processing to relatively simple tasks. The transfer of NMR spectra to personal computers can be accomplished through the use of transfer programs (e.g. Kermit), as discussed in Section IV.A.

1. Teaching programs

The relatively low cost and wide availability of PCs make them extremely useful in a teaching environment. A number of programs have been written to illustrate various aspects of NMR phenomena, and some representative examples are listed in Table 8.

The program MacNMR, written by Robert Boyko and Brian Sykes for the Macintosh computer, allows users to implement pulse sequences used in

TABLE 8

PC NMR programs.

Program	Description	Source
LAOCN 3	Computer simulation of complex NMR spectra. IBM PC Microsoft Fortran and Basica	QCPE 013
MacNMR	Pulse simulation for homo- and hetero-AX systems (Macintosh)	(a)
FTNMR	Principles of FT NMR (Apple II)	(b)
NMR Simulator	Simulation of Varian EM360 operation	(c)
3JHHPC	Vicinal coupling constants from known geometry	QCPE 025
CRYSX	3D Molecular graphics for IBM PC Microsoft Fortran	(d)

(a) R. Boyko and B.O. Sykes, Department of Biochemistry, 474 Medical Sciences Building, University of Alberta, Edmonton, Alberta T69 2H7, Canada.
(b) J.W. Blunt, Department of Chemistry, University of Canterbury, Christchurch 1, New Zealand.
(c) COMPress, Division of Wadsworth Inc., PO Box 102, Wentworth, NH 03282, USA. Author P. Schatz, University of Wisconsin, Milwaukee, WI, USA.
(d) CRYSX, RACI Agricultural & Medicinal Chemistry Division.

NMR spectroscopy and to see the theoretical response of the spin system. The program is widely distributed in the NMR community for a nominal cost of $US20, which includes the program disc and a useful manual. The program runs on both the 512 k Mac and Mac Plus machines; it handles both homonuclear AX and heteronuclear AX spin systems, and so sequences such as COSY or INEPT can be readily simulated. The system graphically displays net magnetization vectors for both A and X spins, and illustrates their response to a sequence of user-defined pulses, delays and RF phases. Density matrix elements are also presented. An example of the display on the Mac is shown in Fig. 20.

Another useful teaching aid is the program FTNMR, written by John Blunt (Table 8). This program runs on the Apple II computer and is useful as a graphic demonstration for explaining basic principles of FT NMR. The program displays a set of magnetic vectors processing at the Larmor frequency (somewhat slowed down for display purposes!), and also illustrates the concepts of the rotating frame of reference and the net magnetization vector. FIDs are also displayed and the concepts of T_1 and flip-angle effects are conveniently demonstrated. Multiple FIDs can be accumulated to show signal-to-noise improvement.

The program "NMR Simulator" is useful as an undergraduate teaching aid to simulate operation of a simple CW 60 MHz NMR spectrometer. This

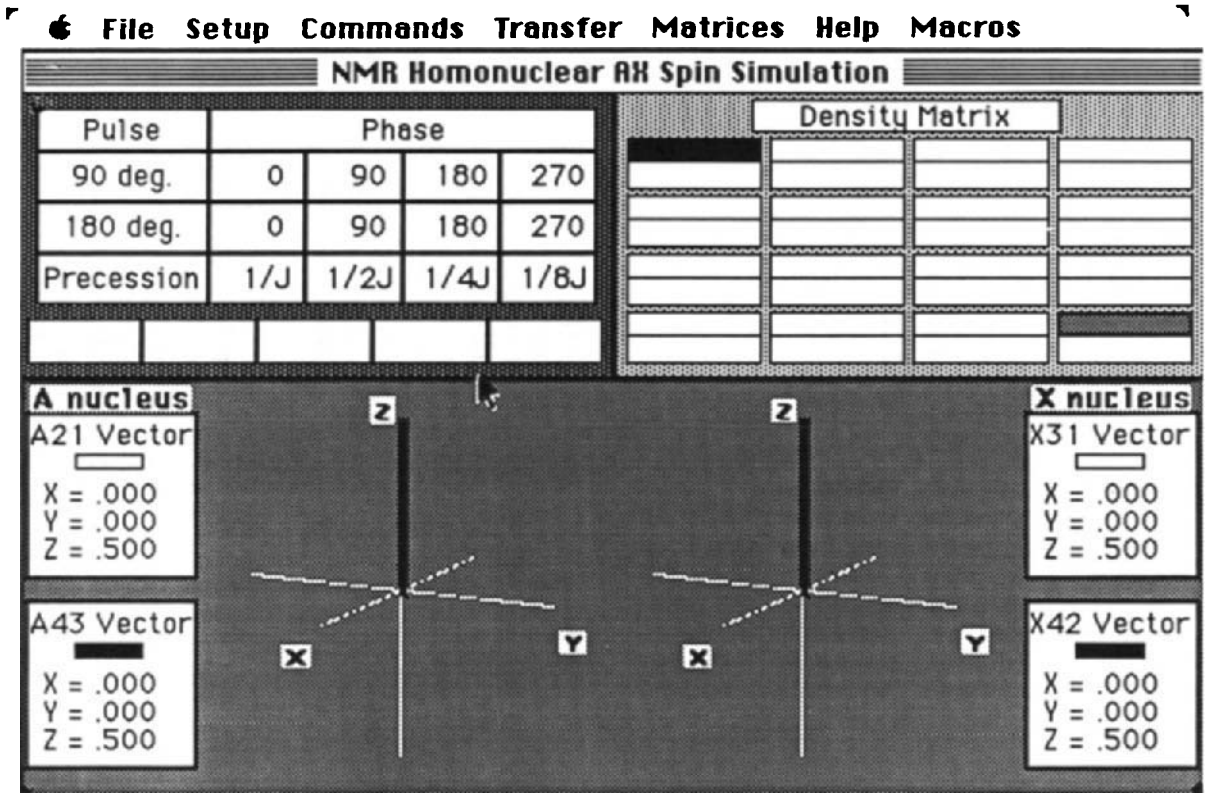

FIG. 20. Example of graphics output for the program MacNMR. (Reproduced with permission of the authors—see footnote to Table 8.)

software is programmed for the IBM PC, XT- or AT-compatibles, and allows a student to investigate the effects of spectrometer controls on an NMR spectrum. Thus the effects of saturation, amplitude and filter bandwidth may be seen and the resulting spectrum plotted on the standard dot-matrix printers or plotters.

2. *In-house programs*

The ease of graphical operations on PCs has resulted in many in-house programs being developed to manipulate NMR data. In many cases, these are written for particular applications and not openly published. We have written a software package to transfer spectra from a Bruker Aspect 3000 system to a Macintosh using Kermit. Once stored on the Macintosh disc, spectra may be rephased, integrated, and scaled both vertically and horizontally. Spectra may be plotted onto a high-resolution Hewlett Packard 7470A plotter, or transferred via the clipboard onto other Macintosh applications, such as Macdaw. This allows the spectra to be labelled and incorporated into word-processing packages, and eventually included in papers printed on a laser printer.

Two other examples of in-house PC programs that we have found useful are an ABC simulation program and a lineshape simulation program for uncoupled two-site exchange. The ABC simulation program, written for a Macintosh, calculates the frequencies and intensities for an ABC (and ABX or AB) spin system given the chemical shifts and coupling constants. This considerably simplifies the analysis of this most common spin system. The correct analysis of an uncoupled two-site exchange system requires estimation of the lifetimes of the two sites from the NMR linewidths, which can be calculated from the known equations,[68,69] and a program written to show the lineshape of the peaks as a function of population, lifetime, chemical-shift difference between the two peaks, and spectrometer inhomogeneity broadening.

3. *Larger programs converted to run on PCs*

The recent improvement in memory and computing power of PCs has resulted in the transition of a number of programs written for mainframe computers to the PC environment. Table 8 shows some of these. CRYSX is a molecular graphics package used to build, store and energy-minimize the structures of medium sized molecules. Its utility in NMR applications derives from the fact that it can estimate coupling constants using Karplus-type relationships, or check internuclear distances from comparison with NOE data.

VI. SUMMARY AND CONCLUSIONS

Over the last few years, there have been very significant increases in the graphics resources (both software and hardware) available to the NMR spectroscopist. The rapid incorporation of these resources into NMR spectrometers and off-line processing stations has reflected the extensive data-reduction demands of methods such as 2D NMR.

In the future, high-resolution, high-speed graphics displays with the ability to zoom, make 2D and 3D rotations under hardware control, and to display several windows simultaneously, will become standard features of NMR spectrometers.

The power of associated workstations will be greatly increased and the spectrometer companies will offer industry-standard workstations of great power and memory. These will have inbuilt high-speed communication and use standard operating systems so that the manufacturers' software can be integrated with commercial and QCPE packages.

Software will be available to detect peaks and assign 2D NMR spectra automatically for peptides of known sequence. There will be considerable development of software to convert NMR data directly into three-dimensional structures.

ACKNOWLEDGMENTS

We thank Jackie King for her excellent work in typing the manuscript, and Malea Kneen and Sharon Munro for their valuable assistance with preparation of diagrams, and for helpful comments. We also thank Jessie White for additional help with diagrams, and Sergio Scrofani, Louis Kyratzis and Tony Wedd for providing the angiotensin I data.

REFERENCES

1. E.G. Hoffman, W. Stempfle, G. Schroth, B. Weimann, E. Ziegler and J. Brandt, *Angew. Chem. Int. Ed.*, 1972, **11**, 375–386.
2. P. Anstey and R.K. Harris, *Chem. in Br.*, 1977, **13**, 303.
3. G.C. Levy, D. Terpstra and C.L. Dumoulin, in *Computer Networks in the Chemical Laboratory* (G.C. Levy and D. Terpstra, eds), Wiley-Interscience, New York, 1981, Ch. 5.
4. C. Thibault and J.W. Cooper, *Magn. Res. Rev.*, 1980, **5**, 101.
5. J.W. Cooper, *The Minicomputer in the Laboratory*, Wiley-Interscience, New York, 1983.
6. W.E. Hull, in *Two-Dimensional NMR Spectroscopy: Applications for Chemists and Biochemists* (W.R. Croasmur and R.M.K. Carbon, eds), VCH Publishers, New York, 1987, Ch. 2.

7. A. Allerhand and M. J. Dohrenwend, *J. Am. Chem. Soc.*, 1985, **107**, 6684.
8. S. R. Maple and A. Allerhand, *J. Am. Chem. Soc.*, 1987, **109**, 6609.
9. K. Prout, in *Molecular Graphics and Drugs Design* (A. S. V. Burgen, G. C. K. Roberts and M. S. Tute, eds), Elsevier, Amsterdam, 1986, Ch. 1.
10. J. G. Vinter, in *Molecular Graphics and Drug Design* (A. S. V. Burgen, G. C. K. Roberts and M. S. Tute, eds), Elsevier, Amsterdam, 1986, Ch. 1.
11. *Graphics Technology*, February Edn, Business Press International, Sydney, 1987, p. 33.
12. E. Fukushima and S. B. W. Roeder, *Experimental Pulse NMR*, Addison-Wesley, London, 1981, Ch. VI.
13. D. M. Doddrell, D. T. Pegg and M. R. Bendall, *J. Magn. Reson.*, 1982, **48**, 323.
14. D. T. Pegg, D. M. Doddrell and M. R. Bendall, *J. Chem. Phys.*, 1982, **77**, 2745.
15. P. R. Andrews, R. T. C. Brownlee, M. F. Mackay, D. B. Poulton, M. Sadek and D. A. Winkler, *Aust. J. Chem.*, 1983, **36**, 2219.
16. D. J. States, R. A. Haberkorn and D. J. Ruben, *J. Magn. Reson.*, 1982, **48**, 286.
17. D. Marion and K. Wuthrich, *Biochem. Biophys. Res. Commun.*, 1983, **113**, 967.
18. A. Bax, *Two-Dimensional Nuclear Magnetic Resonance in Liquids*, Delft University Press, D. Reidel, Dordrecht, 1982.
19. K. Nagayama, P. Bachmann, K. Wuthrich and R. R. Ernst, *J. Magn. Reson.*, 1978, **31**, 133.
20. R. Baumann, G. Wider, R. R. Ernst and K. Wuthrich, *J. Magn. Reson.*, 1981, **44**, 402.
21. J. D. Mersh and J. K. M. Sanders, *J. Magn. Reson.*, 1982, **50**, 171.
22. M. Sass and D. Ziessow, *J. Magn. Reson.*, 1977, **25**, 263.
23. J. Kowalewski, G. C. Levy, L. F. Johnson and L. Palmer, *J. Magn. Reson.*, 1977, **26**, 533.
24. D. J. Craik and G. C. Levy, in *Topics in Carbon-13 NMR Spectroscopy*, Vol. 4 (G. C. Levy, ed.), John Wiley & Sons, London, 1984, Ch. 9.
25. A. A. Bothner-By and S. M. Castellano, in *Computer Programs for Chemistry*, Vol. 1 (D. F. de Tar, ed.), Benjamin, New York, 1968, Ch. 3.
26. J. D. Swalen, in *Computer Programs for Chemistry*, Vol. 1 (D. F. de Tar, ed.), Benjamin, New York, 1968, Ch. 4.
27. S. Brumby, *Magn. Reson. Rev.*, 1983, **8**, 1.
28. A. Ellison, *J. Chem. Ed.*, 1983, **60**, 425.
29. G. Hagele, M. Engelhardt and W. Boenik, *Simulation and Automated Analysis of Nuclear Magnetic Resonance Spectra*, VCH Verlagsgesellschaft, Weinheim, 1987.
30. E. Pretsch, T. Clerc, J. Seibl and W. Simon, *Tables of Spectral Data for Structural Determination of Organic Compounds*, Springer, Berlin, 1983.
31. W. Bremser, B. Franke and H. Wagner, *Chemistry Shift Ranges in Carbon-13 NMR Spectroscopy*, Verlag Chemie, Weinheim, 1982.
32. M. Razinger, J. Zupan, M. Penca and B. Barlic, *J. Chem. Inf. Comput. Sci.*, 1980, **20**, 158.
33. N. A. B. Gray, J. G. Nourse, C. W. Crandell, D. H. Smith and C. Djerassi, *Org. Magn. Reson.*, 1981, **15**, 375.
34. C. A. Shelley and M. E. Munk, *Anal. Chem.*, 1982, **54**, 516.
35. H. Egli, D. H. Smith and C. Djerassi, *Helv. Chim. Acta*, 1982, **65**, 1898.
36. B. U. Meier, G. Bodenhausen and R. R. Ernst, *J. Magn. Reson.*, 1984, **60**, 161.
37. P. Pfandler, G. Bodenhausen, B. U. Meier and R. R. Ernst, *Anal. Chem.*, 1985, **57**, 2510.
38. L. R. Brown, Private communication, 1988.
39. K. Wuthrich, G. Wider, G. Wagner and W. Braun, *J. Mol. Biol.*, 1982, **155**, 311.
40. K. Wuthrich, *NMR of Proteins and Nucleic Acids*, Wiley-Interscience, New York, 1986, Ch. 8.
41. K. P. Neidig, H. Bodenmueller and H. R. Kalbitzer, *Biochem Biophys. Res. Commun.*, 1984, **125**, 1143.
42. K. H. Gross and H. R. Kalbitzer, *J. Magn. Reson.*, 1988, **76**, 87.

43. G. Wagner, A. Kumar and K. Wuthrich, *Eur. J. Biochem.*, 1981, **114**, 375.
44. M. Billeter, V.J. Basus and I.D. Kuntz, *J. Magn. Reson.*, 1988, **76**, 400.
45. W.P. Aue, E. Bartholdi and R.R. Ernst, *J. Chem. Phys.*, 1976, **64**, 2229.
46. H. Widmer and K. Wuthrich, *J. Magn. Reson.*, 1987, **74**, 316.
47. L.R. Brown, *J. Magn. Reson.*, 1984, **57**, 513.
48. M. Rance, G. Wagner, O.W. Sorensen, K. Wuthrich and R.R. Ernst, *J. Magn. Reson.*, 1984, **59**, 250.
49. T.H. Mareci and R. Freeman, *J. Magn. Reson.*, 1983, **51**, 531.
50. G. Wagner, *J. Magn. Reson.*, 1983, **55**, 151.
51. H. Kessler, W. Bermel, A. Muller and K-H. Pooh, in *The Peptides*, Vol. 7 (S. Udenfriend and J. Meinhofer, eds), Academic Press, Orlando, 1985, pp. 547-575.
52. T.F. Havel, I.D. Kuntz and G.M. Crippen, *Bull. Math. Biol.*, 1983, **45**, 665.
53. T.F. Havel and K. Wuthrich, *Bull Math. Biol.*, 1984, **46**, 673.
54. T.F. Havel and K. Wuthrich, *J. Mol. Biol.*, 1985, **182**, 281.
55. G.M. Crippen, *J. Comp. Phys.*, 1977, **24**, 96.
56. G.M. Crippen, *Distance-Geometry and Conformational Calculations*, Chemometrics Research Studies Series, Vol. 1, Research Studies Press (Wiley), New York, 1981.
57. W. Braun and N. Go, *J. Mol. Biol.*, 1985, **186**, 611.
58. A.T. Brunger, R.I. Campbell, G.M. Clore, A.M. Gronenborn, M. Karplus, G.A. Petsko and M.M. Teeter, *Science*, 1987, **235**, 1049.
59. R. Kaptein, E.R.P. Zuiderweg, R.M. Scheek, R. Boelens and W.F. van Gunsteren, *J. Mol. Biol.*, 1985, **182**, 179.
60. C.H. Hassall, *Chem. in Br.*, 1985, **32**, 39.
61. J.G. Vinter, *Chem. in Br.*, 1985, **32**, 32.
62. J.G. Vinter, A. Davis and M.R. Saunders, *J. Comp.-Aided Molec. Design*, 1987, **1**, 31.
63. G.R. Marshall, in *Computer-Aided Molecular Design*, Oyez Scientific and Technical Services Ltd, London, 1985, pp. 1-22.
64. G.R. Marshall, *Ann. Rev. Pharm. Toxicol.*, 1987, **27**, 193.
65. H. Fruhbeis, R. Klein and H. Wallmeier, *Angew. Chem. Int., Ed. Engl.*, 1987, **26**, 403.
66. C.A.G. Haasnoot, F.A.A.M. Leeuw and C. Altona, *Tetrahedron*, 1980, **76**, 2783.
67. D.J. Craik, A. Kumar and G.C. Levy, *J. Chem. Inf. Comp. Sci.*, 1983, **23**, 30.
68. R.K. Harris, *"Nuclear Magnetic Resonance Spectroscopy"*, Pitman, London, 1983, Section 5.4.
69. H. Gunther, *NMR Spectroscopy*, Wiley, Chichester, 1980, Ch. VIII.
70. R. Freeman, *Proc. Roy. Soc. Lond.*, 1980, **A373**, 149.

Some Recent *Ab Initio* Calculations of the NMR Chemical Shift

D. B. CHESNUT

Department of Chemistry,
Duke University,
Durham, North Carolina 27706, USA

I. INTRODUCTION

The chemical shift in nuclear magnetic resonance is certainly one of the more important second-order effects in chemistry. Although it has now been nearly forty years since Ramsey's theoretical description,[1] it has only been in the last decade that significant progress has been made in the calculation of this quantity. As more sophisticated computational facilities have become available and more satisfactory approximate methods employed we have reached the point today where, at least for certain species such as carbon, quite good calculations of the chemical shift in a rigid molecular environment are possible. Indeed, Jameson and Jameson[2] indicate that we have reached the position where theoretical calculations of ^{13}C shielding in small molecules are within experimental error, and require better experimental values with which to compare. The purpose of this review article is to display the current state of affairs, to review the progress which has occurred in recent years which makes today's results so encouraging, and to discuss briefly a few applications of shielding calculations.

ANNUAL REPORTS ON NMR SPECTROSCOPY
VOLUME 21 ISBN 0-12-505321-5

The approach used in this chapter is characterized by the choice of title. We restrict the discussion to *ab initio* calculations for several reasons. First of all, as mentioned already, since first principle calculations are becoming sufficiently facile, the emphasis upon understanding and predicting chemical shifts lies now more in the *ab initio* domain than, out of necessity in the past, in the semi-empirical area. Secondly, at least for small molecules, *ab initio* calculations are generally better than semi-empirical ones at this point in time. For whatever reason, the semi-empirical approaches seem to have run into what for ^{13}C chemical shifts appears to be a 10 ppm "barrier" in accuracy. No such barrier is yet obvious (or anticipated) for *ab initio* calculations, and results seem to be getting better and better. *Recent* results will be discussed but with no real definition of that term. To see the progress that has been made one has to examine some of the past difficulties, and follow the eradication of these problems over a number of years. One needs temporal flexibility to appreciate the current state of affairs. Finally, the scope of the chapter is certainly limited in that only *some* calculations will be discussed, in contrast to a rigorous review of all efforts on all fronts. The latter approach is currently being followed each year in an excellent manner in a number of review articles, such as, for example, the thorough discussions by C.J. Jameson in the Specialist Periodical Reports on Nuclear Magnetic Resonance.[3] The approach adpoted in this chapter allows us to avoid the terse style required in such review articles; at the same time, of course, more lengthy discussions require that the area and range of topics be reduced. The topics discussed here, then, reflect in great part my own interests, and the omission of a great many examples of chemical shift calculations in no way makes any statement concerning their importance.

We begin with a section on basic principles which tries to lay the theoretical foundations for chemical shift calculations. Detailed derivations of the various theoretical approaches are not given since these are better found in other references. A review of the classical picture of the origin of chemical shifts precedes the quantum mechanical fundamentals; because it is so easy to become lost in the symbolism and mathematics of quantum mechanics, it is desirable to keep in mind the basic classical picture of what the quantum theory is attempting to describe. Furthermore, our "understanding" a quantum mechanical calculation usually leads back to a classical "picture" that we find helpful in lieu of the mathematics. The gauge problem, still a thorn in the side of shift calculations, is discussed, and a variety of approaches designed to overcome this problem are described.

We present the current best results of NMR chemical shifts and shift anisotropies for heavy (non-hydrogen) atoms in order to see the level of agreement today between theory and experiment. Since most calculations are sensitive to choice of basis set, a review of the evolution of choice of basis sets is given

so that we can decide on the level required for adequate calculated results. As an illustration of the uses to which chemical shift calculations can be put, the effects of geometry on the chemical shift are discussed, mainly from the standpoint of the effect of bond length modifications. Some theoretical results for calculations on hydrogen are given, and we conclude with brief remarks on some recent chemical shift calculations that are examples of our continuing progress in the ability to treat successfully larger and more complex chemical systems.

II. BASIC PRINCIPLES

It has been nearly forty years since Ramsey's initial paper on the theory of chemical shifts appeared in a 1950 issue of *Physical Review*.[1] We have known for a long time how to calculate the chemical shift, but only recently have we been able to carry out such calculations to a meaningful accuracy. The calculation still needs to be done in an approximate manner, and the final equations which need to be solved often depend upon the particular approximation one is employing. However, there is a certain commonality of basic ideas and approaches, and it is this which we present briefly in this section.

The energy of a magnetic moment, μ, in the presence of an external magnetic field, $\mathbf{B}$, is given by:

$$\begin{aligned} E_\mu &= -\boldsymbol{\mu}\cdot\mathbf{B} + \boldsymbol{\mu}\cdot\boldsymbol{\sigma}\cdot\mathbf{B} \\ &= -\boldsymbol{\mu}\cdot(\mathbf{1}-\boldsymbol{\sigma})\cdot\mathbf{B} \end{aligned} \tag{1}$$

where the first scalar interaction represents the coupling to the external field of the bare moment μ while the second term involving the shift tensor σ is the effective coupling provided between the magnetic field and the nuclear moment by the electronic fluid in a molecular environment. That is, the electrons of a system provide an effective magnetic field of $-\sigma\cdot\mathbf{B}$. If σ is positive, the effective field opposes the external field, the nucleus is shielded, and a diamagnetic effect results. If σ is negative, the effective field provided by the electrons is generally supportive of the external field, a de-shielding or paramagnetic effect. Note that the shielding tensor, σ, is an asymmetric second-rank tensor. That is, because it couples two physically distinct quantities (the nuclear moment and the external field), σ_{ij} will in general not be the same as σ_{ji}.

A. The classical picture

It may be helpful at this point to recall the classical origin of the electron-induced field–nucleus coupling. A particle of charge q at position $\mathbf{r}$ from the

origin moving with a velocity **v** creates a magnetic field $\mathbf{B}_{ind}$ at the origin given by:

$$\mathbf{B}_{ind} = (\mu_0/4\pi)\frac{q\hbar\mathbf{L}}{mr^3} \tag{2}$$

where μ_0 is the magnetic permeability of free space and **L** is the particle's angular momentum (in units of $h/2\pi = \hbar$). Picture a nucleus μ residing at this origin and determine the field induced at the nucleus by an electron (of charge $q = -e$) moving in a circular orbit in the xy plane. In the presence of an external magnetic field $\mathbf{B}_0$ along the z-axis, the energy of the electron is given by:

$$E = \frac{e\hbar}{2m}\mathbf{L}\cdot\mathbf{B}_0 \tag{3}$$

and one sees that to minimize its energy, the electron would prefer an orbit such that its angular momentum is directed in the negative z direction. Since $q = -e$ in equation (2), the field induced by the electron is then *parallel* to the applied field, thus adding to it. This is the paramagnetic shift due to the orbital motion of the electron. Because the angular momentum of the electron prefers to align itself in a particular way with respect to an external field, the resulting motion induces a field that adds to the external field. If we carry out a resonance experiment at fixed frequency to observe the nuclear spin flip, a particular total field is required. Since the orbiting electron provides a positive part of this field, an external part smaller than usual is needed, an effect referred to as a downfield shift.

Apparently, electrons that are already moving (i.e. those that have non-zero angular momentum) lead to paramagnetic shifts. How, then, do we understand the presence of diamagnetic shifts, those effects whereby fields in opposition to the applied field are created? This is most easily understood by considering an arbitrary classical distribution of charge, initially at rest, about our nuclear origin. Being static, there is no orbital angular momentum (no velocities) and, therefore, no magnetic field is induced at the nuclear origin. Suppose we now turn on a magnetic field in the positive z direction and ask what happens classically to the charges that make up this distribution. Maxwell's equations tell us that:

$$\nabla \times \boldsymbol{\xi} = -\frac{\partial \mathbf{B}}{\partial t} \tag{4}$$

that is, a changing magnetic field occurs with an accompanying electric field. If we start from a situation of zero magnetic and external electric fields and proceed to turn on the magnetic field in the z direction, an accompanying

tangential electric field will exist as long as **B** is changing. This will give to particles that are initially static an orbital motion about the z-axis, the direction of the changing magnetic field. This tangential electric field accelerates the particles for a time t during which the magnetic field is being turned on, and it is not difficult to show that at the time the external field has reached its final value, $\mathbf{B}_0$, the various charges in the distribution have reached a velocity such that the average field they induce at the origin is given by:

$$\mathbf{B}_{\text{ind}} = -(\mu_0/4\pi)\frac{e^2\mathbf{B}_0}{2m}\int \frac{x^2 + y^2}{r^3}\rho(\mathbf{r})d\mathbf{r} \tag{5}$$

where we have integrated over a presumed continuous distribution of charge specified by the distribution function $\rho(\mathbf{r})$. Note that the induced field in this case is in opposition to the applied field because the electric field in existence during the time we turn on the magnetic field causes an orbital motion that the electrons would otherwise consider "unsatisfactory."

This is the diamagnetic effect. The action of turning on the magnetic field induces a motion that produces a field in opposition to the applied field. Accordingly, when carrying out a nuclear magnetic resonance experiment at fixed frequency, more than the normal applied field must be used to achieve resonance, an effect referred to as an upfield or diamagnetic shift.

B. The quantum mechanical picture

We now present the general basics of chemical shielding. The theory has been treated in many texts and review articles, and many of the recent theoretical treatments have preceded numerical results with a derivation of the theory pertinent to the particular approximation involved. What we outline here is a more or less general approach at the beginning stages of the theoretical development.

The Hamiltonian of a molecular system can be written as:

$$\mathscr{H} = \sum_j \frac{1}{2m}(\mathbf{p}_j + e\,\mathbf{A}_j)^2 + V \tag{6}$$

where the potential V includes both one- and two-electron potential energy terms as well as the nuclear repulsion terms in a generally assumed rigid nuclear framework (the Born–Oppenheimer approximation). $\mathbf{A}_j$ is the vector potential experienced by the jth electron and is made up of contributions from the external field, **B**, and a nuclear magnetic moment, μ, whose coupling we treat. This total vector potential is given by:

$$\mathbf{A}_j(\mathbf{r}_j) = \mathbf{A}_B(\mathbf{r}_j) + \mathbf{A}_\mu(\mathbf{r}_j) \tag{7a}$$

$$\mathbf{A}_B(\mathbf{r}) = \frac{1}{2}\mathbf{B} \times \mathbf{r} \tag{7b}$$

$$\mathbf{A}_\mu(\mathbf{r}) = (\mu_0/4\pi)\ \frac{\mu \times \mathbf{r}_N}{r_N^3};\quad \mathbf{r}_N = \mathbf{r} - \mathbf{R}_N \tag{7c}$$

where the vector potential from the magnetic field **B**, $\mathbf{A}_B$, is a fairly standard form and is written with respect to an arbitrary origin, while the contribution from the magnetic moment μ is more specific, with distances being measured relative to the nuclear moment located at $\mathbf{R}_N$. Employing the usual coulomb gauge ($\nabla \cdot \mathbf{A} = 0$), the Hamiltonian can be expanded in terms of the cartesian coordinates ($\alpha,\beta = x,y,z$) of the magnetic moment and the external field to various orders:

$$\mathscr{H} = \sum_j \frac{1}{2m}\,\mathbf{p}_j^2 + V + \sum_j \left(\frac{e}{m}\,\mathbf{A}_j \cdot \mathbf{p}_j + \frac{e^2}{2m}\,\mathbf{A}_j \cdot \mathbf{A}_j\right) \tag{8}$$

$$\left.\begin{aligned} &= \mathscr{H}_0 + \sum_\alpha \mu_\alpha \mathscr{H}_\alpha^{(0,1)} + \sum_\rho H_\beta \mathscr{H}_\beta^{(1,0)} + \sum_{\alpha,\beta} \mu_\alpha H_\beta \mathscr{H}_{\alpha\beta}^{(1,1)} \\ &\quad + \sum_{\alpha,\beta} \mu_\alpha \mu_\beta \mathscr{H}_{\alpha\beta}^{(0,2)} + \sum_{\alpha,\beta} H_\alpha H_\beta \mathscr{H}_{\alpha,\beta}^{(2,0)} \\ &\quad \alpha,\beta = x,y,z \end{aligned}\right\} \tag{9}$$

where the order for a particular component of the Hamiltonian with respect to the magnetic field is indicated first within the superscript parentheses, while the order with respect to the nuclear moment is indicated second; particle indices are suppressed henceforth for ease of notation. That term which is pure second-order in the magnetic field is important in the calculation of the magnetic susceptibility but is not of interest for chemical shielding; neither is the pure second-order term for the nuclear moment, μ. As we shall see, the terms which are of interest to us here are those which are first-order in either the magnetic moment or the external field and are given below:

$$\mathscr{H}_\alpha^{(1,0)} = \frac{e}{2m}\,(\mathbf{r} \times \mathbf{p})_\alpha \tag{10a}$$

$$\mathscr{H}_\alpha^{(0,1)} = \frac{e}{m}\,r_N^{-3}\,(\mathbf{r}_N \times \mathbf{p})_\alpha \tag{10b}$$

$$\mathscr{H}_{\alpha,\beta}^{(1,1)} = \frac{e^2}{2m}\,r_N^{-3}\,(\mathbf{r}\cdot\mathbf{r}_N\delta_{\alpha\beta} - (\mathbf{r}_N)_\alpha \mathbf{r}_\beta) \tag{10c}$$

The chemical shielding arises from the effect on the *electronic* energy of the system by the moment μ and the external field **B**. Given the appropriate Hamiltonian for the system we now can define the chemical shielding tensor as:

$$\sigma_{\alpha\beta} = \left.\frac{\partial^2 E}{\partial \mu_\alpha \partial B_\beta}\right|_{\mu = \mathbf{B} = 0} \tag{11}$$

Since this electron-induced shielding is generally small, perturbation theory is appropriate, and that is now briefly outlined.

Energy derivatives such as that given in equation (7) are generally most readily obtained by starting with the Hellmann–Feynman theorem.[4,5] Although the Hellmann–Feynman theorem is usually derived presuming energy eigenfunctions of the corresponding Hamiltonian, it has been shown that under appropriate conditions it also obtains for approximate wave functions. Stanton[6] has given a short proof of its applicability to Hartree–Fock wave functions, while Pople and co-workers[7] present a nice derivation in their 1968 paper based on the prior work of Hurley.[8] We will parallel the development of Pople *et al.* with a slight generalization in terms of the parameters that the wave function can depend upon.

In order to see this development, consider a Hamiltonian of a system that can be written as an analytical function of the parameters a, b:

$$\begin{aligned}\mathscr{H} &= \mathscr{H}(a,b) \\ &= \mathscr{H}_0 + a\mathscr{H}^{(1,0)} + b\mathscr{H}^{(0,1)} + ab\mathscr{H}^{(1,1)} + \ldots \end{aligned} \tag{12}$$

The ground state wave function associated with $\mathscr{H}$, $\Psi = \Psi(a,b)$ will also be a function of a and b, as will the energy:

$$E = E(a,b) = \langle \Psi(a,b) | \mathscr{H}(a,b) | \Psi(a,b) \rangle \tag{13}$$

We assume that Ψ and E may be expanded in a power series about the point $a = b = 0$:

$$E = E_0 + aE^{(1,0)} + bE^{(0,1)} + abE^{(1,1)} + \ldots \tag{14a}$$

$$\Psi = \Psi_0 + a\Psi^{(1,0)} + b\Psi^{(0,1)} + ab\Psi^{(1,1)} + \ldots \tag{14b}$$

and wish to calculate the quantity

$$\left.\frac{\partial^2 E}{\partial b \partial a}\right|_{a=b=0} = E^{(1,1)} \tag{15}$$

Suppose we write the wave function as:

$$\Psi(a,b) = \phi(s;a) \tag{16}$$

where the wave function ϕ now contains a set of parameters, $s_j \epsilon s$, that are mainly variational parameters chosen to minimize the energy, and where generally the parameters s_j depend upon a and b, $s_j = s_j(a,b)$. The form of ϕ we have chosen also indicates an *explicit* dependence on one of the Hamiltonian parameters, a, as well as the implicit dependence contained in the set s. (This explicit dependence in ϕ on the parameter a illustrates treatments later on of the chemical shift in which orbitals (atomic or molecular) are employed that contain a complex exponential linear in the external magnetic field, **B**.) Just as we can rewrite the wave function Ψ in terms of the equivalent function ϕ, so, too, can we rewrite the energy:

$$E(a,b) = \epsilon(s;a) = \langle \phi(s;a) | \mathscr{H}(a,b) | \phi(s;a) \rangle \tag{17}$$

That is, the energy's total dependence on a and b is contained implicitly in the parameter set s and in an explicit dependence on the parameter a since we have allowed it to appear in the wave function ϕ.

To this point it has not been necessary to stipulate whether or not Ψ (or ϕ) satisfies an energy eigenvalue equation or not, that is, whether or not it is exact. The set s will usually contain expansion coefficients in a basis. If the basis is complete, then Ψ will be exact; if the basis is incomplete, Ψ will be an approximation. The key point is, however, under whatever conditions we work, members of the set s either provide the lowest energy for these conditions

$$\frac{\partial \epsilon}{\partial s_j} = 0 \text{ (first subset)} \tag{18a}$$

or are fixed in the sense that they do not depend on a or b.

$$\frac{\partial s_j}{\partial a} = \frac{\partial s_j}{\partial b} = 0 \text{ (second subset)} \tag{18b}$$

We can use this fact to derive the Hellmann–Feynman theorem for Ψ, be it approximate or exact, in the following way. We first take the derivative of E with respect to the parameter b:

$$\frac{\partial E}{\partial b} = \frac{\partial \epsilon}{\partial b} + \sum_j \frac{\partial \epsilon}{\partial s_j} \frac{\partial s_j}{\partial b} \tag{19}$$

and see that the second sum vanishes because of either equation (18a) or (18b) above. Thus, since $\phi(s;a)$ does not explicitly depend upon b, it follows that:

$$\frac{\partial E}{\partial b} = \frac{\partial \epsilon}{\partial b} = \langle \Psi | \frac{\partial \mathscr{H}}{\partial b} | \Psi \rangle \tag{20}$$

It is important to note at this juncture that a similar result could not be obtained if we were to start by taking the energy derivative with respect to the parameter a for which ϕ does have an explicit dependence. We can complete the determination of $\partial^2 E/\partial a \partial b$ by taking the derivative with respect to a in equation (20):

$$\frac{\partial^2 E}{\partial a \partial b} = \langle \frac{\partial \Psi}{\partial a} | \frac{\partial \mathscr{H}}{\partial b} | \Psi \rangle + \langle \Psi | \frac{\partial \mathscr{H}}{\partial b} | \frac{\partial \Psi}{\partial a} + \langle \Psi | \frac{\partial^2 \mathscr{H}}{\partial a \partial b} | \Psi \rangle \tag{21}$$

where now the derivative of Ψ with respect to a is the total derivative of that function. Finally, recalling the expressions (15), (12), and (14) we find the desired end result:

$$\left.\begin{aligned}\left.\frac{\partial^2 E}{\partial a \partial b}\right|_{a=b=0} &= \langle \Psi^{(1,0)} | \mathscr{H}^{(0,1)} | \Psi_0 \rangle \\ &+ \langle \Psi_0 | \mathscr{H}^{(0,1)} | \Psi^{(1,0)} \rangle \\ &+ \langle \Psi_0 | \mathscr{H}^{(1,1)} | \Psi_0 \rangle\end{aligned}\right\} \tag{22}$$

$\Psi_{(1,0)}$ is that part of Ψ first-order in the parameter a and will contain that part of ϕ explicitly first-order in a as well as the first-order contribution through the parameter set s, usually found by ordinary perturbation theory.

As indicated above, this simple result could not be obtained if we had taken initially the derivative of E with respect to a. If, as is usually done in derivations of this kind, no explicit dependence of either a or b is contained in ϕ, then an equivalent result could be obtained by starting in the second way. The apparent asymmetric result obtained in these two cases illustrates the interchange theorem of Dalgarno and Stewart.[9] When, however, there is an explicit dependence in the wave function on one of the Hamiltonian parameters, the corresponding equations for the interchange theorem take on a much more complicated form.

The application of equation (22) to the chemical shift calculation is clear. Instead of the parameters a and b we have the cartesian components μ_α and H_β ($\alpha,\beta = x,y,z$). In terms of our previous notation it is easy to see that

$$\left.\begin{aligned}\sigma_{\alpha\beta} &= \left.\frac{\partial^2 E}{\partial B_\beta \partial \mu_\alpha}\right|_{\mu=\mathbf{B}=0} \\ &= \langle \Psi_\beta^{(1,0)} | \mathscr{H}_\alpha^{(0,1)} | \Psi_0 \rangle \\ &+ \langle \Psi_0 | \mathscr{H}_\alpha^{(0,1)} | \Psi_\beta^{(1,0)} \rangle \\ &+ \langle \Psi_0 | \mathscr{H}_{\alpha,\beta}^{(1,1)} | \Psi_0 \rangle\end{aligned}\right\} \tag{23}$$

where $\sigma_{\alpha\beta}$ is the desired tensor quantity. This result is valid whether the $\mathbf{B}_\alpha$ appear explicitly in the basis set or not, but would not be correct if the basis contained the μ_α.

Accordingly, to calculate σ we need to know the wave function linear (first-order) in each of the components of the magnetic field, **B**. The way we determine $\Psi_\beta^{(1,0)}$ will depend upon the particular approach involved. In this review we consider wave functions compiled from large basis sets with no explicit dependence in the basis of the magnetic field as well as those cases where the magnetic field enters explicitly into the basis set in the atomic or molecular orbitals of a Hartree–Fock calculation.

The expression for the shielding tensor in equation (23) brings us full circle with the classical picture. The wave function of the system is perturbed by an external magnetic field. The magnetic field induces preferred currents in the

system, and it is these currents which, through the modified wave function, interact with the nuclear moment. The paramagnetic effects are contained in the first two expressions in equation (23), while the last term involving $\mathscr{L}_{\alpha,\beta}^{(1,1)}$ is an expression of the diamagnetic effect.

Before leaving this section we point out again that the chemical shielding tensor is in general an asymmetric second rank tensor with nine independent components.[10,11] The number of components is often reduced by symmetry but, generally, this asymmetry will be present both experimentally and, of course, theoretically. Fortunately, through linear terms in the shielding only the effects of the symmetric part of the tensor manifest themselves experimentally;[12] accordingly, principal values of the shielding tensor and anisotropies that are reported are derived from the tensor symmetrized prior to diagonalization.

C. The gauge problem

The vector potential employed in the previous section for the external magnetic field is more or less the standard one but is not unique. This lack of uniqueness, normally expressed in terms of the choice of gauge origin, poses problems in approximate calculations in that they may not be gauge invariant. In this section we give a brief review of the gauge problem and cite several approaches to overcoming it.

Because in Maxwell's equations the divergence of the magnetic field, **B**, vanishes, one is allowed to introduce the idea of the vector potential **A**, given by

$$\mathbf{B} = \nabla \times \mathbf{A} \tag{24}$$

since the divergence of the curl of an arbitrary vector is equal to zero. The choice of the vector potential is not unique; if one defines a new vector potential $\mathbf{A}'$ in terms of **A** and an arbitrary scalar function f

$$\mathbf{A}' = \mathbf{A} - \nabla f \tag{25}$$

the potential $\mathbf{A}'$ yields the same physical magnetic field as the vector potential **A** since the curl of the gradient of an arbitrary scalar function vanishes. This freedom of choice allows us to select gauges which greatly simplify situations, such as choosing **A** such that its divergence is zero (div $\mathbf{A} = 0$), the Coulomb gauge, or the Lorentz gauge

$$\nabla \cdot \mathbf{A} + \frac{1}{c^2} \frac{\partial \phi}{\partial t} = 0 \tag{26}$$

where ϕ is the scalar potential introduced in a manner similar to that of **A**; the Lorentz gauge leads to symmetrical field equations. Where one is dealing

with a static uniform magnetic field the scalar potential can be set equal to zero, so that the Coulomb and Lorentz gauges become equivalent.

The freedom to select different gauges would seem to add flexibility to calculations. Since the particular gauge involved can certainly not affect the physical observables of a system, one should be able to select a gauge which, in a particular situation, leads to a particularly transparent interpretation. Unfortunately, this gauge invariance holds for *exact* calculations but, as with many theorems, not necessarily for approximate ones. Fortunately for us, it has been shown that the coupled Hartree–Fock approximation *is* gauge invariant,[13] even though it is an approximate theory. Even so, one seldom does a full Hartree–Fock treatment of a system; we are usually forced to work with finite basis sets, and our incomplete Hartree–Fock SCF approach, an approximation to an approximation, is found to be no longer independent of the chosen gauge.

For a uniform external field, **B**, the standard choice for the vector potential is given by:

$$\mathbf{A}(\mathbf{r}) = \frac{1}{2}\mathbf{B} \times \mathbf{r} \tag{27}$$

where **r** is the vector distance of a particle from an arbitrary origin. An equivalent potential is arrived at by the gauge transformation defined by:

$$\mathbf{A}'(\mathbf{r}) = \frac{1}{2}\mathbf{B} \times (\mathbf{r} - \mathbf{R}) \tag{28}$$

which clearly yields the same physical external field, but where now distances are measured relative to the arbitrary vector **R**. That is, this gauge transformation defines a reselection of the origin for our problem. The choice of origin in a completely and properly solved problem cannot, of course, affect any physical observable. Yet here the choice of origin arises in the gauge of the vector potential and, because most calculations are to some degree incomplete, a gauge dependence is introduced.

There are several ways to attack this problem. One is to select an "optimum" gauge to minimize the problem, and a number of discussions of this approach are in the literature. It is generally held that the larger errors in calculating the chemical shift arise from the paramagnetic term. Rebane[14] showed that for one-electron systems there exists a gauge such that the paramagnetic susceptibility vanishes identically. Chan and Das[15] selected as gauge origin the electronic centroid because this choice causes the paramagnetic part of the susceptibility to be a minimum. However, as Sadlej[16] points out, while the arguments of Chan and Das appear convincing for the magnetic susceptibility, they do not provide criteria for the choice of gauge origin for nuclear magnetic shielding. He further comments that this choice of gauge

origin does not imply additionally that the error due to incompleteness of the basis set is also minimized.

Another approach is to choose a sufficiently complete basis so that the effects of choice of origin are minimal; this is the approach taken by several authors whose calculations we discuss in the present review. Yet another approach, and one which is finding more widespread acceptance at present, is to introduce gauge factors into either the atomic orbitals of the basis set or the molecular orbitals themselves in a Hartree–Fock calculation in such a manner that the calculation, approximate though it is, is independent of gauge origin.

When one uses London orbitals,[17] or, as they are often called, gauge invariant atomic orbitals (GIAOs), instead of using the usual, real atomic orbital, ϕ_n, located at $\mathbf{R}_n$, one employs the complex orbital, χ_n,

$$\chi_n = \phi_n \exp[-(ie/\hbar)\mathbf{A}(\mathbf{R}_n)\cdot\mathbf{r}] \tag{29}$$

where the complex phase factor contains the vector potential (as defined in equation (7b)) evaluated at the point $\mathbf{R}_n$. It is easy to see how using such orbitals will lead to translational gauge independence in coupled Hartree–Fock theory. The potential energy integrals (both one- and two-electron integrals) will have complex exponential terms depending upon the *differences* of the vector potentials of the centres involved. The integral involving $\mathbf{p} + e\mathbf{A}(\mathbf{r})$, the kinetic momentum, likewise will involve the difference of the vector potentials at the sites of the two centres involved, and the operator itself is modified as follows:

$$\begin{aligned}(\mathbf{p} + e\mathbf{A}(\mathbf{r}))\phi_n \exp[-(ie/\hbar)\mathbf{A}(\mathbf{R}_n)\cdot\mathbf{r}] = \\ \exp[-(ie/\hbar)\mathbf{A}(\mathbf{R}_n)\cdot\mathbf{r}]\,[\mathbf{p} + e\mathbf{A}(\mathbf{r}) - e(\mathbf{A}(\mathbf{R}_n))]\phi_n\end{aligned} \tag{30}$$

The action of the momentum derivative operator causes $\mathbf{A}(\mathbf{r})$ in the Hamiltonian to be replaced by $\mathbf{A}(\mathbf{r}) - \mathbf{A}(\mathbf{R}_n)$. Thus, all the integrals involve *differences* of vector potentials and are clearly invariant to choice of gauge origin.

We should note that the important point in the argument just given is not that the vector $\mathbf{R}_n$ be specifically the vector defining the position of centre n, but rather that it be some *constant* vector. The use of $\mathbf{R}_n$ is convenient, however, in that in the magnetic field perturbation part of the calculation the angular momentum integrals that arise will have the angular momentum operator defined with respect to the vector $\mathbf{R}_n$. Clearly, such integrals are easier to evaluate if this is the atomic centre since our basis functions are also atom centred.

Whereas in Ditchfield's GIAO Hartree–Fock approach[18] to the chemical shift calculation the gauge factors premultiply the usual *atomic* orbitals, the types of calculations carried out by Kutzelnigg and Schindler[19-22] involve

complex exponential gauge factors in the *molecular* orbitals. Schindler and Kutzelnigg wanted an approach that would allow both circumvention of the gauge origin problem and the ability to define atomic and bond contributions to both the magnetic susceptibility and the chemical shift. In order to do this they worked with localized molecular orbitals, orbitals that do not differ very much from spherical orbitals, and which have a natural gauge origin each. Rather than working with molecular orbitals Ψ_k which satisfy the Hartree-Fock equation

$$F\Psi_k(\mathbf{r}) = \epsilon_k \Psi_k(\mathbf{r}) \tag{31}$$

where F is the usual Fock operator, they define molecular orbitals Ψ_k'

$$\Psi_k'(\mathbf{r}) = \mathrm{e}^{-i\Lambda_k(\mathbf{r})}\,\Psi_k(\mathbf{r}) \tag{32}$$

where Λ_k is any real local function (of $\mathbf{r}$) linear in the external magnetic field, $\mathbf{B}$. These new orbitals satisfy the modified Fock equations

$$\left.\begin{aligned} F_k'\Psi_k'(\mathbf{r}) &= \epsilon_k \Psi_k'(\mathbf{r}) \\ F_k' &= \mathrm{e}^{-i\Lambda_k(\mathbf{r})} F_k \mathrm{e}^{+i\Lambda_k(\mathbf{r})} \end{aligned}\right\} \tag{33}$$

where F_k' is the Fock operator transformed as indicated. If one uses for the gauge factor the function

$$\Lambda_k(\mathbf{r}) = \frac{e}{2\hbar}(\mathbf{R}_k \times \mathbf{B})\cdot\mathbf{r} \tag{34}$$

then, just as was the case with the use of GIAO orbitals, the term containing the momentum and vector potential terms in the Hamiltonian is transformed according to:

$$\mathrm{e}^{-i\Lambda_k(\mathbf{r})}(\mathbf{p} + e\tfrac{1}{2}\mathbf{B}\times\mathbf{r})\mathrm{e}^{+i\Lambda_k(\mathbf{r})} = \mathbf{p} + e\tfrac{1}{2}\mathbf{B}\times(\mathbf{r}-\mathbf{R}_k) \tag{35}$$

and a simple shift of the gauge origin is effected.

As shown by Kutzelnigg,[19] a similar treatment can be devised for a localized coupled Hartree-Fock scheme. The advantages of the localized representation appear when one uses, in addition, different gauge transformations for the different localized orbitals. Although the vector $\mathbf{R}_k$ associated with the transformed localized molecular orbitals could be any constant vector, it is clearly advantageous to associate it with some property of the localized orbitals, and Schindler and Kutzelnigg select it to be equal to the electronic centre of gravity of the localized orbital. Levy and Ridard[23] have suggested a similar method in which different gauge origins are used for different pairs of orbitals (either AOs or MOs); however they have only treated the molecule PH_3 so few data are available to assess their method.

Yet another approach has been taken by Hansen and Bouman[24] involving a local origin variant of the coupled Hartree-Fock method in which the

random phase approximation is applied.[25] Complex (gauge-independent) orbitals are not introduced, but rather by expanding angular momentum terms relative to a local origin for each orbital and using properties of the random phase approximation they are able to arrive at shielding expressions that contain no reference to an overall gauge origin. This localized-orbital-local-origin (LORG) approach yields quite good results for the carbon species studied, and employs some of the smallest basis sets that we discuss. As in the IGLO method of Schindler and Kutzelnigg, a localization of the molecular orbitals and the use of local origins allows the decomposition of the total shielding into individual local bond contributions and so-called "bond-bond" contributions involving all other bonds.

According to Jameson,[3] the success of these methods employing local origins (Ditchfield's GIAO approach, the IGLO approach of Schindler and Kutzelnigg, the LORG method of Hansen and Bouman, or the different origins of different pairs of orbitals proposed by Levy and Ridard) in some way seems to be that when these methods are employed, the calculations leave out large terms of opposite sign which would have been exactly cancelling in the limit of a complete basis set. Evidently the use of local origins provides an effective damping of basis set errors in the long-range contributions to shielding, and leads to better agreement with experiment than the conventional coupled Hartree–Fock approach which employs a common gauge origin.

As we shall see, all of these approaches employ different levels of basis sets that achieve a similar and reasonably good degree of success in the calculation of the chemical shift. The reader is referred to the original references for a detailed discussion and derivation of the various approaches.

III. SOME THEORETICAL RESULTS FOR HEAVY ATOMS

A. Shieldings and shielding anisotropies

In this section we give a general overview of calculated isotropic shieldings and shielding anisotropies as determined by four groups with differing approaches to the shielding calculation itself in terms of the gauge problem. The calculated results are shown in Tables 1 and 2, which also contain the corresponding experimental data. The experimental data, for the most part, have been taken from the recent ^{13}C gas phase work of Jameson and Jameson[2] or from the recent compilation of data by C.J. Jameson[3] in her review article. Where results must be converted to an absolute scale for ^{13}C, the Jamesons' data[2] has been employed. Most of the experimental data quoted are gas phase data, although there are some liquid and solid data as

TABLE 1

Representative isotropic chemical shifts (ppm) for C, N, O, and F nuclei from the work of Chesnut and Foley (CF), Schindler and Kutzelnigg (SK), Hansen and Bouman (HB), and Höller and Lischka (HL). Experimental results are generally gas phase data, or, as indicated, liquid (l) or solid (s). Several shift values are obtained from spin rotation constants and theoretical diamagnetic shieldings (sr). Primary ^{13}C standards are taken from Jameson and Jameson.[2]

	CF	SK	HB	HL	Experiment	Ref.
C: CH_4	193.0	196.7	196	195.8	195.1	2
$H_2\overset{*}{C}CO$		189.9			182.4(s),182.9(l)	29
$\overset{*}{C}_2H_6$	181.2	183.5	184	186.2	180.9	2
$CH_3\overset{*}{C}H_2CH_3$			179		170.9,170.9	32,33
$CH_3CH_2CH_3$			177		169.2,169.3	32,33
$\overset{*}{C}H_3NH_2$	162.5				158.3	2
$\overset{*}{C}H_3CHO$			166		157.2	2
CH_3OH	145.1[a]	157.2[b]	145		136.6	2
C_2H_2	118.3	116.4[c]	122	119.1	117.2	2
CH_3F	128.1	139.8[b]			116.8	2
$H_2\overset{*}{C}CCH_2$	114.5[a]	116.7			115.2	2
HCN	74.8	72.9[c]	78		82.1	2
C_2H_4	62.2	61.6	63	60.4	64.5	2
OCO	54.6[a]	50.7[c]			58.8	2
CO	−21.3	−23.8[c]		−21.1[d]	1.0(sr)	2
CN^-	2.0[a]				18(l)	3
$CH_3\overset{*}{C}HO$			−8		−6.7	2
$H_2\overset{*}{C}CO$		−6.8			−8.3(s), −8.6(l)	29
$H_2\overset{*}{C}O$	2.6	−5.5	4		−8.4(l)	34
$H_2\overset{*}{C}CCH_2$	−37.0[a]	−37.8			−29.3	2
N: NH_3	265.2	265.4[e]		266.1	264.5(sr)	36
CH_3NH_2	253.2				249	37
HCN	−46.9	−46.0[c]			−20.4	38
CN^-	−73.3[a]				−29.7(l)	38,40
N_2	−109.4	−108.4[c]			−61.6	38
O: H_2O	332.0	327.4[e]		328.1	344.0	41
CH_3OH	347.0[a]				270.9(l)	3
CO	−88.0	−84.1[c]			−42.3(sr)	41,42
H_2CO	−459.4	−456.1[e]			−312.1	41
OCO	220.0[a]	223.7[c]				
F: CH_3F	484.5				471.6	43
HF	412.4	413.5[e]		415.0	410	44
F_2	−181.5	−172.5			−232.8	43

[a]D. B. Chesnut and K. D. Moore, unpublished results. The results for CH_3NH_2 and CH_3OH are corrections to the data in ref. 26 where a slightly incorrect geometry was employed.

[b]Basis I of ref. 21.

[c]Ref. 22.

[d]Ref. 28.

[e]Ref. 20.

TABLE 2

Representative chemical shifts anisotropies (ppm) for C, N, O, and F from the work of Chesnut and Foley (CF), Schindler and Kutzelnigg (SK), Hansen and Bouman (HB), and Höller and Lischka (HL). The shift anisotropy, $\Delta\sigma$, is defined as $\Delta\sigma = \sigma_{\parallel} - \sigma_{\perp}$ when axial symmetry is present, or as $\Delta\sigma = \sigma_{33} - \frac{1}{2}(\sigma_{22} + \sigma_{11})$, $\sigma_{33} \geq \sigma_{22} \geq \sigma_{11}$. Experimental data are gas phase (unlabelled) or indicated otherwise as liquid (l), liquid crystal (lc), solid (s), or a combination of spin-rotation constants plus standard diamagnetic shieldings (sr).

	CF	SK	HB	HL	Experiment	Ref.
C: C_2H_6	11.3	13.5	8	10.4		
$CH_3CH_2CH_3$			24			
$CH_3CH_2CH_3$			11			
CH_3NH_2	38.6					
CH_3CHO			47			
CH_3OH	63.8[a]		61		63(s)	45
C_2H_2	241.0	243.8	235	240.4	240 ± 5(s)	46
CH_3F	85.9	86.9			68 ± 15	47
H_2CCCH_2	98.6[a]	100.5[b]			83	30
HCN	304.8	306.0	301		284.6 ± 20(lc)	48
C_2H_4	172.0		180	176.3	153(s)	46
OCO	342.9[a]	346.5			335(s)	46
CO	439.0	442.2		438.4[c]	405.5 ± 1.4(sr), 406 ± 30(s)	49,50
CN^-	413.4					
CH_3CHO			193			
H_2CO	196.5	183.8	183			
H_2CCCH_2	72.4[a]	55.0			58	30
N: NH_3	−45.2	−37.7		−40.4	−40(sr)	36
CH_3NH_2	47.7					
HCN	579.7	574.4			563.8 ± 8(sr)	53
CN^-	625.0[a]					
N_2	662.3	670.8			676 ± 20(sr), 603 ± 28(s)	55,56
O: H_2O	39.0	55.8		56.9		
CH_3OH	96.9[a]					
CO	748.1	742.0		740.1[c]	676.1(sr)	57
H_2CO	1330.5	1318.0			1252	55
OCO	292.4	286.2				
F: CH_3F	−71.5				−60.8 ± 15(sr)	58
HF	105.8	102.3		99.9	108	59
F_2	1005.3	991.6			1050 ± 50(s)	60

[a] D. B. Chesnut and K. D. Moore, unpublished data. See footnote *a* of Table 1.
[b] See ref. 30.
[c] Ref. 28.

well; in some instances, the paramagnetic part of the shift has been determined from spin rotation studies and coupled with a theoretical determination of the diamagnetic shielding to yield an "experimental" result. This is a generally permissible procedure since the diamagnetic part of the chemical shift can generally be calculated quite accurately. Although most of the gas phase data have been reported in the zero-pressure limit, such experiments are usually carried out at finite temperatures (typically 300 K) so that the effects of rotation and vibration on the chemical shift are present in the experimental results. For the data discussed here, the calculations have been carried out for a rigid nuclear framework, generally for the molecule in its equilibrium configuration. Although occasionally geometries optimized for the particular basis set are employed, for the most part investigators employ experimental geometries in their calculations.

The isotropic chemical shifts for some carbon, nitrogen, oxygen, and fluorine species are shown in Table 1 taken from the calculations of Chesnut and Foley,[26] Schindler and Kutzelnigg,[21] Hansen and Bouman,[24] and Höller and Lischka.[27] Generally speaking, all four approaches illustrated here yield essentially equivalent results. Hansen and Bouman report only carbon chemical shifts, while the data of Höller and Lischka are limited to the simple hydrocarbons and some additional hydrides. All the results for carbon are quite impressive and show that we can today, with a variety of approaches, calculate carbon chemical shifts to within 5–10 ppm of experiment. One awkward case which shows up in all calculations is that of CO, where all of the theoretical approaches underestimate the net shielding.

The results for nitrogen, oxygen and fluorine are not as impressive, although there are relatively few data for fluorine on which to make any serious judgement at this time. The nitrogen species that have the worst agreement with experiment involve multiply bonded nitrogens. Clearly, while we can take pride in the results for carbon, there is still a great deal of work yet to be done for these other elements of the first long row of the periodic table.

In Table 2 are shown the calculated and observed anisotropies for representative molecules containing as resonant nuclei again carbon, nitrogen, oxygen and fluorine, again using the four sets of calculations that appear in Table 1. While a good theory of chemical shielding must, of course, reproduce the isotropic chemical shifts, the ability to calculate shielding anisotropies can be a more severe test since accurate evaluation of the three individual components of the diagonalized symmetrized shielding tensor are required. Like the isotropic shifts for carbon, the carbon anisotropies shown in Table 2 compare quite favourably to experiment; for the other resonant nuclei, the comparison is not so good. It is interesting to note that for those nitrogen and oxygen species where the isotropic shift is difficult to calculate,

the calculated anisotropy has a smaller error. This can be rationalized if it turns out that there is a more or less uniform error in the same algebraic direction of the various shielding tensor components. If this is true, it also suggests that comparing differences of isotropic shifts is more likely to match experimental data than comparing their absolute values. While this could be a useful approach in terms of making predictions, still the problem remains theoretically of finding the best approaches to reproduce absolute measurements.

Some calculations on simple hydrides of the second long row of the periodic table are shown in Table 3 where the data have been taken from the calculations of Chesnut,[61] Höller and Lischka,[62] and Lazzeretti and Zanasi.[63] The various calculations agree quite well with each other and, in those two instances where experimental data can be estimated, with experiment. Calculations involving second row elements pose a more difficult problem than those involving first row elements; larger basis sets must be employed and the calculations show that a much larger range for the (sensitive) paramagnetic terms is present. Calculations on hydrides are fairly easy to do, and one should indeed hope that calculations which are going to be adequate for more complicated systems certainly should reproduce those of the simple hydrides.

B. Basis set effects

The test of any approximate theory is how well it reproduces and helps to

TABLE 3

Representative isotropic shift calculations for second row hydrides using the data of Chesnut (C), Höller and Lischka (HL), and Lazzeretti and Zanasi (LZ).

	C[a]	HL[b]	LZ[b]	Experiment
NaH	580.9	566.3		
MgH_2	491.0	472.2		
AlH_3	376.0	352.8		
SiH_4	499.3	480.9	492.2	
PH_3	591.1	584.9	577.6	594[c]
H_2S	703.1	716.5	701.9	
HCl	940.0	947.6	983.9	950[c]
AlH_4^-	535.7			
PH_4^+	483.3			

[a]Optimized geometries.

[b]Experimental geometries.

[c]Based on σ_p from ref. 55 with σ_d averaged from the theoretical calculations of refs 62 and 63.

explain experimental observation. Studies which suggest additions or modifications to the theory which bring it more in line with experiment are obviously desirable. Such is the case with the effect of basis sets in the Hartree–Fock SCF calculation of the chemical shift. Hartree–Fock theory is an approximation; because one normally must deal with finite basis sets, we are then dealing with an approximation to an approximation. The theory can be made to work better, perhaps, by using appropriate basis sets. These basis sets, to be appropriate, may either need to bring us sufficiently close to the Hartree–Fock limit for the observable in question, or reproduce in a controllable way the experimental observation one is hoping to understand. Several readable and extensive reviews on this subject have appeared.[64,65]

While there have not been any exhaustive basis set studies of the chemical shift in the Hartree–Fock approach, enough comparisons have been carried out in recent years to afford us a good view of what types of basis sets are required in the various approaches taken to give reasonable agreement with experiment.

1. Basis set notation

In recent years the basis functions employed in nearly all quantum mechanical calculations in chemistry involve gaussian-type orbitals (GTOs) where instead of the $\exp(-r)$ type of exponential found in hydrogen-type orbitals (HTOs) one employs $\exp(-r^2)$ functions, which allow significantly easier integral determination. Single gaussian-type orbitals are referred to as primitive gaussians and are characterized by the exponential factor and the type of angular dependence they represent (s,p,d, . . .). One may also take linear combinations of these primitives with fixed coefficients to form what are called contracted gaussians. In general, a basis set will consist of a mixture of contracted and primitive gaussians. While generally it is necessary to consult the appropriate literature to determine the exact nature of the orbitals represented by the particular mix of gaussians, in recent years a fairly standard notation has arisen which allows one in a relatively concise way to convey the general nature of the gaussian basis set. A simple example best illustrates this notation. For example, for carbon a fairly common gaussian basis would be denoted as (6311/311/1) where the numbers in parentheses indicate the contraction of the gaussian orbitals for s,p,d, . . . functions, in that order. In this example, there are four s orbitals made up of one contraction of six gaussians, one contraction of three gaussians and two primitive gaussians; there are three p functions (actually three (x,y,z) sets of p functions) consisting of one contraction of three gaussians and two primitive gaussians; finally, there is a single set of d functions consisting of primitive gaussians. This basis could also be denoted as (11s5pd), which indicates the

total number of primitive gaussians which are involved in the various s, p, d, . . . contractions; this notation of course does not, by itself, show the particular contractions used nor the number of orbitals actually involved in the calculation. Finally, this particular basis might also be denoted as [4s,3p,d], which indicates the number of atomic orbitals involved; that is, four s-type orbitals, three sets of p-type orbitals, and one set of d-type orbitals. This latter notation also suffers in that it does not indicate the appropriate contraction of the gaussians involved. Usually one finds a mixture of these notations; we find it useful here to denote basis sets such as the one in this example by (6311/311/1) = [4s, 3p, d] which quickly allows one to determine both the number and types of orbitals involved as well as the particular contraction. Finally, beyond the p-type functions (i.e. for d, f, . . .) one should somehow note whether such functions represent the complete set of cartesian gaussians or the more restricted set of gaussians corresponding to the $2l+1$ spherical harmonics. That is, for the d functions one may employ the five gaussians corresponding to the set of spherical harmonics, or one may employ the six cartesian gaussians (x^2, y^2, z^2, xy, xz, yz) which actually contain the five second-order spherical harmonics plus an additional function of s-type symmetry. Similar arguments arise for the seven spherical harmonics for f-type functions as opposed to the ten third-order cartesian gaussians, and so on to higher angular momentum.

2. *Results of some basis set studies*

That the chemical shift was not going to be an easy thing to calculate was demonstrated quite early by the work of Lazzeretti and Zanasi[66] involving calculations of the magnetic shielding constants of heavy nuclei in some of the first row hydrides, illustrated in Table 4. The first two basis sets in that table are minimal basis sets, the first using atom-optimized orbitals, while the second involves some partial optimization of the orbital exponents for use in molecular calculations. The molecular optimization does make a difference but the results obtained are still poor. Use of a double-zeta set as illustrated in the third basis set of that table produces some improvement in the results, but leaves them still woefully short of the mark. Not until the last basis set involving multiple s and p functions and polarization functions on both the heavy (non-hydrogen) and hydrogen atoms does one achieve the type of agreement with experiment hoped for. The last basis set in the table requires twenty-six atomic orbitals on the non-hydrogen centres and six orbitals on each hydrogen. It is evident, then, that calculations not involving gauge factors require rather large basis sets for success.

Another example of the need for large basis sets with non-gauge calculations is illustrated in Table 5, taken from some of the early work of Höller

TABLE 4

Isotropic chemical shifts (ppm) for the heavy atom (X) and hydrogen (H) from ref. 66 for several simple hydrides.

		CH_4	NH_3	H_2O
X:	(55/5) = [2s,p][a]	159.0	124.7	111.1
H:	(5) = [s]			
X:	(55/5) = [2s,p][b]	156.5	175.7	221.5
H:	(5) = [2s]			
X:	(5211/32) = [4s,2p]	217.0	207.8	213.3
H:	(32) = [2s]			
X:	(6,5xl/3,4xl/2) = [6s,5p,d]	196.0	263.5	316.9
H:	(311/2) = [3s,p]			
	Experiment	195.1	264.5	344.0

[a]Exponents from atomic SCF calculations.
[b]Exponents partially optimized for the molecular calculation.

TABLE 5

Isotropic chemical shifts (ppm) for HCl for a variety of basis sets. The data are taken from ref. 62.

	σ_{Cl}	σ_H
Cl: [8s,6p,3d]	923.7	29.33
H: [4s,2p]		
Cl: [9s,6p,3d]	923.8	29.31
H: [4s,2p]		
Cl: [9s,6p,3d] + [s,p][a]	939.0	28.89
H: [4s,2p]		
Cl: [9s,6p,3d][b] + [s,p]	948.7	29.26
H: [4s,2p]		
Cl: [9s,6p,4d] + [s,p]	947.5	29.23
H: [4s,2p]		
Cl: 9s,6p,5d] + [s,p]	947.3	29.23
H: [4s,2p]		
Experiment	950.0[c]	32[d]

[a]Diffuse s,p functions added.
[b]d set more diffuse here (smaller exponents).
[c]See footnote *c* in Table 3.
[d]See refs 55 and 67.

and Lischka,[62] who carried out some of the first very extensive chemical shift calculations. Höller and Lischka carried out calculations on both the first and second row hydrides[27,62] as well as on the additional standard hydrocarbons ethane, ethylene and acetylene.[27] Table 5 shows the results for six different basis sets in the calculation of HCl.[62] A perusal of the table shows that the addition of a diffuse set of s and p orbitals (the third basis set) is evidently quite important; as one compares the results of the third and fourth basis sets in that table it is also clear that the nature of the d exponents has a noticeable effect on the calculated results. Making the d functions more diffuse as in the fourth basis set can be mimicked by using the d functions used in basis set three plus an additional d function as shown in the fifth basis set. The addition of a fifth set of d functions has virtually no effect on the calculations. Accordingly, then, basis set five is representative of the type of set necessary for such a simple second row molecule as HCl where fifty-one atomic orbitals are required for chlorine and ten for hydrogen. Second row molecules are going to require more basis functions than those of the first row, but Höller and Lischka's papers show that large sets are needed even for first row molecules. For example, to achieve a reasonable convergence for HF it is necessary to have [7s,5p,2d] plus a diffuse set [s,p] on fluorine and [4s,2p] on hydrogen, representing thirty-six atomic orbitals for fluorine and, again, ten for hydrogen. The problem is two-fold in that one will require large basis sets to minimize any lack of origin gauge dependence in such calculations and to obtain chemical shift results which are sufficiently close to experiment to allow a significant interpretation of the corresponding wave functions.

We have mentioned earlier the IGLO method of Kutzelnigg and Schindler[19-22] and the GIAO approach of Ditchfield,[18] two theories which involve the explicit use of gauge factors. Table 6 shows the calculated shifts for the standard set of simple hydrocarbons for three bases in the IGLO approach.[21] The first basis is essentially a double-zeta basis, the second involves a triply split valence set plus polarization on carbon and hydrogen polarization functions as well, and the third set extends the second by using four p functions on carbon. The data are analysed on the right-hand side of the table in terms of the root-mean-square error (rmse) between calculated and observed shifts and the SD, which is the standard deviation of the errors; SD gives a measure of the goodness of the calculation on a *relative* basis. In terms of the absolute shifts neither the double-zeta nor the triply split valence calculation is sufficient, whereas extremely good results are obtained for the third basis set which involves twenty-two atomic orbitals on carbon and six on each hydrogen. Both in terms of the rmse and SD, so far as the proton shift is concerned the second basis set having polarization function on hydrogen along with three s functions is satisfactory. For carbon on a relative basis (as

TABLE 6

Isotropic chemical shifts (ppm) for carbon (C) and hydrogen (H) for a standard set of hydrocarbons in the IGLO approach. The data are from ref. 21.

		CH_4	C_2H_6	C_2H_2	C_2H_4	rmse	SD
C:	(4111/21) = [4s,2p]	212.3	206.6	130.3	82.7	19.1	4.6
H:	(21) = [2s]	32.55	32.47	28.56	26.43	1.74	1.25
C:	(5,4xl/311/1) = [5s,3p,d]	209.2	197.3	127.0	75.0	13.0	2.7
H:	(311/1) = [3s,p]	31.14	30.55	29.04	25.88	0.50	0.35
C:	(5,4xl/2111/1) = [5s,4p,d]	196.7	183.5	117.4	61.6	2.1	2.1
H:	(311/1) = [3s,p]	31.06	30.48	29.02	25.83	0.45	0.33
	Experiment C:	195.1	180.9	117.2	64.5		
	H:	30.61	29.86	29.27	25.43		

TABLE 7

Differences between calculated and observed carbon chemical shifts ($\sigma_{calc} - \sigma_{obs}$, in ppm) for a number of small molecules and a variety of basis sets of increasing complexity. The data are taken from refs 26 and 68.

	[3s,2p]		[3s,2p,d]		[4s,3p,d]	
	(321/21)[a]	(431/31)	(321/21/1)[a]	(431/31/1)	(4211/211/1)	(6311/311/1)
CH_4	15.5	6.9	6.7	2.2	2.1	−2.1
CH_3CH_3	23.7	12.1	14.2	6.7	4.6	0.3
CH_3NH_2	27.1	16.8	18.0	10.7	9.1	4.2
CH_3OH	32.5	20.7	23.8	13.1	12.1	8.5
$HC{\equiv}CH$	24.4	13.0	23.1	12.4	7.7	1.1
CH_3F	36.8	23.2	28.2	16.9	17.3	11.3
HCN	17.9	0.7	23.2	5.4	1.0	−7.3
$H_2C{=}CH_2$	27.2	8.3	24.8	8.1	5.4	−2.3
$\bar{x}$	25.6	12.7	20.3	9.4	7.4	1.7
SD	6.6	7.0	6.5	4.4	5.1	5.7
$(\bar{x}^2)^{1/2}$	26.5	14.5	21.3	10.4	9.0	5.9

[a]Ref. 68.

measured by SD) all the calculations on this very small molecular subset are quite good. Comparing the third basis of Schindler and Kutzelnigg with the hydrogen fluoride calculations by Höller and Lischka,[27] we see that inclusion of specific gauge terms has reduced the size of the basis set required.

By combining work on carbon carried out by Rohlfing and co-workers[68] with some of our own[26] we show in Table 7 some of the more extensive comparisons of bases in the GIAO approach using a variety of the basis sets

developed by Pople and co-workers.[69] In this table are listed the *differences* between calculated and observed shifts along with the mean difference $\bar{x}$, the standard deviation SD, and the factor representing the rmse between calculated and observed chemical shifts. These latter two factors can be compared directly with those given in Table 6, which illustrates the data of Schindler and Kutzelnigg in their IGLO approach.[21] The first two columns of values contrast the so-called 3-21G and 4-31G bases,[70] columns three and four the same bases with a single set of six d polarization functions included on the heavy atoms, while the fifth and sixth columns of values compare the relaxed 4-31G(d) basis with the 6-311G(d) approach. It should be noted that in all of these calculations the hydrogen basis was maintained at the small (31) = [2s] level. The grouping of data in the table allows us to evaluate the effectiveness of bases with the same number of atomic orbitals but made up of different numbers of contracted gaussians, as well as the effect of polarization functions and the necessity of having at least a triply split valence set. An inspection of the first two columns of values shows that the 4-31G basis is significantly superior to the 3-21G set. The addition of six d polarization functions helps both bases, but in terms of these two the 4-31G(d) is to be preferred. If one goes from a double to a triple valence split (columns four and five) further improvement is seen, indicating the need to have at least a triply split valence basis in order to achieve good results. Finally, the comparison of the last two columns at the [4s,3p,d] level shows that the energy-optimized basis (the 6-311G(d)) is the basis of choice among those considered. The GIAO approach succeeds with fewer basis functions than those approaches which use no explicit gauge factors, and may be slightly more efficient in this regard than the IGLO method of Kutzelnigg.[19]

Comparing the gaugeless bases of Höller and Lischka[27,62] with those required by the IGLO method[19-22] and with those needed in the GIAO approach,[26] we find that, respectively, [7s,5p,d], [5s,4p,d], [4s,3p,d] bases are needed for the first row heavy atoms along with [5s,p], [3s,p], [2s] hydrogen bases. In these three approaches for the methane molecule fifty-nine, forty-six, and twenty-seven atomic orbitals are required. It seems clear that polarization functions will be required to describe adequately the chemical shielding of hydrogen, although the success of the GIAO approach for non-hydrogen atoms using the very simple [2s] basis indicates that a very simple hydrogen basis may suffice for the calculation of screening on the *heavy* nuclei.

One must not be misled, however, with the apparent success of these various calculations on carbon and, to some extent, hydrogen. The results for nuclei such as nitrogen, oxygen and fluorine in the first row are not as encouraging, and molecules of the second row, while not so extensively studied, can be expected to pose more difficult problems. In some of our

work which established the (6311/311/1) = [4s,3p,d] heavy atom, (31) = [2s] basis as being a generally good one for first row molecules, we investigated briefly the effects of going beyond this particular basis.[26] It was found that the addition of a second set of six d polarization functions had little effect on these first row molecules, and that for carbon as the resonant nucleus the addition of a set of diffuse s,p functions also had little effect. The effect of the addition of diffuse s,p functions on nuclei such as nitrogen, oxygen and fluorine was more noticeable. Atoms with lone pair electrons seem to be more sensitive to the basis set employed, and we concluded in this work that if additional extensions to our primary basis were to be made, the addition to the diffuse s,p functions would be the extension of choice.

While a single set of d polarization functions seems to be adequate in the GIAO approach for molecules containing first row atoms, this appears not to be the case for molecules involving second row atoms. Carrying out shift calculations for PH_3 as a prototype molecule of the second row, a triple valence split with two sets of (six) d polarization functions, (66211/6211/11) = [5s,4p,2d], appears to be adequate.[71] In this study a variety of bases was employed with the results, to be discussed, indicated in Fig. 1. The hydrogen basis was maintained at the (31) = [2s] level as before with the phosphorus basis sets being derived from the 6-31G(d) basis sets due to Francl *et al.*[72] along with the diffuse s and p functions of Clark and co-workers.[73] All scale factors were set equal to unity. The Pople standard basis without polarization or diffuse functions in its (6631/631) = [4s,3p] form was progressively increased in size by relaxing the three-fold contraction in the valence shell to 2,1 and 1,1,1 forms. The progressive relaxation of this particular shell was done by freeing up initially that primitive with the lowest exponent while retaining the two-fold contraction made up of those primitives with the two highest exponents, and finally freeing all of the primitives in the original three-fold contraction. Diffuse s,p functions were considered as well as multiple d polarization functions; the multiple d polarization functions were created from the original primitives by multiplying and dividing the original exponent by two as suggested by Frisch *et al.*[74] so that the d-exponent ratios were always equal to 4.

The results of this investigation for phosphine in both its pyramidal C_{3v} and planar D_{3h} forms are shown in Fig. 1. The notation in Fig. 1 indicates the inner core contractions of six gaussians for the first and second inner shells, with the figures after the dash indicating the s,p contractions in the valence shells. Data are plotted as a function of the number, n_d, of sets of six d polarization functions. The basic contractions are indicated beside each line of data and correspond to the solid circle data; open circle data have one additional diffuse s,p set of functions.

A variety of conclusions can be reached from these data. First of all, the

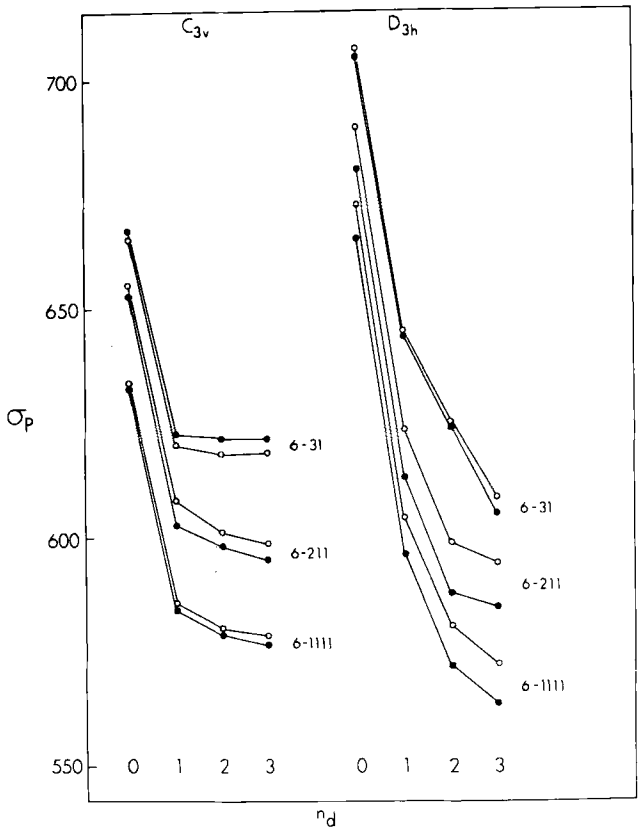

FIG. 1. Variation of the isotropic chemical shift in PH_3 as a function of basis set for both pyramidal and planar structures. The basic sp contractions are indicated beside each line of data and correspond to the solid circle data; open circle data have one additional sp-diffuse set of functions. The number of sets of d polarization functions, n_d, is indicated below the appropriate points. The PH bond length was kept constant at its experimental value in these particular studies, taken from ref. 71.

data clearly show that the addition of the diffuse s,p functions has a relatively minor effect on the chemical shift. Changing the valence split (from (6-31G) to (6-211G) to (6-111G)) has a large effect, and within each type of split valence set the effect of the addition of d orbitals is quite noticeable. The addition of the first set of d functions has a very great effect in all cases, while the effect of the addition of a second set is smaller but still significant; the addition of a third set of d polarization functions causes relatively minor changes, of the order of a few ppm, and in all likelihood does not present any

great gain in the calculation of the shift, especially in view of the increased size of the basis set required.

Although the effect of added d functions seems to indicate a kind of convergence in the shift calculation, such is not the case with the general relaxation of the s,p valence functions. We suggested in our work that a good compromise was to go with the triple valence split for second row molecules. Until calculations can be carried out on larger systems, the question of whether or not it is necessary to go beyond this type of valence split must remain unanswered.

Because we have an interest in the effects of geometry on the calculated chemical shift, data were also obtained for phosphine in its planar form and are also contained in Fig. 1. Generalizations in this case regarding the need of various functions are not as clear as for the pyramidal structure. The effect of the addition of diffuse s,p functions is more important for the planar molecule.

IV. EFFECTS OF GEOMETRY

In the Born–Openheimer approximation the electronic properties of molecules are determined for a rigid nuclear framework, most often a 0 K structure in its equilibrium configuration. Experimental measurements, however, are carried out at finite temperatures, for NMR typically 300 K. While calculations generally are on an isolated molecule, experimental measurements, even in the gas phase, must be carried out at finite densities; data can often be extrapolated to the limit of zero density, removing intermolecular effects. As Jameson and Osten[75] point out, the pressure in a system must be high enough so that collisional interactions allow a molecule to sample representative numbers of the accessible vibrational and rotational states on the NMR timescale.

The effect of rotational–vibrational corrections to the equilibrium-structure calculation can be sizeable. Jameson and Osten report corrections for fluorine at 300 K of -9.5 to -18.0 ppm in some haloethanes,[76] and -6.8 to -16.4 in some halomethanes.[77] Ditchfield[78] calculates a -11.2 ppm correction for fluorine in HF at 300 K, while Fowler and Raynes[79] report a -13.1 ppm zero point correction for oxygen in H_2O. Corrections for carbon species seem not to be so large. Jameson and Jameson[2] in their recent extensive gas phase studies on carbon chemical shifts estimate corrections at 300 K of -1.5 ppm in CO_2 to -3.4 ppm in CH_4, fairly representative for this type of nucleus. As they point out, the degree of success of current chemical shift calculations is approaching the point where such rotation–vibration corrections are becoming significant in comparing theory and experiment.

Calculated values of electronic properties obviously depend on the bond lengths and angles of the molecular structure involved. Because of anharmonic terms in the internuclear potential, different vibrational states will have different values for the expectation value of the bond extension; as the temperature is changed, the thermal average over the vibrational states changes, and so, too, will the bond extension. Owing to centrifugal stretching, as a molecule rotates its bonds tend to increase in length. These effects give rise to changes in the structure of the molecule with temperature and, accordingly, changes in the calculated and observed chemical shift. The well-known isotope effect[75] in nuclear magnetic resonance occurs because the vibrational and rotational effects on geometry depend on the masses of the species involved; for example, the shift of carbon in a CH bond will change when the hydrogen is replaced by deuterium. The effects of temperature or isotopic substitution on a particular shift is then greatly dependent on a knowledge of the chemical shift surface as a function of geometry for a particular species, as well as on a knowledge of the vibrational and rotational energy surfaces. The energy surface is dependent upon the particular structure involved and, accordingly, it is important to know how the chemical shift changes with bond angle deformations or bond length modifications. In fact, with suitable models, experimental observation of isotope effects or temperature effects can be used to determine the derivative of the chemical shift with respect to these structural modifications. In their review article Jameson and Osten[75] give an extensive tabulation of such experimentally determined derivatives compared to theoretical calculations.

A. Temperature effects in H_2, HF and LiH

As a first example of the effects of geometry on nuclear shielding, we discuss the calculations of Ditchfield[78] on the temperature dependence of shielding in several small diatomic molecules. The purpose of Ditchfield's work was to determine the difference between chemical shielding at the equilibrium 0 K structure compared with that at experimental temperatures (300 K), to determine the various shielding derivatives as a function of bond extension in order to assess the effect of higher order derivatives, and to study the lithium and fluorine hydrides, two cases where apparently opposite temperature dependences of the chemical shielding occur. The situation is relatively simple for diatomic molecules since both shielding and potential energy surfaces are one-dimensional. Thus, for example, the shielding constant σ is expanded in a power series in the reduced coordinate ξ

$$\sigma(\xi) = \sigma_e + \sigma_e'\xi + \tfrac{1}{2}\sigma_e''\xi^2 + \ldots \tag{36}$$

where σ_e is the shielding constant for the equilibrium structure defined by the equilibrium bond length R_e and where ξ and the σ derivatives are defined as:

$$\left.\begin{aligned} \xi &= \frac{R - R_e}{R_e} \\ \sigma_e' &= \left(\frac{d\sigma}{d\xi}\right)_e \\ \sigma_e'' &= \left(\frac{d^2\sigma}{d\xi^2}\right)_e \end{aligned}\right\} \quad (37)$$

For a particular vibration–rotation state specified by the quantum numbers v and J one will have

$$\sigma_{vJ} = \sigma_e + \sigma_e'\langle\xi\rangle_{vJ} + \tfrac{1}{2}\sigma_e''\langle\xi^2\rangle_{vJ} + \ldots \quad (38)$$

where the expectation values of the reduced coordinate are taken over the appropriate vibration–rotation wave function. By applying Boltzmann weighting to such contributions one can at last write down an expression for the chemical shielding at temperature T as

$$\sigma_0(T) = \sigma_e + \sigma_e'\langle\xi\rangle_T + \tfrac{1}{2}\sigma_e''\langle\xi^2\rangle_T + \ldots \quad (39)$$

where the subscripts T on the expectation values show that the appropriate thermal averagings have been carried out. Assuming that the potential energy surface, and therefore the vibration–rotation states, can be ascertained, one must then determine the value of σ_e and its various derivatives (to whatever order is necessary) in order to complete the calculation.

Ditchfield assumed a Dunham potential[80] of the form

$$V(R) = a_0\xi^2(1 + a_1\xi + a_2\xi^2 + \ldots) \quad (40)$$

Dunham has solved the vibrational–rotational problem for this potential using the WKB method in terms of the a_i coefficients. Fitting experimental observations to the Dunham solutions allows one to determine these coefficients for any particular case, and from these and Dunham's solutions the expectation values $\langle\xi\rangle_{vJ}$. By calculating theoretically the chemical shielding and its various derivatives at the molecule's equilibrium configuration, Ditchfield was then able to determine the temperature dependence of the shielding for the various nuclei.

Ditchfield carried out his calculations using his GIAO formalism[18] and the Pople 6-31G** basis[69] (in our standard notation, (631/31/1) = [3s,2p,d] for the heavy atoms, (31/1) = [2s,p] for hydrogen), a basis with polarization functions on both the heavy atoms (a set of six d functions) and hydrogen (one set of three p functions). Geometries were varied over a small region near the equilibrium bond distance in order to fit the chemical shift to an

equation of the type given in equation (36) above. Although Ditchfield carried out some of his calculations with derivatives as high as the sixth order in the expansion, he found that the major results could be obtained by retaining derivatives only up to the second order. The results of some of these calculations are given in Table 8 for the equilibrium geometry (σ_e), for the chemical shift averaged over the ground rotation-vibration state (σ_{00}), and for the fully thermally averaged chemical shift at 300 K ($\sigma_0(300)$).

We may note the following observations based on the data in Table 8. First, the differences between $\sigma_0(300)$ and σ_{00} are relatively small, indicating a weak temperature dependence of the predicted chemical shifts. Indeed, the chemical shift as a function of temperature is virtually linear in all cases; for HF Ditchfield quotes a temperature coefficient for F of -1.56×10^{-3} ppm K^{-1}. The second point, and the important one here, is that when the chemical shift either averaged simply over the ground vibration-rotation state or completely thermally averaged is compared with that obtained in the rigid equilibrium structure without any vibration or rotational effects, the difference is quite noticeable, except for the case of lithium hydride. For HF the difference in the fluorine chemical shift is approximately 11 ppm, while that for hydrogen is 0.35, both figures significant in terms of the chemical shift ranges of the two nuclei. Similarly large differences show up in the shift anisotropies as seen in the second part of the Table 8, the differences there being larger than those observed for the isotropic shift. Evidently rotation and vibration can lead to significant corrections to the shift calculated for a nucleus in a rigid nuclear environment.

Both H_2 and HF show a decrease in the chemical shift with increasing temperature, while LiH is predicted to have a weakly positive temperature coefficient. As we discuss later, the situation for Li in lithium hydride

TABLE 8

Chemicals shifts, σ, and shift anisotropies, $\Delta\sigma$, in ppm calculated for H_2, HF, and LiH in their rigid equilibrium structures (σ_e), averaged over the $v = 0$, $J = 0$ vibration-rotation state (σ_{00}), and the fully thermally averaged state at 300 K ($\sigma(300)$). σ_e values are the optimal fits of $\sigma(\xi)$ to ξ; the σ_{00} and $\sigma(300)$ data shown were obtained from fitting $\sigma(\xi)$ up through quadratic terms. The data are taken from ref. 78.

Molecule	Nucleus	σ_e	$\Delta\sigma_e$	σ_{00}	$\Delta\sigma_{00}$	$\sigma_0(300)$	$\Delta\sigma_0(300)$
H_2	H	26.58	1.68	26.25	1.63	26.21	1.63
HF	H	28.88	23.01	28.54	22.36	28.51	22.31
	F	424.69	86.14	414.03	102.12	413.58	102.78
LiH	H	26.34	3.04	26.23	3.01	26.21	2.98
	Li	93.15	12.68	93.21	12.50	93.23	12.44

appears to be typical of hydrides in the left-hand portion of the periodic table in terms of their shift derivatives being positive, while the behaviour of F in hydrogen fluoride is representative of those in the right-hand portion of the periodic table whose shift derivatives are generally negative.

Ditchfield also carried out calculations for the deuteriated forms of the diatomics and found that the variations of the shielding tensor as a function of temperature basically paralleled those for the undeuterated or normal hydride forms. For example, in HF at 300 K the chemical shift is increased by 3.07 ppm when hydrogen is replaced by deuterium, in good agreement with the experimental value for the isotope shift of 2.5 ± 0.5 ppm reported by Hindermann and Cornwell.[44] Ditchfield's results for shieldings and shielding anisotropies are generally in good agreement with experiment.

Jameson and Osten[75] have reanalysed Ditchfield's data retaining only the leading terms in the potential energy of the diatomic, which is regarded as behaving like a perturbed harmonic oscillator in three dimensions. Owing to their simplified treatment they were able to derive explicit formulae for the various contributions. They can thus divide the contribution to the various bond stretching terms in terms of vibrational and rotational corrections, and can furthermore break down the vibrational contribution into that arising purely from the unperturbed oscillator (referred to as "harmonic vibrational contributions"), the contribution from the anharmonicity involved (the a_1 term in equation (40)), and that due purely to effects of rotation. Their table of data shows that the anharmonic vibration contribution is the largest in determining the difference between σ and σ_e or $\sigma(300)$, and the rotational contribution generally the smallest. On the other hand, they find that the temperature dependence of the shielding depends almost entirely on the rotational term, which is basically linear with respect to temperature; their calculations show that vibrational effects account for less than 2% of the total change. Since the rotational contribution dominates the linear term in equation (39), empirical fits of the temperature dependence of σ and the linear nature of the rotational contribution allow one to determine experimentally a measure of the first derivative of the chemical shift with respect to bond extension.

B. Bond length modifications

While the various rotation–vibration states in diatomic molecules are relatively easily determined, such is not the case for more complex molecules. Even so, it is possible to determine the effects of bond modification or angle changes in small molecules to obtain a general idea of how these geometry modifications affect the chemical shift. There is relatively little documentation of bond angle effects on chemical shifts.[71] In this section we discuss

chemical shift derivatives as a function of bond modification and take as examples some of our own work[26] on some small first row atom molecules and the first and second row hydrides. For heavy atoms of the first long row of the periodic table the 6-311G* basis[69] ((6311/311/1) = [4s, 3p, d]) was used with a (31) = [2s] set for hydrogen based on the 4-31G basis.[69] The smaller hydrogen basis (with no polarization functions) was employed for efficiency since the heavy atom chemical shifts seem to be relatively insensitive to the hydrogen basis set employed with a [2s] representation for hydrogen being adequate. For second row heavy atoms the 6-31G* basis[69] was used in the partially relaxed form (66211/6211/11) = [5s, 4p, 2d]. All scale factors, including those of hydrogen, were set equal to unity. The multiple d polarization functions for second row atoms were created from the original primitives by multiplying and dividing the original exponents by two as suggested by Frisch *et al.*[74] so that the d exponent ratios were always equal to four. Optimized geometries were employed for the first and second row hydrides while experimental geometries were used in all other cases. Estimates of the first and second derivatives of the chemical shift were determined by lengthening and shortening appropriate bonds by 0.01 Å from their equilibrium length.

1. Modifications of bonds between heavy atoms

Table 9 contains both the calculated isotropic shift, σ, and the calculated first derivative of the shift, σ', for a variety of small molecules involving carbon, nitrogen, oxygen, and fluorine resonant atoms. Experimental determinations of the shift derivative are also indicated and compare favourably with the calculated results. In the table there is also included the shift derivative reported by Wasylishen[40] for CN^- in a 0.2 M solution of KCN, and compared to that calculated for CN^- with a presumed bond length of 1.1791 Å. The theoretical bond length employed was determined by optimizing the geometry at the 6-311G* level and then correcting (lengthening) by the observed versus optimized CN bond length in HCN.

Keeping in mind that the resonant nuclei involved in this example are in the right-hand portion of the first row of the periodic table (*vide infra*), we note that for all the molecules illustrated the first derivative term is negative. Although not indicated in Table 9, the second derivative terms were found to be negative in all cases except ethane, and of comparable order of magnitude to the first derivative term. Since the first and second derivative terms seem to be generally negative, and since one would only expect increases in bond distances with increasing temperature, one may conclude that for those cases dominated by bond length changes the change in the chemical shift with increase in temperature generally will be negative. That such is indeed the

TABLE 9

Calculated first derivatives, σ' (ppmÅ^{-1}), of the (calculated) isotropic chemical shift, σ (ppm), for heavy atoms with modification of the bond between heavy atoms. Literature references are given in parentheses. The theoretical results are taken from ref. 26.

	σ	σ'	Experiment σ'
C: C_2H_6	181.2	−6.3	
CH_3F	128.1	−91.6	
C_2H_2	118.3	−103.2	
HCN	74.8	−263.0	
C_2H_4	62.2	−187.7	
H_2CO	2.6	−406.6	
CN^-	2.0	−538.7	−473 ± 90(40)
CO	−21.3	−573.9	−456 ± 15(81)
N: HCN	−46.9	−625.4	
CN^-	−73.3	−892.2	−872 ± 160(40)
N_2	−109.4	−1132.5	−774 ± 110(82), −910 ± 42(83)
O: CO	−88.0	−1166.3	−1150 ± 130(81)
H_2CO	−459.4	−1726.5	
F: CH_3F	484.5	−131.4	−338(84)
F_2	−181.4	−2782.0	−4530(85)

case for molecules of the type illustrated in Table 9 is seen in the data tabulated by Jameson *et al.*[43] for changes in chemical shifts in going from 300 to 350 K in a variety of molecules. With the exception of NH_3 and PH_3, all the changes are negative for the fluorine, carbon, hydrogen, and phosphorus examples fited.

The data in Table 9 also indicate that the magnitude of the first derivative of the chemical shift is related to the chemical shift itself. That is, the shift derivatives tend to become more negative as the chemical shielding decreases (less positive σ); the data for C—C bond changes are shown in Fig. 2. A prediction of this type was made by Jameson[86] early on based on experimental work concerning the temperature dependence of the chemical shift for fluorine in some fluoromethanes as well as for carbon in some carbonyl compounds. Further work by Jameson and Osten[87] used temperature dependences and force field estimates of bond extensions to calculate shift derivatives in some halomethanes and the series of compounds represented by $CH_{3-n}F_n$.[88] These results, all for fluorine, show the same general trend as that given in Table 9. Their data are not linear and show a slight negative curvature when the shift derivative is plotted as a function of the chemical shift, as do the carbon data shown in Fig. 2.

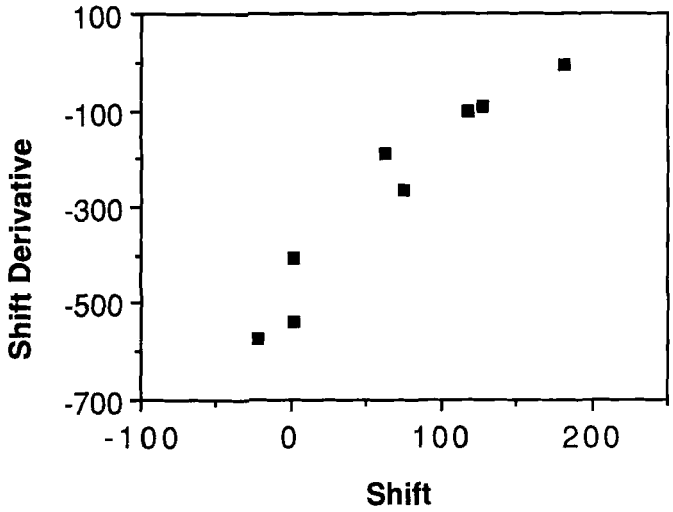

FIG. 2. Calculated chemical shift derivatives as a function of the calculated shift for carbon-carbon bond modifications. The data are included in Table 9 and are taken from ref. 26.

The theoretical calculations of Chesnut and Foley show that in the case of heavy atom bond modification the change in the paramagnetic term dominates, being greater than 90–95% in virtually all examples. Ethane is somewhat unusual in that the value of the paramagnetic contribution of the equilibrium geometry appears to be a minimum as a function of the C—C bond length. This is undoubtedly why the shift derivative for this bond in that molecule is so small.

2. *Effects of heavy atom–hydrogen bond modifications*

The shift derivative for a heavy atom upon modification of an attached hydrogen bond is not quite as straightforward as the results found in the previous section. While the shift derivative of the heavy atom tends to be negative for such cases as methane, ethane, ethylene, acetylene, and fluoromethane, the carbon shifts in HCN and H_2CO are positive. Furthermore, the effect on a heavy atom two bonds removed from hydrogen involved in the modified bond can have either sign, and is of comparable magnitude to that of the primary heavy atom.

In Table 10 are given the calculated chemical shifts and shift derivatives for hydrogen for the various primary, secondary, and tertiary hydrogens involved when a specific carbon—hydrogen bond is modified. In general, the

TABLE 10

Calculated hydrogen chemical shifts, σ, and first derivatives, σ', due to C–H^1 and CX (X = C, N, O, F) bond modifications. Shifts are in ppm and distances are measured in Å units.

			CH bond		CX bond
		σ	σ'	σ'(exp)	σ'
	H^1	31.85	−25.47	−38 ± 3[a]	—
	H^2		−2.60	−1.3 ± 0.2[a]	
	H^1	31.14	−23.37		0.32
	H^2		−3.09		
	H^3		−0.83		
	H^1	26.74	−15.66		−9.07
	H^2		−1.47		
	H^3		0.45		
	H^4		−0.26		
$H^2-C=C-H^1$	H^1	30.89	−33.40		−5.50
	H^2		−0.25		
$H-C\equiv N$	H	29.74	−35.02		−4.79
	H^1	28.27	−20.00		−2.86
	H^2		−2.38		
	H^1	23.08	−11.48		−11.25
	H^2		−0.52		

[a]Ref. 89.

derivatives of the chemical shift for primary hydrogens (those involved in the bond modified) are comparable in magnitude to those for the corresponding heavy atom. Effects on hydrogens one bond removed are generally lower by an order of magnitude, and effects on those still further away are quite small. The signs of the first derivative terms are all negative and, as before, it is found that the second derivative terms (not shown) are comparable in magnitude to the first derivative ones. The last column in Table 10 shows that the indirect effect on the hydrogen shift derivative of modifying the heavy atom bond (CX) is generally smaller than the direct effect due to a primary bond modification, but is generally larger than indirect effects due to an XH bond modification.

3. *Effects of choice of equilibrium geometry*

The magnitudes of the calculated (and observed) shift derivatives show that the chemical shift may vary significantly depending upon the choice of molecular geometry, particularly for multiply bonded atoms. What difference does it make whether one uses experimental geometries or those geometries optimized by the Hartree–Fock SCF method? For the molecules in Tables 9 and 10, geometry optimizations were carried out and the chemical shifts recalculated for the optimized geometries. Generally, bonds involving both heavy atoms and hydrogen atoms were shortened by anywhere from 0.01 to 0.03 Å. With the exception of F_2 the shortenings were remarkably uniform; F_2, a pathological case, showed a shortening of 0.089 Å relative to the experimental value. Because the bonds are generally shortened in the optimized geometries, an increase in the chemical shift is predicted. In most incidences it was found that this increase was only a few ppm, but for those situations where nuclei show a large shift derivative the effect is not at all small. For example, the carbon and oxygen atoms in carbon monoxide showed increases in the chemical shift of 13.3 and 26.7 ppm, respectively, in changing from experimental to optimized geometry; the carbon and nitrogen atoms in HCN showed changes of 6.5 and 15.7 ppm, respectively, while the carbon and oxygen atoms in formaldehyde changed by 10.4 and 46.0 ppm, respectively. F_2, with its very large change in bond length, showed an increase in its chemical shift of 147.7 ppm! The chemical shift, then, is quite sensitive to choice of geometry in general and is clearly so for multiply bonded species. The typical shift change with the change in bond length of 0.01 Å may, in many cases, be comparable to the error between the calculated and experimental shift itself.

4. *The first and second row hydrides*

While the previous bond modification's shift derivatives were found to be negative in general, Ditchfield's calculations on LiH[78] indicated that the derivative there was small and positive. Ditchfield's calculations on LiH and HF, two extremes in terms of electronegative hydrides, prompted an investigation of all the hydrides of the first and second long rows of the periodic table.[61] The behaviour for lithium hydride, previously thought to be "anomalous", was shown to be part of a general trend in the shift derivative as one passes across the appropriate row of the periodic table. Table 11 illustrates the calculations of the shift and shift derivative and compares the latter with available experimental data. For the hydride studies optimized geometries were employed using the same basis set as was used for the chemical shift calculation itself. Although experimental

TABLE 11

Calculated and observed heavy atom isotropic shifts, σ (ppm), and shift derivatives, σ' (ppm Å^{-1}), for bond length modification for first and second row hydrides and several hydride ions. Literature references are given in parentheses. The calculations are taken mainly from ref. 61.

	σ		σ'	
	Calc.	Obs.	Calc.	Obs.
LiH	90.1	—	8.8	—
BeH_2	88.3	—	16.4	—
BH_3	36.5	—	3.5	—
CH_4	192.9	197.4(32)	−51.1	−35 ± 3(89)
NH_3	266.4	264.5(36)	−130.3	−124(90)
H_2O	335.9	344 (41)	−267.1	−296(90), −294(91)
HF	414.5	410 (44)	−436.6	—
BH_4^-	154.1	—	−27.0	−26.7(92)
NH_4^+	238.5	223.8(38)	−67.9	−60(90), −65(92)
H_3O^+	306.6[a]	—	−117.3[a]	−60(90)
NaH	580.9	—	49.4	—
MgH_2	491.0	—	107.3	—
AlH_3	376.0	—	84.2	—
SiH_4	499.3	—	−17.4	—
PH_3	591.1	594[b]	−150.8	−180 ± 20(93)
H_2S	703.1	—	−431.8	—
HCl	940.1	950[b]	−704.8	—
AlH_4^-	535.7	—	11.6	—
PH_4^+	483.3	—	−52.9	0 ± 10(93)
PH_2^-	631.1[a]	—	−456.3[a]	−585 ± 65(93)

[a] D. B. Chesnut, unpublished results.

[b] Based on σ_{para} from experimental work (ref. 55) and σ_{dia} averaged from the theoretical calculation of refs 62 and 63.

geometries could have been employed, it was felt more appropriate in this instance to use the optimized geometries for all the molecules under study for a variety of reasons. Some of the Be, B, Mg, Al hydrides are not known in their monomeric form, although BH_4^- and AlH_4^- ions exist. The question of experimental versus optimized geometries here is really a moot one since the optimized structures were found to agree very well with those known experimentally; for example, the average absolute deviation in the bond lengths was 0.009 Å, and angles were good to one degree.

The variation of the shift derivative with position in the row of the periodic table can readily be seen in Table 11 and, for the neutral hydrides, is also

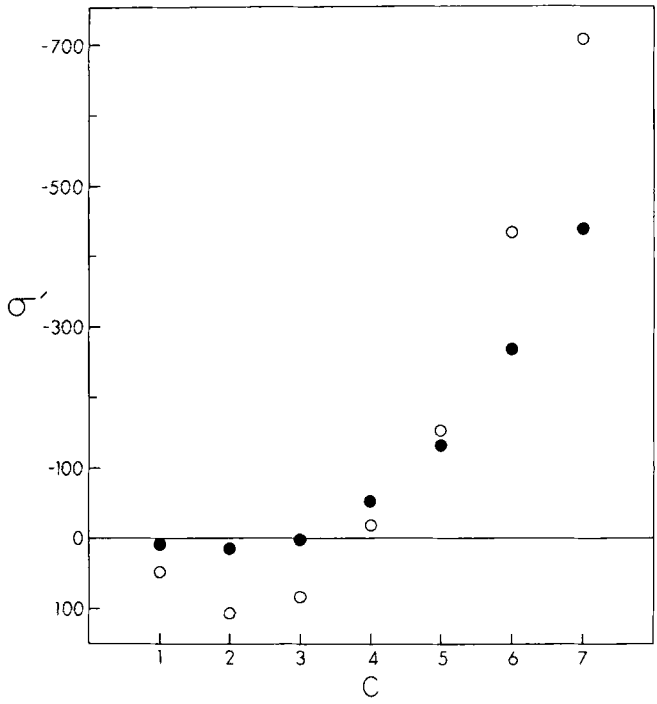

FIG. 3. Variation of the bond length derivative of the chemical shift, j′ (ppm Å^{-1}), with column, C, of the periodic table of the heavy atom for the first row (closed circles) and second row (open circles) hydrides. The data are taken from ref. 61.

shown graphically in Fig. 3. The chemical shifts calculated for the heavy atoms are in good agreement with those determined by others and are in reasonably good agreement with experiment. Recall again that these are rigid structures at their presumed equilibrium geometries with no rotational-vibrational corrections applied.

Figure 3 shows the key result of this work. For both first and second row hydrides the shift derivative is positive and small at the low end of the periodic row, and is large and negative at the high end of the row in which the heavy atom is located. Ditchfield[78] has provided an explanation in some detail for the cases of HF and LiH. In the case of HF the major interaction involves the occupied π states interacting with the σ^* anti-bonding state. Since hydrogen fluoride is polarized toward fluorine in its bonding molecular orbitals, the σ^* anti-bonding orbital is polarized in the opposite way. Furthermore, when hydrogen fluoride is stretched this polarization is enhanced, thus allowing a greater use of the inner p-type orbitals which, due to the r^{-3}

dependence in the paramagnetic term, leads to a larger and more negative paramagnetic contribution to the shift. Ditchfield points out that a different situation obtains for lithium hydride. There the chief interaction is between the occupied σ bonding orbital and the vacant π states of the system. Lithium hydride is polarized in the form Li^+H^- and, as with HF, this polarization is enhanced as the internuclear separation is increased. The effect of this polarization enhancement in the σ bonding orbital decreases the extent of p character involved, thus giving rise to a positive change in the paramagnetic contribution. Although in both cases there are changes in the energy gap between the coupled orbitals, it is apparently the polarization effects which dominate. Thus, in these two extreme examples it is the relative polarity of the heavy atom with respect to hydrogen as well as the presence of p electrons in the system which dictate the behaviour of the shift derivative, positive in the case of lithium hydride and negative in the case of hydrogen fluoride. The results tabulated in Table 11 and shown in Fig. 3 illustrate how this behaviour changes in a smooth way going across the first and second rows of the periodic table.

The gross atomic charges as determined by a Mulliken population analysis also illustrate the effect. Lithium and beryllium are slightly positive, and boron is slightly negative; the remainder of the first row heavy atoms are significantly negative. Sodium, magnesium, and aluminium are significantly positive, while silicon is slightly positive; phosphorus, sulphur, and chlorine are significantly negative. The ranges of the chemical shifts increase across the rows of the periodic tables as more electrons with non-zero angular momentum are added to the atom. Combined with the changing polarization character, this offers a reasonable description in these hydrides of the behaviour of the shift derivative as a function of atomic number.

The behaviour of the ions treated in this study is consistent with the idea of addition or removal of charge from the heavy atom. The formation of BH_4^- relative to BH_3 involves an addition of charge to the boron nucleus and results in an algebraic decrease in its shift derivative from 3.5 to -27.0 ppm Å^{-1}. The ammonium ion shows a decrease of charge at the nitrogen nucleus relative to ammonia and exhibits an algebraic increase in its shift derivative from -130.3 to -67.9 ppm Å^{-1}. Similar behaviour is observed for H_3O^+ and for the second row hydride ions AlH_4^-, PH_4^+ and the recently experimentally determined PH_2^- ion[93] relative to their uncharged species. In the study of these hydrides it was again found that the derivative of the paramagnetic term controlled the magnitude and sign of the shift derivative in all cases. The contribution from the diamagnetic term was relatively small and surprisingly uniform, as was also Ditchfield's magnetic dipole term.[18] Where shift derivatives were positive, so was the derivative of the paramagnetic term; where shift derivatives were negative, there the derivative of the paramagnetic term was also found to be negative.

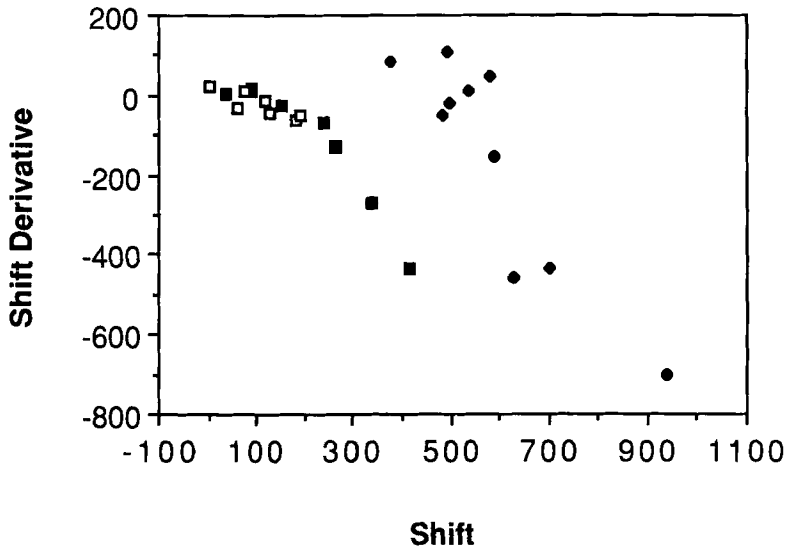

FIG. 4. Calculated chemical shift derivatives as a function of the calculated shift for CH (□), XH (■, first row hydrides), and XH (♦, second row hydrides). The data are taken from Tables 10 and 11 and are from refs 26 and 61.

Figure 4 illustrates the relationship between the heavy atom shift derivative and the corresponding shift for these hydrides and also for some CH data. In contrast to the behaviour of the shift derivative upon bond modification between heavy atoms, the shift derivatives for species bonded to hydrogen tend to become more negative as the chemical shift increases. The behaviour of the first row hydrides is similar to that found for the derivatives of carbon upon carbon—hydrogen bond modification. This different behaviour evidently reflects the clear difference between a bond between heavy atoms and a bond between a heavy atom and hydrogen.

V. SOME THEORETICAL RESULTS FOR HYDROGEN ATOMS

The discussion to this point concerning the comparison of theoretical and experimental results has dealt with the so-called heavy or non-hydrogen atoms. Proton magnetic resonance is of great importance and the large abundance and relatively high sensitivity of ^1H makes it a significant nucleus to study. We present in Table 12 a representative selection of calculations on hydrogen that involved only first row elements. The basis sets range in complexity from the gaugeless, best origin calculations of Höller and Lischka[27]

TABLE 12

Calculated from observed proton chemical shifts in ppm. The correlations are taken from refs 18, 68 (RAD), 26 (CF), 20, 21, 22 (SK), and 27 (HL). References to the experimental data are given in parentheses.

	Molecule	RAD	CF	SK	HL	Experiment
Set I	NH_3	33.59	32.71	31.51	31.41	32.43 (94)
	CH_4	32.73	31.85	31.14	31.39	30.61 (96)
	H_2O	32.79	32.04	30.56	30.08	30.09 (97)
	C_2H_6	32.38	31.14	30.55	30.63	29.86 (98)
	C_2H_2	31.48	30.89	29.04	29.85	29.27 (98)
	HF	30.61	30.18	28.05	27.85	28.72 ± 0.5 (99)
	C_2H_4	27.12	26.74	25.88	25.42	25.43 (98)
Set II	$CH_3O\underline{H}$	35.10	33.65	31.64	—	30.73 (97)
	$C\underline{H}_3CH_2CH_3$	32.49	—	—	—	29.93 (100)
	$CH_3C\underline{H}_2CH_3$	32.12	—	—	—	29.45 (100,101)
	$C\underline{H}_3CHO$	31.22	—	29.72	—	28.82 (102)
	HCN	29.78	29.74	28.76	—	27.78 (103)
	$C\underline{H}_3OH$	29.95	29.16	28.59	—	27.34 (97)
	$C\underline{H}_3F$	28.69	28.27	27.50	—	26.61 (102)
Set I	SD	0.48	0.48	0.60	0.69	
	$\langle x^2 \rangle^{1/2}$	2.10	1.39	0.60	0.69	
Sets I and II	SD	0.70	0.65	0.66	0.69	
	$\langle x^2 \rangle^{1/2}$	2.46	1.65	0.79	0.69	

that use large numbers of orbitals per atom to the relatively simple but nonetheless reasonably accurate results of Rohlfing, Allen, and Ditchfield[18,68] whose 4-31G results are selected for display. The calculations are broken into a set where one can compare results from all four approaches (Set I), along with an additional extended set of calculations on some other molecules (Set II). The standard deviation, SD, represents the spread of the differences between calculated and experimental results and is, therefore, a measure of the goodness of the calculations on a *relative* scale. The parameter $\langle x^2 \rangle^{1/2}$ represents the root-mean-square error between experiment and theory and is a measure of the *absolute* error. The four sets of results quoted and the bases employed give a good indication of the range of results that can be obtained using the various approaches.

The most extensive bases are those of Höller and Lischka[27] who use no gauge factors but many functions in order to minimize the gauge problem. Schindler and Kutzelnigg[20-22] are able to employ fewer basis functions in their IGLO approach, while the somewhat more efficient approach of Chesnut and Foley[26] using Ditchfield's GIAO method[18] can give reasonable results

with yet fewer orbitals. The data of Rohlfing, Allen, and Ditchfield using the rather small 4-31G basis is significant in that, while yielding the least accurate absolute results of those shown, it competes very well on a relative scale. Their calculations, like those of Chesnut and Foley, employ Ditchfield's approach. To get an idea of the size of the basis sets employed we note the number of atomic orbitals employed for the calculation of the HF molecule; Höller and Lischka use 71, Schindler and Kutzelnigg 53, Chesnut and Foley 21, and Rohlfing, Allen, and Ditchfield 11. The same groups in the calculation of ethane employ, respectively, 100, 93, 50 and 43 orbitals. The number of basis functions is, of course, large on the heavy atoms but can also be large on the hydrogen species. For example, in HF Schindler and Kutzelnigg employ a hydrogen basis of [4s,2p], Höller and Lischka [5s,3p,d], while Chesnut and Foley, and Rohlfing, Allen, and Ditchfield use the much smaller [2s] basis.

The analysis of the data in terms of the root-mean-square error and the parameter $\langle x^2 \rangle^{1/2}$ shown in Table 12 is informative. For those seven molecules of Set I the more extensive calculations of Höller and Lischka and Schindler and Kutzelnigg show a root-mean-square error of 0.6–0.7 ppm, better by a factor of approximately 2 or 3 than the other calculations cited. A comparison of Sets I and II again shows that these authors with their larger basis sets and more functions on hydrogen yield better absolute results. It is instructive, however, and most useful to note that if one looks at the measure of the relative results in this sampling as given by the parameter $\langle x^2 \rangle^{1/2}$ there is really very little to choose among the various approaches. The work of Chesnut and Foley and Rohlfing, Allen, and Ditchfield that use rather efficient and small basis sets have results which are as good as, if not slightly better than, those involving more complicated bases. Pragmatically, then, it is encouraging to note that one can do proton chemical shift calculations with a rather small basis and hope to achieve reasonable relative results. The large number of hydrogen species in organic compounds, for example, rapidly increases the number of atomic orbitals needed in a molecular calculation; the more efficient basis one can employ on hydrogen the easier such calculations become.

Although hydrogen chemical shifts can be calculated more accurately on an absolute basis than those for C, N, O and F, for example, the error as a percentage of the chemical shift range is comparable in the various cases. Taking the data of Schindler and Kutzelnigg as given in Tables 1 and 12 one finds that the root-mean-square error expressed as a percentage of the reported range of shifts is a little over 11% in each case. The ranges for the other nuclei such as nitrogen, oxygen and fluorine are increasingly greater; this in part explains the difficulty in reproducing absolute shifts for these species that are as good as those for carbon or hydrogen.

VI. CONCLUDING REMARKS

There has been great progress during the last decade in the calculation and interpretation of the chemical shift in nuclear magnetic resonance. This has been due to the availability of larger and faster computers, to the ability to carry out calculations with very large basis sets, and to the development of various sound approaches to the treatment of the gauge problem using various explicit gauge factors in the wave function. While most of the examples we have cited in this review article have been on small, first row heavy atom molecules, various groups have made significant progress in recent years in handling larger systems including molecules involving atoms in the second row of the periodic table.

The ability to carry out reasonably accurate relative proton chemical shift calculations has been employed by a variety of authors to study hydrogen bonding and the structure of water *n*-mers. Rohlfing *et al.*[104] have determined magnetic shielding tensors for hydrogen bonded systems in the species $(H_3O_2)^-$, $(H_2O)_2$, and $(H_5O_2)^+$ using a 4-31G basis. In an effort to explain empirically observed correlations between certain structural features of hydrogen bonds and the corresponding proton chemical shift parameters, they also carried out studies of fourteen OH· · ·O dimers involving substituted carboxylic acids and alcohols.[105] Giessner-Prettre and Pullman[106] used a minimal basis to determine the shielding constants of the formamide nuclei for the isolated molecule, the molecule surrounded by its "first hydration shell", and the molecule surrounded only by the four water molecules engaged in the short solute–solvent hydrogen bond. Their work shows that the six "remote" water molecules produced significant shift variations, and accordingly must be used in a correct description of the solvated molecule. Hinton and Bennett[107] used a 4-31G split valence basis to calculate the magnetic shielding tensors for the monomer, dimer, trimer, and pentamer of water in the ice structure, and conclude that secondary hydrogen bonding has a significant effect on both the proton shielding constant and its anisotropy.

Lazzeretti and Tossell[108] have invoked near-Hartree–Fock bases of gaugeless gaussian orbitals to calculate the ^{31}P NMR shielding constants in P_4, P_2, and PN. These authors have also studied the phosphorus chemical shift in PF_3, PF_4^+, PF_5, PF_6^-, and PO_4^{3-}, and comment on angular effects upon the shift in these systems.[109] Calculations involving silicon in the molecules SiH_4, Si_2H_6, Si_2H_4, and H_2SiO have been carried out,[110] as well as those involving SiO_4^{4-} and the fluorides SiF_4, SiF_5^-, and SiF_6^{2-}.[111] Tossell and Lazzeretti[112] have also looked at the series $SiH_nF_{(4-n)}$ for $n=1$ to 4, as a function of hydrogen content.

Fleischer *et al.*[113] have also carried out a very nice set of calculations on

many of the same phosphorus and silicon compounds using their IGLO approach. Of particular importance in this work is their study of basis sets. They conclude that on the whole a basis set of [7s,6p,2d] is required in the calculation of phosphorus (similar to the example of PH_3 cited in Section III.B.2 of this review), but for high accuracy three or four sets of d functions are necessary. They conclude that somewhat smaller basis sets are sufficient for silicon, again illustrating the fact that systems with non-bonding electrons are more difficult to handle than those with fully saturated valence shells.

Schindler[114] has shown that quite large systems can now be handled by applying the IGLO method to nitrogen chemical shifts in a wide variety of compounds. He has studied the amines $NH_m(CH_3)_{3-m}$ ($m = 0$, 1, 2, 3), $C_6H_5NH_2$, the three-membered ring aziridine ($(CH_2)_2NH$), the nitriles CH_3CN and C_6H_5CN, the isonitrile CH_3NC, diazomethane (CH_2NN), hydrazine (N_2H_4), and some diazines $RN=NR$ ($R = H$, CH_3). Schindler notes the importance of being aware of experimental conditions when comparing theoretical and experimental values for the chemical shift; due to the nitrogen lone-pair electrons, temperature and solvent shifts are much more pronounced for nitrogen than for carbon. A number of basis sets were employed in this study including some of near-Hartree–Fock quality. Schindler finds that the calculated NMR chemical shifts of nitrogen involved in NN double bonds are too paramagnetic, even in the limit of near-Hartree–Fock quality of the basis sets. Because of the large magnitude of the deviations between theory and experiment, gas-to-liquid shifts or asymmetry effects cannot explain these differences. It is concluded that correlation effects, which are neglected in the IGLO methods as well as in the other coupled Hartree–Fock approaches, are likely to play an important role in the calculation of NMR shifts for nitrogen atoms involved in NN multiple bonds. No one has yet attempted such extensive calculations with large basis sets.

Finally, while great progress has been made in the use of coupled Hartree–Fock techniques, still another level of calculation involving electron correlation may be required before a fully satisfactory understanding of this important chemical phenomenon can be had.

REFERENCES

1. N.F. Ramsey, *Phys. Rev.*, 1950, **78**, 699.
2. A.K. Jameson and C.J. Jameson, *Chem. Phys. Lett.*, 1987, **134**, 461.
3. C.J. Jameson, in *Specialist Periodical Report on NMR* (G.A. Webb, ed.), Vol. 16, Royal Society of Chemistry, London, 1987, p 1.
4. H. Hellmann, *Einfuhring in die Quantenchemie*, Franz Deuticke, Leipzig, Germany, 1937.
5. R.P. Feynman, *Phys. Rev.*, 1939, **56**, 340.

6. R.E. Stanton, *J. Chem. Phys.*, 1962, **36**, 1298.
7. J.A. Pople, J.W. McIver, Jr., and N.S. Ostlund, *J. Chem. Phys.*, 1968, **49**, 2960.
8. A.C. Hurley, *Proc. R. Soc. Lond.*, 1954, **A226**, 179.
9. A. Dalgarno and A.C. Stewart, *Proc. R. Soc. Lond.*, 1958, **A247**, 245.
10. A.D. Buckingham and S.M. Malm, *Mol. Phys.*, 1971, **22**, 1127;
11. A.D. Buckingham and J.A. Pople, *Trans. Faraday Soc.*, 1963, **59**, 2421.
12. R.F. Schneider, *J. Chem. Phys.*, 1968, **48**, 4905.
13. S.T. Epstein, *J. Chem. Phys.*, 1965, **42**, 2897; see also *J. Chem. Phys.*, 1973, **58**, 1592.
14. T.K. Rebane, *Soviet Phys. JETP*, 1960, **11**, 694.
15. S.I. Chan and T.P. Das, *J. Chem. Phys.*, 1962, **37**, 1527.
16. A.J. Sadlej, *Chem. Phys. Lett.*, 1975, **36**, 129.
17. F. London, *J. Phys. Radium*, 1937, **8**, 397.
18. R. Ditchfield, *Mol. Phys.*, 1974, **27**, 789.
19. W. Kutzelnigg, *Israel J. Chem.*, 1980, **19**, 193.
20. M. Schindler and W. Kutzelnigg, *J. Chem. Phys.*, 1982, **76**, 1919.
21. M. Schindler and W. Kutzelnigg, *J. Am. Chem. Soc.*, 1983, **105**, 1360.
22. M. Schindler and W. Kutzelnigg, *Mol. Phys.*, 1983, **48**, 781.
23. B. Levy and J. Ridard, *Mol. Phys.*, 1981, **44**, 1099.
24. Aa.E. Hansen and T.D. Bouman, *J. Chem. Phys.*, 1985, **82**, 5035.
25. Aa.E. Hansen and T.D. Bouman, *Adv. Chem. Phys.*, 1980, **44**, 545; T.D. Bouman, Aa.E. Hansen, B. Voigt and S. Rettrup, *Int. J. Quant. Chem.*, 1983, **23**, 595.
26. D.B. Chesnut and C.K. Foley, *J. Chem. Phys.*, 1986, **84**, 852.
27. R. Höller and H. Lischka, *Mol. Phys.*, 1980, **41**, 1017.
28. Th. Weller, W. Meiler, H.-J. Köhler, H. Lischka and R. Höller, *Chem. Phys. Lett.*, 1983, **98**, 541.
29. Calculated in ref. 3 based on data from refs 30 and 31.
30. A.J. Beeler, A.M. Orendt, D.M. Grant, P.W. Catts, J. Michl, K.W. Zilm, J.W. Downing, J.C. Facelli, M.S. Schindler and W. Kutzelnigg, *J. Am. Chem. Soc.*, 1984, **106**, 7672.
31. J. Mason, *J. Chem. Soc. Perkin Trans.* 1976, **2**, 1671.
32. K. Jackowski and W.T. Raynes, *Mol. Phys.*, 1977, **34**, 465.
33. L.J.M. van DeVen and J.W. de Haan, *J. Chem. Soc., Chem. Commun.*, 1978, 94.
34. Estimated in ref. 3 from the combined data of refs 30 and 35.
35. D.B. Newmann and J.W. Moskowitz, *J. Chem. Phys.*, 1969, **50**, 2216.
36. S.G. Kukolich, *J. Am. Chem. Soc.*, 1975, **97**, 5704.
37. Calculated in ref. 3 based on data from refs 38 and 39.
38. C.J. Jameson, A.K. Jameson, D. Oppusunggu, S. Wille, P.M. Burrell and J. Mason, *J. Chem. Phys.*, 1981, **74**, 81.
39. M. Alei, A.E. Florin, W.M. Litchman and J.F. O'Brien, *J. Phys. Chem.*, 1971, **75**, 932.
40. R.E. Wasylishen, *Can J. Chem.*, 1982, **60**, 2194.
41. R.E. Wasylishen, S. Mooibroek and J.B. Macdonald, *J. Chem. Phys.*, 1984, **81**, 1057.
42. M.A. Frerking and W.D. Langer, *J. Chem. Phys.*, 1981, **74**, 6990.
43. C.J. Jameson, A.K. Jameson and P.M. Burrell, *J. Chem. Phys.*, 1980, **73**, 6013.
44. D.K. Hindermann and C.D. Cornwell, *J. Chem. Phys.*, 1968, **48**, 4148.
45. A. Pines, M.G. Gibby and J.S. Waugh, *Chem. Phys. Lett.*, 1972, **15**, 373.
46. Quoted in ref. 3 based on data in ref. 31.
47. B.P. Appleman and B.P. Dailey, *Adv. Magn. Reson.*, 1974, **7**, 231.
48. F. Millett and B.P. Dailey, *J. Chem. Phys.*, 1971, **54**, 5434.
49. Calculated in ref. 3 from the data of refs 51 and 52.
50. A.A.V. Gibson, T.A. Scott and E. Fukushima, *J. Magn. Reson.*, 1977, **27**, 29.
51. W.L. Meerts, F.H. de Leeuw and A. Dymanus, *Chem. Phys.*, 1977, **22**, 319.

52. R.D. Amos, *Chem. Phys. Lett.*, 1979, **68**, 536.
53. Calculated from spin rotation data of ref. 54 and diamagnetic σ of ref. 55.
54. R.M. Garvey and F.C. DeLucia, *J. Mol. Spectrosc.*, 1974, **50**, 38.
55. T.D. Gerke and W.H. Flygare, *J. Am. Chem. Soc.*, 1972, **94**, 7277.
56. L.M. Ishol and T.A. Scott, *J. Magn. Reson.*, 1977, **27**, 23.
57. Calculated in ref. 3 from the data of refs 41, 42 and 52.
58. S.C. Wofsy, J.S. Muenter and W. Klemperer, *J. Chem. Phys.*, 1971, **55**, 2014.
59. F.H. de Leeuw and A. Dymanus, *J. Mol. Spectrosc.*, 1973, **48**, 427.
60. D.E. O'Reilly, E.M. Peterson, Z.M. El Saffer and C.E. Scheie, *Chem. Phys. Lett.*, 1971, **8**, 470.
61. D.B. Chesnut, *Chem. Phys.*, 1986, **110**, 415.
62. R. Höller and H. Lischka, *Mol. Phys.*, 1980, **41**, 1041.
63. P. Lazzeretti and R. Zanasi, *J. Chem. Phys.*, 1980, **72**, 6768.
64. S. Wilson, in *Ab Initio Methods in Quantum Chemistry* (K.P. Lawley, ed.), Vol. I, John Wiley and Sons, New York, 1987, p. 439.
65. E.R. Davidson and D. Feller, *Chem. Rev.*, 1986, **86**, 681.
66. P. Lazzeretti and R. Zanasi, *Int. J. Quant. Chem.*, 1977, **12**, 93.
67. H.L. Tigelaar and W.H. Flygare, *Chem. Phys. Lett.*, 1970, **7**, 254.
68. C.M. Rohlfing, L.C. Allen and R. Ditchfield, *Chem. Phys.*, 1984, **87**, 9.
69. W.J. Hehre, L. Radom, P.v.R. Schleyer and J.A. Pople, *Ab Initio Molecular Orbital Theory*, J. Wiley and Sons, New York, 1986.
70. See ref. 69 for an explanation of the special basis set notation employed by Pople and co-workers.
71. D.B. Chesnut and C.K. Foley, *J. Chem. Phys.*, 1986, **85**, 2814.
72. M.M. Francl, W.J. Piefro, W.J. Hehre, J.S. Binkley, M.J. Gordon, D.J. DeFrees and J.A. Pople, *J. Chem. Phys.*, 1982, **77**, 3654.
73. T. Clark, J. Chandrasekhar, G.W. Spitznagal and P.v.R. Schleyer, *J. Comp. Chem.*, 1983, **4**, 294.
74. M.J. Frisch, J.A. Pople, and J.S. Binkley, *J. Chem. Phys.*, 1984, **80**, 3265.
75. C.J. Jameson and H.J. Osten, in *Annual Reports on NMR Spectroscopy* (G.A. Webb, ed.), Vol. 17, Academic Press, London, 1986, p. 1.
76. C.J. Jameson and H.J. Osten, *J. Chem. Phys.*, 1985, **83**, 5425.
77. C.J. Jameson and H.J. Osten, *Mol. Phys.*, 1985, **55**, 383.
78. R. Ditchfield, *Chem. Phys.*, 1981, **63**, 185.
79. P.W. Fowler and W.T. Raynes, *Mol. Phys.*, 1981, **43**, 65.
80. J.L. Dunham, *Phys. Rev.*, 1932, **41**, 713; *Phys. Rev.*, 1932, **41**, 721.
81. R.E. Wasylishen, J.O Friedrich, J. Mooibroek and J.B. MacDonald, *J. Chem. Phys.*, 1985, **83**, 548.
82. C.J. Jameson, A.K. Jameson, S. Willie and P.M. Burrell, *J. Chem. Phys.*, 1981, **74**, 853.
83. J.O. Friedrich and R.E. Wasylishen, *J. Chem. Phys.*, 1985, **83**, 3707.
84. C.J. Jameson and H.J. Osten, *Mol. Phys.*, 1985, **56**, 1083.
85. C.J. Jameson and H.J. Osten, *J. Chem. Phys.*, 1977, **66**, 4977.
86. C.J. Jameson, *Mol. Phys.*, 1985, **54**, 73.
87. C.J. Jameson and H.J. Osten, *Mol. Phys.*, 1985, **55**, 383.
88. C.J. Jameson and H.J. Osten, *Mol. Phys.*, 1985, **56**, 1083.
89. H.J. Osten and C.J. Jameson, *J. Chem. Phys.*, 1984, **81**, 4288.
90. R.E. Wasylishen and J.O. Fredrich, *Can. J. Chem.*, 1987, **65**, 2238.
91. H.J. Osten and C.J. Jameson, *J. Chem. Phys.*, 1985, **82**, 4595.
92. C.J. Jameson and H.J. Osten, *J. Chem. Phys.*, 1984, **81**, 4300 (Erratum: *J. Chem. Phys.*, 1985, **83**, 915).

93. R.E. Wasylishen and N. Burford, *Can. J. Chem.*, 1987, **65**, 2707.
94. Liquid phase value of 30.68 reported by G. Arrighini, M. Maestro and R. Moccia, *J. Chem. Phys.*, 1970, **52**, 6411, corrected to the gas phase for 300 K by adding 1.75 as reported in ref. 95.
95. C.J. Jameson, A.K. Jameson, S.M. Cohen, H. Parker, D. Oppusunga, P.M. Barrell and S. Willie, *J. Chem. Phys.*, 1981, **74**, 1608.
96. W.T. Raynes, in *Nuclear Magnetic Resonance* (R.K. Harris, ed.), Vol. 7, The Chemical Society, London, 1978, p. 1.
97. J.P. Chauvel and N.S. True, *Chem. Phys.*, 1985, **95**, 435.
98. L. Petrakis and C.H. Sederholm, *J. Chem. Phys.*, 1961, **35**, 1174.
99. Average of results quoted in ref. 20.
100. J.B. Cavanaugh and B.P. Dailey, *J. Chem. Phys.*, 1961, **34**, 1099.
101. R.E. Wasylishen and T. Schaefer, *Can. J. Chem.*, 1974, **52**, 3247.
102. J.W. Ensley, J. Feeney and H. Sutcliffe, *High Resolution Nuclear Magnetic Resonance Spectroscopy*, Vol. 2, Pergamon Press, New York, 1968.
103. W.G. Schneider, H.J. Bernstein and J.A. Pople, *J. Chem. Phys.*, 1958, **28**, 601.
104. C.M. Rohlfing, L.C. Allen and R. Ditchfield, *Chem. Phys. Lett.*, 1982, **86**, 380.
105. C.M. Rohlfing, L.C. Allen and R. Ditchfield, *J. Chem. Phys.*, 1983, **79**, 4958.
106. C. Giessner-Prettre and A. Pullman, *Chem. Phys. Lett.*, 1985, **114**, 258.
107. J.F. Hinton and D.L. Bennett, *Chem. Phys. Lett.*, 1985, **116**, 292.
108. P. Lazzeretti and J.A. Tossell, *J. Phys. Chem.*, 1987, **91**, 800.
109. J.A. Tossell and P. Lazzeretti, *J. Chem. Phys.*, 1987, **86**, 4066.
110. J.A. Tossell and P. Lazzeretti, *Chem. Phys. Lett.*, 1986, **128**, 420.
111. J.A. Tossell and P. Lazzeretti, *J. Chem. Phys.*, 1986, **84**, 369.
112. J.A. Tossell and P. Lazzeretti, *Chem. Phys. Lett.*, 1986, **132**, 464.
113. A. Fleischer, M. Schindler and W. Kutzelnigg, *J. Chem. Phys.*, 1987, **86**, 6337.
114. M. Schindler, *J. Am. Chem. Soc.*, 1987, **109**, 5950.

This Page Intentionally Left Blank

NMR Studies of Membrane Transport

B.P. HILLS and P.S. BELTON

AFRC Institute of Food Research, Colney Lane, Norwich, NR4 7UA, UK

I. INTRODUCTION

Membrane transport processes are fundamental to life, without them growth and reproduction are impossible. Improved methods for studying transmembrane transport are thus of key importance in biology and medicine. Over the last decade nuclear magnetic resonance (NMR) has made a major contribution to the understanding of the transport of small molecules and ions across membranes, both in model membrane systems as well as in living cells and perfused organs. This has resulted in a rapid increase of papers dealing with NMR membrane transport covering a wide range of disciplines. In physiology, for example, the effect of substances such as hormones,[1,2]

ANNUAL REPORTS ON NMR SPECTROSCOPY
VOLUME 21 ISBN 0-12-505321-5

anaesthetics,[3,4] antibiotics[5,6] and cryoprotectants[7] in selectively altering membrane permeabilities has been studied with NMR techniques. Clinical research into the molecular basis of illnesses such as hypertension,[8,9] manic depression,[10] human epilepsy,[11] cancer,[12] muscular dystrophy,[13] cataract formation[14] and malaria[15] has been facilitated by NMR determinations of membrane permeabilities. The current interest in using liposomes as drug microencapsulation and delivery systems has led to NMR studies of membrane permeabilities in liposomes.[16]

In cell biology changes in membrane permeability can play a key role not only in nerve response, but also in such fundamental processes as cell growth, mitogenesis and differentiation. This has stimulated a number of NMR studies[17,18] and reviews.[19-21] As we will show, under favourable conditions it is even possible to monitor the *in vivo* fluxes of metabolites between the various membrane-bound compartments within cells using NMR techniques. At the molecular level it is necessary to understand the chemical factors determining the binding constants and transport rates characterizing membrane carriers such as the ionophore antibiotics. This is especially important for the design of new drugs. NMR can provide a unique way of measuring these parameters and considerable progress has been made in this direction.

Despite these varied applications it cannot yet be said that such NMR measurements have become "routine". Several different NMR techniques are available and to some extent these need to be adapted to the biological system of interest. In some cases the techniques themselves are still in the process of development. In other cases the technique is well established but the data are hard to interpret because of the lack of appropriate theoretical models. For these reasons we will not, in this review, merely attempt to catalogue the large number of papers dealing with NMR studies of membrane transport or to review critically the results obtained for any one type of biological system such as erythrocytes or yeasts, since this would entail a detailed discussion of results obtained with other non-NMR methods. Rather, we intend to review the strengths and limitations of each NMR technique currently available and will attempt to point out areas for future development. We will exclude, for the most part, publications dealing with NMR studies of membrane structure and function unless transport is specifically measured. Similarly NMR studies of carrier–substrate interactions in homogeneous solutions and micelle suspensions will be excluded except in the important case of gramicidin. Though tempting, we will also refrain as far as possible, from discussing the intricacies of theories for membrane transport except in so far as they impinge on the NMR techniques used to measure the transport rates. The basic theory of membrane transport has already been reviewed in a number of monographs[22-24] and articles.[25-27] Table 1 lists a number of other reviews that are relevant to NMR membrane transport studies.

TABLE 1

Reviews relevant to NMR studies of membrane transport.

	Ref.
(1) NMR and compartmentation in biological tissues (1985)	44
(2) NMR studies of ion-binding in biological systems (1987).	45
(3) NMR studies of intracellular metal ions in intact cells and tissues (1984).	46
(4) NMR study of epithelia (1986).	47
(5) Water in plants: A review of some NMR studies concerning the state and transport in leaf, root and seed (1982).	48
(6) NMR studies of ion transport across membranes (1983).	49
(7) Dynamic aspects of carrier-mediated cation transport through membranes (1977).	25
(8) Kinetic properties of ion carriers and channels (1980).	26
(9) Water movement through lipid bilayers, pores and plasma membranes. Theory and reality (1987).	27

As we hope to illustrate in this review, there remain many exciting possibilities for future development of NMR transport techniques. One general area that might be mentioned at this point is the future application of localized NMR spectroscopy and NMR imaging techniques together with suitable contrast reagents to allow the spatial resolution of *in vivo* transport throughout whole organs. However, at present this development is in its infancy.[28]

In the next section we will make a general comparison of NMR methods with some other non-NMR techniques for measuring membrane transport.

II. COMPARISON WITH OTHER TRANSPORT METHODS

The standard method for measuring membrane permeabilities by monitoring the flux of a radioactive labelled compound (or ion) through the membrane is restricted to relatively slow transport with time constants longer than a few seconds. It requires repetitive and painstaking analysis and usually involves destruction of the sample. In contrast, NMR methods can conveniently measure transport processes over a range of timescales varying from milliseconds to hours and allows almost continuous monitoring of small amounts of sample in a non-destructive way. This means that it is straightforward with NMR methods to monitor the effect of varying parameters such as temperature, osmolarity or concentration of effectors on the transport process.

Unstirred layers either side of the membrane can be a problem with the classical radiolabelling technique, especially when the membrane exchange is fast. In such cases diffusion of the labelled molecules up to the membrane

may become rate limiting.[29] Because fast exchange rates are usually measured by magnetically labelling the whole sample under conditions when there is no net mass flux through the membrane, unstirred layers are not usually a problem with NMR methods. In most experiments the distances that need be traversed by diffusion up to the membrane will be only a few thousand ångströms which can be done by small molecules in a few milliseconds. This timescale is usually shorter than the membrane exchange rate. Plant cells can be exceptional in that membrane exchange is often extremely fast and the cells very large so that diffusion through unstirred layers can be rate limiting even in NMR determinations.[30]

Electrical conductance methods have been exceedingly useful in characterizing ion transport across Black lipid membranes (BLM)[31-34] and across the plasma membrane of large cells such as the spiral giant axon.[35] While this method is very sensitive, allowing the observation of single ion events, physical limitations mean it cannot be used as a general method for vesicle or cell suspensions. Furthermore measurements of BLMs may suffer from problems of membrane heterogeneity, solvent residues within them and the difficulty of incorporating viable membrane protein mediators. NMR methods suffer no such restriction and have the advantage that ionic flows do not have to be perturbed by externally applied potential differences.

Stopped flow light scattering has been used to measure fast osmotic water permeability coefficients (P_f) through vesicle membranes on a short millisecond timescale.[36] The method relies on the dependence of the light scattering intensity on vesicle volume as the vesicles swell (or shrink) in hypo- (or hyper-) osmotic solutions. In contrast, NMR methods can measure the tracer permeability (P_{dw}) for water under steady state conditions without perturbing the volume of the system. Such NMR determinations have yielded water exchange lifetimes as short as 8–9 ms in human erythrocytes (Table 7). These values compare well with those obtained with the much more difficult radioactive tritiated water method which uses a steady state flow tube apparatus, and requires large volumes of blood, cell enrichment, filtration and counting.[37] It may be possible to use NMR to measure the osmotic permeability coefficient for water (P_f) as well as the tracer permeability (P_{dw}). This possibility will be discussed in Section III.A.5, though so far no attempt has been made to do this.

The main disadvantage of NMR is its low sensitivity. This is a problem with all nuclei but is exacerbated when the nuclei have low natural abundance, low magnetogyric ratios and give broad resonance signals. In general even under the most favourable circumstances relatively high concentrations of compounds (> 1 mM) are usually required. These concentrations may be greater than desirable, especially if *in vivo* physiological responses are being monitored. Some biologically important ions such as calcium or magnesium

are especially difficult to measure since they have low magnetogyric ratios, low natural abundances and, being quadrupolar, are likely to have broad lines if involved in ion pairing or complexing.

The recent advance of sensitive ^{19}F NMR indicators for these particular metal ions (Section III.A.4) holds great future potential. Nevertheless, the vast majority of NMR transport studies to date are concerned with the transport of nuclei with relatively high nuclear receptivity such as $^{23}Na^+$, $^{7}Li^+$ and with molecules containing phosphorus (^{31}P) or fluorine (^{19}F). There have been some reports (Tables 3 and 6) on $^{39}K^+$, which has a low magnetogryric ratio but 100% natural abundance; however, these have been at fairly high concentrations. Proton (^{1}H) NMR has been widely used to study water transport, and proton spin-echo NMR methods (Section V) and pulsed field gradient methods (Section VI) hold promise of being applicable to a wide range of organic compounds such as amino-acids and sugars. However the proton spin-echo method has so far only been tested on erythrocytes and algal cells and it remains to be seen to what extent it can be usefully applied to other cellular or vesicular systems.

III. METHODS BASED ON CHEMICAL SHIFT DIFFERENCES

To monitor the transport of a substance across a cell (or vesicle) membrane using NMR it is necessary to have some way of distinguishing between the signals originating from spins in the compartments on either side of the membrane. In this section we will discuss the case where the spins have different chemical shifts. There are at least four ways of using such chemical shift differences to measure transport rates and these will be reviewed in Subsections III.A-D below.

A. Peak intensity changes

1. Theory

Perhaps the simplest case conceptually occurs when the spins in each compartment have sufficiently large chemical shift differences that they give rise to separate peaks in the NMR spectrum. If the transport of spins across the membrane separating the compartments is slow compared to the minimum time required to acquire a high resolution spectrum (usually a few seconds), or to halt the transport chemically, the transport can be monitored by adding the transported material to the outer compartment and following the changes in inner and outer integrated peak intensity as the material crosses the membrane. Of course the concentrations of transporting material must be

sufficient for separate peaks to be detectable from each compartment and the relaxation times must be much longer than the instrument recovery time.

Before reviewing experimental results it is worthwhile considering how such NMR intensity changes can be analysed to give membrane transport rates. The spectral intensity originating from a compartment is proportional to the number of spins (N) in that compartment. The changes in peak intensity can therefore be used to measure the net flux (J) of spins through the membrane encompassing the compartment since $J = -A^{-1}(dN/dt)$, where A is the membrane area. It is important to note that intensity changes are related to the *net* flux J, not the unidirectional (or tracer) flux.[22] One of the many models of membrane transport can then be used to relate the next flux J to parameters characterizing the membrane and the transported material. These theories have been discussed in a number of standard texts.[22-24] The simplest case is the passive, diffusive carrier-independent transport of small uncharged molecules. For this case $J = -P(c^i - c^0)$ where c^i and c^0 are the concentrations of transporting material in the inner and outer compartments and P is the membrane permeability coefficient given as $\beta D/L$, where D is the diffusion coefficient in the membrane, L is the membrane thickness and β is the distribution coefficient between the aqueous phase and the membrane. The carrier-independent transport of ions is more complicated. As a first approximation the Goldman–Hodgkin–Katz equation can be used to relate the ion flux to the membrane potential difference ($\Delta\Psi$) and the concentration difference, provided the potential field is linear,[23]

$$J = \frac{-PzF\Delta\Psi}{RT}\left\{\frac{c^0 - c^i \exp(zF\Delta\Psi/RT)}{1 - \exp(zF\Delta\Psi/RT)}\right\} \quad (1)$$

Many models have been proposed for carrier-mediated transport (facilitated transfer) for both neutral molecules and ions.[22] In contrast to passive diffusive transport, facilitated transport can show the phenomena of carrier saturation, competitive inhibition, counter-transport and cotransport.

In living systems, as distinct from model vesicle studies, the analysis can be complicated by rapid metabolism of the transported material, by feedback control mechanisms and by changing areas and volumes due to cell growth. In such cases it may be possible to analyse the NMR intensity data using more complex kinetic schemes.[38,39] Alternatively the membrane transport step can in some cases be isolated by inhibiting the metabolism of the transported material with drugs.[40] The specificity of the transport system can also be studied using non-metabolizable substrates[41,42] if these are easily available.

2. *Chemical shifts created by pH gradients*

In principle any difference in the chemical environment that affects the chemical shift may be used to separate the inner and outer peaks, but the most

important differences are those arising from pH gradients across the membrane and those induced by the so-called "shift reagents" which are usually paramagnetic complexes. In this subsection we will review the use of pH gradients. For this method to be useful the transporting material must have a pH-dependent chemical shift in the pH range for which the cell (or vesicle) is viable and its transport needs to be slow compared to the chemical shift difference. Ideally the material should not be rapidly metabolized. In model vesicle suspensions the pH and concentrations can usually be adjusted to meet these conditions but in cellular systems there are fewer degrees of freedom since the pH in intracellular compartments is often under tight metabolic control. The description of the pH-dependent chemical shifts method will be split into two parts: the application of ^{31}P NMR (Section III.A.2(a)) and other nuclei (Section III.A.2(b)).

(a) ^{31}P spectra. In 1973 Moon and Richards[43] first demonstrated that inorganic phosphate (P_i) has a significant ^{31}P chemical shift range over a pH of 5.5–8.5. Since many living cells maintain significant pH gradients across their organelle and cytoplasmic membranes, separate peaks corresponding to extracellular, cytoplasmic and even organelle phosphate can often be resolved in the ^{31}P spectrum. Since the chemical shift of these peaks depends on the pH, many studies have used ^{31}P spectra to measure intracellular pHs and this has been reviewed.[44] Fewer studies (see Table 2) have used intensity changes in the resolved ^{31}P peaks to measure the transport of phosphate or phosphate analogues. This is no doubt because of a number of experimental difficulties that need to be overcome before meaningful transport rates can be determined from the ^{31}P spectra. The low ^{31}P signal sensitivity and slow transport mean that high cell densities must be used with extended acquisition times. The cell suspensions must therefore be kept viable by oxygenation and perfusion with nutrients.[240] In some cells the peaks of diphosphoglycerate (DPG) overlap with internal phosphate so that it may be necessary to deplete the cells of DPG before phosphate influx can be measured. In plant cell systems several micronutrients such as Mn^{2+} and Fe^{3+} are paramagnetic and broaden the phosphate resonances. In these cases the plant cells may need to be cultured in media low in paramagnetics.

Notwithstanding these difficulties, some very interesting transport studies have been undertaken. The transport of phosphate and phosphate analogues across human erythrocyte membranes by a specialized membrane-spanning "Band 3" protein has been reported.[41] The concentration dependent influx rates were analysed using Michaelis–Menten type kinetics and used to discuss the specificity of the transport protein for the different phosphate analogues. Phosphite (HPO_3^{2-}), the anion most closely resembling bicarbonate (a natural substrate for anion exchange), was found to have the highest influx rate. In this study the intracellular concentration of phosphate was initially

TABLE 2

Transport of phosphate or phosphate analogues using ^{31}P NMR intensity changes.

System	Nuclei studied	Transport system	Ref.
Human erythrocytes	^{31}P, ^{19}F	Phosphate analogues, by Band 3 protein	41,42
Human erythrocytes	^{31}P	Link between P_i transport and muscular dystrophy	50
Human erythrocytes	^{31}P, ^{35}Cl	Phosphate and chloride transport by Band 3 protein.	51
Rat erythrocytes	^{31}P, ^{23}Na	Na^+ transport and P metabolism	8
Yeast	^{31}P, ^{23}Na	Na^+ transport and P metabolism	52
Yeast	^{31}P	Phosphate and proton transport	17,53
Clostridium thermocellum	^{31}P, ^{13}C	Phosphate uptake	54
Alga	^{31}P	Phosphate uptake	55
Cultured *Catharanthus roseus* and *Daucus carota* cells	^{31}P	Phosphate uptake	56
Catharanthus roseus treated with DMSO	^{31}P	Phosphate transport	57
Maize root tips	^{31}P	Phosphate uptake	58,59
Corn root tips	^{31}P, ^{23}Na	Na^+ transport, pH_{in} and P metabolism	60
Pea root tips	^{31}P	Phosphate uptake	61
Potato tubers and maize seedlings	^{31}P	Phosphate transport and metabolism	59
Escherichia coli	^{31}P	Phosphate transport	62

lowered to below 2 mM by washing with 145 mM NaCl and incubating in humidified O_2 for 60 min at 37°C with gentle agitation followed by rewashing. The influx rates of many of the phosphate analogues were so fast that exchange for intracellular Cl^- reached equilibrium within seconds. Therefore the anion exchange inhibitor SITS (4-acetamido-4′-isothiocyanatostilbene-2,2′-disulphonic acid) was used to "freeze" the transmembrane anion distribution ratios at specified times so that NMR analysis could be performed. Later work[42] studied the pH dependence of the influx rates for the phosphate analogues and concluded that the erythrocyte membrane carrier has a titratable positive charge with a pK of 5.5.

The potential of ^{31}P NMR in studying the *in vivo* transport and metabolism of phosphate in plant tissues has barely begun to be exploited. This has great practical importance in the selection of genotypes for efficient growth under conditions of low availability of particular nutrients.[59] The transport of phosphate through the plasmalemma in plant cells is thought to

be extremely fast so that the diffusion of phosphate through the soil solution to the root surface can be rate limiting.[63] However, the uptake is dependent on the availability of ions, particularly calcium, boron[64] and zinc.[65,66]

^{31}P NMR studies of four varieties of maize root tips 48 h after germination show major differences in the distribution of inorganic phosphate between cytoplasm and vacuole. The phosphate absorption rates of 10-day-old seedlings from the same variety differ by a factor of three.[59] Other recent studies of phosphate uptake by maize root tips include the effects of anions (Cl^- and NO_3^-), cations (Zn^{2+}, Mg^{2+}, Al^{3+}) and protonophores on the transport.[58]

The uptake and utilization of phosphate in cultured *Catharanthus roseus* and *Daucus carota* plant cells has been studied.[56] A maximum uptake rate of 1.7 μmol min^{-1} g^{-1} (dry weight of cells) was measured for *C. roseus*. The phosphate is first stored in the vacuoles; subsequently one part of the vacuolar pool is used to keep a constant cytoplasmic P_i level while another part is apparently accumulated as an NMR invisible P_i store. In contrast *D. carota* transports P_i at a much slower rate (0.05 μmol min^{-1} g^{-1}) and the P_i is not accumulated in vacuoles. Changing the external pH did not lead to detectable changes in the positions of the P_i or sugar phosphate resonance so that proton transport could not be measured. Further studies on phosphate transport in plant tissues are to be anticipated.

There have been several noteworthy NMR studies on transport in yeast. In one report simultaneous ^{23}Na and ^{31}P NMR spectra were obtained from sodium-loaded yeast cell suspensions to monitor the Na^+ efflux and the phosphate uptake under a variety of metabolic conditions.[52] In the absence of exogenous glucose the phosphate taken up accumulated first as intracellular inorganic phosphate; otherwise it accumulated first in the "sugar phosphate" pool. Another report[53] focused on phosphate uptake in glycolysing yeast cells which had been grown on a variety of different carbon sources and subsequently supplied with glucose, both in the presence and absence of oxygen. Table 2 lists a number of other transport studies using ^{31}P NMR intensity changes.

The studies so far discussed have used intensity changes in the ^{31}P spectra to monitor the transport of phosphate or phosphate analogues. However, time-resolved changes in the chemical shifts of these peaks can also be used to follow the time course of intra- or extracellular pH changes and so give information on the transport of protons across membranes. Several examples are listed in Table 3. Proton transport across model vesicle membranes has been studied with P_i as the pH-dependent probe.[67,68,190] It was shown that below the lipid transition temperature (42°C in L-α-dipalmitoylphosphatidylcholine vesicles) there is no significant proton transport. But above the transition temperature there is a slow proton–cation exchange

TABLE 3

Proton transport studies using ^{31}P chemical shifts.

System	Nucleus	Transport system	Ref.
Vesicles	^{31}P	H^+ transport	67, 190
Vesicles	^{31}P, ^{1}H	H^+ transport	68
Yeast	^{31}P, ^{23}Na, ^{39}K	Na^+, K^+ and H^+ transport	69
Yeast	^{31}P	Glycine–proton symport	38
Rosc damascena	^{31}P	UV-stimulated bicarbonate efflux	70

which is accelerated by the ionophore valinomycin. Unfortunately quantitative interpretation of these changes has not yet been attempted and the potential of this method for investigating protonophore kinetics and the dependence on membrane composition and membrane potential has not yet been explored. Proton (or OH^-) fluxes through membranes can also control intravesicular precipitation reactions.[68] This may be an important controlling factor in the formation and dissolution of calcium carbonate or calcium phosphate in shells and bones, or of calcium oxalate in some plants. In their investigations of precipitation within a model vesicle system, Mann *et al.*[68] used phosphate chemical shifts to follow the intravesicular pH under steady state conditions as the external pH was varied between 6 and 12.6 units. It was concluded that pH is changed mainly by exchange of external OH^- for internal diffusive anions such as Cl^- or NO_3^-. But highly charged anions such as HPO_4^{2-} or PO_4^{3-} could not be exchanged for OH^- through the vesicle membrane. Despite the importance of such transport processes the kinetics of OH^- (or H^+) transport in model vesicle systems has yet to be investigated quantitatively.

In living systems ^{31}P NMR would seem to be ideally suited to study the cotransport of protons along with various solutes into the cells. In many bacterial, fungal, algal and higher plant cells the entry of solute into the cells is accompanied by uptake of protons and by depolarization of the plasma membrane; and maximal steady state levels of accumulated solute appear quantitatively related to the energy available from the electrochemical gradient of protons. ^{31}P NMR determinations of intracellular pH changes allow quantitative studies of this phenomenon. One such study on glycine–proton symport in yeast[38] used ^{31}P NMR with phosphate to monitor pH_{in} and pH_{out} while the ^{13}C-labelled glycine transport was measured radiochemically. Spin-echo NMR methods might have provided an easier alternative way of measuring the glycine transport (see Sections V and VI) in this system. In another study on yeast the pH_{in} was monitored by ^{31}P NMR and the intimately connected transport of the cations K^+ and Na^+ was followed

using ^{23}Na and ^{39}K NMR.[69] It was concluded that upon energizing the cells by oxygenation H^+ efflux is correlated with K^+ influx and the fluxes are reversed when the cells were de-energized after the aerobic period. The ultraviolet-stimulated efflux of K^+ and HCO_3^- ions from *Rosa* cells has been studied by ^{31}P NMR. Here the efflux of bicarbonate led to an acidification of both the cytoplasm and the vacuolar regions which was monitored using the shifts in the phosphate resonances.[70] The acidification was not as great as predicted from the HCO_3^- loss. Analysis of nitrogenous material in the cell suggested that reduction of nitrate and synthesis of γ-aminobutyric acid absorbed some of the protons formed by the synthesis and dissociation of bicarbonate.

(b) Other nuclei with pH-dependent chemical shifts. In principle any molecule having a nucleus with a pH-dependent chemical shift in the physiological pH range can be used to measure both proton (or OH^-) transport as well as its own transport flux. Table 4 gives some representative examples. Membrane permeabilities have been measured for maleic acid in model phospholipid vesicles using a kinetic analysis based on the flux equation $J = -P(c^i - c^0)$. In this case the vinyl protons showed a pH-dependent chemical shift that was used to distinguish internal and external resonances.[38,39] Although, in principle, many other simple compounds have pH-dependent chemical shifts of ^1H, ^{13}C or ^{15}N resonances, very little work has been done in this area. One example, however, is the use of the ^{13}C resonance in malate to study vacuolar compartmentation in *Kalanchöe tubiflora*.[72] The ^{15}N resonance in ^{15}N-enriched histidine has been used to probe vacuolar pH in intact mycelia of *Neurospora crassa*.[78] There would

TABLE 4

Transport studies involving nuclei other than ^{31}P with pH-dependent chemical shifts.

System	Nucleus	Transport system	Ref.
Vesicles	^1H	Maleic acid	71, 39
Kalanchöe tubiflora	^{13}C	Malate	72
Human erythrocytes	^{19}F	Trifluoroethylamine	73
Human lymphocytes	^{19}F in fluorinated α-methylamino-acids	H^+ (pH_{in})	18, 74
E. coli	^{13}C	Succinate	75
Staphylococcus	^{13}C	Lactate	76
Mouse thymocytes	^{19}F in Fquene	H^+ (pH_{in})	1
Chromaffin granule membranes	^1H in EDTA	H^+ (pH_{in}) and Ca^{2+} uptake	77

seem to be considerable potential in these approaches which so far have not been exploited for transport measurements.

^{19}F-NMR resonances can show significant pH-dependent chemical shifts and have the advantage of greater nuclear sensitivity than phosphorus. Furthermore, inorganic phosphate can show shifts arising from interactions with enzymes and metal ions and can be metabolized. Fluorine compounds can be chosen to avoid these problems. Trifluoroethylamine has a pK_a of 6.0 and has been used to measure the intracellular pH of erythrocytes.[73] At 37°C the transmembrane exchange is so fast that only a single averaged peak can be observed. Temperatures as low as 4°C are necessary to resolve the inner and outer resonances and allow pH determination. This precludes its general use as a pH indicator, but observation of such fast exchange at 37°C is itself of interest and may provide a good model system to test theories of fast membrane transport as will be discussed in Section III.B. The problem of the rapid exchange of trifluoroethylamine was overcome in later work[18,74] by using fluorinated α-methylamino-acids as pH probes. These underwent slow exchange, were non-toxic and non-metabolizable. An alternative ^{19}F-NMR pH probe (Fquene) has been developed by Metcalfe and co-workers.[1] It has a pK_a of 6.7 and also acts as a fluorescence pH indicator, so providing pH_{in} measurements in the same cell samples by independent spectroscopic assays.

A possible disadvantage of fluorine resonances as pH probes may be their sensitivity to internal magnetic field gradients, since the magnetic dipole moments of fluorine and protons are similar. Another potential problem is that these compounds are foreign to living systems and may thus interfere with the metabolic processes they are designed to study. It will be necessary to carry out independent assessments of the metabolic state of the system before results obtained by fluorine probes can be accepted as representing the unperturbed *in vivo* state. Even given these problems, however, the high signal-to-noise ratio intrinsic to ^{19}F NMR makes such compounds an attractive option.

3. *Lanthanide shift reagents for metal cations*

A number of complex anions containing paramagnetic lanthanides bind reversibly and rapidly to metal cations and cause substantial shifts in their resonance frequency. With these anionic shift reagents in the external compartment it is possible to resolve the internal and external resonances of the physiologically important cations $^{7}Li^{+}$, $^{23}Na^{+}$ and $^{39}K^{+}$. The characteristics of these shift reagents have been reviewed[44] and Table 5 is adapted from ref. 44. Of course, the shift reagent must not penetrate the cell or vesicle membrane or adversely affect the metabolism of living cells. The reagents in Table 5 have been chosen to avoid these problems as far as possible, but a number of recent studies have drawn attention to other factors which may

TABLE 5

Anionic shift reagents[a] (taken from ref. 44, Table 2).

Shift reagent	Acid anion	Ref.
$[Dy(PPP)_2]^{7-}$	Tripolyphosphate $(P_3O_{10})^{5-}$	19, 79, 80
$[Dy(DPA)_3]^{3-}$	Dipicolinate	81, 82
$[Dy(NTA)_2]^{3-}$	Nitrilotriacetate $[N(CH_2COO)_3]^{3-}$	82
$[Dy(CA)_3]^{6-}$	Chelidamate	83
$[Dy(THHA)]^{3-}$	Triethylenetetraminehexa-acetate $[(OOCCH_2)_2N(CH_2)_2N(CH_2)_2N(CH_2)_2N(CH_2COO)_2]^{6-}$ (with CH_2COO CH_2COO)	84
$[Dy(EDTA)_2]^{5-}$	Ethylenediaminetetra-acetate	85

[a] Thalium analogues of several of these complexes have also been used.[83, 84] The shifts induced by thalium complexes are smaller in magnitude and opposite in sign to the dysprosium-induced shifts.

limit their effectiveness in some systems. For example, the tripolyphosphate anion is readily degraded by phosphatases which may be present in living systems[6] and the free dysprosium ions can then leak into the cell.[180] The tripolyphosphate anion can also chelate extracellar Ca^{2+} and so perturb the system.[86] Agitation of the cell suspension can cause leakage of the shift reagent.[87] Care must be taken when using the integrated intracellular peak intensities to measure ion concentrations inside cells or tissues. ^{23}Na and ^{39}K are spin 3/2 nuclei and the nuclear quadrupolar interaction can have a profound effect on resonance lineshapes. For example, in the case of fast exchange between a very small immobilized pool and a large free pool 60% of the intensity will be broadened beyond detection so that the intensity of the observed intracellular ^{23}Na or ^{39}K resonance is only expected to correspond to 40% of the total cation content.[88, 89]. It is generally necessary to calibrate the peak intensities before the intensities are used to measure intracellular ion concentrations and transport.

Table 6 lists some papers reporting measurements of the slow transport of metal ions across lipid membranes using anionic shift reagents. Space does not permit a detailed review of all of these reports, but representative examples will be considered briefly.

Because of the importance of alcohol-induced changes in electrolyte handling in the kidneys, Elgavish and Elgavish[85] undertook a study on the effect of small doses of alcohol on sodium transport across large unilamellar vesicles of both egg L-α-lecithin and of brush border membrane vesicles isolated from the rat kidney cortex. The vesicles were loaded with 100 mM NaCl and the external medium contained 100 mM LiCl and only 0.5 mM NaCl. $[Dy(EDTA)_2]^{5-}$ was used to shift the outer sodium resonance. In the

TABLE 6

NMR transport studies using anionic shift reagents.

System	Nucleus	Mediator or inhibitor	Shift reagent	Ref.
Large unilamellar vesicles (LUV)	^{23}Na	Ethanol	$[Dy(EDTA)_2]^{5-}$	85
LUV	^{23}Na	Valinomycin	$[Dy(NTA)_2]^{3-}$	90
LUV	^{23}Na, ^{39}K, ^{7}Li	Ionophores	$[Dy(DPA)_3]^{3-}$	81
LUV	^{23}NA	Gramicidin	$[Dy(NTA)_2]^{3-}$	91
LUV	^{23}Na	Gramicidin	$[Dy(PPP)_2]^{7-}$	92
Human erythrocytes	^{23}Na, ^{39}K	Ouabain, Gramicidin	$[Dy(PPP)_2]^{7-}$	93
Human erythrocytes	^{23}Na, ^{39}K, ^{31}P, ^{35}Cl	Lasalocid A	$[Dy(PPP)_2]^{7-}$	94
Human erythrocytes (uremic)	^{23}Na	Ouabain	$[Dy(PPP)_2]^{7-}$	95
Human erythrocytes	^{7}Li	None	$[Dy(PPP)_2]^{7-}$	10, 96, 239
Hypertensive rat erythrocytes	^{23}Na, ^{31}P	Ouabain	$[Dy(TTHA)]^{3-}$	209
Millet cells (*Panicum miliaceum*)	^{23}Na	None	$[Dy(PPP)_2]^{7-}$	96
Yeast	^{23}Na, ^{7}Li	None	$[Dy(NTA)_2]^{3-}$	52, 69, 90, 97
Amoeba (*Dictyostelium discoideum*)	^{23}Na	Nystatin	$[Dy(PPP)_2]^{7-}$	6
Perfused frog heart	^{23}Na, ^{39}K, ^{7}Li	None	$[Dy(PPP)_2]^{7-}$	98
Rabbit proximal tubule	^{23}Na	Ouabain	$[Dy(PPP)_2]^{7-}$	86, 99
Perfused rat mandibular gland	^{23}Na	Acetylcholine	$[Dy(TTHA)]^{3-}$	100
Perfused rat heart	^{23}Na, ^{39}K	Ouabain	$[Dy(TTHA)]^{3-}$	101
Corn root tips	^{23}Na, ^{31}P	None	$[Dy(PPP)_2]^{7-}$	60
Human lenses from patients with cataracts	^{23}Na	None	$[Dy(PPP)_2]^{7-}$	14

absence of alcohol there was no detectable sodium transport out of the egg lecithin vesicles. A concentration of 0.1% alcohol allowed equilibrium of the sodium concentrations after 100 min. A similar effect was found in the amiloride-insensitive pathways in the renal brush border vesicles. It was suggested that the alcohol alters the membrane structure and increases the quantity of an isotropic, possibly inverted, micellar component of the membrane which is instrumental in the sodium transport. ^{31}P NMR spectra of the membrane were used to support this contention. Future work might involve quantitative modelling of the transport fluxes as a function of cation concentration gradient and alcohol concentration.

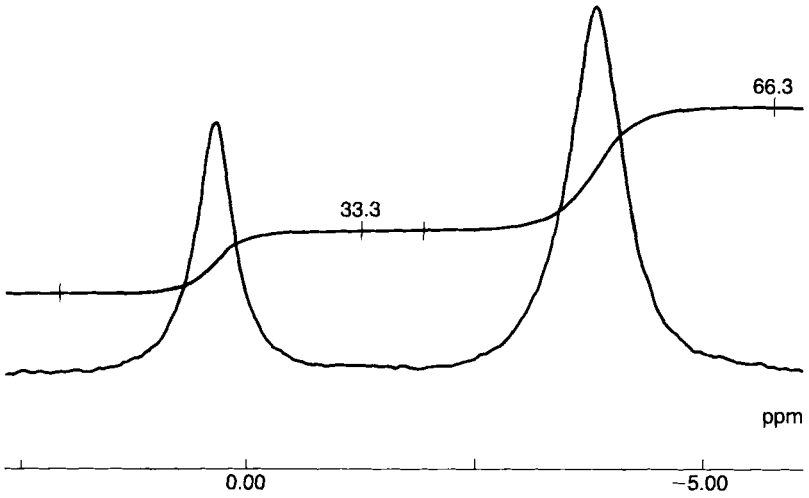

FIG. 1. ^{7}Li NMR spectrum of erythrocytes incubated at 37°C for 24 h in plasma containing 50.0 mM LiCl. 5.0 mM dysprosium:tripolyphosphate shift reagent was added just before the experiment. The number of scans is 100. Taken from Pettegrew *et al.* (1987), ref. 10.

Lithium transport into human erythrocytes has been studied using $^{7}Li^{+}$ NMR by Pettegrew and co-workers.[10] This study was motivated by the demonstrated efficacy of lithium ions in the prophylactic treatment of manic depressive illness. Figure 1 shows a representative spectrum where the inner and outer lithium resonances are clearly resolved. Figure 2 shows the single exponential time-course for lithium uptake. A time constant of 14.7 ± 1.2 h was found, showing that the transport is very slow. Comparative studies on the effect of ionophores or drugs such as oubain which inhibits the Na^{+}-K^{+} pump on lithium transport were not undertaken in this exploratory report, which focused attention primarily on the interpretation of the intracellular lithium T_1 and T_2 relaxation times. It remains to be investigated whether the lithium transport pathway is via the Na^{+}-Li^{+} countertransport system, the (Na^{+},K^{+})-ATPase pathway, or by some other enzyme system.

In a recent study[94] a multinuclear approach was used to monitor the ion fluxes through erythrocyte membranes. ^{23}Na and ^{39}K NMR with a shift reagent were used to follow the ion fluxes after addition of the ionophore lasalocid A. ^{35}Cl NMR was also used to follow the transport of chloride (see Section IV.A), while ^{31}P was used to check the energy status of the cells. An interesting aspect of this work was the use of the Na^{+} chemical shift as an indicator of the extracellular potassium concentration. Both potassium and sodium compete for the $[Dy(PPP)_2]^{7-}$ shift reagent so that the sodium shift depends on the potassium concentration. Other ions, including Mg^{2+} and

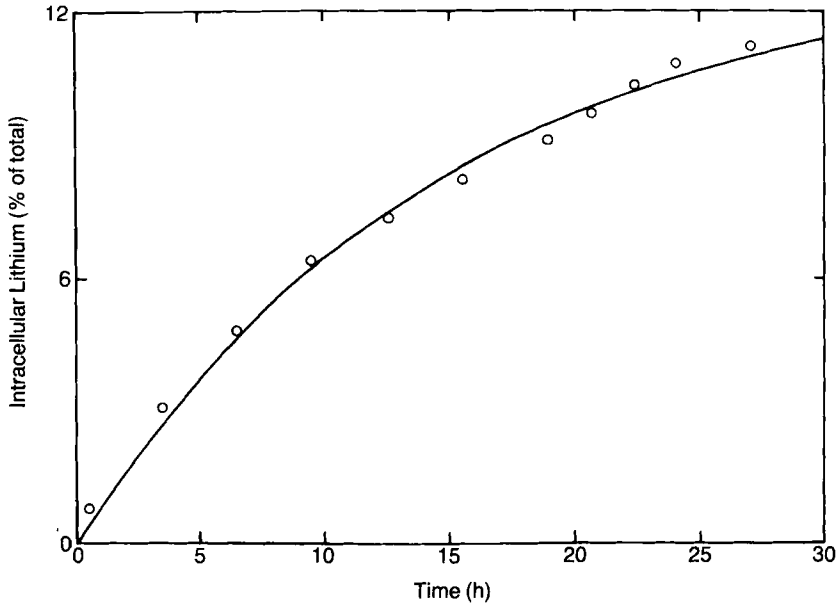

FIG. 2. Plot of the intracellular Li^+ content as a function of time, t(h), for erythrocytes incubated with 50 mM LiCl at 25°C. The intracellular Li^+ concentration is expressed as a percentage of the total lithium concentration. The data are fitted with the function $y = A[1-\exp(-x/k_t)]$, which yields a time constant $k_t = 14.7 \pm 1.2$ h. Taken from Pettegrew *et al.* (1987), ref. 10.

Ca^{2+}, compete with sodium and cause shifts, so this might be a useful indirect way of following the ion fluxes.

Table 6 includes a number of perfused whole organ studies where intracellular and extracellular ion concentrations were separated with a shift reagent in the perfusate allowing the time-course of *in vivo* transmembrane ion fluxes to be investigated under a variety of pharmacological and physiological interventions. Such NMR investigations have recently become important in physiological and medical research. The apparatus for perfusion of isolated frog hearts is shown in ref. 98. Intracellular sodium, potassium and lithium concentrations were observed and the time-course of the intracellular sodium level was monitored during:

(1) the addition of 10 μM ouabain to inhibit the Na^+-K^+ pump;
(2) the perfusion with zero-potassium, low calcium perfusate;
(3) replacement of two-thirds of the sodium in the perfusate with lithium; and

(4) variation of the pacing rates of the heart (which was externally stimulated).

In these exploratory experiments no attempt at quantitative modelling of the observed changes in terms of membrane fluxes was made. An exciting possibility for future work is the application of localized spectroscopic techniques to these perfused organ studies. This may allow the observation of local changes in intracellular ion content in the organ.

4. Other chemical shift indicators for metal ions

Just as the binding of protons shifts the ^{31}P resonance of phosphate or the ^{19}F resonance in Fquene and provides a method for measuring pH_{in} and proton transport, so the binding of metal ions can shift the resonances of suitable ligands and provide a method for measuring metal ion concentrations (p M) and metal ion transport. This approach is especially valuable for ions such as Ca^{2+} and Mg^{2+} which play an important physiological role and yet have a very low nuclear receptivity, making direct observation by ^{43}Ca or ^{25}Mg NMR at physiological concentrations difficult if not impossible.

The general specification for an ideal spectroscopic indicator of cytosolic free M^{n+} would include the following characteristics:[1]

(a) The indicator should bind only M^{n+} in the presence of physiological concentrations of other cations, with an apparent dissociation constant for M^{n+} close to the normal $[M^{n+}]_i$.
(b) The spectroscopic properties of the indicator should be very sensitive to M^{n+} binding and provide direct identification of the metal ion.
(c) The kinetics of M^{n+} binding to the indicator should not be rate limiting in following the time-course of changes in $[M^{n+}]_i$.
(d) The indicator should not itself perturb $[M^{n+}]_i$ or normal cellular functions and responses or add significantly to the cytosolic buffering capacity for M^{n+}.

Considerable progress has been made in meeting these criteria for Ca^{2+}, Mg^{2+} and Na^+ indicators. The first Ca^{2+} indicator was reported by a research group in Cambridge who have pioneered this approach.[1,102] It is based on the shift of the ^{19}F resonance in symmetrically substituted difluoro derivatives of 1,2 bis-(*o*-aminophenoxy)ethane-*N*,*N*,*N'*,*N'*-tetra-acetic acid (*n*FBAPTA), where *n* denotes the position of the fluorine atom. The free and bound forms of 3FBAPTA and 5FBAPTA complexes with Ca^{2+} were in slow exchange, whereas for 4FBAPTA the two forms were in fast exchange on the NMR timescale. The shift of the fast-exchange-averaged 4FBAPTA complex gives an accessible $[Ca^{2+}]$ range of 300 nM to 30 μM and is insensitive to Mg^{2+} and

pH. Measurement of the relative areas of the slow exchanging 5FBAPTA resonances enabled the calcium concentration in mouse thymocytes to be estimated as 250 nM. Selective compartmentation of the indicators can be achieved by introducing them into the cells as their membrane-permeable acetoxymethyl esters, which are subsequently hydrolysed inside the cells by natural esterases, generating and trapping the impermeable carboxylate form of the indicator inside the cells. The line broadening of Ca 5FBAPTA and free 5FBAPTA gives a dissociation rate for Ca^{2+}-5FBAPTA complexes of $5.7 \times 10^2\ s^{-1}$ and a forward rate constant of $8.1 \times 10^8\ s^{-1}$. This sets a limit of approximately 10 ms to the response time for $[Ca^{2+}]$ changes, which is sufficiently fast to follow most Ca^{2+} signals in cells.

In Table 7 we have listed a number of experiments where changes in the internal calcium ion concentration has been determined using 5FBAPTA following the addition of physiologically active compounds such as mitogenic stimulants (ConA) or ionophores to the external medium. The success of these preliminary studies opens up many exciting future possibilities.

The fluorine-cryptanol derivative FCryp-1 has recently been shown to have appropriate properties as an indicator of intracellular free sodium[106] and has been used to estimate the free sodium content in pig lymphocytes as 13.8 mM. However, the method has not yet been used for time-resolved transport measurements.

The intracellular level of free Mg^{2+} is of fundamental importance since it may regulate the activity of enzyme systems requiring this metal ion, includ-

TABLE 7

Use of metal ion indicators in time-course experiments.

System	Cellular perturbation	Metal ion	Indicator	Ref.
Mouse thymocytes	Addition of succinylated ConA and ionophore A23187	Ca^{2+}	5FBAPTA	1, 102
Ehrlich ascites tumour cells	Serum addition	Ca^{2+}	5FBAPTA	1
Rat basophile leukaemic (2H3) cells	Antigen (ovalbumin)	Ca^{2+}	5FBAPTA	1
Human erythrocytes	Ionophore A23187	Ca^{2+}	5FBAPTA	103
Perfused rat heart	Adrenaline, D600 and external calcium	Ca^{2+}	5FBAPTA	1
Perfused ferret heart	Heart beats	Ca^{2+}, Mg^{2+}	5FBAPTA(Ca^{2+}) (+)fluorocitrate (Mg^{2+})	104, 105

ing membrane transport proteins. There is evidence that Ca^{2+} transport may be influenced by Mg^{2+} in some systems.[107] Only very recently has a fluorine shift complexing indicator been developed for magnesium.[104,105] This is the non-toxic (+) isomer of fluorocitrate which is loaded as its acetoxymethyl ester and has a K_D for magnesium of 0.84 mM at 37°C. So far it has only been used to monitor magnesium transients in beating, perfused ferret heart, but many other applications are to be anticipated. The chemical shift separation between the α and β ^{31}P resonances of ATP are sensitive to Mg^{2+} concentration and this, together with knowledge of the dissociation constant of $(MgATP)^{2-}$, has enabled the determination of free magnesium in a variety of cells and tissues.[108-112] Whether this method can also be used to monitor the time-course of magnesium transients remains to be investigated.

5. *Shift reagents for protons*

There are only two reports where paramagnetic metal cations have been used to shift proton resonances and determine membrane transport. The first report, made by Fritz and Swift in 1967, used $Co^{2+}{}_{aq}$ ions in the external medium to separate the contributions from intracellular and extracellular water in ^1H spectra of frog nerves.[113] The success of this experiment depends on the impermeability of the cell membrane to cobalt and the relatively slow exchange of water between the two compartments. It is surprising that no further work using water proton shift reagents has been reported since 1967. Fritz and Swift used a continuous wave spectrometer operating at 60 MHz and the induced shift was small (13.6 Hz). With a 400 or 500 MHz spectrometer the splitting should be more easily resolved, though increased field gradient effects might also spoil the resolution. An alternative shift reagent which might be considered is $[Dy(en)]^{3+}$ (en = ethylenediamine). This gives a water proton shift of 0.11 ppm mM^{-1} and is temperature independent between 3°C and 25°C.[114] Naritomi *et al.*[115] also report that the anionic shift reagent $[Dy(TTHA)]^{3-}$ gives a resolvable shift of intra- and extracellular water in brain and muscle tissue. However, no transport measurements have been undertaken. If water transport is sufficiently slow to allow it to be followed from inner and outer peak intensities this method would, in principle, enable measurement of P_f, the osmotic or filtration water permeability coefficient, in contrast to the tracer permeability coefficient determined by lineshape analysis (Section III.B) or by NMR relaxation methods (see Section IV).

In 1979 Alger and Prestegard[116] used a similar approach with Pr^{3+} to resolve the internal and external acetic acid resonances and study its transport across vesicle membranes. Whether this approach could be used for other organic anions (including amino-acids) has yet to be explored. Possible limitations on the general use of lanthanide cations as shift reagents for

organic compounds are: (1) unless the pH is slightly acid the ions readily hydrolyse and precipitate as complex hydroxides; and (2) at high concentrations they tend to aggregate vesicle suspensions.

B. Exchange rates from spectral lineshape analysis

If the transport across the membrane is fast compared to the time required to acquire the NMR spectrum (typically a few seconds), it is not possible to follow the time-course of the changing peak intensities. However, the exchange rate can still be measured from the dynamic effect of the exchange on the NMR spectral lineshape in the steady state. In this case the lineshape does not depend on the net flux, J (this will be zero in the steady state), but on the unidirectional (or tracer) fluxes due to diffusive exchange across the membrane. Thus experiments based on lineshape analysis measure an essentially equilibrium property in which the fluxes in either direction across the membrane are equal; whereas experiments based on intensity changes measure the rate of attainment of equilibrium from a situation in which there is an electrochemical potential difference across the membrane.

The simplest theoretical model relating the lineshape to the unidirectional flux assumes that the cell or vesicle exchange process is describable by the traditional equations for homogeneous, two-site chemical exchange.[117-119] The lineshape can then be used to calculate the mean lifetime (τ_{in}) of the molecule (or ion) in the vesicle or cell as well as the lifetime in the outer compartment (τ_{out}). The mean lifetimes are related to the unidirectional flux, $J^{(1)}$, since $1/\tau_i = AJ^{(1)}/V_i c$, where V_i is the volume of the compartment i, τ_i is the mean lifetime in the compartment i, A is the membrane area and c is the concentration of transporting material (equal in both compartments). Alternatively we can relate the lifetimes to the effective permeability coefficient, P, since $J^{(1)} = Pc$ so that $1/\tau_i = AP/V_i$. One of the many transport models can then be used to relate $J^{(1)}$ (or P) to rate constants describing the membrane transport process.[22-24] For example, for the carrier-mediated model.

$$J^{(1)} = \frac{k_{diff} k_b [L]_T c}{(k_b + 2k_{diff})(c + (k_b/k_f))} \tag{2}$$

where k_{diff} is the first-order transinterfacial jump rate, k_f and k_b are the rate constants for the formation and the breakdown of the carrier–substrate complex, and $[L]_T$ is the total carrier concentration in the membrane.

Table 8 lists some NMR transport studies involving spectral lineshape analysis. One of the first quantitative determinations of exchange rates (actually permeation coefficients) from a total lineshape analysis (TLA) was reported by Alger and Prestegard in 1979.[116] They studied the fast exchange of acetic acid across large unilamellar vesicles (LUV) with Pr^{3+} in the outer

TABLE 8

NMR transport studies using spectral lineshape analysis.

System	Nucleus	Mediator or inhibitor	Shift reagent	Ref.
LUV	^{1}H (acetic acid)	None	Pr^{3+}	116
Thylakoid membranes	^{1}H (water)	None	$[Dy(en)]^{3+}$	114
LUV	^{23}Na	Lasalocid A	$[Dy(NTA)_2]^{3-}$	90
LUV	^{23}Na	Monensin	$[Dy(PPP)_2]^{7-}$	5
LUV	^{23}Na, ^{39}K	Nigericin	$[Dy(PPP)_2]^{7-}$	120
LUV	^{23}Na	Gramicidin	$[Dy(PPP)_2]^{7-}$	92

compartment to resolve the ^{1}H acetic acid resonances at pH 5.5. At 7°C the exchange was slow and gave two resolved resonances, but as the temperature was raised to 65°C the peaks coalesced to a single resonance. Total lineshape analysis gave an inside compartment lifetime varying from 15 ms at 7°C to 2.5 ms at 65°C. The observed average activation energy was 10 ± 4 kcal mol^{-1}. No attempt was made to relate the lifetimes to models for the membrane transport.

A related method was used by Sharp and Yocum in 1980[114] to measure the very fast exchange of water across intact thylakoid membranes. They used $[Dy(en)]^{3+}$ (en = ethylenediamine) as a shift reagent for water protons and used analytical solutions of the general two-site chemical exchange equations to derive the mean lifetime of water inside the thylakaloids from the lineshape changes observed as increasing aliquots of shift reagent were added to the external medium. As an independent check on the results they also calculated the exchange rate from the τ dependence of the transverse relaxation rate (T_2^{-1}) measured with the CPMG pulse sequence, (see Section III.C). Values for the mean lifetime as short as 1.1 ms at 25°C were observed. It is surprising that this method has not been more extensively applied to determine fast water exchange times in other systems such as erythrocytes.

Since this pioneering work there have been few attempts at quantitative TLC. Balschi and co-workers[90] reported that addition of the anionic ionophore lasalocid A (X-537A) to vesicle preparations where the inner and outer sodium peaks were separated with a shift reagent caused the inner sodium peak to broaden and, at higher lasolocid A concentrations, to coalesce with the outer resonance. Unfortunately no quantitative lineshape analysis was attempted. Riddell and Hayer[5] in their study of the monensin-mediated transport of sodium ions across egg phosphatidylcholine vesicles found that the inner sodium peak broadened linearly with increasing monensin concentration and narrowed with increasing sodium concentration

as the carrier became saturated. A total lineshape analysis was not necessary in this case since the exchange lifetime (τ_{in}) is simply π x (the excess line broadening due to exchange). This simple relationship pertains whenever the exchange is sufficiently slow that the peaks are well separated, yet fast enough to cause perceptible broadening. It assumes that the peak lineshapes remain Lorentzian, which for quadrupolar ions such as sodium ($I = 3/2$) requires that the extreme narrowing conditions hold in each compartment. As is often the case, the intracellular or intravesicular volume is much less than the external volume, with the result that only the inside peak is broadened since the exchange of a very small fraction of the external nuclei leaves its width essentially unaffected. Buster *et al.*[92] have recently reported the broadening of the inner sodium peak with increasing concentrations of gramicidin D incorporated by heating into LUVs. In this case the mean lifetime ($1/\tau_{in}$) increased linearly with the square of the gramicidin concentration, which is consistent with formation of channels by dimers of gramicidin. Unfortunately no attempt was made to interpret the lifetime data in terms of models for the channel transport, despite the fact that Urry *et al.* have already extensively characterized sodium–gramicidin transport using a two-site kinetic model and NMR binding studies (see Section VII). In another study on the nigericin-mediated transport of sodium and potassium, Riddell and co-workers[120] not only determined the exchange lifetime (τ_{in}) but also interpreted its dependence on nigericin concentration using a model for carrier-mediated transport (equation (2)). It was argued that dissociation of the nigericin–metal ion complex (k_b) is the rate-determining step. This was tested by adding cholesterol to the membrane, which although "stiffening" the membrane, did not alter the exchange rate significantly.

An important problem in the use of NMR exchange data to test models of membrane transport is that the membrane exchange experiments do not determine uniquely all the required rate constants. In order to do this it is necessary to combine them with other experiments to determine reaction rates within the membrane. This may be accomplished by the use of micellar suspensions. For example, the relaxation times of the ions in micellar suspensions containing the carrier can give the rate constants for the formation (k_f) and breakdown (k_b) of the carrier–ion complex. With knowledge of these, k_{diff}, the rate constant for interfacial diffusion (or jumping), can be deduced from the NMR transport measurements across vesicle membranes. Alternatively, values of k_f, k_b and k_{diff} can, in suitable circumstances, be obtained from electrical conductivity measurements across Black lipid membranes.[31-34] These can then be checked or complemented by the NMR method. The possibilities of exploiting a combination of approaches in this way are very promising. Unfortunately the monensin- and nigericin-mediated transport studied by Riddell and co-workers has not yet been

complemented by NMR micelle studies or by electrical conductivity measurements.

The simple theoretical approach outlined above relating the lineshape to the mean lifetime (τ) and then to the unidirectional flux, $J^{(1)}$, has a number of shortcomings. It takes no account of the effect of unstirred layers in the inner and outer fluid compartments on the observed spectrum. Such effects could be important in large cells with high membrane permeabilities such as plant cells. The spectral lineshape could then be diffusion limited and independent of the membrane transport rate. The decay of the magnetization within the membrane itself could be a significant broadening mechanism, especially for ions with large electric quadrupole moments binding reversibly to carriers. The simple two-site chemical exchange model takes no account of this.

The correct treatment of these problems requires a more general theoretical approach relating the observed lineshape to membrane transport models. Two recent theoretical papers have used the generalized Bloch–Torrey equations[121] to calculate the observed spectral lineshape. The first paper[122] dealt with the effects of diffusion through unstirred layers in the outer and inner fluid compartments on the spectrum. The Bloch–Torrey equations were solved for diffusive exchange between two compartments separated by a membrane of permeability P. The spins in each compartment (n) were characterized by a resonance frequency (w_n), intrinsic relaxation rate (γ_n) and diffusion coefficient (D_n). Exact analytical solutions for the spectrum were derived for the simplest morphology of two planar compartments of width a and b. Numerical methods could be used for more realistic morphologies.

A second theoretical paper[123] took account of the time evolution of the magnetization within the membrane by assigning the transport complex within the membrane its own chemical shift and intrinsic relaxation rate. These can be estimated from homogeneous solution or micelle studies. The paper also treated the morphological aspects consistently by explicitly calculating the fluxes of magnetization through the two interfaces between the membrane and the inner and outer aqueous compartments. The motion within the membrane was modelled using both diffusive and jump-type transport models. Although analytical lineshape expressions have only been derived for the case of planar compartments, it may be possible to obtain solutions for more realistic (spherical) morphologies using numerical methods. Experimentally, the significance of membrane relaxation could be determined using inversion recovery experiments along with lineshape analysis.

Quadrupolar effects are another complicating feature whose effects on the spectral lineshape have yet to be properly evaluated. All the metal cations of interest (Li, Na, K, Rb, Cs, Ca, Mg) have nuclear spin $I > \frac{1}{2}$ and have

electrical quadrupole moments which can give multiexponential relaxation.[89] However, the experimental results for Na^+ and K^+ so far reported suggest that the extreme motional narrowing condition pertains so that, at least in these cases, the metal ions can be treated as pseudo spin $-\frac{1}{2}$ systems. Ion transport through gramicidin channels is exceptional in that quadrupolar effects must be taken into account explicitly. This will be discussed in Section VII.

C. Exchange rates from CPMG studies

Measurements of fast reaction rates in homogeneous solutions using the Carr-Purcell-Gill-Meiboom (CPMG) technique are well documented.[124] The same technique can, of course, be applied to measure fast exchange rates between membrane-bound compartments. By fitting the observed dependence of the transverse relaxation rate (T_2^{-1}) on the delay time (t_{cp}) between the 90° and 180° pulses using, for example, the general two-site exchange analysis of Allerhand and Gutowsky,[125] it is possible to determine the mean lifetimes in the compartments. The only example of this approach so far reported is the determination of rapid water exchange across thylakoid membranes by Sharp and Yocum.[114] They used this method as an independent check on their lineshape fitting results referred to in the previous section.

Unfortunately magnetic field gradients generated at the membrane boundaries can also give rise to a t_{cp}-dependence in the observed relaxation rate. The field gradients become larger with increasing differences in bulk magnetic susceptibility generated by the paramagnetic shift reagent and with smaller radii of curvature of the membrane-bound compartment. Unless the magnetic susceptibility in the compartments is equalized there is no simple way to remove this complication. It would seem that the replacement of Dy^{3+} by an equal concentration of diamagnetic La^{3+} as a control, as suggested by Sharp and Yocum, would not completely remove this difference in magnetic susceptibility. Nevertheless, their results agreed with those obtained with total lineshape analysis.

D. Magnetization transfer methods

Since its introduction in 1963 by Forsen and Hoffman,[126,127] the double resonance methods of transfer of saturation and inversion recovery have been widely used to study relatively slow chemical exchange. Procedures for selectively inverting NMR resonances and analysis of the subsequent time evolution of intensities have been described.[128,129] However, the potential of double resonance methods in measuring membrane transport rates appears to have been largely neglected. Magnetization transfer complements the

method of total lineshape analysis (TLA, Section III.B). TLA is limited to observing fast exchange rates of the order of 10–100 ms because inherent linewidths in membrane preparations are often broad. In contrast, magnetization transfer methods are sensitive, not to short transverse relaxation times, but to longitudinal relaxation times which can be several seconds for small molecules. This means that magnetization transfer can monitor slower exchange rates than can TLA.

Alger and Prestegard[116] first used both magnetization transfer and TLA to quantify the exchange of acetic acid across LUV membranes. The acetic acid inner compartment lifetime at 7°C is 1 s at pH 6.9 and progressively decreases with pH to 0.01 s at pH 5.4. This was found to fit the relationship

$$\tau_{in} = \frac{1}{P_{HOAc}} \times \frac{V_{in}}{A}\left\{\frac{K_A}{[H^+]} + 1\right\} \quad \text{with } P_{HOAc} = 5 \pm 2 \times 10^{-4}\ \text{cm s}^{-1} \text{ at } 7°C \tag{3}$$

This assumes that only neutral acetic acid molecules can permeate the membrane. A stacked plot showing their magnetization transfer data is shown in Fig. 3 (reproduced with permission from ref. 116).

In Table 9 we have listed some other transport studies which use magnetization transfer. McCain and Markley[131] measured the *in vivo* water permeability of chloroplast envelope membranes in tulip tree leaves. Here the chloroplast water gave an orientation-dependent shoulder to the high field of the isotropic signal from water in the cytoplasm, vacuole and extracellular water. The mean residence time of the water protons was calculated from the recovery of the spectrum following selective saturation of the chloroplast water peak. An effective permeability coefficient of $9 \pm 2 \times 10^{-4}$ cm s^{-1} was deduced.

In another recent paper, Kirk and Kuchel[133] used saturation recovery methods to measure the permeability of dimethyl methylphosphonate (DMMP) across erythrocyte membranes. DMMP gives two resonances corresponding to the intra- and extracellular compartments. The intracellular resonance was selectively saturated with a DANTE pulse sequence[134,135] and the resulting lowering in the extracellular resonance intensity was measured, ΔM^{out}. This is related to the extracellular lifetime (τ_{out}) using the two-site exchange model for which

$$\frac{1}{\tau_{out}} = \frac{\Delta M^{out}/M^{out}}{T_1^{out}(1 - (\Delta M^{out}/M^{out}))} \tag{4}$$

T_1^{out} was measured for the surrounding fluid after separating off the cells. M^{out} was obtained from a control experiment in which the saturating radiofrequency was applied downfield of the extracellular resonance. The

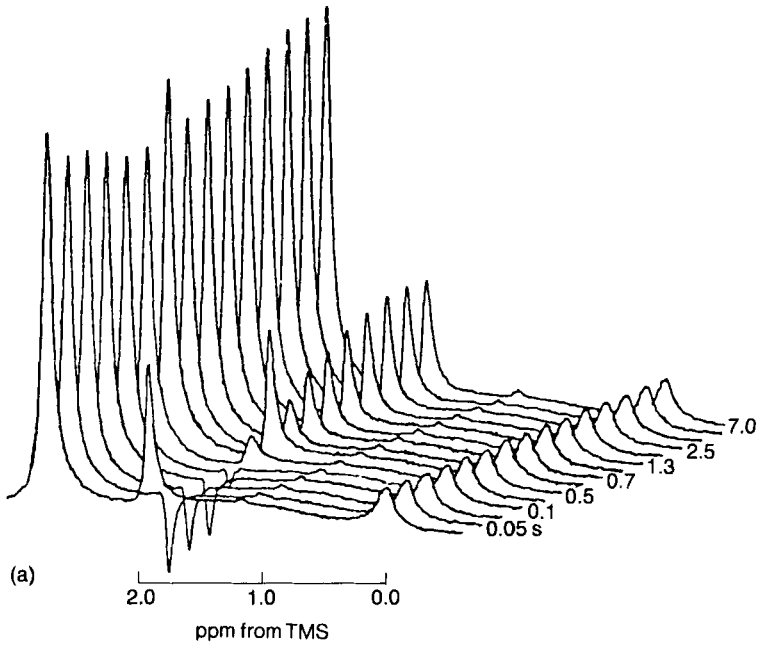
7.0
2.5
1.3
0.7
0.5
0.1
0.05 s
(a)
2.0
1.0
0.0
ppm from TMS

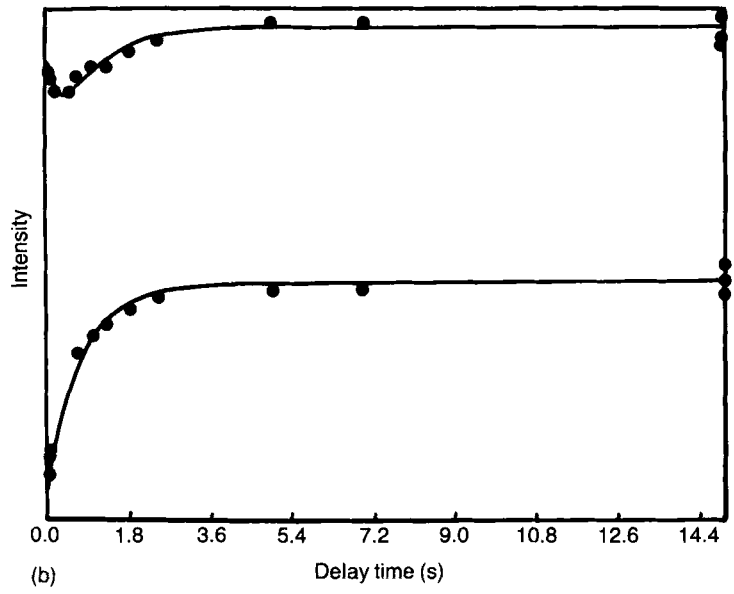
Intensity
0.0
1.8
3.6
5.4
7.2
9.0
10.8
12.6
14.4
(b)
Delay time (s)

TABLE 9

Transport studies using magnetization transfer.

System	Nucleus	Mediator	Ref.
Vesicles (LUV)	^{1}H (acetate)	None	116
Vesicles (LUV)	^{7}Li	Monensin	130
Vesicles (LUV)	^{23}Na	Gramicidin	92
Chloroplasts	$^{1}H(H_2O)$	None	131
Human erythrocytes	^{13}C (bicarbonate)	None	132
Human erythrocytes	^{31}P (dimethyl methylphosphonate)	None	133

membrane permeability coefficient $P\ (= V^{out}/\tau^{out}A)$ was found to be 1.1×10^{-4} cm s^{-1}. In a more recent paper Kuchel *et al.*[132] reported measurements of the rapid exchange of bicarbonate across human erythrocyte membranes using a saturation transfer technique. In this case, however, the inner and outer resonances were not resolved; instead the method relied on differences in chemical exchange rate between bicarbonate and CO_2 inside and outside the cell. ^{13}C NMR was used to resolve CO_2 and $HCO^{-}{}_3$ resonances but there was no chemical shift difference between the inside and outside compartments. This method is therefore limited to relatively few systems. Preliminary work has been reported on glucose exchange based on differences in the chemical exchange rate of the α- and β-anomeric forms inside and outside the cells.

E. Choline headgroup shift methods

The interaction between aqueous paramagnetic ions such as $Pr^{3+}{}_{aq}$ and $Eu^{3+}{}_{aq}$ with the phosphate sites on the phospholipid headgroups of lipid bilayer membranes causes a chemical shift in the headgroup resonances which can be observed in ^{1}H, ^{13}C and ^{31}P spectra. If vesicles are prepared with the paramagnetic ion localized in either the internal or external space the vesicle spectra show separate peaks from the internal and external headgroups. Vesicles prepared under these conditions are stable for long periods

FIG. 3(a) Stacked plot of selective population transfer ^{1}H 270 MHz spectra of a large unilamellar vesicle preparation, with the inner and outer acetate (methyl) peaks at 1.9 and 2.8 ppm respectively. 0.10 M NaOAc, pH 6.7, 7°C with 5 mM $Pr(NO_3)_3$ was used as shift reagent. Delay times appear to the right of every other spectrum. TMS, tetramethylsilane. Reproduced from ref. 116. (b) Comparison of observed relaxation and best fit simulation (solid line) for the stacked plot data in Fig. 3(a). Outside/inside resonances correspond to the upper/lower curves respectively. Reproduced from ref. 116.

and the membranes are impermeable to the lanthanide cations. However, if a pathway is introduced between the inside and outside compartments, e.g. by adding an ionophore, it is possible to model transmembrane cation transport by monitoring the time dependence of the internal and external boundary resonances.

Unfortunately the method is restricted to model vesicle systems because useful boundary signals are not generally detected in cellular systems. It is also restricted to the transport of paramagnetic ions, whose permeation rates may differ from those of the biologically important cations such as Ca^{2+} and Mg^{2+}. Nevertheless the method has an advantage over other NMR methods in allowing a clear experimental distinction between processes that allow the ions to enter the vesicles singly (such as via a diffusive carrier) and those in which the ions enter in large bursts (such as by pore activation). This aspect was first analysed theoretically by Springer and co-workers[136] using both a continuous flow (diffusive) model and a stochastic flow model.

It was found that the time-course of the inner headgroup resonances exhibits three qualitatively different types of behaviour. The first is an "all-or-nothing" process in which there are only two kinds of vesicle: those that have the equilibrium number of paramagnetic ions and those that have transported none. The intensity of the inner resonance decreases but its chemical shift and linewidth remain unchanged. This is shown in Fig. 4a, which is reproduced from ref. 136. This behaviour is exemplified by ion transport mediated by ultrasonic irradiation (which causes vesicles to disintegrate and re-form) or by the operation of an efficient "pore" mechanism. It has been observed for thermally induced transport by cycling through the gel to liquid-crystal phase transition in bilayers containing cholesterol or hexadecane,[137] as well as in bilayers containing Triton X-100.[138] Large amounts of phytanic acid, vitamin E or phytol[139] also give similar "all-or-nothing" behaviour.

A slightly less efficient pore can give rise to a "something-or-nothing" process. As time progresses new peaks arise corresponding to vesicles which have suffered none, one, two, etc. transport events or pulses. The various spectral lines do not shift with time but only change intensities, giving the appearance of "standing waves". This is depicted in Fig. 4b and has been observed for the chenodeoxycholate-mediated transport of Pr^{3+} into cholesterol-containing DPL vesicles.[140] Small vesicles formed by sonication favour the observation of this "something-or-nothing" behaviour. Discrete peaks will only be seen if the exchange of the mediator between different vesicles is slow. If it is not, the discrete nature of the peaks in Fig. 4b will be lost and the intermediate time spectra will show broadening (Fig. 4c). An example of intermediate broadening has been reported by Pierce and co-workers[141] for nystatin-mediated Pr^{3+} translocation into small vesicles.

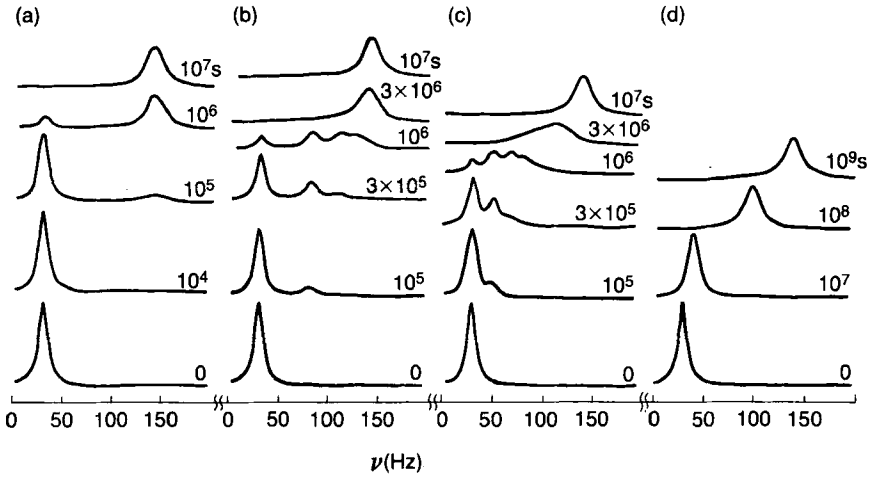

FIG. 4. Simulated time evolutions of inner headgroup NMR spectra. Taken from Ting *et al.*, ref. 136.

The most commonly found behaviour occurs when there is a "slow leakage" process such as a diffuse ionophore-mediated ion transport. For this, the inner headgroup resonance will move along the chemical shift scale in such small jumps that its motion appears continuous. This is shown in Fig. 4d.

The literature based on this method was reviewed by Springer and coworkers[136] in 1981. Table 10 extends their review by including several more recent reports.

Unlike the lanthanide ions Pr^{3+}, Dy^{3+} or Eu^{3+}, manganese ions cause relaxation broadening of the lipid headgroups. Small unilamellar vesicles prepared by sonication have an internal radius of only about 75 Å so that the transport of a single manganese ion produces an internal concentration of approximately 1 mM. This concentration is high enough to broaden substantially the ^1H NMR signal to the extent that it is not observable. The observed ^1H NMR signal thus arises predominantly from those vesicles that have no manganese ions in the intravesicular space. As manganese ions are transported into the vesicles the signal decreases in intensity but does not broaden. This allows a determination of the permeability coefficient for Mn^{2+}.[2,147,148]

To avoid the development of diffusion potentials the vesicles are usually prepared by sonication in the presence of a diamagnetic lanthanide ion. The paramagnetic lanthanide is added to one compartment and the concentrations adjusted to give equal total lanthanide concentrations on both sides of the membrane.

TABLE 10

List of transport studies based on choline headgroup shifts.

Metal ion transported	Mediator	Lipid[a]	Nucleus	Ref.
Pr^{3+}	Lasalocid A	Lecithin	^{1}H	142
Pr^{3+}	Lasalocid A and calcimycin	DPL	^{1}H	143
Pr^{3+}	Lasalocid A	DPL	^{1}H	144
Pr^{3+}	Mixtures of lasalocid A, monensin, etheromycin	Lecithin	^{31}P	145
Pr^{3+}, Nd^{3+}, Eu^{3+}	Lasalocid A and calcimycin	DML, DPL	^{1}H	146
Mn^{2+}	Lasalocid A	Lecithin	^{1}H	147
Mn^{2+}	Lasalocid A	DPL	^{1}H	148
Mn^{2+}	Angiotensin II	Lecithin	^{1}H	2
Pr^{3+}	Etheromycin and polyether ligands	Lecithin	^{31}P	149
Pr^{3+}	Alamethicin 30 and lasalocid A	Lecithin	^{1}H	150
Eu^{3+}	Alamethicin	DPL	^{1}H	151, 152
Pr^{3+}	Positive cooperativity of two ionophores	Lecithin	^{31}P	153
Pr^{3+}	Ethanol, ether, chloroform	Lecithin	^{1}H	3
Pr^{3+}	Organophosphate insecticide GA41	Lecithin + cardiolipin	^{1}H, ^{31}P	154
Pr^{3+}	Lysolecithin	EL	^{1}H	155
Eu^{3+}	Lysolecithin	DPL and DML	^{1}H	156
Eu^{3+}	Ultrasonic irradiation	EL	^{31}P	157
Eu^{3+}	Ultrasonic irradiation	DPL and DSL	^{1}H	158
Pr^{3+}	Ultrasonic irradiation	DPL	^{31}P	159
Eu^{3+}, Nd^{3+}	Thermal	DSL, DPL, DML and DLL	^{1}H	242
Pr^{3+}	Thermal with cholesterol Thermal with hexadecane	DPL	^{1}H	137
Pr^{3+}	Phytanic acid, vitamin E, phytol	EL	^{31}P, ^{13}C	139
Eu^{3+}	Rhodopsin	EL	^{1}H	160
Pr^{3+}	Nystatin, Triton X-100	EL, DCP, Sterol	^{31}P	141
Dy^{3+}	Glycophorin	DOL	^{13}C	161
Pr^{3+}	Bile salts	DPL	^{1}H	140
Pr^{3+}	Triton X-100, taurocholate, Thermal	DPL	^{1}H	138
Pr^{3+}	Phosphatidic acid, alamethicin, melittin, nystatin	EL, DPL	^{1}H	162

[a]Key: EL, egg lecithin; DPL, dipalmitoyllecithin; DML, dimyristoyllecithin; DSL, distearoyllecithin; DLL, dilauroyllecithin; DCP, dicetyl phosphate; DOL, dioleoyllecithin.

If there are no intravesicular diamagnetic lanthanide ions transport must be associated either with the symport of anions or the antiport of cations to maintain charge neutrally. Under these conditions lasalocid A and etheromycin, which have carboxylic acid groups, have been shown to antiport protons[149] which led to an acidification of the external medium.[66] Neutral ionophores which could not transport protons were much less effective as ionophores unless used in conjunction with an uncoupler molecule such as picric acid which serves to antiport protons. In the most recent study reported[146] it was shown that the rates of transport of Pr^{3+}, Nd^{3+} and Eu^{3+} by lasalocid A and calcimycin (A23187) were 5–10 orders of magnitude faster in the absence of intravesicular La^{3+} compared to the rates of transport observed in its presence. It was speculated that this was caused by the more rapid back-diffusion of the free carrier.

Although a variety of ionophores and transport mediators have been studied using this method (Table 10), membrane proteins are conspicuously absent. This is surprising since reconstitutions of active membrane proteins in vesicles have been successfully accomplished. The sensitivity of the method to the mechanism of ion transport makes it an attractive tool for such protein-mediated transport studies.

IV. METHODS BASED ON RELAXATION TIME DIFFERENCES

In the previous section differences in chemical shift were used to distinguish the NMR signals originating from spins in compartments either side of the membrane. In this section we will discuss the case where the spins are distinguished on the basis of their different intrinsic relaxation times. In many ways the two sections are analogous so our discussion will follow a similar order to that of Section III.

A. Peak intensity changes

If the transport is slow compared to the spectrum acquisition time and there are sufficiently large differences in the transverse relaxation times (T_2) between the inner and outer compartments, the transport can be monitored by adding the transported material to the external medium and following the time-course of the "inner" and "outer" peak intensities. Since we assume there are negligible chemical shift differences either side of the membrane, the "inner" and "outer" peak intensities correspond to the areas of the broad and narrow spectral components, or, equivalently in the time domain, to the amplitudes of the fast and slow decaying components in the free induction decay (FID). The difference in transverse relaxation time (T_2) between the compartments can be increased by selective addition of an impermeable, paramagnetic relaxation reagent (broadening probe) such as $Mn^{2+}{}_{aq}$,

$Mn(EDTA)^{2-}$ or Dextran-magnetite[241] to one of the compartments.

In practice there have been few reports so far where the transport has been sufficiently slow to allow the time-course of the influx (or efflux) to be followed by this method. One example is the slow transport of PEP across erythrocyte membranes.[40] Here sufficient $Mn^{2+}{}_{aq}$ was added to the external medium so that the external (^{31}P NMR) PEP signal was entirely eliminated (broadened into the baseline). The passage of PEP into the cell was followed from the increasing intensity of the inner, narrow component. Fluoride was added to inhibit glycolysis and allow observation of the accumulation of PEP inside the cells. When no fluoride is added the PEP was rapidly metabolized so that no signal could be detected.

A variation of this method which avoids the need to add concentrations of relaxation reagent so high that one signal is entirely eliminated was suggested by Degani and Elgavish in 1978.[163] Provided sufficient relaxation reagent is added to create observable broad and narrow components, the broad component can be essentially eliminated using the T_1-null method. This uses the pulse sequence $180°$–τ–$90°$ (FID) with τ fixed so that the fast decaying longitudinal magnetization has recovered to the null-point which occurs when $\tau = T_1^f \ln 2$, where T_1^f is the fast relaxing component. This essentially eliminates the fast relaxing outer component while the slow relaxing component is still inverted (Fig. 5).

If the transport is sufficiently slow the change in intensity of the inverted, inner signal can be followed in an influx experiment. So far there have been no reports using this approach (Degani and Elgavish[163] followed the line broadening since the transport was fast). In principle, slow influxes of alkali metal cations into cells (or vesicles) could be followed using this method using $Gd(EDTA)^-$, $La(PPP)_2^{7-}$ or $Lu(PPP)_2^{7-}$ as relaxation reagents.[243]

The slow transport of chloride ions across erythrocyte membranes has been followed using ^{35}Cl NMR intensity changes.[51,94] Here the intracellular $^{35}Cl^-$ resonance is intrinsically so broad as to be unobservable, so that the transport can be followed directly from the intensity of the remaining extracellular peak.

B. Relaxation time determinations of exchange rates

The mean exchange lifetime of water molecules in human erythrocytes is about 10 ms, so that peak intensity changes discussed in the previous section cannot be used to follow its transport. However there are several ways of using relaxation time measurements to determine such fast exchange rates and these will be discussed in this section. These methods have been developed primarily to measure water transport across human erythrocyte membranes, as this can have important clinical diagnostic value. Neverthe-

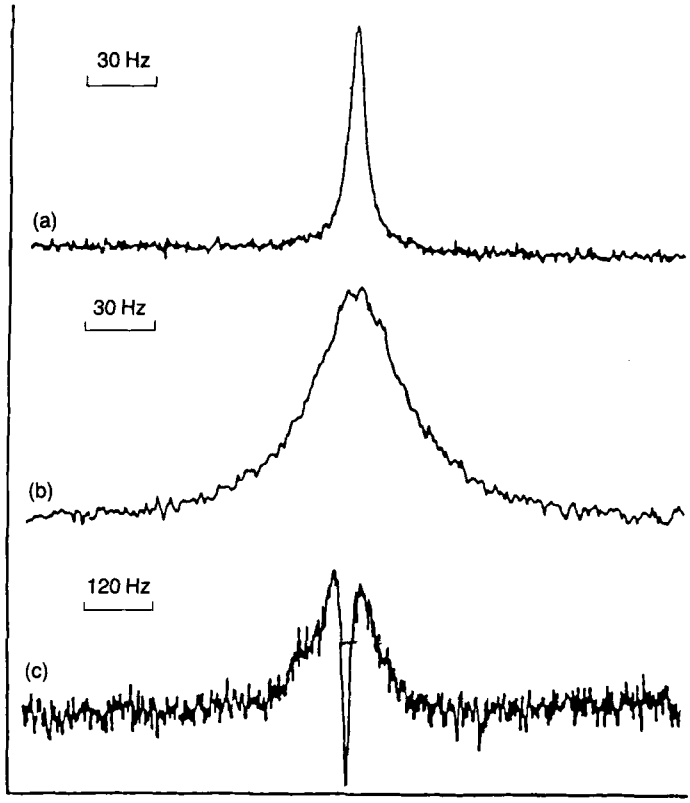

FIG. 5. ^{23}Na NMR spectra of: (a) 150 mM NaCl dissolved in phosphatidylcholine vesicle suspension pH 9.2 at 28°C; (b) the same as (a) after addition of 11.6 mM $Gd(EDTA)^-$; (c) the same as (b) using 180°-τ-90° pulse sequence in order to separate the inner and outer signals as explained in the text. Forty transients were accumulated in (a) and (b) and 4800 transients with τ = 4 ms in (c), with a recycle time of 1.1 s. Taken from Degani and Elgavish, ref. 163.

less they are not confined to this system. In Tables 11 and 12 we have collected a number of determinations of water transport in erythrocyte and non-erythrocyte systems respectively. Table 13 lists some applications to molecules other than water.

1. Transverse relaxation measurements

Stated in the most general terms, the fast exchange of a molecule (or ion) across cell (or vesicle) membranes can be determined by introducing a relaxation contrast reagent to one compartment (e.g. the outside medium) so that there is a difference in transverse relaxation times (T_2), and then deducing the

exchange rate from measurements of the decay of the transverse magnetization of the whole system. While this is experimentally straightforward, the extraction of a meaningful exchange rate from the decay data has been a source of theoretical difficulty. Here we will attempt to review some of the approximations used in the literature.

There are two common methods for observing the transverse relaxation and both have been used to measure exchange rates. The first, usually called the Hahn spin-echo, uses a simple ($90°_x$–τ–$180°_y$–echo) pulse sequence with a variable delay time τ. The echo height is plotted as a function of τ to give a decay curve. The second method uses the CPMG (Carr–Purcell–Meiboom–Gill) pulse train $90°_x$–[τ–$180°_y$–τ–echo–]$_n$ to measure the decay envelope of the echo amplitudes. As is well known, these two methods differ primarily in the dependence of the observed decay envelope on diffusion of the spins through magnetic field gradients within the sample.[197] In some transport experiments this can be an important distinction. For example deoxygenated erythrocytes contain paramagnetic deoxyhaemoglobin which can generate magnetic field gradients at the membrane boundaries.[198,199] Ignoring this complication for the moment, the decay curves for both Hahn and CPMG sequences will depend, in general, on: (a) the relaxation times of the compartments; (b) any chemical shift differences between the compartments; (c) on the morphology of the compartments and on the diffusion coefficients of the spins; (d) on the membrane permeability, P; and (e) on relaxation of the spins in the membrane. Unfortunately, a general thoretical treatment which incorporates all of these possibilities is not yet available. Nevertheless theoretical solutions for various limiting cases have been presented and to the extent that the experimental system approaches these limiting cases, meaningful membrane exchange rates can be extracted from the data.

The first and simplest limiting case was proposed by Conlon and Outhred[166] in 1972 for measuring water exchange across human erythrocyte membranes suspended in plasma doped with manganese. Sufficiently high concentrations of manganese were used (9.5–48 mM) to give a plasma relaxation time of less than 2 ms. Under these conditions it was reasoned that the relaxation of water molecules passing through the membrane into the plasma was so fast that the effects of field gradients, back-flux, incomplete diffusive averaging within the plasma and chemical shift differences could be ignored. The observed decay for either the Hahn or CPMG sequences is then biexponential, the fast decay component arising principally from the relaxation of the doped plasma and the slow decaying component with relaxation time T'_{2a} arising from the water inside the erythrocytes relaxing both intrinsically and by passage through the membrane into the plasma. The observed slow decay rate $(T'_{2a})^{-1}$ is then simply $(\tau_a^{-1} + T_{2a}^{-1})$, where τ_a is

the mean water lifetime in the erythrocyte and T_{2a} the intrinsic transverse relaxation time inside the erythrocytes, measured for packed cells suspended in plasma.

This level of approximation was subsequently critically evaluated in a number of papers. Morariu and Benga[165] suggested using a more accurate limit to the two-site chemical exchange equations such that $(T'_{2a})^{-1} = (T_{2a})^{-1} + P_b/(P_b\tau_a + T_{2b})$, where P_b is the population of plasma protons and T_{2b} their intrinsic relaxation rate. They suggested that this gave an improvement over the Conlon–Outhred method for erythrocytes. Pirkle *et al.*[167] and Fabry and Eisenstadt[179] believed that the high concentrations of manganese required by Conlon–Outhred altered the membrane permeability and led to errors ranging from 35–45% and suggested using much lower Mn^{2+} concentrations. They interpreted the CPMG decay data with the equations describing two-site chemical exchange in homogeneous solution,[119] of which the Conlon–Outhred expression is only an extreme limiting case.

Unfortunately, there are several other sources of systematic error which could be significant. These are: (a) the lack of complete diffusive averaging, including the back-flux of intracellular water, which could become significant at low manganese concentrations; (b) internally generated field gradients; (c) the Mn-induced chemical shift between cell and plasma water;[200] (d) Rouleaux formation;[175] and (e) the age of the blood.

From a theoretical viewpoint, the two-site chemical exchange equations referred to above do not strictly describe the Hahn or CPMG decays, even for homogeneous chemical exchange, since they fail to include the effect of varying τ. The exchange equations of Richards and Carver[124] would give a better description of the system, but even these equations do not include the effects of diffusion through two unstirred water compartments or through internally generated field gradients. The effect of Rouleau formation on the T_2 method has been nicely treated by Herbst and Goldstein[175] using a three-compartment exchange model which includes cell aggregation. However, from a practical view it is better to observe the water–erythrocyte system in dilute plasma or in artificial media where Rouleaux do not form, unless, of course, the kinetics of their formation is of prime interest.

Notwithstanding the problems of the interpretation and the absolute values of the exchange rates, the T_2 relaxation method is of value in comparative studies since large numbers of samples can be examined quickly. Table 11 shows that the effects of drugs, anaesthetics and cryoprotectants on erythrocyte–water transport have been examined. Significant differences between healthy and pathological subjects have been observed.[4,165] The effects of temperature, cell volume and osmolality have been investigated.

Many authors have explored the possibility of applying the Conlon–Outhred method to measure water transport in systems other than

TABLE 11

Water permeability measurements across human erythrocyte membranes using relaxation methods.

Effect of interest	Relaxation method	Ref.
Technique development	Proton T_2 (high Mn^{2+})	165, 166
Technique development	Proton T_2 (low Mn^{2+})	167
Membrane defect and human epilepsy	Proton T_2	11
Temperature and drugs	Proton T_2 (high Mn^{2+})	169, 170
Cell volume	Proton T_2 (high Mn^{2+})	171
Cryoprotectants (DNSO, Glycerol)	Proton T_2 (low Mn^{2+})	7
Osmolality	Proton T_2 and T_1	172
Cetiedil (anti-sickle cell drug)	Proton T_2 and ^{13}C	173
Procaine anaesthetic	Proton T_2 (low Mn^{2+})	174
Rouleau formation	Extension of Proton T_2 method	175
Dextran-magnetite as a relaxation agent	Proton T_2	176
Apparent thermal membrane transition	Proton T_2	174, 177
Osmolality cell volume and medium	Proton T_1, T_2 and T_{12} hybrid relaxation	178
Role of halothane anaesthetic	Proton T_1	4
Technique development	Proton T_1 and ^{17}O	179
Duchenne muscular dystrophy	Proton T_2	13
Effect of inhibitors and chemical modification	Proton T_2	181
Technique development	^{17}O	182

TABLE 12

Water permeability in non-erythrocyte systems by relaxation methods.

System	Relaxation method	Ref.
Dipalmitoyllecithin vesicles	Proton T_1 and T_2	183
Dipalmitoyllecithin vesicles	Proton T_1 and T_2, ^{17}O	184
Egg lecithin and cholesterol vesicles	^{17}O	185
Neoplastic mouse cells (Lettree cells)	Proton T_1	186
Halotolerant alga (*Dunaliella*)	Proton T_1 and ^{17}O	187
Giant algal cells (*Nitella mucronata*)	Proton T_2	188
Chlorella vulgaris cells	Proton T_1 and T_2	189
Friend leukaemia cells	^{17}O	12
Maize root	Proton T_1	191
Winter wheat cells following freeze-thaw injury	Proton T_2	192
Ivy bark	Proton T_2 and T_1	193
Elodea leaf	Proton T_2	30
Necturus gall bladder epithelial cells	Proton T_1	194
Renal proximal tubules	Proton T_2	195

erythrocytes (Table 12). However, new problems can arise that necessitate modification of the method. For example water exchange across vesicle membranes is very fast, typically 1 or 2 ms, so that very high external concentrations of manganese would be required in the Conlon–Outhred method to reduce the external medium T_2 substantially below the exchange lifetime. At such high concentrations the vesicles risk osmotic rupture. The signal from the lipid protons in vesicle suspensions also complicates the relaxation behaviour. Accordingly Andrasko and Forsen[183] introduced manganese inside rather than outside the vesicles. The limiting expression for fast, two-site exchange when there is a preponderance of slowly relaxing nuclei, corresponding to the water outside the vesicles, was used to extract the exchange rate from the CPMG decay which was single exponential.

Many difficulties beset proton T_2 studies on water transport in plant cells. First, plant cells can be large so that diffusion through intracellular and extracellular unstirred layers can be an important rate-determining factor.[30,193] This requires a more refined theoretical approach than simple two-site chemical exchange. The recent theoretical work based on the Bloch–Torrey equations[122] has pointed the way by treating the effects of diffusion through unstirred layers on the FID of two exchanging one-dimensional compartments. The extension of this approach to more realistic morphologies can perhaps be performed numerically. Another problem with plant cells is the high concentration of paramagnetic ions in cell walls during growth; this is the case with ivy bark, but not with *Elodea* leaves.[193] When manganese does bind to the cell wall the intrinsic relaxation of the intracellular water cannot be directly measured as the relaxation rate of the packed cells (as was the case with erythrocytes), since the intracellular water can still be in contact with the cell wall through the plasmalemma. Stout *et al.*[193] suggested that in this case the intracellular lifetime and relaxation time could be obtained from the slope and intercept of the straight line obtained by plotting the observed relaxation rate against the extracellular relaxation time (T_b) for increasing concentrations of added manganese. Unfortunately the fractional proton populations in the intra- and extracellular compartments then need to be independently determined and it has to be assumed that the extracellular relaxation rate equals that of the separated external medium. This is only an approximation since the cell wall relaxation effect is still present. Quite apart from this problem, the binding of manganese to the cell wall creates a surface relaxation "sink" which is not described by any of the above two-site exchange schemes. Surface relaxation can, however, be incorporated into theories based on the Bloch–Torrey equations[122,201] and can give rise to multiexponential relaxation so that even assigning the decay populations in relaxation studies on multicellular plant tissues can become problematic. The cells themselves are multicompartmental with up to 90% of the water residing in

vacuoles separated from the cytoplasm (symplast) by the tonoplast membrane. The cytoplasm itself is separated from the cell wall by the plasmalemma. When whole tissues are studied the time-course of the penetration of the relaxation reagent into the tissue via the extracellular water spaces (apoplast) is another interesting, but complicating, feature that can be explored indirectly from the time-course of the water relaxation. This is especially significant in plant tissues where some essential micronutrients (e.g. Mn, Fe, Co) are paramagnetic.[191] The spin-echo recovery method is an attractive alternative for studying the uptake of such paramagnetic micronutrients (see Section V.D) and NMR mini-imaging techniques are beginning to be applied to this problem.[28] It is surprising that more use is not made of combinations of relaxation and chemical shift reagents to aid in the assignment of water compartments and the determination of membrane permeabilities in these complex, multicellular tissues.

2. *Spin lattice relaxation measurements*

Although the idea behind the T_1 relaxation method is similar to that behind the T_2 method already discussed, there are some new aspects that warrant special attention. The longitudinal relaxation time T_1 of cells suspended in a doped medium is usually determined by the inversion-recovery method using the pulse sequence $[180°\text{-}\tau\text{-}90°(\text{FID})\text{-}T_d]_n$ where the delay time T_d must be much longer than the longest T_1 to be measured. The accumulated FID is Fourier-transformed and the peak height recorded. The whole determination is then repeated at various τ and the peak height plotted against τ to generate a point-by-point decay curve. Since T_d needs to be at least five times the longest T_1 in the system, the method is more time consuming than T_2 determinations. A more serious problem arises because protein protons can give a significant signal since their T_1 relaxation times can be quite long (e.g. 100 ms). The protein signal manifests itself as a third, slowly decaying component in the relaxation curve.[179] This signal cannot simply be subtracted since there can be spin diffusion between water protons and the protein protons. In erythrocytes this is especially important since the cells are packed with haemoglobin. The effect of spin diffusion is to make the effective cell water lifetime appear longer than in T_2 determinations unless it is correctly taken into account. If spin exchange with haemoglobin protons is included in the theoretical analysis, three coupled differential equations for the magnetization must be solved and fitted to the observed decay curve. Although this has been done[4, 178] and yields reasonable water exchange times, reliable fitting of three exponentials is notoriously difficult and requires independent determinations of the spin exchange rates and protein–proton T_1 relaxation times.

A quite different situation can pertain with T_1 measurements in non-

erythrocytes. In the halotolerant alga *Dunaliella*[187] the T_1 of the intracellular water fraction is intrinsically fast compared to the slow relaxing external water protons, so no relaxation agent is required and spin-exchange effects can be neglected.

The other difficulties already discussed in the context of T_2 determinations apply equally to T_1 determinations. Manganese ions bind to the surface of Lettree cells (neoplastic mouse cells) and enter the cytoplasm, preventing quantitative determination of the water exchange rate.[186] Cell wall binding, unstirred layers and compartmental assignment complicate plant tissue studies.[188,191] Animal tissue studies are more promising. A recent paper on suspension of renal proximal tubules[195] presented a simplified three-compartment analysis of the proton T_1 relaxation in this multicellular structure and derived an apparent basolateral membrane water permeability of 2×10^{-3} cm s^{-1}. Intracellular unstirred layers were estimated to give at most a 20% underestimate of the true basolateral permeability. Further applications of this sort of analysis to other animal tissues are to be anticipated.

3. *^{17}O relaxation methods*

The ^{17}O nucleus ($I = 5/2$) has a quadrupole moment of moderate size so that, in diamagnetic molecules such as $H_2{}^{17}O$, the quadrupole relaxation mechanism dominates and leads to relatively short relaxation times T_1 and T_2 of the order of milliseconds. Addition of low concentrations of Mn^{2+} dramatically shortens the transverse relaxation time (T_2) of $H_2{}^{17}O$, presumably through a direct electron–nuclear interaction, but T_1 is unaffected. However the $H_2{}^{17}O$ T_1 is reduced in the presence of protein so that intracellular and extracellular relaxation times can differ even in the absence of added paramagnetic relaxation agents. This means that, provided the water exchange rate is sufficiently fast (e.g. water exchange lifetimes < 20 ms), ^{17}O NMR relaxation can be used to determine the water exchange rate.

Fabry and Eisenstadt[179] found that T_1 of $H_2{}^{17}O$ in plasma at 25°C is 3.9 ms, whereas T_1 in the red cell interior is 1.7 ms. Unfortunately these rates are both considerably shorter than the water exchange lifetime in erythrocytes, so the observed T_1 for erythrocyte suspensions is insensitive to the exchange. Nevertheless their two-site analysis set a lower limit to the exchange lifetime of 20 ms. Curiously, this is considerably longer than the proton relaxation results discussed in the previous section. Shporer and Civan[182] reported a similar determination and found water exchange times of 16.7 ms at 25°C and 9.35 ms at 37°C. Why their results should differ from those of Fabry and Eisenstadt is unclear.

The exchange of water across vesicle membranes is much faster than in

erythrocytes so that the ^{17}O method can be used with reliability. However, since there is no intravesicular protein, T_1 and T_2 for $H_2{}^{17}O$ inside the vesicles do not differ from that of pure water. Accordingly T_2 measurements are used with low concentrations (approximately 5 mM) of manganese in the extravesicular medium. Haran and Shporer[185] used this method to derive an exchange lifetime of 1 ± 0.1 ms at 22°C for vesicles consisting of 5% egg lecithin and 2.5% cholesterol. They found no evidence for internally generated field gradients so that the CPMG pulse sequence gave similar results to the free induction decay.

A similar method was used by Lipschitz-Farber and Degani[184] for water transport across egg phosphatidylcholine and dipalmitoyllecithin vesicles. A combination of T_2 and T_1 proton relaxation with ^{17}O water relaxation measurements were used to follow water permeability as a function of temperature. A sharp reduction in permeability was found below the lipid phase transition.

The ^{17}O method has been used to study water permeability changes during the DMSO-induced differentiation of Friend leukaemia cells.[12] Manganese even in low concentrations poisons the cells so that $T_1{}^{17}O$ relaxation had to be used. T_1 in the $H_2{}^{17}O$-enriched supernatant was 8 ms at 36°C, only about twice as long as the intracellular T_1 measured for the pelletized cells. This small difference limited the range of exchange rates that could be accurately determined.

4. Relaxation time methods for molecules (or ions) other than water

So far there have been few reports where the transport of molecules other than water has been studied by relaxation time methods (Table 13).

The fast exchange of glycerol across egg phosphatidylcholine vesicles was determined by incorporating Gd^{3+} inside the vesicles and measuring the T_1 relaxation time of the glycerol protons with the inversion-recovery sequence.[164] The limiting expression for fast, two-site exchange when there is a preponderance of slowly relaxing nuclei (corresponding to the glycerol in the external medium) was used to extract the exchange rate. This is the T_1

TABLE 13

Fast transport of molecules (ions) other than water by relaxation methods.

System	Transported molecule/ion	Method	Ref.
Erythrocytes	Bicarbonate ions	^{13}C	196
Vesicles	Li^+, Na^+ by monensin	Relaxation reagent $Gd(EDTA)^-$	163
Vesicles	Glycerol	Gd^{3+}, Proton T_1	164

equivalent of the Andrasko and Forsen method[183] already discussed in Section IV.B.1.

The rate of exchange of ^{13}C-labelled bicarbonate across human erythrocyte membranes was measured using ^{13}C NMR.[196] The decay of the transverse magnetization was followed using the CPMG sequence. The extracellular bicarbonate relaxation rate was reduced by addition of 25 μM of Mn^{2+} while the fast CO_2–HCO_3^- exchange reaction was inhibited with methazolamide. A standard two-site exchange analysis gave a permeability coefficient of 3.34×10^{-4} cm s^{-1}, which agrees well with previous non-NMR determinations. In more recent work[132] no methazolamide was added and the membrane permeability was deduced from the differences in intra- and extracellular CO_2–HCO_3^- exchange rates (see Section III.D).

5. *Relaxation methods using other pulse sequences*

Up to now we have discussed methods based on the "standard" textbook pulse sequences for measuring either transverse or longitudinal relaxation times. These are not the only pulse sequences that can be used in relaxation studies, and in this section we discuss two other possible pulse sequences that have been used in membrane transport studies.

(a) T_1-null method and lineshape analysis. In their study on the fast, monensin-mediated exchange of Li^+ and Na^+ ions across vesicle membranes,[163] Degani and Elgavish added $Gd(EDTA)^-$ as a relaxation reagent to the outer medium and used the sequence $180°$–τ'–$90°$(FID) with $\tau' = T_1^{ex} \ln 2$ to eliminate the fast decaying outer signal. Here T_1^{ex} is the external T_1 relaxation time. The monensin-induced broadening of the remaining, inverted peak corresponding to the more slowly relaxing, intracellular ions was then used to derive the exchange rate. Of course, rather than use measurements of the linewidth they could presumably have followed the decay using a CPMG sequence after the initial T_1-null sequence $180°$–τ'–$90°$.

(b) Hybrid "T_{12}" measurements. This method was used by Fabry and Eisenstadt[178] to measure water exchange across erythrocyte membranes. It is based on the pulse sequence $[90°$–τ_2–$(180°)$–τ_2–$90°$–$\tau_1]_n$. This places the magnetization in the x–y plane during the time interval $2\tau_2$ and in the z direction during τ_1. Using such sequences Edzes[202] has shown that two recovery measurements with different τ_1 and τ_2 can yield both T_1 and T_2. Fabry and Eisenstadt[178] used this method from a desire to measure T_1 in just one (or two) scans rather than with the much slower inversion-recovery method. The algebraic analysis of the hybrid decay using two-site exchange is complex but easily programmable and gives the mean water lifetime in the erythrocyte.

V. METHODS BASED ON BULK MAGNETIC SUSCEPTIBILITY DIFFERENCES

A. General

In Section III the spins in different compartments were distinguished on the basis of their chemical shift, while in Section IV relaxation time differences were used. In this section we will consider how differences in compartmental bulk magnetic susceptibility can be used to distinguish the spins. Large differences in magnetic susceptibility can be created by selective addition of so-called "susceptibility reagents" such as the diethylenetriaminepenta-acetic acid complex of dysprosium (DyDPTA) or the desferrioxamine complex of iron (III), to the outer compartment.[203] In the static B_0 magnetic field these differences in bulk susceptibility give rise to strong magnetic field gradients in the extracellular space. Field gradients also exist inside the cells, but these are expected to be smaller so that the internal magnetic field remains relatively uniform. The external field gradients reduce the amplitude of the echo observed using a simple Hahn 90°–τ–180°–τ–echo pulse sequence, so that the intensity observed in the spin-echo sequence for a molecule in the extracellular space is more rapidly attenuated than the intensity of the same molecule in the intracellular space. Thus the detection sensitivity depends on the compartmental location of the observed molecule and by a suitable choice of the paramagnetic concentration and the delay (τ) before the 180° refocusing pulse, it is possible to eliminate the external signal from the spectrum. The transport of a small molecule from the external medium to the intracellular space is associated with an increase in intensity and this provides a direct method for studying the kinetics of membrane transport.

To understand the strengths and limitations of this method it is necessary to look more closely at its theoretical basis. This we will do in the next subsection.

B. Theory of spin-echo amplitudes using a cellular field gradient model

The physical principles of the spin-echo method have been clearly elucidated by a number of authors.[198,203] Consider, for simplicity, an unbounded spin system having an intrinsic, bulk transverse relaxation time T_2, to which a linear magnetic field gradient G is applied. It can be shown[204] that the echo amplitude of a simple Hahn 90°–τ–180°–(τ–echo) sequence is given by

$$I(2\tau) = I(0) \exp\left\{\frac{-2\tau}{T_2} - \frac{2D\gamma^2 G^2 \tau^3}{3}\right\} F(J) \qquad (5)$$

where γ is the magnetogyric ratio, D is the diffusion coefficient of the

observed molecules in solution, and the term $F(J)$ is a phase correction if there is homonuclear spin–spin coupling. The physical meaning of the term in $DG^2\tau^3$ is that the echo is not properly refocused if a molecule diffuses to a region of different applied field in the time (2τ) required to produce the echo. In the cellular systems we are considering the above expression for the echo amplitude is inadequate for three reasons, namely: (1) the field gradients generated at the boundary of a cell are non-linear; (2) the expression has been derived for the case of unbounded diffusion whereas diffusion in vesicular and cellular suspensions is restricted; and (3) it takes no account of the effects of exchange between the intra- and extracellular compartments characterized by different relaxation times, diffusion coefficients and field gradients. To date there is no general theoretical treatment which encompasses all these effects. According to Glasel and Lee[205] who performed experiments with glass beads, the mean field gradient $\overline{G}$ at a radial distance $r(r>r_0)$ from a sphere of radius r_0 is

$$\overline{G} = K B_0 \Delta\chi [r_0^2/(r_0^2 + r_0 r + r^2)r] \tag{6}$$

Here K is a constant, B_0 the applied magnetic field, and $\Delta\chi$ is the difference in magnetic susceptibility between the inside and outside media, usually increased by the addition of the susceptibility reagents.

Just outside the surface of the sphere, $\overline{G}$ is proportional to $1/r_0$ but falls off as r increases. This means that the field gradients will be sensitive to the size (and shape) of the cells. To our knowledge the spin-echo method has been tested only on small cells such as erythrocytes and algae. Whether it is applicable to larger cell systems such as plant cells where field gradients might be smaller remains to be seen.

The field gradients will depend on cell packing density and on the distribution of cell sizes and shapes. This has been confirmed in erythrocytes by measuring changes in spin-echo signal amplitudes as cell volume was altered by changing the osmotic pressure of the medium.[206] $\overline{G}$ is proportional to B_0 so that there is a clear advantage in using larger magnetic fields. This is also a gain in sensitivity and spectral dispersion.

In order to monitor the time-course of influx experiments from the changing spin-echo intensities, the transport must be reasonably slow (with a half-life of at least a few minutes). Indeed, the theory for the effects of more rapid exchange on echo heights in this sort of experiment is non-existent.

Expressions for restricted diffusion have been derived by Robertson for a linear field gradient between two parallel plates separated by a distance Z[244]. When $\tau \gg Z^2/\pi^2 D$, the diffusion term was calculated to be

$$I(2\tau) = \exp - \{(Z^4\gamma^2G^2/120D)\,[2\tau - (17Z^2/56D)]\} \tag{7}$$

In constrast to unbounded diffusion the decay is now linear in τ and varies as

$1/D$ rather than D. This dependence has been found by F.F. Brown in his careful empirical studies on packed erythrocytes,[198] confirming that restricted diffusion exists in this system.

In general the data may be acquired in two different ways. In the first the time-course of the spin-echo intensity is followed for a constant spin-echo decay time (τ). τ is usually chosen to be quite long (e.g. 60 ms) since this increases the contribution of the field gradient term and also removes the signal from high molecular weight material which has short transverse relaxation times. The signal intensity $I(t)$ is then given, for a two-compartment slow influx experiment, as $I(t) = n_{out}(t)f_{out} + n_{in}(t)f_{in}$, where n refers to the number of molecules and the f factors are normalization constants which relate the numbers of molecules in the compartment to the integrated peak intensity. These normalization constants can depend on all the factors mentioned above but are assumed to be independent of the transport process. This means that changes in cell volume due to the influx should be minimized by using isotonic media.[206]

The observed signal intensity $I(t)$ is related to the net influx $J(t)$ as $J = (dI/dt)/A(f_{out} - f_{in})$, where A is the membrane area. The net influx can then be related to any of the membrane transport models appropriate to the system. To determine f_{out} and f_{in} it is necessary to calibrate the initial intensity $I(0)$ of the outer compartment by addition of a known amount of transporting material. f_{in} can be determined from $I(t = \infty)$ when equilibrium has been reached and the net flux is zero. The large water peak in the proton spin-echo spectrum of biological systems can be suppressed by gated irradiation or by using D_2O as a solvent.

In the second method of data acquisition spin-echo plots (i.e. plots of ln $I(2\tau)$ against τ) obtained by varying τ are acquired at increasing time intervals (t) so producing stacked spin-echo plots along the time axis (t). An individual spin-echo decay plot is, in general, multiexponential because each compartment in the system has its own characteristic spin-echo decay constant (T_2^*). The redistribution of material in an influx (or efflux) experiment can be monitored through the time-course of the $\tau = 0$ intercepts obtained by multiexponential "unpeeling" of the decay curve.[207]

In chicken erythrocytes the spin-echo decays for DMSO were triexponential (Fig. 6, reproduced with permission from ref. 198), the third, most slowly decaying component being assigned to DMSO in the nucleus. The assignments of the other components to the cytoplasm and extracellular regions was straightforward since their slopes (T_2^*) corresponded to those of endogenous/ergothionine and freshly added extracellular AIB (α-aminoisobutyric acid). This plot shows how, in principle, the method can be used to measure the transport of material not only across the cytoplasmic membrane, but also across organelle membranes. However, before meaningful transport

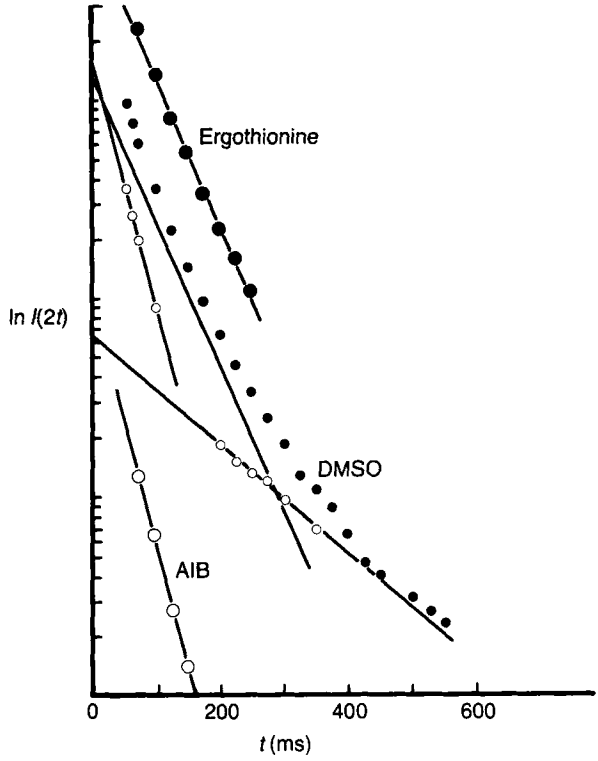

FIG. 6. A curved spin-echo plot from dimethyl sulphoxide distributed throughout a chicken erythrocyte suspension. Plots from freshly added AIB (extracellular) and endogenous ergothionine (cytoplasmic) are shown for comparison with the two shorter T_2* components from the dimethyl sulphoxide. The small open circles are the points peeled from the adjacent line and the experimental data. Measurements were made on a sample of 66% haematocrit. Taken from ref. 198.

rates can be deduced, care must be taken to eliminate a number of possible practical complications. Some of these are listed below.

(1) Cell sedimentation which can alter field gradients
(2) Gross degradation of signal by large bubbles in oxygenated samples
(3) Production of paramagnetic deoxyhaemoglobin in erythrocytes. This can alter the field gradients during deoxygenation
(4) Cell volume changes during influx or efflux experiments
(5) Saturation effects from too short delays between scans
(6) Emergence of endogenous protein signals at short times in the spin-echo plots

(7) Changes of curvature in spin-echo decays ($I(2\tau)$ plotted against τ) due to influx of permeant.

C. Applications of the spin-echo method to transport studies

In Table 14 we have listed a number of reports of membrane transport using spin-echo methods. The time-course of spin-echo intensity was used by K.M. Brindle and co-workers[203] to determine the permeability coefficients of L- and-D-alanine and L-lactate into human erythrocytes. Results were in good agreement with other non-NMR methods. Similar methods were used in later work[164] to determine the glycerol permeability of pig erythrocytes and the alga *Dunaliella*. The latter showed an exceptionally low permeability to glycerol; to our knowledge, it is the only example so far reported where the method has been applied to transport studies of cells other than erythrocytes.

Proton spin-echo methods have been used by King and co-workers in a series of reports on the transport of di-, tri- and tetrapeptides into human erythrocytes.[210-212] These peptides are hydrolysed by intracellular peptidases to the constituent amino-acids, and the rate of reaction can be analysed using Michaelis–Menten kinetics from the spin-echo intensity changes of the reactant (peptide) and product amino-acids. By comparing the rate of reaction of lysates with intact cell suspensions it was shown that for α-glutamylpeptides the membrane transport was the rate-limiting step. The steady-state Michaelis–Menten kinetic parameters for the membrane transport of α-glutamyl-L-alanine was $K_t = 2.35 \pm 0.41$ mmol litre^{-1} and $V_{max} = 3.26 \pm 0.13$ mmol h^{-1} per litre of packed cells. Fe^{3+}-desferrioxamine was used to increase the extracellular bulk magnetic susceptibility. This example shows the potential of spin-echo methods in

TABLE 14

Spin-echo determinations of membrane transport.

Cell type	Transported molecule	Susceptibility reagent	Ref.
Human erythrocytes	D- and L-alanine, L-lactate	Dy-DTPA	203
Human erythrocytes	Cd^{2+} uptake	None	208
Pig erythrocytes and algae (*Dunaliella salina*)	Glycerol	Dy-DTPA	164
Chicken erythrocytes	3-*O*-methylglucose and aminobutyric acid, thymidine, ergothionine	None	207
Maize roots	Mn^{2+} uptake	Spin-echo recovery	191
Human erythrocytes	Di-, tri- and tetrapeptides	Fe^{3+}-desferrioxamine	210,211,212

following not only the transport, but also the subsequent metabolism of cell nutrients.

Although in this section we have emphasized the importance of differences in bulk susceptibility in distinguishing inner and outer spin populations, there would appear to be no reason why a mixture of susceptibility and relaxation reagents should not be used to create a difference in f_{out} and f_{in}, at least in slow influx experiments. Thus Section IV and this section are not mutually exclusive. Such combinations have not yet, to our knowledge, been tried.

D. Spin-echo recovery methods

In the usual Hahn spin-echo method the pulse sequence is not repeated until the echo has completely decayed and the longitudinal magnetization has fully recovered its equilibrium value. This requires a repetition time $T \gg 5T_1$ where T_1 is the longitudinal relaxation time. If short repetition times are used such that $T \ll T_1$ the echo amplitude is suppressed through saturation. In 1984 Bacic and Ratkovic[191] used this phenomenon to measure the multiphasic influx of the paramagnetic relaxation reagent Mn-EDTA^{2-} into multicellular plant root tissue (maize roots). They employed the pulse sequence $(90°\text{-}\tau\text{-}180°\text{-}T)_n$ with a fast repetition rate (T = 200 ms $\ll T_1$) to completely suppress the echo intensity. The pulse space τ ($\geqslant$20 ms) was also adjusted to be much longer than the proton transverse relaxation time (T_2) of the external Mn-EDTA solution. This removed the external water signal. After addition of the Mn-EDTA solution the Mn-EDTA^{2-} ions started to enter the root and an echo signal appeared due to the shortening of the internal T_1 of the root water and the concomitant removal of proton saturation. The echo intensity plotted against time gives the time-course of the ion uptake into the tissue. Maize roots soaked in Mn(EDTA)$^{2-}$ showed a multiphasic uptake of manganese with time. It was suggested that the initial phase, which fitted the exponential function $I(t) = I(\infty)(1 - \exp(-kt))$, corresponded to diffusion of the ions into the root apoplast which is continuous with the external solution. The second phase (initiated after about 78 min) was thought to involve ions crossing the plasmalemma into the cytoplasmic continuum (symplasm) and being transported to the leaves. In the third stage the ions crossed the tonoplast into the vacuoles. Mn(EDTA)$^{2-}$ was chosen in preference to Mn^{2+}_{aq} since it is non-toxic to plants and does not bind to cell walls.[191]

VI. METHODS BASED ON DIFFERENCES IN EFFECTIVE DIFFUSION COEFFICIENT USING PULSED FIELD GRADIENTS

A. General

This method distinguishes the intra- and extracompartmental spins on the basis of their different effective (restricted) translational self-diffusion coefficients. Fourier transform pulsed gradient spin-echo studies of molecular diffusion have been recently reviewed by P. Stilbs[213] so that only a brief description of the theoretical basis of the methods as they apply to membrane permeability determinations (Table 15) will be given here. For unrestricted diffusion with no chemical exchange the factor R by which diffusion will attenuate the spin-echo amplitude in a simple pulsed field gradient experiment is given by the well-known expression

$$R = \exp[-\gamma^2\delta^2G^2(\Delta - 1/3\delta)D] \tag{8}$$

where δ is the duration of each gradient pulse of magnitude G, Δ is the spacing between gradient pulses (i.e. the time over which diffusion is measured), γ is the magnetogyric ratio and D is the self-diffusion coefficient of the nuclear species studied.[219] The above expression does not apply to restricted diffusion found in cells or vesicles. The expression for echo attentuation for a molecule diffusing inside an impermeable spherical cavity has been given[220] and shows that R decreases with Δ less rapidly than predicted by unrestricted diffusion and approaches a limiting value when Δ is longer than the time the molecule takes to traverse the cavity. Theoretical expressions for the echo attentuation R when there is exchange of molecules through a membrane of permeability P separating intracellular and extracellular compartments characterized by different relaxation times, self-diffusion coefficients and volumes are not yet available. Nevertheless, the method can still be used to measure both slow and fast transport and we will consider each of these cases separately.

TABLE 15

Membrane permeabilities by pulsed field gradient methods.

System	Transported material	Ref.
Human erythrocytes	H_2O	214,215,216
Human erythrocytes	Li^+	217
Yeast	H_2O	214
Chlorella vulgaris	H_2O	189
Wheat roots	H_2O	218

B. Echo intensity changes

If there is slow exchange of spins between intra- and extracellular compartments the observed echo amplitude $R(t)$ will be a sum of amplitudes from each compartment

$$R(t) = P_i(t)R_i + P_0(t)R_0 \tag{9}$$

where $P_i(t)$ is the time dependent fraction of intracellular spins and R_i is the effective intracellular amplitude per spin. This is entirely analogous to the case of spin-echos discussed in Section V. Here, however, the amplitudes R_i and R_0 depend on the parameters characterizing the externally applied field gradient pulses, δ, G and Δ. By choosing sufficiently long delay times Δ and suitable values for δ and g, R_0 can be made much smaller than R_i. For a slow influx experiment the observed echo amplitude $R(t)$ will then increase as spins enter the inner compartment. A kinetic analysis enables the permeability coefficient to be measured.

Andrasko first used this approach in 1976 to measure the slow influx of lithium ions into human erythrocytes.[217] He chose conditions which entirely eliminated the outer signal, though this is not an absolute necessity. It is surprising that the potential of this method has not been more fully explored. The slow influx of many simple organic molecules with ^1H, ^{19}F or ^{31}P resonances could, in principle, be studied. Nor is there any obvious reason why the method should not be used in conjunction with relaxation contrast reagents and/or magnetic susceptibility reagents to increase the difference between R_0 and R_i through T_2 differences and non-linear cellular field gradients, respectively. If restricted intracellular diffusion alone is to produce significant differences in R_0 and R_i, the intracellular relaxation time (T_2) must be sufficiently long to make the intracellular spin-echo observable for long diffusion times Δ. If this is the case then no contrast reagent need be used and truly *in vivo* transport rates can be measured.

C. Exchange rates from echo decay plots

When exchange is too fast to permit echo intensity changes to be monitored the transport rate can still, in principle, be deduced from its dynamic effect on a plot of echo amplitude R versus diffusion time (Δ). Of course an appropriate theoretical model for the echo attenuation is required if meaningful exchange rates are to be extracted, and this has been a source of difficulty. Andrasko[215] assumed that the membrane exchange can be modelled using the equations for exchange between two sites developed by Kärger.[221] Kärger showed that when the spins exchange between sites A and B characterized by different diffusion coefficients D_A and D_B, the echo attenuation is, in general, a superposition of two exponentials

$P_1 \exp(-KD_1\Delta) + P_2 \exp(-KD_2\Delta)$, where $K = \gamma^2\delta^2G^2$ and P_1, P_2, D_1 and D_2 are functions of the mean lifetimes at each site τ_A and τ_B as well as the fractional populations of each site P_A and P_B. More complex expressions including relaxation terms were also derived.[222] Kärger's results were only derived for the case of unrestricted diffusion; nevertheless Andrasko assumed that the same expression could be used for membrane exchange where D_A and D_B now become effective extracellular and intracellular diffusion coefficients. For long delay times Δ the intracellular diffusion will be restricted so that $D_B \gg D_A$. In this limit the intracellular lifetime τ_B is given as

$$\tau_B = \frac{D_A - D_1(1 + P_B/P_A)}{KD_1(D_A - D)} \tag{10}$$

Although this theoretical model lacks rigorous justification, Andrasko obtained results for erythrocyte water exchange[215] in good agreement with those obtained with other methods.

A different approach was used by Stout *et al.*[189] to measure water exchange across *Chlorella* cells. They used loosely packed cells so that the extracellular diffusion was essentially unrestricted, and a long delay time so that the intracellular echo had reached its asymptotic restricted limit which is independent of Δ and D. Under these conditions they reasoned that only the unexchanged intracellular echo amplitude remained for which

$$R(2\tau)\alpha \exp\left\{-\left(\frac{2\tau}{\tau_B}\right) - \gamma^2G^2\delta^2\frac{R^2}{5}\right\} \tag{11}$$

where τ_B is the mean intracellular lifetime.

A plot of $\ln R(2\tau)$ against the square of field gradient strength ($G^2\delta^2$) for varying τ then gives a set of straight lines whose intercepts can be used to extract τ_B. For *Chlorella* cells τ_B was found to be 25 ± 5 ms, corresponding to a permeability coefficient $P(= V/A\tau_B)$ of 2.1 ± 0.4 × 10^{-3} cm s^{-1}, in agreement with values obtained using the Conlon–Outhred method (Section IV).

A quite different method of analysis has been used by Tanner.[214] He modelled the echo attenuation in a cell suspension using a theoretical expression for diffusion through a set of equally spaced, parallel, permeable barriers. Defining the apparent diffusion coefficient, D, in such a system as $D = \ln R/\gamma^2\delta^2G^2t_d$, he showed that the value at long diffusion times D_∞ is related to that at short times D_0 as $1/D_\infty = 1/D_0 + 1/aP$, where a is the barrier spacing and P is the membrane permeability.[223,224] The barrier spacing a can be calculated separately from the intermediate value diffusion time when $D = (D_0 + D_\infty)/2$. Reasonable values for a and P were found for water exchange in human erythrocytes.[214] The method has also been applied to yeast cells.[214] The model assumed only one diffusion coefficient (D_0) char-

acterized the space between the equally spaced barriers so that, for comparison with experiment, the amount of extracellular material should be minimized by using packed cell suspensions.

Clearly more theoretical work is required to make these methods reliable. Numerical stochastic methods are promising for this purpose[168,225] and could allow the treatment of unstirred layers and multicompartment systems, characterized by various morphologies, diffusion coefficients and relaxation times.

VII. TRANSPORT INFORMATION FROM BINDING STUDIES: GRAMICIDIN

Most of the NMR studies of gramicidin to be discussed in this section do not involve direct measurements of transport through vesicle or cell membranes. Rather they involve measurement of the various binding constants for alkali metal ions with gramicidins dissolved in micelle suspensions. Nevertheless we include these reports in this review since they illustrate how NMR binding studies can complement other transport methods such as electrical conductivity in providing a uniquely detailed description of the transport mechanism. They also show how quadrupolar effects, which do not seem to manifest themselves in other systems, can be used to determine rate constants.

Gramicidin A forms a single transmembrane channel which allows single-file conductance of water and alkali metal cations. Each channel has sites situated near each end which can bind cations tightly. But when one site is occupied the vacant site at the other end becomes a weak binding site, presumably because of cation–cation repulsion. This "two-site" model can be represented kinetically by the diagram[226] shown below.

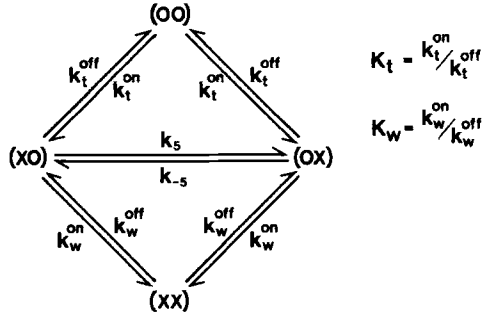

Here (OO) means the two sites are unoccupied, (XX) means both are occupied, etc. The subscripts t and w refer to tight and weak binding

respectively. This and more complex three- and four-site kinetic models can be used with Eyring rate theory[226] to relate the single channel current observed in conductivity measurements to the individual rate constants k_t^{on}, k_t^{off}, etc. As will be shown, in favourable circumstances NMR binding studies can give values for all the rate constants except k_5 (or k_{-5}), the rate constant for intra-channel jumping. However k_5 can be determined by fitting the calculated and observed single channel currents. Thus a combination of NMR binding studies with conductivity measurements can, in favourable circumstances, yield all the rate constants of the model. The observation that the activation energy for NMR determined Na^+-gramicidin binding is roughly the same as that for transport measured by conductivity methods at equimolar concentrations suggests that, in most cases, $k_5 > k_t^{off}$, which places a lower limit on the possible value of k_5. Urry and co-workers[226] have developed this approach and applied it to most of the alkali metal ions (Table 16). A variety of NMR methods were used to obtain information on the rate constants. These include relaxation time measurements (T_1 and T_2) as well as chemical shift (δ) and linewidth ($\nu_{1/2}$) studies. Which NMR measurements gives useful information depends largely on the choice of metal ion and channel type (Table 16). For example there is no significant chemical shift of $^7Li^+$ on binding to gramicidin, but there are substantial changes in T_1.[227] Unfortunately T_1 measurements alone only allow a determination of the tight and weak equilibrium binding constants K_t and K_b, but even this information provides a valuable check on conductivity data. Table 16 shows that the sodium–gramicidin system provides the most comprehensive set of NMR data for determination of the rate constants, so we will choose this system to discuss the method.

^{23}Na longitudinal relaxation times (T_1) were obtained using the inversion-recovery method for a series of sodium concentrations in the micellar-

TABLE 16

NMR studies of ion binding to gramicidin channels.

Ion	Gramicidin type	Observed NMR parameter	Ref.
Li^+	Malonyl gramicidin A	T_1	227
Na^+	Gramicidin A	T_1, T_2, $\nu_{1/2}$, ν	228
Na^+	Malonyl gramicidin A	T_1, T_2, $\nu_{1/2}$, ν	226, 229
K^+	Gramicidin A	T_1, T_2	230
$^{87}Rb^+$	Gramicidin A	T_1, T_2, ν	231
Cs^+	Gramicidin A, malonyl gramicidin	T_1, ν	232, 233
Tl^+	Gramicidin A, B and C	ν	234
K^+, Tl^+	Gramicidin A	ν of ^{13}C-labelled carbonyl	235

malonyl gramicidin in NaCl system. The relaxation was in the fast exchange regime so that the excess longitudinal relaxation rate $(R_1 - R_{1f})$ is simply

$$(R_1 - R_{1f}) = P_t(R_{1t} - R_{1f}) + P_w(R_{1w} - R_{1f}) \tag{12}$$

where P_t and P_w are fractions of ions bound to the tight and weak sites respectively. The exact details of the multiple occupancy model determines the relationship between the bound fractions P_t and P_w and the binding constants K_t and K_w. Urry *et al.*[226] used a least-squares fitting of experimental data to determine K_t and K_w.

The off-rate, k_t^{off}, of the tight-binding site was determined using the variation of the ^{23}Na chemical shift (ν) and linewidth ($\nu_{1/2}$) with increasing sodium concentration. The tight-binding site was selected using low sodium concentrations. The fast exchange condition was shown to hold for which

$$\left.\begin{aligned} \nu &= P_f\nu_f + P_t\nu_t \\ (\nu_{1/2} - \nu_{1/2}^f) &= P_t(\nu_{1/2}^t - \nu_{1/2}^f) + 4\pi P_t(1 - P_t)^2\nu_t^2/k_t^{off} \end{aligned}\right\} \tag{13}$$

Fitting to the experimental data gave both K_t and k_t^{off}. This also determines k_t^{on}, since $K_t = k_t^{on}/k_t^{off}$.

The corresponding off-rate, k_w^{off}, for the weak binding site was determined from the transverse relaxation at high sodium concentration (so that at least one site is occupied). This relies on the specifically quadrupolar effect first analysed by Bull[89] that a spin-3/2 nucleus exchanging between two states f and b will, in general, show biexponential transverse relaxation with components T_2' and T_2''. These are related to the correlation time, τ_c, for sodium ions bound on the gramicidin and this can be calculated if T_2' and T_2'' are known. In general, for quadrupolar ions, the correlation time, τ_c, is determined mainly by fluctuations in electric field gradients at the nucleus produced for example by reorientation and vibration. But Urry *et al.* have argued that for large gramicidin channels in micelles the reorientation contribution will be too slow to contribute significantly to the observed relaxation, while vibrational motions can be discounted since they would give a τ_c on the picosecond rather than the observed nanosecond timescale. In this case they propose that the correlation time τ_c is the same as the lifetime of the ion bound to the channel so that τ_c^{-1} is simply k_w^{off}. Thus the high concentration transverse relaxation allows determination of k_w^{off} and, with K_w, of k_w^{on}. Finally k_5 was determined by fitting the experimental channel current to that calculated using k_t^{on}, K_t^{off}, k_w^{on} and k_w^{off}. In this way the system is completely characterized at a kinetic level.

The extent to which this sort of approach can be applied to other ionophores packaged in micellar systems remains to be investigated. The majority of binding studies to date have been done in homogeneous solution. In

general, however, the binding constants obtained in homogeneous solution are not appropriate for membrane-bound systems where the reactions are largely confined to membrane–aqueous interfaces. For this reason micelle or vesicle packaging of the carrier is better.

VIII. MISCELLANEOUS NMR METHODS

In previous sections we have reviewed the main NMR techniques for membrane transport. In this section we consider just three examples of papers that do not fall neatly into the previous categories. The first concerns the transport of vitamin C (ascorbic acid) across dipalmitoyllecithin vesicles.[236] Here the transport is slow and can be followed from the changing intensities of the inner and outer CH_2-6 resonance (^1H NMR) of ascorbic acid during an efflux experiment. Unlike previous examples, the splitting of the ascorbate peak is caused not by shift reagents but by direct interaction of the ascorbate anion with the vesicle membrane, presumably by coulombic interaction.

The second paper concerns the study of the uptake of ammonium and nitrate ions by plant roots using ^{14}N NMR.[237] Here the intra- and extracellular media are distinguished on the basis of their isotopic (but not chemical) composition. The plant tissue is first equilibrated with a medium containing natural abundance ^{14}N-nitrate or ammonium ions. The external medium is then changed to one enriched in the ^{15}N analogue, but having the same chemical composition. Fresh medium is continuously circulated over the tissue so that the intensity of the ^{14}N resonance decreases as the ^{15}N isotope exchanges with the intratissue ^{14}N ions. The slow uptake or efflux kinetics can then be followed from the time-course of the intensity changes. Ammonium and nitrate ^{14}N resonances were chosen since these give narrow ^{14}N-resonances due to the high electronic symmetry of the ions. In principle this sort of experiment could be done with other isotope pairs such as $^{13}C/^{12}C$ or $^2H/^1H$ resonances, but we know of no instances where this has been tried. Both the transport and metabolism of suitably labelled substrates could in principle be studied by this approach.

The last example demonstrates that it is possible to measure transport of a chemical species into cells directly using NMR if the species is actively metabolized in the cell at a rate much faster than the transport rate. This was found to be the case for transport of arginine into human erythrocytes where its subsequent hydrolysis to ornithine by arginase as measured by proton spin-echo NMR in erythrocyte cell lysates was much faster than in intact cell suspensions. A Michaelis–Menten analysis was used to characterize the transport enzyme in the membrane.[238]

REFERENCES

1. J.C. Metcalfe, T.R. Hesketh and G.A Smith, *Cell Calcium*, 1985, **6**, 183.
2. H. Degani and R.E. Lenkinski, *Biochemistry*, 1980, **19**, 3430.
3. G.R.A. Hunt and I.C. Jones, *Biochim. Biophys. Acta*, 1983, **736**, 1.
4. J.A. Dix and A.K. Solomon, *Biochim. Biophys. Acta*, 1983, **773**, 219.
5. F.G. Riddell and M.K. Hayer, *Biochim. Biophys. Acta*, 1985, **817**, 313.
6. M. Jean-Baptiste, G. Klein and M. Satre, *Arch. Biochem. Biophys.*, 1987, **254**, 559.
7. W.C. Small and J.H. Goldstein, *Biochim. Biophys. Acta*, 1982, **720**, 81.
8. C.Y. Kwan, Y. Seo, M. Murakomi, H. Ito, H. Watari, *Biochem. Arch.*, 1987, **3**, 13.
9. C.Y. Kwan, S. Yoshiteru, H. Ito, M. Murakami and H. Watari, *J. Hypertension*, 1987, **5**, 359.
10. J.W. Pettegrew, J.F.M. Post, K. Panchalingam, G. Withers and D.E. Woessner, *J. Magn. Reson.*, 1987, **71**, 504.
11. G. Benga and V.V. Morariu, *Nature (Lond.)*, 1977, **265**, 636.
12. N. Haran, Z. Malik and A. Lapidot, *Proc. Natl Acad. Sci. USA*, 1979, **76**, 3363.
13. T. Conlon, P.S. Lingard and J.K. Tomkins, *Clin. Chim. Acta*, 1983, **130**, 139.
14. M. Fossarello, N. Orzalessi, F.P. Corongui, S. Biagini, M. Casu and A. Lai, *FEBS Lett.*, 1985, **184**, 245.
15. R.C. San George, R.L. Nagel and M.E. Fabry, *Biochim. Biophys. Acta*, 1984, **803**, 174.
16. I.C. Jones and G.R.A. Hunt, *Biochim. Biophys. Acta*, 1985, **820**, 48.
17. J.M. Thevelain, M. Beullens, F. Honshoven, G. Hoebeck, K. Detremerie, J.A. den Hollander and A.W.H. Jans, *J. Gen. Microbiol.*, 1987, **133**, 2191.
18. J.S. Taylor and C. Deutsch, *Biophys. J.*, 1983, **43**, 261.
19. R.K. Gupta and P. Gupta, *Biophys. J.*, 1982, **37**, 76a.
20. W.B. Busa and R. Nuccitella, *Am. J. Physiol.*, 1984, **246**, R409.
21. P.G. Morris, in *NMR Specialist Periodical Reports*, Vol. 15 (G.A. Webb, ed.), The Royal Society of Chemistry, London, 1986.
22. S.G. Schultz, *Basic Principles of Membrane Transport*, Cambridge University Press, Cambridge, 1980.
23. M.C. Mackey, *Ion Transport through Biological Membranes*, Springer, Berlin, 1975.
24. W.D. Stein, *The Movement of Molecules across Cell Membranes*, Academic Press, London, 1967.
25. E. Grell and I. Oberbäumer, in *Chemical Relaxation in Molecular Biology*, Vol. 24 (I. Pecht and R. Rigler, eds), Springer, Berlin, 1977.
26. P. Lauger, *J. Membrane Biol.*, 1980, **57**, 163.
27. A. Finkelstein, *Water Movement through Lipid Bilayers, Pores and Plasma Membranes. Theory and Reality*, John Wiley and Sons, Chichester, 1987.
28. A. Connelly, J.A.B. Lohman, B.C. Loughman, H. Quiquampoix and R.G. Ratcliffe, *J. Exp. Bot.*, 1987, **38**, 1713.
29. T.E. Andreoli and S.L. Troutman, *J. Gen. Physiol.*, 1971, **57**, 464.
30. D.G. Stout, R.M. Cotts and P.L. Steponkus, *Can. J. Bot.*, 1977, **55**, 1623.
31. R. Benz, *J. Memrane Biol.*, 1978, **43**, 367.
32. R. Benz and G. Stark, *Biochim. Biophys. Acta*, 1975, **382**, 27.
33. R. Benz, G. Stark, K. Janko and P. Lauger, *J. Membrane Biol.*, 1973, **14**, 339.
34. R. Benz and P. Lauger, *J. Membrane Biol.*, 1976, **27**, 171.
35. F. Conti and E. Neher, *Nature*, 1980, **285**, 140.
36. P. Bennekou and P. Christophersen, *J. Membrane Biol.*, 1986, **93**, 221.
37. F.L. Viera, R.I. Sha'afi and A.K. Solomon, *J. Gen. Physiol. (Lond.)*, 1970, **55**, 451.
38. A. Ballarin-Denti, J.A. den Hollander, D. Sanders, C.W. Slayman and C.L. Slayman, *Biochim. Biophys. Acta*, 1984, **778**, 1.

39. J.H. Prestegard, J.A. Cramer and D.B. Viscio, *Biophys. J.*, 1979, **26**, 575.
40. N. Hamasaki, A.M. Wyrizicz, H.J. Lubansky and A. Omachi, *Biochem. Biophys. Res. Commun.*, 1981, **100**, 879.
41. R.J. Labotka and A. Omachi, *J. Biol. Chem.*, 1987, **262**, 305.
42. R.J. Labotka and A. Omachi, *Biomed. Biochim. Acta*, 1987, **46**, 560.
43. R.B. Moon and J.H. Richards, *J. Biol. Chem.*, 1973, **248**, 7276.
44. P.S. Belton and R.G. Ratcliffe, *Prog. NMR Spectrosc.*, 1985, **17**, 241.
45. S. Forsen, T. Drakenberg and H. Wennerstrom, *Q. Rev. Biophys.*, 1987, **19**, 83.
46. R.K. Gupta, P. Gupta and R.D. Moore, *Ann. Rev. Biophys. Bioengng*, 1984, **13**, 221.
47. M.M. Civan, *Biomed. Res.*, 1986, **7**, 1.
48. S. Ratkovic, G. Bacic, C. Radenovic and Z. Vucinic, *Studia Biophysica*, 1982, **91**, 9.
49. J. Grandjean and P. Laszlo, *Studies Phys. Theor. Chem.*, 1983, **24**, 289.
50. G. Sarpel, H.J. Lubansky, M.J. Danon and A. Omachi, *Arch. Neurol.*, 1981, **38**, 271.
51. M. Brauer, C.Y. Spread, R.A.F. Reithmeier and B.D. Sykes, *J. Biol. Chem.*, 1985, **260**, 11643.
52. H. Höfeler, D. Jenson, M.M. Pike, J.L. Delayre, V.P. Cirillo, C.S. Springer Jr., E.T. Fossel and J.A. Balschi, *Biochemistry*, 1987, **26**, 4953.
53. J.A. Den Hollander, K. Ugurbil, T.R. Brown and R.G. Shulman, *Biochemistry*, 1981, **20**, 5871.
54. C.J. Tolman, S. Kanodia and M.F. Roberts, *J. Biol. Chem.*, 1987, **262**, 11088.
55. A. Elgavish, G.A. Elgavish, M. Holmann, T. Berman and I. Shomer, *FEBS Lett.*, 1980, **117**, 137.
56. P. Brodelius and H.J. Vogel, *J. Biol. Chem.*, 1985, **260**, 3556.
57. P. Lundberg, L. Linsefors, H.J. Vogel and P. Brodelius, *Plant Cell Rep.*, 1986, **5**, 13.
58. J.R. Cavanaugh and S.-I. Tu, *Biophys. J.*, 1987, **51**, 74a.
59. B.C. Loughman, *Plant and Soil*, 1987, **99**, 63.
60. W.V. Gerasimowicz, S.-I. Tu and P.E. Pfeffer, *Plant Physiol. (Bethesda)*, 1986, **81**, 925.
61. R.B. Lee and R.G. Ratcliffe, *J. Exp. Bot.*, 1983, **34**, 1222.
62. K. Ugurbil, R.G. Shulman and T.R. Brown, in *Biological Applications of Magnetic Resonance* (R.G. Shulman, ed.), Academic Press, London, 1979, pp. 537–589.
63. K.K.S. Bhat and P.H. Nye, *Plant and Soil*, 1973, **38**, 161.
64. A.J. Parr and B.C. Loughman, in *Metals and Micronutrients* (D.A. Robb and W.S. Pierpoint, eds), Academic Press, London, 1983.
65. B.C. Loughman and R.S. Russell, *J. Exp. Bot.*, 1957, **8**, 280.
66. B.C. Loughman, M.J. Webb and J.F. Loneragan, in *Plant Nutrition* (A. Scaife, ed.), CAB, Wallingford, Oxon, 1982, pp. 335–340.
67. S. Trandinh, T. Prigent, J.J. Lacapere and C.M. Gary-Bobo, *Biochem. Biophys. Res. Commun.*, 1981, **99**, 429.
68. S. Mann, M.J. Kime, R.G. Ratcliffe and R.J.P. Williams, *J. Chem. Soc. Dalton Trans.*, 1983, 771.
69. T. Ogino, J.A. Den Hollander and R.G. Shulman, *Proc. Natl Acad. Sci. USA*, 1983, **80**, 5185.
70. T.M. Murphy, G.B. Matson and S.L. Morrison, *Plant Physiol.*, 1983, **73**, 20.
71. J.A. Cramer and J.H. Prestegard, *Biochem. Biophys. Res. Commun.*, 1977, **75**, 295.
72. M.A. Stidham, D.E. Moreland and J.N. Siedow, *Plant Physiol.*, 1983, **73**, 517.
73. J.S. Taylor, C. Deutsch, G.G. McDonald and D.F. Wilson, *Anal. Biochem.*, 1981, **114**, 415.
74. C. Deutsch, J.S. Taylor and M. Price, *J. Cell Biol.*, 1984, **98**, 885.
75. K. Ugurbil, H. Rottenberg, P. Glynn and R.G. Shulman, *Biochemistry*, 1982, **21**, 1068.
76. F.S. Ezra, D.S. Lucas, R.V. Mustacich and A.F. Russell, *Biochemistry*, 1983, **22**, 3841.

77. P.S. Yoon and R.R. Sharp, *Biochemistry*, 1985, **24**, 7269.
78. T.L. Legerton, K. Kanamori, R.L. Weiss and J.D. Roberts, *Biochemistry*, 1983, **22**, 899.
79. R.K. Gupta and P. Gupta, *J. Magn. Reson.*, 1982, **47**, 344.
80. M.K. Hayer and F.G. Riddell, *Inorg. Chim. Acta.*, 1984, **92**, L37.
81. C.S. Springer Jr., M.M. Pike and J.A. Balschi, *Biophys. J.*, 1982, **37**, 337A.
82. M.M. Pike and C.S. Springer, *J. Magn. Reson.*, 1982, **46**, 348.
83. M.M. Pike, D.M. Yarmush, J.A. Balschi, R.E. Lenkinski and C.S. Springer, *Inorg. Chem.*, 1983, **22**, 2388.
84. S.C. Chu, M.M. Pike, E.T. Fossel, T.W. Smith, J.A. Balschi and C.S. Springer, *J. Magn. Reson.*, 1984, **56**, 33.
85. A. Elgavish and G.A. Elgavish, *J. Membrane Biol.*, 1986, **88**, 123.
86. S.R. Gullans, M.J. Avison, T. Ogino, G. Giebisch and R.G. Shulman, *Am. J. Physiol.*, 1985, **249**, F160.
87. Y. Boulanger, P. Vinay and M. Desroches, *Biophys. J.*, 1985, **47**, 553.
88. M.M. Pike, E.T. Fossel, T.W. Smith and C.S. Springer, *Am. J. Physiol.*, 1984, **246**, C528.
89. T.E. Bull, *J. Magn. Reson.*, 1972, **8**, 344.
90. J.A. Balschi, V.P. Cirillo, W.J. LeNoble, M.M. Pike, E.C. Schreiber, S.R. Simon and C.S. Springer, Jr, *Rare Earths Mod. Sci. Technol.*, 1982, **3**, 15.
91. M.M. Pike, S.R. Simon, J.A. Balschi and C.S. Springer Jr, *Proc. Natl. Acad. Sci. USA*, 1982, **79**, 810.
92. D.C. Buster, J.F. Hinton, F.S. Millett and D.C. Shungu, *J. Biophys.*, 1988, **53**, 145.
93. T. Ogino, G.I. Shulman, M.J. Avison, S.R. Gullans, J.A. den Hollander and R.G. Shulman, *Proc. Natl Acad. Sci. USA*, 1985, **82**, 1099.
94. E. Fernandez, J. Grandjean and P. Laszlo, *Eur. J. Biochem.*, 1987, **167**, 353.
95. J.P. Monti, P. Gallice, A. Crevat, M. El-Mehdi, C. Durand and A. Murisasco, *Clin. Chem.*, 1986, **32**, 104.
96. M.C. Espanol and D. Mota de Freitas, *Biophys. J.*, 1986, **49**, 326a.
97. J.A. Balschi, V.P. Cirillo and C.S. Springer Jr, *Biophys. J.*, 1982, **38**, 323.
98. D. Burstein and E.T. Fossel, *Am. J. Physiol.*, 1987, **252**, H1138.
99. M.J. Avison, S.R. Gullans, T. Ogino, G. Giebisch and R.G. Shulman, *Am. J. Physiol.*, 1987, **253**, C126.
100. Yoshiteru Seo, Masataka Murakami, Takehisa Matsumoto, Hiroyasu Nishikawa and Hiroshi Watari, *J. Magn. Reson.*, 1987, **72**, 341.
101. M.M. Pike, J.C. Frazer, D. Dedrick, J.S. Ingwall, Allen, P.D., T.W. Smith and C.S. Springer, *Biophys. J.*, 1984, **45**, 33a.
102. G.A. Smith, R.T. Hesketh, J.C. Metcalfe, J. Feeney and P.G. Morris, *Proc. Natl Acad. Sci. USA.*, 1983, **80**, 7178.
103. R.K. Gupta and F.A.X. Schanne, *Fed. Proc.*, 1986, **45**, 549.
104. P.G. Morris, G.A. Smith, J.C. Metcalfe and G.C. Rodrigo, in *Sixth Annual Meeting, and Exhibition, Society of Magnetic Resonance in Medicine*, New York, USA, 1987, pp. 31.
105. M. Eduardo, K. Kitakaze, H. Kusuoka, J.K. Porterfield, D.T. Yue and V.P. Chacko, *Proc. Natl Acad. Sci. USA*, 1987, **84**(16), 6005.
106. G.A. Smith, P.G. Morris, R. Hesketh and J.C. Metcalfe, *Biochim. Biophys. Acta*, 1986, **889**, 72.
107. E.W. Stephenson and R.J. Podolsky, *J. Gen. Physiol.*, 1977, **69**, 1.
108. R.K. Gupta, P. Gupta, W.D. Yushok and Z.B. Rose, *Biochem. Biophys. Res. Comm.*, 1983, **117**, 210.
109. L. Garfinkel and D. Garfinkel, *Biochemistry*, 1984, **23**, 3547.

110. L.M. Resnick, R.K. Gupta and J.H. Laragh, *Proc. Natl Acad. Sci. USA*, 1984, **81**, 6511.
111. R.K. Gupta, J.L. Benovic and Z.B. Rose, *J. Biol. Chem.*, 1978, **253**, 6172.
112. R.K. Gupta and R.D. Moore, *J. Biol. Chem.*, 1980, **255**, 3987.
113. O.G. Fritz and T.J. Swift, *Biophys. J.*, 1967, **7**, 675.
114. R.R. Sharp and C.F. Yocum, *Biochim. Biophys. Acta*, 1980, **592**, 169.
115. H. Naritomi, M. Kanashiro, M. Sasaki, Y. Kuribayashi and T. Sawada, *Biophys. J.*, 1987, **52**, 611.
116. J.R. Alger and J.H. Prestegard, *Biophys. J.*, 1979, **28**, 1.
117. H.M. McConnell, *J. Chem. Phys.*, 1958, **28**, 430.
118. D.E. Woessner, *J. Chem. Phys.*, 1961, **35**, 41.
119. C.F. Hazlewood, D.C. Chang, B.L. Nichols and D.E. Woessner, *Biophys. J.*, 1974, **14**, 583.
120. F.G. Riddell, S. Arumugam, P.J. Brophy, B.G. Cox, M.C.H. Payne and T.E. Southon, *J. Am. Chem. Soc.*, 1988, **110**, 734.
121. H.C. Torrey, *Phys. Rev.*, 1956, **104**, 563.
122. P.S. Belton and B.P. Hills, *Molec. Phys.*, 1987, **61**, 999.
123. B.P. Hills and P.S. Belton, *J. Magn. Reson.* 1988, **80**.
124. J.P. Carver and R.E. Richards, *J. Magn. Reson.*, 1972, **6**, 89.
125. A. Allerhand and H.S. Gutowsky, *J. Chem. Phys.*, 1965, **42**, 1587.
126. S. Forsen and R.A. Hoffman, *J. Chem. Phys.*, 1963, **39**, 2892.
127. S. Forsen and R.A. Hoffman, *J. Chem. Phys.*, 1964, **40**, 1189.
128. I.D. Campbell, C.M. Dobson, R.G. Ratcliffe and R.J.P. Williams, *J. Magn. Reson.*, 1978, **29**, 397.
129. G.M. Clore, G.C.K. Roberts, A. Gronenborn, B. Birdsall and J. Feeney, *J. Magn. Reson.*, 1981, **45**, 151.
130. F.G. Riddell, S. Arumugam and B. Cox, *J. Chem. Soc. Commun.*, 1987, Com. 1034, 1890.
131. D.C. McCain and J.L. Markley, *FEBS Lett.*, 1985, **183**, 353.
132. P.W. Kuchel, B.T. Bulliman, B.E. Chapman and K. Kirk, *J. Magn. Reson.*, 1987, **74**, 1.
133. K. Kirk and P.W. Kuchel, *J. Magn. Reson.*, 1986, **68**, 311.
134. G. Robinson, B.E. Chapman and P.W. Kuchel, *Eur. J. Biochem.*, 1984, **143**, 643.
135. G.A. Morris and R. Freeman, *J. Magn. Reson.*, 1978, **29**, 433.
136. D.Z. Ting, P.S. Hagan, S.I. Chan, J.D. Doll and C.S. Springer Jr, *Biophys. J.*, 1981, **34**, 189.
137. G.R.A. Hunt and L.R.H. Tipping, *Biochim. Biophys. Acta*, 1978, **507**, 242.
138. G.R.A. Hunt, *FEBS Lett.*, 1980, **119**, 132.
139. R.J. Cushley and B.J. Forrest, *Can. J. Chem.*, 1977, **55**, 220.
140. G.R.A. Hunt and K. Jawaharlal, *Biochim. Biophys. Acta*, 1980, **601**, 678.
141. H.D. Pierce, A.M. Unrau and A.C. Oehschlager, *Can. J. Biochem.*, 1978, **56**, 801.
142. M.S. Fernandez, H. Celis and M. Montal, *Biochim. Biophys. Acta*, 1973, **323**, 600.
143. G.R.A. Hunt, *FEBS Lett.*, 1975, **58**, 194.
144. G.R.A. Hunt, L.R.H. Tipping and M.R. Belmont, *Biophys. Chem.*, 1978, **8**, 341.
145. J. Grandjean and P. Laszlo, *Biochem. Biophys. Res. Commun.*, 1982, **104**, 1293.
146. B.P. Shastri, M.B. Sankaram and K.R.K. Easwaran, *Biochemistry*, 1987, **26**, 4925.
147. H. Degani, *Biochim. Biophys. Acta*, 1979, **508**, 364.
148. H. Degani, S. Simon and A.C. McLaughlin, *Biochim. Biophys. Acta*, 1981, **646**, 320.
149. J. Donis, J. Grandjean, A. Grosjcan and P. Laszlo, *Biochem. Biophys. Res. Commun.*, 1981, **102**, 690.
150. G.R.A. Hunt and I.C. Jones, *Biosci. Rep.*, 1982, **2**, 921.
151. A.L.Y. Lau and S.I. Chan, *Proc. Natl Acad. Sci. USA*, 1975, **72**, 2170.
152. A.L.Y. Lau and S.I. Chan, *Biochemistry*, 1976, **15**, 2551.
153. J. Grandjean and P. Laszlo, *J. Am. Chem. Soc.*, 1984, **106**, 1472.

154. I.I. Addrashitova, T.F. Aripov, F.G. Kamaev, B.A. Salakhutdinov and A.A. Abduvakhabov, *Biofizika*, 1987, **32**, 679.
155. L.D. Bergelson and V.F. Bystrov, in *Biomembranes: Structure and Function* (G. Gardos and I. Szasz, eds), Vol. 35, American Elsevier, New York, 1975, p. 33.
156. Y. Lee and S.I. Chan, *Biochemistry*, 1977, **16**, 1303.
157. D.M. Michaelson, A.F. Howitz and M.P. Klein, *Biochemistry*, 1973, **12**, 2637.
158. R. Lawaczek, D. Blackman and M. Kainosho, *Biochim. Biophys. Acta*, 1976, **443**, 313.
159. A. Chrzeszczyk, A. Wishia and C.S. Springer Jr, *Am. Chem. Soc. Symp. Ser.*, 1976, **34**, 483.
160. D.F. O'Brien, N. Zumbulyadis, F.M. Michaels and R.A. Ott, *Proc. Natl Acad. Sci. USA*, 1977, **74**, 5222.
161. W.J. Gerritsen, E.J.J. Van Zoelen, A.J. Verkleij, B. Dekruijff and L.L.M. Van Deenen, *Biochim. Biophys. Acta*, 1979, **551**, 248.
162. G.R.A. Hunt, I.C. Jones and J.A. Veiro, *Biosci. Rep.*, 1984, **4**, 403.
163. H. Degani and G.A. Elgavish, *FEBS Lett.*, 1978, **90**, 357.
164. F.F. Brown, I. Sussman, M. Avron and H. Degani, *Biochim. Biophys. Acta*, 1982, **690**, 165.
165. V.V. Morariu and G. Benga, *Biochim. Biophys. Acta*, 1977, **469**, 301.
166. T. Conlon and R. Outhred, *Biochim. Biophys. Acta*, 1972, **288**, 354.
167. J.L. Pirkle, D.L. Ashley and J.H. Goldstein, *Biophys. J.*, 1979, **25**, 389.
168. G.P. Zientara and J.H. Freed, *J. Chem. Phys.*, 1980, **72**, 1285.
169. C. Jalobeanu, M. Jalobeanu and V.V. Morariu, *Revue Roumain de Physique*, 1983, **28**(9), 831.
170. T. Conlon and R. Outhred, *Biochim. Biophys. Acta*, 1978, **511**, 408.
171. R. Outhred and T. Conlon, *Biochim. Biophys. Acta*, 1973, **318**, 446.
172. D.Y. Chien and R.I. Macey, *Biochim. Biophys. Acta*, 1977, **464**, 45.
173. C. Narasimhan and L.W.M. Fung, *Biophys. J.*, 1985, **47**, 401A.
174. V.V. Morariu, M.S. Ionescu, M. Frangopol, R. Grosescu, M.F. Lupu and P.T. Frangopal, *Biochim. Biophys. Acta*, 1986, **860**, 155.
175. M.D. Herbst and J.H. Goldstein, *J. Magn. Reson.*, 1984, **60**, 299.
176. D.I. Ashley and J.H. Goldstein, *Biochem. Biophys. Res. Commun.*, 1980, **97**, 114.
177. V.V. Morariu, M.S. Ionescu, M. Frangopol, R. Grosescu, M.F. Lupu and P.T. Frangopol, *Biochim. Biophys. Acta*, 1985, **815**, 189.
178. M.E. Fabry and M. Eisenstadt, *J. Membrane Biol.*, 1978, **42**, 375.
179. M.E. Fabry and M. Eisenstadt, *Biophys. J.*, 1975, **15**, 1101.
180. Y. Boulanger, P. Vinay and M. Desroches, *Biophys. J.*, 1985, **47**, 553.
181. G. Benga, V.I. Pop, O. Popescu, W. Ionescu and V. Mihele, *J. Membrane Biol.*, 1983, **76**, 129.
182. M. Shporer and M.M. Civan, *Biochim. Biophys. Acta*, 1975, **385**, 81.
183. J. Andrasko and S. Forsen, *Biochem. Biophys. Res. Commun.*, 1974, **60**, 813.
184. C. Lipschitz-Farber and H. Degani, *Biochim. Biophys. Acta*, 1980, **600**, 291.
185. N. Haran and M. Shporer, *Biochim. Biophys. Acta*, 1976, **426**, 638.
186. D. Getz, J.F. Gibson, R.N. Sheppard, K.J. Micklem and C.A. Pasternak, *J. Membrane Biol.*, 1979, **50**, 311.
187. H. Degani and M. Avron, *Biochim. Biophys. Acta*, 1982, **690**, 174.
188. S. Ratkovic and G. Bacic, *Bioelectrochem. and Bioenergetics*, 1980, **7**, 405.
189. D.G. Stout, P.L. Steponkus, L.D. Bustard and R.M. Cotts, *Plant Physiol.*, 1978, **62**, 146.
190. Y. Prigent, S. Trandinh and C.M. Gary-Bobo, *Biochem. Biophys. Res. Commun.*, 1980, **95**, 1218.
191. G. Bacic and S. Ratkovic, *Biophys. J.*, 1984, **45**, 767.

192. P.M. Chen, L.V. Gusta and D.G. Stout, *Plant Physiol.*, 1978, **61**, 878.
193. D.G. Stout, P.L. Stephonkus and R.M. Cotts, *Plant Physiol.*, 1978, **62**, 636.
194. M.C. Steward and M.J. Garson, *J. Membrane Biol.*, 1985, **86**, 203.
195. A.S. Verkman and K.R. Wong, *Biophys. J.*, 1987, **51**, 717.
196. B.E. Chapman, K. Kirk and P.W. Kuchel, *Biochem. Biophys. Res. Comm.*, 1986, **136**, 266.
197. A. Abragam, *The Principles of Nuclear Magnetism*, Oxford University Press, Oxford, 1961, pp. 57-63.
198. F.F. Brown, *J. Magn. Reson.*, 1983, **54**, 385.
199. M.E. Fabry and R.C. San George, *Biochem.*, 1983, **22**, 4119.
200. Z. Frait, D. Fraitora and D. Doskocilova, *Czech, J. Phys.*, 1973, **B23**, 908.
201. K.R. Brownstein and C.E. Tarr, *Phys. Rev. A.*, 1979, **19**, 2446.
202. H.T. Edzes, *J. Magn. Reson.*, 1975, **17**, 301.
203. K.M. Brindle, F.F. Brown, I.D. Campbell, C. Grathwohl and P.W. Kuchel, *Biochem. J.*, 1979, **180**, 37.
204. H.Y. Carr and E.M. Purcell, *Phys. Rev.*, 1954, **94**, 630.
205. J.A. Glasel and K.H. Lee, *J. Am. Chem. Soc.*, 1974, **96**, 970.
206. Z.H. Endre, P.W. Kuchel and B.E. Chapman, *Biochim. Biophys. Acta*, 1984, **803**, 137.
207. F.F. Brown, G. Jaroszkiewicz and M. Jaroszkiewicz, *J. Magn. Reson.*, 1983, **54**, 400.
208. D.L. Rabenstein, A.I. Anvarhusein, K. Webe and P. Mohanakrishnan, *Biochim. Biophys. Acta*, 1983, **762**, 531.
209. L.O. Sillerud and J.W. Heyser, *Plant Physiol.*, 1984, **75**, 269.
210. G.F. King, M.J. York, B.E. Chapman and P.W. Kuchel, *Biochem. Biophys. Res. Commun.*, 1983, **110**, 305.
211. G.F. King and P.W. Kuchel, *Biochem. J.*, 1985, **227**, 833.
212. J.I. Vandenberg, G.F. King and P.W. Kuchel, *Biochim. Biophys. Acta*, 1985, **846**, 127.
213. P. Stilbs, *Prog. NMR Spectrosc.*, 1987, **19**, 1.
214. J.E. Tanner, *Arch. Biochem. Biophys.*, 1983, **224**, 416.
215. J. Andrasko, *Biochim. Biophys. Acta*, 1976, **428**, 304.
216. R.L. Cooper, D.B. Chang, A.C. Young, C.J. Martin and B. Ancker-Johnson, *Biophys. J.*, 1974, **14**, 161.
217. J. Andrasko, *J. Magn. Reson.*, 1976, **21**, 479.
218. A.S. Yevarestov, A.V. Anisimov and I.F. Samuilova, *Biophysics*, 1984, **29**, 92.
219. E.O. Stejskal and J.E. Tanner, *J. Chem. Phys.*, 1965, **42**, 288.
220. J.S. Murday and R.M. Cotts, *J. Chem. Phys.*, 1968, **48**, 4938.
221. J. Kärger, *Ann. Phys. (Leipzig)*, 1969, **24**, 1.
222. J. Kärger, *Ann. Phys. (Leipzig)*, 1971, **27**, 107.
223. J.E. Tanner, *J. Chem. Phys.*, 1978, **69**, 1748.
224. J.E. Tanner, *J. Chem. Phys.*, 1981, **74**, 6959.
225. E.D. Von Meerwall and R.D. Ferguson, *J. Chem. Phys.*, 1981, **74**, 6959.
226. D.W. Urry, C.M. Venkatachalem, A. Spisni, A.J. Bradley, T.L. Trapane and K.U. Prasad, *J. Membrane Biol.*, 1980, **55**, 29.
227. D.W. Urry, T.L. Trapane, C.M. Venkatachalem and K.U. Prasad, *J. Phys. Chem.*, 1983, **87**, 2918.
228. D.W. Urry, C.M. Venkatachalem, A. Spisni, and Md. Abu Khaled, *Proc. Natl Acad. Sci. USA*, 1980, **77**, 2028.
229. C.M. Venkatachalam and D.W. Urry, *J. Magn. Reson.*, 1980, **41**, 313.
230. D.W. Urry, T.L. Trapane and C.M. Venkatachalem, *J. Membrane Biol.*, 1986, **89**(1), 107.
231. D.W. Urry, T.L. Trapane, C.M. Venkatachalem and K.U. Prasad, *J. Am. Chem. Soc.*, 1986, **108**, 1448.

232. D.W. Urry and T.L. Trapane, *J. Magn. Reson.*, 1987, **71**, 193.
233. D.W. Urry, T.L. Trapane, R.A. Brown, C.M. Venkatachalam and K.U. Prasad, *J. Magn. Reson.*, 1985, **65**, 43.
234. J.F. Hinton, R.E. Keoppe, D. Shungu, W.L. Whaley, J.A. Paczkowski and F.S. Millett, *Biophys. J.*, 1986, **49**(2), 571.
235. D.W. Urry, T.L. Trapane, C.M. Venkatachalem and K.U. Prasad, *Can. J. Chem.*, 1985, **63**(7), 1976.
236. H. Sapper, in *Liposomes as Drug Carriers*, (K.H. Schmidt, ed.), G. Thieme, Stuttgart, 1986.
237. P.S. Belton, R.B. Lee and R.G. Ratcliffe, *J. Exp. Bot.*, 1985, **36**, 190.
238. P.W. Kuchel, B.E. Chapman, Z.H. Endre, G.F. King, D.R. Thorburn and M.J. York, *Biomed. Biochim. Acta*, 1984, **43**, 719.
239. M.C. Espanol and D. Mota de Freitas, *Inorg. Chem.*, 1987, **26**, 4356.
240. R.H. Knop, C.W. Chen, J.B. Mitchell, A. Russo, S. McPherson and J.S. Cohen, *Biochim. Biophys. Acta*, 1984, **804**, 275.
241. M. Oghuski, K. Nagayama and A. Wada, *J. Magn. Reson.*, 1978, **29**, 599.
242. R. Lawaczeck, D. Blackman and M. Kainosho, *Biochim. Biophys. Acta.*, 1977, **468**, 411.
243. F.G. Riddell and T.E. Southon, *Inorg. Chim. Acta.*, 1987, **136**, 133.
244. B. Robertson, *Phys. Rev.*, 1966, **151**, 273.

This Page Intentionally Left Blank

Recent Developments in Multiple Pulse NMR

DAVID L. TURNER

Department of Chemistry,
University of Southampton, Highfield,
Southampton SO9 5NH, UK

ANNUAL REPORTS ON NMR SPECTROSCOPY
VOLUME 21 ISBN 0-12-505321-5

I. INTRODUCTION

Five years is a long time in any branch of science which relies as heavily on computers as does NMR. Even so, nothing very dramatic has appeared since McFarlane and Rycroft reported on the literature up to mid-1983 in their chapter on Multiple Resonance in Vol. 16 of this series.[1] Some change of emphasis is reflected in the title for this chapter, but major advances such as the general introduction of two-dimensional NMR techniques, the DEPT sequence for editing heteronuclear spectra, and composite pulse decoupling were covered in the earlier article and have not been surpassed. A detailed commentary covering most of this period will be found in the recent *Specialist Periodical Report on Nuclear Magnetic Resonance.*[2] In general terms, the developments of the last five years have involved the clarification of many detailed points and the establishment of conventions as well as the evaluation of particular methods in practical applications.

Jargon such as "coherence transfer" is now widely understood while its earlier equivalent, the "supertransition", has disappeared without trace. Other conventions have yet to be established; Ernst chooses arbitrarily to detect coherence of order -1 while some authors[3,4] prefer the more optimistic $+1$ and may use "phase cycling" to select a "route" for transferring coherence between orders, or levels, rather than the more pedestrian "pathway". Multidimensional NMR experiments show up particular weaknesses in notation: insisting on labelling frequency dimensions in the order of the evolution periods means that the familiar single quantum spectrum is sometimes denoted "F_2" and may even be relegated to F_3. This is unfortunate since the set of frequencies appearing in the new dimensions is quite arbitrary while the first dimension observed in NMR, the detectable free induction decay, remains unchanged. This may seem less important if the two-dimensional experiment correlates essentially identical sets of frequencies as in the homonuclear COSY experiment, but, since the F_2 (or F_3) dimension is normally transformed first to be followed by transposition and a second Fourier transform (of F_1), the notation could be made more helpful to the spectrometer user. It is no longer even safe to assume that spectra will be presented with the second dimension running vertically, though it is vital to avoid confusion since the types of artifact appearing in the two dimensions are quite different.

Consolidation of a field is important because the accessibility of methods is important. Several articles have addressed fundamental topics such as phase cycling and sensitivity, and much effort has gone into simplifying use of the density operator and into the adaptation of existing experiments and their presentation. Despite the efforts and acronyms of some of these interpreters, a clearer view of the development and scope of the subject is emerging. Essen-

tially, the growing number of end users is beginning to sort the wheat from the chaff.

One of the earlier attempts to provide a coherent framework for understanding multiple pulse experiments[3] has been superseded by the book by Ernst, Bodenhausen and Wokaun[5] *The Principles and Applications of NMR in One and Two Dimensions* which achieves, as one reviewer put it, "a comprehensive review spiked with interesting new viewpoints" and, unlike the former work, is essentially free of unexpected contributions from the word processor. Much of the contents have been published separately in review articles covering phase cycling,[6] sensitivity of two-dimensional experiments,[7] "violations" of selection rules for coherence transfer,[8] magnetic resonance imaging,[9] the product operator formalism,[10] and multiple-quantum NMR.[11] A useful discussion of average Hamiltonian theory is added to this, and further details of the application of two-dimensional methods to biological systems can be found in the book by Wüthrich and other reviews.[12-19]

Two-dimensional NMR is now well enough accepted to be included in textbooks from a somewhat faltering start for undergraduates[20] through a new edition of Shaw[21] and a "guide for chemists"[22] to the expansive descriptions of Derome.[23] Freeman[24] takes a more nostalgic view and although the modern undergraduate might wonder just what a buck out coil looks like or where a lock-in detector might be found he will have no problem with the density matrix, which is referred to only by name. This is a simple and entertaining book but, despite the caveats of the preface, fuller referencing would have enhanced its value both as an index and outline of topics since articles such as that which introduced decoupling by 180° pulses,[25] or indeed Ernst's book,[5] do contain important additional insights.

Despite the importance of two-dimensional methods, it should not be forgotten that many of the most useful multiple pulse experiments applied to liquids are one-dimensional: these have been described clearly and comprehensively in a review by C. J. Turner[26] (no relation).

I. COMPUTATIONAL METHODS

A. Operator bases

While the density matrix formalism provides an undisputed foundation for understanding almost every aspect of pulse NMR, it is sometimes difficult to see the wood for the trees. The development of various bases for expansion of the density operator has provided considerable insight into the origin of certain effects, and the products of single spin operators, or PROPs, have been used and illustrated widely.[27-34] There are two principle groups of PROPs which use the Cartesian basis, E, I_x, I_y, I_z, which has the advantage of

being more easily related to the vector picture[29] but is not well suited to calculations involving multiple quantum coherences or phase cycling, and the alternative basis of shift operators, E, I_+, I_-, I_z. It is important to bear in mind the limitations of calculations which use PROPs: they are effectively restricted to small groups of weakly coupled spins[35] and although the mathematical operations which describe the effects of pulses or free precession simply involve substituting two terms for one, the expressions become unwieldy unless groups of terms can be dropped safely. The principal advantages of the formalism therefore emerge when discussing experiments with hindsight, and some useful nomenclature has been generated for labelling different types of signal which has helped in developing experiments such as "zz" COSY.

The built-in approximations have spawned a small industry of spotting "selection rule violations". This is an unfortunate expression, discussed further in Section V, because the selection rules derive from a model of weak coupling in which relaxation is neglected and are not of the same character as those derived from group theory. There are two main classes of violation, the first is trivial and the second nearly so. Trivial violations result from strong coupling, in which case it is simply not meaningful to assign transitions to a single nucleus: an AB pattern is the joint property of the two spins and any effect, such as a nuclear Overhauser enhancement, which affects spin A will naturally show up in the part of the pattern trivially ascribed to spin B.[36] Degeneracy provides the basis of the less trivial class. The simplest example shows up in the absence of COSY cross-peaks between nuclei with a vanishingly small coupling constant which may be regarded as a consequence of the cancellation of degenerate components which have opposite signs.[3] Any relaxation phenomenon which produces differential effects among those components may spoil that cancellation and a cross-peak or multiplet can reappear, but only with distorted lineshapes which have zero integrated intensity.

Basis sets derived from irreducible tensor operators[37-46] are better suited to analyses of systems including equivalent spins, and Sanctuary's operators have been adopted, albeit with modifications to conform to the Ernst's inversion of the physical conventions, to discuss the violations of rules derived from their simpler brethren.[8]

B. Computer simulations

While PROPs are widespread in discussions, with a very few exceptions[47] the full blown density matrix remains at the heart of computer simulations of spectra. Simulations are important to help distinguish artifacts and predict effects which might not be expected on the basis of a superficial considera-

tion. Simulations may also be used in fitting spectra to extract chemical shifts and coupling constants. All of these aspects were exploited well before the period covered by this review,[48-49] but the growing use of multiple pulse techniques has led to considerable new activity in the area. Examples of shift correlation spectra,[50-52] multiple-quantum spectra,[53,54] and multiple-quantum filtered spectra[55] have been presented recently. Dynamic properties of the spin system are also being taken into account,[56,57] though not yet at the same level of sophistication as is common in studies of relaxation or chemical exchange modified bandshapes in one-dimensional spectra.

The effects of poor digitization in two-dimensional spectra are also important and difficult to predict analytically. There is some renewed interest therefore in subjecting simulated data to processing similar to that used in experiments. To date, this approach has simply confirmed that COSY cross-peaks will appear in the absolute value spectrum even if the point spacing exceeds the coupling constant,[58] but it is likely that there will be further developments to compete with linear prediction and maximum entropy methods for handling experimental data in the time domain.

C. Data processing

The computer is, of course, central to processing experimental data as well as simulating it. The physical chemist likes to see graphs, and if they cannot be straight lines then spectra are acceptable. However, the information sought at the end of the day is usually a structure or a conformation. Few people would look at an X-ray diffraction picture with more than polite interest (with the possible exception of the DNA helix pattern); they would rather see atomic coordinates. Similarly, the spectroscopist is usually interested in very few of the NMR parameters—shifts and coupling constants, possibly intensities, and occasionally linewidths. All of this information is present in the free precession signal and the Fourier transformation is really only necessary to give spectroscopists something comprehensible to look at. If computers could perform the complete analysis, and tell the operator when to adjust the spectrometer, then spectra might become a thing of the past.

A few steps have been taken in that direction by finding alternatives to the Fourier transform to unscramble the free precession signal and, secondly, in automating the interpretation of spectra. The connection between the two activities is not helped by the tendency to cling to traditional spectral forms and enter into arguments over the relative sensitivity of the Fourier transform spectrum and reconstructions which are based on restrictive models. On the analytical side, maximum entropy methods[59-62] and linear prediction[63-69] are attracting most attention. Both involve assumptions about the nature of the noise and the lineshape and require lengthy computation, and both methods

avoid the restrictions on sampling imposed by the fast Fourier transform algorithm. This has attractions for those who dislike truncation artifacts[70] and, more importantly, opens the possibility for using geometrically spaced samples to maximize the efficiency of data collection, particularly in two-dimensional experiments. The methods are well established in other fields and are only being demonstrated, rather than used, in NMR at present. No doubt the next *Annual Report* will have further progress to discuss.

The second step toward spoiling spectroscopists' employment prospects involves the automated interpretation of spectra. Pattern recognition applied to one-dimensional spectra, in particular for the analysis of complex exchange-broadened bandshapes, has been highly sophisticated for some years. Recent developments concentrate on homonuclear two-dimensional spectra of weakly coupled spin systems and tend to be limited to dealing with the frequency coordinates of the component lines of cross-peak multiplets rather than their intensities. Apart from the overall symmetries observed in, for example, a COSY spectrum, there is considerable symmetry within cross-peaks. The basic AX cross-peak is a square pattern with four components, two positive and two negative, separated in each dimension by the coupling constant J_{AX}. If spin A is coupled to some other spin M then the pattern is reproduced with an offset J_{AM} in the dimension of spin A, and similarly for spin X. The computer is set the task of recognizing these simple patterns and determining the coupling constants. To some extent the tail has begun to wag the dog and considerable effort has gone into obtaining spectra which are amenable to analysis using relatively primitive software. This involves obtaining both very high resolution and high signal-to-noise ratios which require extremely long two-dimensional experiments. Even this may be insufficient, so small flip angle pulses and multiple-quantum filters have been employed to simplify multiplets further, and further multiply the acquisition time.[71-84] There has been relatively little use made of spin-echo spectroscopy recently[85-90] despite the existence of iterative simulation programmes and the value of vicinal proton coupling constants in conformational analysis, and it may be timely to reconsider this comparatively easy method for obtaining resolved and simplified multiplets with high resolution.

Apart from extracting coupling constants, the analysis of a cross-peak multiplet naturally identifies the chemical shifts of spins A and X as the coordinates of the centre of the cross-peak. This is also achieved directly by plotting the double dispersion component for which the maximum intensity normally appears at the centre. Once this has been done, the interpretation of connectivities in terms of structure may be sufficiently straightforward to be left to the computer,[91] but the incomplete information usually obtained from macromolecules leaves a massive bookkeeping problem which may also be alleviated by employing a computer to keep records and check the consistency of assignments proposed by human spectroscopists.[92]

III. GENERAL ASPECTS OF TWO-DIMENSIONAL EXPERIMENTS

A. "t_1" noise

The useful sensitivity of a two-dimensional experiment, or any spectrum for which data are not gathered in real time, is usually determined by noise levels on signal bearing cross-sections in the second dimension rather than thermal noise in the detected signal. The influence of random noise on sensitivity in two-dimensional spectra is well understood;[7,93,94] so are the effects of digitization and sampling which are central to the optimization of two-dimensional experiments[93,94] and can even cause apparent phase anomalies in one-dimensional spectra.[95] The additional noise in the second dimension is generally known as "t_1 noise" since it arises from the incremented evolution period. The real NMR signals act as amplifiers for any instability in the spectrometer, including transmitter power, radio-frequency phase and signal amplification, or in the spin system, which includes non-equilibrium states and temperature-dependent chemical shifts, which has components varying on the timescale of the pulse repetition. This might make "T_1 noise" a more descriptive term, in contrast to variations which occur on the timescale of T_2 while sampling the free precession signal and contribute to noise in one-dimensional spectra. Slow variations and spatial inhomogeneity tend to cause line broadening rather than noise, though clearly any instability during an experiment is undesirable.

The most disturbing feature of t_1 noise is that it runs right through the second dimension at the frequency of the normal NMR signals, nearly obscuring any weak cross-peaks. Mehlkopf *et al.*[96] have listed the known instabilities in an NMR spectrometer which lead to noise, to which should be added the "t_1 spikes" which are generated by impure reference frequencies[97] and vortexing or the possibility of using flowing liquids to reduce the dependence on T_1 values.[98,99] Among these, thermal instability is possibly the most important when the deuterium lock material has a significantly temperature-dependent frequency, as in water, but here we shall only consider what can be done to improve the data collected using an inherently unstable machine.

Any procedure which cancels diagonal peaks will reduce "t_1 noise" by removing contributions from fluctuations occurring on a timescale longer than the cancellation cycle. This principle is familiar from interleaved difference experiments in one dimension such as modified inversion recovery or nOe difference. Disordering the steps in the evolution periods simply alters the effective timescale and converts potential line-broadening mechanisms into noise.

Quite apart from the apparently random noise, it is common to observe ridges or waves in the second dimension. Waves may be generated by presaturation with non-phase locked irradiation,[100] and a variety of data

massaging procedures has been proposed which use the symmetry expected of two-dimensional signals[101] or the subtraction of empirical masks.[102,103] Ridges, however, are a simple consequence of Fourier transforming data acquired with a finite sampling rate. A certain amount of hand waving leads to the sensible suggestion that the first point of the time-domain signal should be reduced to half the value it would have in the absence of a bandpass filter and the intensity of the transform of the $t_1 = 0$ increment, the first point of the interferogram, should also be halved.[104] This corresponds to the subtraction of a constant value from the baseline which approximates to the height of the ridge.

There should be no mystery about the discrete Fourier transform since numerical values are processed using well-defined algorithms. However, it is important to recognize the distortions which arise as a consequence of the periodicity of the discrete spectrum. The most familiar consequence of this is the folding or aliasing of lines, which can be recognized easily even in two-dimensional spectra so long as the spectroscopist is aware of the possible combinations of real and complex Fourier transforms.[3] The behaviour of the wings of supposedly lorentzian lines may seem more curious, though the principles are identical. The lineshape extends infinitely and must always be modified by folding at the limits of the finite spectral width. In the particular case of a real transform applied to a sine wave, the absorption lineshape has zero intensity at the extremes of the spectrum. This is because the sine transform is antisymmetric so that folding is accompanied by a phase inversion and the wings of the line cancel exactly at the limit of the spectral width. If the reference phase is adjusted so that a real cosine signal is obtained then the absorption lineshape results from a cosine transform and the wings of the line reinforce on folding and create the appearance of a DC offset of the baseline. In neither case, however, does the line have a purely lorentzian character.

It is oversimplistic to justify modifying the first sample point in terms of taking the mean value between the first and last points of the free induction decay to ensure "continuity". It has been shown[105] that a signal recorded at the Nyquist frequency in the form of a cosine generates an offset at zero frequency of $(M_0/2)[1 - \exp(-N\delta/T_2^*)]$, where N points are sampled at intervals δ which are small with respect to the decay constant, and the first point has intensity M_0. This is a smoothly decaying function which disappears if $\delta = 0$, that is for an infinite spectral width, and tends to $M_0/2$ if N is large enough for the free induction decay to be sampled for long enough for the signal to be vanishingly small. This is never allowed to happen in the second dimension because of the disastrous consequences for sensitivity, in which case the first point should be reduced by a factor slightly less than 2 in order to subtract the ridge even though the even numbered samples in this

example are negative. An infinite decay constant actually removes the ridge altogether since sinc wiggles do not appear in the absence of zero filling — yet in that case the mean value of the first and last of 2^n points would be zero, so the amplitude of the first point should be left well alone. Even so, the analytical problems presented by apodization and zero filling are such that halving the amplitude of the $t_1 = 0$ increment is probably a useful rule of thumb for beautifying contour plots. An adjustable weighting of the first point of a free induction decay or interferogram may be as useful a variable as window functions for obtaining interpretable spectra, at least until software improves to the point that full two-dimensional baseplane correction[106] becomes practicable on a routine basis.

B. Phase cycling and 2D absorption lineshapes

If a radio-frequency pulse has its phase shifted with respect to the reference then the magnetization which is eventually detected experiences the same phase shift, multiplied by the change in the order of coherence induced by that pulse. Thus a 90° shift in the phase of a pulse applied to a system at equilibrium, order zero, produces a 90° shift in the phase of the free induction decay, order +1, whereas the same shift in a 180° refocusing pulse used to convert order of −1 into order +1 inverts the phase of the echo. This simple principle is the basis for using phase cycling to select particular routes for coherence transfer in a complex pulse sequence.[6,107,108] The pulse sequence is repeated several times with suitable phase shifts so that all the undesirable signals cancel on addition of the free induction decays. Phase cycling is therefore a form of difference spectroscopy in essence, and this is its weakness. Any of the instabilities which can generate t_1 noise in two-dimensional spectra tend to spoil the cancellation even if the phase shifts are perfectly adjusted, and methods such as multiple-quantum filtration which depend on phase cycling cannot overcome problems with the dynamic range of the receiver, though they do help with long-term time averaging and will reduce quantization errors in the transformed spectrum.

A phase cycle should be designed to eliminate the strongest signals on the shortest possible timescale to optimize cancellation. This usually means that "axial" peaks which result from longitudinal relaxation during the sequence should be cancelled on alternate transients. Signals from protons which are not coupled to heteronuclei present an essentially similar problem in heteronuclear multiple-quantum experiments, and it has been noted that cancellation is usually improved by ensuring that the singlets are generated under identical conditions while the desired signals are inverted.[109] Such pairs may then be nested in cycles to cancel or separate mirror image frequencies present during the evolution period of a two-dimensional experiment to suppress

quadrature images in the second dimension. The cycle may be completed by superimposing four 90° phase shifts according to the "CYCLOPS" procedure on all of the pulses and on the reference phase to suppress normal quadrature images. It is not always possible to manipulate the phase of a particular signal independently. For example, zero-quantum coherence is indistinguishable from longitudinal magnetization. In that case partial cancellation may be achieved by pseudo-random variation of the zero-quantum evolution period to prevent coherent addition of these low frequency terms. High order coherences may also be attenuated by exploiting their sensitivity to their B_0 or B_1 inhomogeneity.[110,111]

These simple principles lend themselves to illustration[112] and to the automatic generation of optimized cycles. The simplest approach to the determination of a complete set of phase combinations is to define the orders of coherence, C_n, to be generated by each of the N pulses having a phase $P_n = \sum_n^N p_n$ where $\Sigma C_n p_n = 2k\pi$. The most coarse phase shift to be of any use is π, and the number of possible sequences increases rapidly as finer steps are considered so it is useful to check sequences which employ shifts of $2\pi/j$ where $j = 2, 3, 4 \ldots$ and use the most economical cycle which will cancel signals from undesired routes. The problem can be simplified a little when fixed elements such as composite pulses are included in the sequence if the orders of coherence between the individual pulses are not specified and they are all given identical phase increments. The "X-approximation", applicable when any group of spins contributes a Zeeman term which commutes with the total Hamiltonian, may also be useful for selective pulses such as those applied to heteronuclei. In that case the orders of coherence and phase shifts may be defined separately for the different groups. Thus, for example, in a heteronuclear multiple-quantum experiment with proton detection all of the pulses applied to the heteronuclei may be given the same additional phase shift without affecting the phase of the proton signal since the route begins and ends with order zero.[3] In practice, there is usually just such an increment and it is completely random unless the phases of the different transmitters are synchronized at the start of each sequence.

The fundamental importance of route selection by phase cycling has led to the development of faster, more stable and more flexible phase shifters based on digital frequency synthesizers. Research workers tied to machines which offer only 90° shifts come up with increasingly ingenious modifications,[113-116] but it is worth nothing that only shifts of exactly $2\pi/n$ are of any use and that 15° steps will serve almost all purposes.

Perhaps the most important development to come into general use is the application of phase cycling to produce effective quadrature detection in the evolution period of two-dimensional experiments. The essential problem is that any single route for coherence transfer will generate a "phase twist" line-

shape which combines double absorption with double dispersion so that it became common to present absolute value spectra and use strong resolution enhancement functions which are extremely costly in terms of sensitivity. There was little point in modifying experiments to produce pure phases when no commercial software existed for phase correcting spectra in two dimensions. Happily, that situation has been improved sufficiently to make phase sensitive two-dimensional spectroscopy a practical proposition in non-specialist laboratories and enough time has passed to forget that the problem was fully worked out before any commercial software existed at all. Taking the absolute value of a spectrum will distort regions with overlapping lines since it is not a linear process,[117] yet some people are still shy of phase correcting the second dimension.[118–120]

The essence of eliminating the dispersion component is as simple as forming a linear oscillation from two counter-rotating vectors. The limitation is that those vectors must have identical magnitude. The requirement is therefore that a pair of routes exist with opposite signs for the order of coherence during the evolution period and identical coherence transfer coefficients. This is no problem for Jeener's NOESY experiment since ± 1 magnetization is created from the spins at equilibrium, order zero, and returned to zero as populations or vectors along the z-axis mix. The situation is therefore perfectly symmetrical. A similar situation obtains in heteronuclear shift correlation since the X-approximation applies: the protons evolve with their own order ± 1 and return to zero as the magnetization is transferred to the heteronucleus for detection. This is true of the cross-peaks but not of the diagonal peaks in homonuclear shift correlation (COSY) spectra except when a 90° mixing pulse is used. Thus it is perfectly normal to have access to signals which are symmetrical about zero frequency in the second dimension with symmetric absorption components and antisymmetric dispersion components; they are sometimes referred to as the P (positive) and N (negative) signals. In Switzerland, the refocused components which generate the N peaks actually have positive orders of coherence during the evolution period, but that is where the P/N nomenclature was introduced. The two components can easily be distinguished by a 90° phase shift of the excitation sequence ($\pi/2n$ for higher orders) which inverts the refocused term so that the free induction decay contains contributions from the difference of the two routes rather than the sum. All subsequent data processing merely amounts to separating the P and N terms, reversing one in the second dimension, and adding it to the other to cancel the dispersion component mixed with absorption. This may be done explicitly in either the time or frequency domains, but the most commonly used methods are implicit because a full "hypercomplex" Fourier transform doubles the storage space required, though it still has its adherents.[121,122] States *et al.*[123] make the switch

implicitly without separating the two components by phase correcting the spectra obtained from the quadrature components after transformation of the free precession signals, then rejecting the dispersive parts before transforming with respect to the evolution period. Marion and Wüthrich[124] achieve the same thing by sampling each quadrature component in alternate increments of a single data set and using a real transform in the second dimension to fold the spectrum, effectively combining the principles of "time-proportional phase incrementation" with Redfield quadrature. The difference between these methods is purely practical; both achieve pure absorption lineshapes through quadrature detection in the evolution period and increase the sensitivity by combining signals from the two routes.[1,35,125]

The attractions of pure absorption lineshapes make it desirable to design experiments which avoid refocusing periods immediately prior to acquisition since they destroy the symmetry required for the mirrored routes. Several experiments, including *J* spectroscopy and multiple-quantum experiments, which have been designed to use refocusing to take advantage of smaller spectral widths in the second dimension, may therefore be improved by allowing folding into a limited spectral width and then unwrapping the frequencies using "foldover correction".[126,127] However, despite the simplicity of the procedure, no example has yet been presented in which the frequency-dependent phase correction in the second dimension is programmed to take account of such folding.

C. Repeated acquisition periods

The similarity of many of the elements appearing in multiple pulse experiments makes the possibility of acquiring signals at different stages in the sequence an attractive possibility which is limited only by the need to balance adequate digitization of the intermediate signal against excessive loss of intensity from subsequent signals through relaxation. The NOESY experiment, which is derived from COSY simply by the addition of a mixing period and a third 90° pulse, is an excellent candidate since the eventual NOESY signal is only attenuated at the longitudinal relaxation rate while a COSY signal is being collected.[128,129] This is a particularly useful combination since assignments are frequently made from COSY spectra before attempting to interpret the NOESY data, and NOESY artifacts typically appear at the coordinates of strong COSY cross-peaks. Keeping signals from different steps in a phase cycle separate for later use in various combinations has a similar flavour, as does the method for obtaining pure absorption lineshapes, but few other possibilities have been proposed.[130] Perhaps the more rapid frequency switching available on modern spectrometers will encourage the development of multiple acquisitions in heteronuclear experiments.

IV. COMPLEX PULSES

A. Selective pulses

Whereas the ability of pulse experiments to excite all the lines of the spectrum simultaneously is usually regarded as an advantage over continuous wave methods, it is occasionally useful to restrict the region of excitation. The most familiar case is perhaps the nOe difference experiment in which significantly higher sensitivity can be obtained in a one-dimensional experiment than from a NOESY spectrum for a single saturated line or multiplet.[131] This is directly analogous to the relationship between normal one-dimensional Fourier transform and continuous wave spectra in which the sensitivity advantage of the Fourier transform method may be viewed as a consequence of the time wasted scanning the baseline in the continuous wave method. However, if it is only necessary to measure the amplitude of a single line of known frequency, then the continuous wave scan can be restricted to the line while the Fourier transform spectrum wastes data points on defining the irrelevant parts of the spectrum. The problem becomes acute in two-dimensional spectroscopy since digitization is generally poor yet there is an increasing drive to use the enhanced resolution which results from dispersing signals in two dimensions to examine multiplet structures in detail or make quantitative nOe measurements, both of which require very good digital resolution. Here lies the rub; not only does the sensitivity advantage of one-dimensional over two-dimensional experiments increase as the digital resolution is improved, but the two-dimensional sensitivity is actually degraded if there is limited storage space for the data matrix.[93,94] One way out is to restrict the spectral width in the second dimension; some folding can be tolerated in double-quantum experiments without causing signal overlap,[132] but this can only be achieved in general by restricting the range of frequencies present during the evolution period by using a selective pulse at the beginning of the sequence. The problem is naturally more acute if an experiment is to be extended to three dimensions, and selective pulses have been demonstrated in this context,[133-135] but the spectral widths and potential applications are extremely limited.

If a single transition or multiplet is excited initially then a one-dimensional analogue of the two-dimensional experiment is obtained, and this has been demonstrated for COSY, MQF-COSY, NOESY, RELAY and TOCSY by using a Gaussian shaped pulse for selectivity.[136-138] The perturbation of a single line can also be spread throughout a multiplet by following a selective pulse by a hard 90° pulse.[139-141] Truncated Gaussians are generally preferred to rectangular soft pulses, though the technology is available to produce an infinite variety of shapes[142,143] and each is sure to find a proposer.[144]

B. Water suppression

There has been renewed interest in the generation of frequency selective pulses, on the one hand as a spin-off from the development of magnetic resonance imaging with all of its consequences for spectrometer technology, and on the other because of the growing importance of discriminating against certain frequencies, usually that of protons in water.

The availability of very high field NMR instruments has made it common to study solutes in very low concentrations so that solvent impurities, either chemical or isotopic, are seen as an increasing problem. The worst possible case, however, arises with the need to observe exchangeable protons in water. The assignment of spectra from peptides and proteins depends on the observation of amide proton resonances and typically involves a relative concentration around 100 ppm. Furthermore, the absolute strength of the water signal is usually sufficient for the famous scapegoat "radiation damping" actually to be significant so that the peak is broad. Finally, the region obscured by the wings of the line includes many peptide αCH resonances.

Multiple-quantum filtration would seem the obvious solution, but the water singlet is cancelled only on completion of a phase cycle so the problem of dynamic range is not relieved. Dumoulin reports suppression ratios of only 100:1 achieved in this manner.[145] Presaturation may help and is indeed used in most experiments, but the underlying αCH resonances are also saturated and the amide protons may also become saturated through chemical exchange. Another possibility is so called "T_1 nulling" which makes use of the differences in relaxation rates of solvent and solute, but residual transverse magnetization may still cause problems. High concentrations of ammonium or hydroxylammonium salts have been used to shorten the T_2 of water to alleviate this in suitable samples.[146-149]

Many combinations of these approaches have been considered,[150-160] but most of the activity in recent years has been directed simply to avoiding excitation of the solvent line by using selective pulses. Redfield's original contribution virtually monopolized the field for some years until Plateau and Gueron proposed the "Jump-return" sequence.[161] These two methods are fundamentally different in approach. Redfield's "214" pulse is a soft pulse modified with reference to the Fourier transform of the pattern of excitation, an approach which assumes a linear response from the spin system, whereas Plateau and Gueron consider the effect of hard pulses in a Bloch vector model. Both methods require considerable adjustment by trial and error and have limited success, as reviewed recently.[162] Trial and error is required for the 214 pulse because the approximation of a linear response is breaking down, and the full advantage of the Jump-return sequence is only realized with good 90° pulses, so some fiddling is necessary in the presence of inhomo-

geneous B_1 fields. Ideally, the solvent magnetization is aligned with the y-axis of the rotating frame when a 90° return pulse is applied along the x-axis so that the remaining transverse magnetization has pure $\pm x$ phase. A null is only obtained at a single frequency, but the wings of the water line which remain are less troublesome because there is no first-order phase correction necessary.

The two approaches have been combined in the "binomial" sequences[163] with the $1\text{-}\tau\text{-}\bar{3}\text{-}\tau\text{-}3\text{-}\tau\text{-}\bar{1}$ "quartet" pulse as the target set up for a host of competitors. The underlying principle of this linear response approach is that the suppression of a line of finite width can be improved by using a sequence which has higher derivatives of the pattern of excitation simultaneously zeroed. The nth order binomial sequence of hard pulses (the single pulse being a zero-order binomial sequence for the purpose of this discussion) has an excitation pattern $\sin^n(\omega\tau)$ with $(n-1)$ derivatives zero at the null. The first advantage of this family of sequences is that it is not sensitive to breakdown of the linear approximation and so requires no adjustment of pulse lengths and is not affected by B_1 inhomogeneity.[163] The sequences with even numbers of pulses are further tolerant of reproducibly misshapen pulses. The poor performance of sequences with an odd number of pulses results from the asymmetric form of real radio-frequency pulses and may be improved by splitting the central pulse into two parts, each of which has the same rise and fall characteristics.[164] The major deficiencies of the scheme are that the flatter nulls are paid for by narrowed regions of excitation and that the resulting spectra require large approximately first-order phase corrections so that residual wings of the solvent line cause severe baseline roll. Two attempts to improve the method simply miss the point: the "OBTUSE" approach[165] fails because it has an odd number of pulses and the square wave synthesis[166] maximizes the derivative of the pattern of excitation at the null. Various groups have tried different methods for optimizing linear combinations of binomial sequences which naturally share the deficiencies of the parents,[167,168] including a tongue-in-cheek attempt at breeding them.[169] Following a binomial sequence by refocusing also has possibilities but depends on finding the perfect 180° pulse.[170]

Coherent averaging theory provides an alternative to trial and error, though Levitt *et al.*[171,172] have not had great success even with extended trains of soft pulses. Criteria for measuring the success of an existing sequence have been discussed.[173] Simplicity seems all important in this area. It may be easy to obtain a good illustration of a new method, but a technique needs to be reproducibly effective and easily implemented if it is to be of general use. Despite its deficiencies, the quartet sequence appears to meet these more demanding criteria, but, if it is to be improved upon, it seems necessary to take a radically different starting point.

The pack has picked up the scent of the Jump-return sequence again with some variations including soft pulses.[174,175] The asymmetric sequence $1\text{-}\tau\text{-}\bar{1}1\text{-}2\tau\text{-}\bar{1}$ in which the second Jump-return component is phase cycled to act as a refocusing pulse seems to show promise since it has the same excitation pattern as the quartet but avoids the large phase correction.[176-178] However, the baseline roll is being traded for a need to obtain good 90° pulses and a simple baseline correction may still be preferable.

Whichever approach is employed, good B_0 homogeneity is essential over the effective sample volume. Dykstra[179] has shown that much of the residual water signal results from pickup by the coil leads from regions of poor homogeneity in the static magnetic field which may result from the materials used in the probe construction or from the discontinuity in magnetic susceptibility at the bottom of the sample tube. He successfully eliminated a massive hump which remained after selected saturation of the water line by screening the coil leads with a zero susceptibility Ag/Pd film. Restricting the effective sample volume has the same effect, but at the cost of a severe reduction in sensitivity.[180]

Santos *et al.*[181] identified the major application for binomial pulses in two-dimensional experiments as the observation of nuclear Overhauser enhancements of amide protons. As singlets or unresolved multiplets, filtration methods are unsuitable, and presaturation is undesirable because of proton exchange. The exchange rates of amide protons with water actually contain significant structural information which may be extracted as a bonus from any NOESY type of experiment. The inclusion of a binomial pulse in the standard NOESY sequence allowed the more rapidly exchanging protons of cytochrome *c* to be identified.[181] The baseline roll associated with binomial sequences may cause difficulties for the less sophisticated software packages if contour plots are sought, but the two-dimensional Fourier transform is not in fact necessary to measure exchange rates. If, as is usual, the reference frequency coincides with the solvent line then a simple addition of the increments of the two-dimensional experiment yields the cross-section at zero frequency in the second dimension which carries the exchange information. The two-dimensional experiment[181] has been applied to the measurement of exchange rates in the cyclic peptide viomycin[182] and similar techniques have employed the basic "Jump-return" or $1\text{-}\bar{1}$ read pulse[183,184] and selective inversion.[158]

C. Pulses for the selection of heteronuclear couplings

The BIRD pulse[185] is designed to provide selectivity with respect to heteronuclear couplings rather than frequency. By using fixed delays and 180° pulses applied simultaneously to both heteronuclei, the J modulation can be

exploited to distinguish couplings of different magnitude. This becomes useful in cases such as ^{13}C–^{1}H coupling since the one-bond coupling is large and roughly constant whereas the longer range couplings are quite small, and the low natural abundance of ^{13}C means that only a few protons in each molecule experience large couplings. It is then possible to apply a selective inversion to all protons which are *not* directly bonded to a carbon-13 nucleus to obtain effective homonuclear decoupling in heteronuclear shift correlation or *J*-resolved spectra, or to choose to observe splittings or coherence transfer arising from long- or short-range couplings.[186–197] This can improve sensitivity by reducing the width of multiplets, particularly those of methylene protons, though variations in coupling constants and short transverse relaxation times can eliminate much of the potential advantage. The usual catch-22 applies insofar as it is possible to devise sequences which are more tolerant of variations in the scalar coupling, but they are much longer and so lose more signal through relaxation.[198,199]

D. Composite pulses

A composite pulse is no different in principle from the shaped or segmented pulses used for selective excitation, but the original and most widely applicable type was designed simply to achieve a broadband population inversion[200] and uses only three segments with varied length and phase. The development of the field has been reviewed recently by its originator.[201] Spin inversion is a more limited capability than a general 180° pulse and most composites are unsuitable for refocusing. The majority of composites which have been proposed are also limited in their compensation — usually to resonance offset — and may be highly sensitive to inhomogeneity in the radio-frequency field or to the adjustment of phase shifts.[202–204] It is also possible to cycle the phase of segments to cancel effects such as acoustic ringing which, unlike the NMR signal, have an approximately linear relationship with the radio-frequency pulse.[205–207]

Whereas the linear response approximation forms the basis for most of the development of selective pulses, all of the early composite pulse schemes were derived by vector waving and Bloch simulations. The same approach can be made more efficient through computer optimization,[208,209] and it has been formalized to some extent by considering the net rotation produced by a series of pulses using the quaternion formalism.[210,211] Attempts have also been made to use average Hamiltonian theory to develop composite pulses with more general applications,[212,213] particularly for use with non-equilibrium spin systems,[214,215] and for multiple-quantum excitation.[216,217]

E. Composite pulse decoupling

Heteronuclear decoupling is one of the most complex problems encountered in NMR. Most simple treatments assume either that the heteronuclei are subject to rapid random spin flips so that the coupling may be ignored as if it were to the quadrupolar chlorine nucleus or to a proton in rapid exchange, or that the decoupling field is not modulated at all so that it can be accounted for easily in the modified Hamiltonian. These two extremes are rarely applicable, and the most successful decoupling schemes use quite deliberate sequences of rotations which bear no resemblance to either.[218] The fact that decoupling involves coherent perturbations rather than a simple disconnection of the interactions was clearly illustrated in some of the earliest two-dimensional experiments and has been reexamined recently[94,219] and used as the basis of an alternative to off-resonance decoupling.[220,221] The deeper understanding of the decoupling process provided by Waugh[222] seems to have put an end to the development of modulation schemes which attempt to improve the efficiency of "noise" decoupling, and it explains the lack of success of the elegant scheme proposed for decoupling with low power input by means of a train of 180° pulses.[25] Despite the advantages of minimizing sample heating and consequent thermal gradients,[223,224] the simple 180° pulse rapidly builds up errors through imperfect inversion. The substitution of composite spin inversion pulses is an obvious development and the process becomes highly efficient when the composite pulses are themselves cycled to provide higher orders of compensation.

The first limitation of composite pulse decoupling sequences is that they generate sidebands. These comprise as much as 10% of the total signal intensity with methods such as "GARP",[225] but they can at least be smeared out by introducing cyclic permutations into successive supercycles. The efforts made to improve on the early sequences have been no more rewarding than those made to improve on binomial solvent suppression. In general, the simpler the better, and in this sense the WALTZ-16 sequence scores heavily by using only 180° phase shifts and avoiding the temperamental behaviour of the MLEV with respect to phase errors.[226,227] More complex sequences are not necessarily better,[228] and it might be interesting simply to check the performance of simple 180° pulses built into supercycles. The second major problem with composite pulse decoupling is that performance can suffer dramatically in the presence of homonuclear couplings because bilinear terms develop which are constant with respect to the cycle.[229] This may be minimized simply by increasing the power[230] and has led to efforts to find improved sequences for dealing with large homonuclear couplings such as the dipolar couplings observed in liquid crystal solvents[227] and sequences which may be useful specifically for suppressing homonuclear dipolar couplings.[231,232]

V. HOMONUCLEAR TWO-DIMENSIONAL AND RELATED EXPERIMENTS

A. Homonuclear shift correlation experiments (COSY)

COSY, the archetype of high-resolution two-dimensional NMR experiments, is now well into its second decade and has virtually superseded homonuclear decoupling experiments for assignment purposes in most laboratories. Interference from the ridges associated with strong diagonal peaks is its greatest weakness, and this is still more apparent in "pure phase" spectra since the multiplets on the diagonal appear as double dispersions with a 90° mixing pulse when the cross-peaks are in pure absorption. The cross-peaks also have zero net intensity and rapidly lose intensity through cancellation if the linewidth approaches the active coupling constant. This has some advantages if the broader lines are of no interest,[233] but if such weak cross-peaks are sought it may be better to inspect the pure dispersion component since the broad peaks actually reinforce in the centre of the multiplet and the diagonal peaks are also less intrusive since they become pure absorptions. A variety of modifications of the evolution period use refocusing to scale down the cross-peak splittings or bring the cross-peak components into phase in a manner similar to that commonly used in heteronuclear shift correlation experiments.[234-239] The experiment can also be modified to have a constant evolution period so that homonuclear couplings are removed from the second dimension.[240] Some intensity is lost through relaxation, but this is partly compensated by the increased peak height resulting from the collapse of multiplet structure and in any case the loss of broad lines is sometimes desirable.[233,241] An alternative proposal uses what is effectively a multiple-quantum filtered refocusing pulse to select the component with the passive spins inverted.[242] The intensity of diagonal peaks may be reduced by difference methods[243] or by reducing the flip angle of the mixing pulse, in which case their phase distortion may be reduced by subtraction.[243]

The basic experiment has found numerous applications, particularly for the assignment of proton spectra from systems of biological interest such as peptides,[245-250] oligonucleotides,[251,252] and complex organic molecules.[253-259] The range of other nuclei to have their homonuclear couplings explored in this way is also increasing with studies of ^{2}H,[260,261] ^{11}B,[262-266] ^{19}F,[267] ^{29}Si,[268,269] ^{31}P,[270] and ^{51}V[271] to name a few.

It is not easy to "violate" a COSY experiment, as the multiple-quantum coherences generated from strongly coupled spin systems through non-equilibrium populations of the second kind if the relaxation delay is too short[272] do not count. Nor do deliberate attempts to spoil its symmetry.[273-275] A mechanism must be found which will generate variations in the transverse

relaxation behaviour between degenerate components of a line. The components then fail to cancel and a spurious cross-peak may appear to connect two spins which are not coupled to each other. This cross-peak has a multiplet structure which differs in the two dimensions, reflecting the structures of the two spins it purports to connect but which do not have a common coupling constant. Cross-correlation between field modulations which cause relaxation provides just such a mechanism and the effects of cross-correlation between dipole–dipole relaxation and chemical shift anisotropy on heteronuclear nOes are quite well known.[276,277] Bull[278] is somewhat further advanced in seeking to vary the flip angles used in the NOESY experiment to favour $I_{kz}I_{lz}I_{mz}$ terms in the mixing period to study cross-correlation effects which couple such "*zzz*" magnetization with simple populations.

It is easier to visualize the effect of cross-correlation between different sources of dipole–dipole relaxation, and an example has been found to illustrate this.[279] Consider the behaviour of the proton in the middle of a line of three: the dipolar fields of its neighbours will reinforce if they have the same spin state or cancel if they are opposite. Now let the central proton couple to just one of the others to give a doublet, and consider one of the two lines. This will comprise two degenerate components of different width which reflect the influence of the spin state of the third proton. The COSY experiment "transfers" these components to the third proton in antiphase and they fail to cancel because of the difference in linewidth. This is essentially identical to the mechanism which generates adventitious peaks in multiple-quantum filtered spectra and will be discussed further under that heading.

B. Multiple-quantum filters

A pulse applied to a system which is not at equilibrium may create higher orders of coherence than the normally observable single quantum order. An extremely weak zero-quantum coherence may be generated by a 90° pulse applied to a system at equilibrium since "weak coupling" is only ever an approximation,[280] though it has been questioned whether this effect is in fact an example of the limitation of the high temperature approximation.[281] This coherence must be converted to order + 1 for detection and cycling the phase of the excitation and detection sequences can be used to cancel out contributions from all but some chosen order. Simply adding a third pulse to the normal COSY sequence immediately after the mixing pulse allows detection of coherence which has been transferred via any chosen order. This allows singlets to be excluded from the COSY spectrum by selecting a double-quantum intermediate since isolated spin-1/2 nuclei naturally are unable to produce higher than single-quantum coherence. Simple AX spin systems can

be rejected also by choosing a triple-quantum intermediate, but this level of filtration is rarely used because the higher orders are inefficiently excited and on balance the simplification of the spectrum does not justify the loss of sensitivity.

A cycle for the selection of order p will pass signals from any system of p or more coupled spins, but the p-quantum magnetization arising from just p spins is a singlet and signals from more complex spin systems can be attenuated by varying the separation of the pulses with refocusing to modulate the phase of the multiplets.[282,283] Keeping the signals from each step in the cycle separate also allows different filters to be selected from the same data set by taking different combinations.[284] The coordinates of the components of the cross-peaks in multiple-quantum filtered COSY spectra are identical to those of normal COSY, but their phases may be inverted.[285,286] For example, the AX cross-peak from an AMX spin system survives double- or triple-quantum filtration. The basic square of the simple AX COSY cross-peak remains with four lines of equal magnitude in a $\pm\mp$ pattern with separations J_{AX} which is then reproduced four times with the same phase as if convoluted with the pattern $\pm\pm$ with separations given by the couplings to the passive spin, J_{AM} and J_{MX}, in each dimension. This is the same for COSY and double-quantum filtered COSY, but in the triple-quantum filtered version two of the groups are inverted with the convoluting pattern $\pm\mp$. In that case, the central components of the pure absorption multiplet tend to coalesce and the resulting pattern is quite similar to that obtained from a simple AX cross-peak shown in the double dispersion mode. As with normal COSY, it is also possible to use an evolution period of constant length with the modulation generated by stepping the position of a refocusing pulse in order to suppress multiplet structure in the second dimension.[287]

Even so, the removal of singlets to produce slightly cleaner spectra than normal COSY seems a small advantage for which to pay at least half the sensitivity of the basic experiment. Rather greater advantages can be obtained by keeping the double-quantum frequencies in the second dimension as discussed in the next section. One of the more interesting aspects of the multiple-quantum filter is that this is where the scandal of selection rule violation first broke. As usual, there are two kinds of affront to the simple minded; a trivial effect of strong coupling and a result of non-exponential relaxation which is most familiar for spins or composite spins which have $I > 1$ in systems outside the extreme narrowing region.

The "rule" for weak coupling[8] is that a cross-peak may connect the multiplets of two spins in a p-quantum filtered COSY spectrum only if the two spins have p-2 coupling partners in common which show resolved splittings. A linear AMX system ($J_{AX} = 0$) should not show an M–X cross-peak in a triple-quantum filtered spectrum. However, an ABX system will produce a

B–X cross-peak since all of the transitions of the AB system are the joint property of the two spins and spin X taps into this by coupling to spin B. The rule for weak coupling is therefore modified to allow that a *strong* coupling partner of either one of the spins acts as a common partner for the other even if the coupling constant is zero. The minimum condition is thus that only one of the spins need have p-2 strong coupling partners to show a cross-peak in a p-quantum filtered spectrum with a spin to which it is weakly coupled and which has no other couplings. Similar effects have been observed in heteronuclear shift correlation[288,290] and RELAY experiments.[291,292]

The biexponential transverse relaxation observed for $I=3/2$ spins when $\omega_0\tau_c \gg 1$ forms the basis of the most widely recognized violation of the selection rules provided by PROPs. This is a common phenomenon within the $I=3/2$ composite spin state of methyl protons in macromolecules and allows the AX_3 spin systems of alanine and threonine to generate up to quadruple-quantum coherence.[285,293–295] The effect can usefully be exploited by preceding the COSY experiment with an inversion-recovery sequence[296,297] $180°$–τ–$90°$–t_1–$90°$–AQ(t_2) which can then be phase cycled to pick out the triple-quantum coherence generated from the modified populations of methyl groups.[298] The principle can be applied to individual $I=3/2$ nuclei such as ^{23}Na and ^{7}Li, for which deconvolution of the double lorentzian lineshape in ordinary one-dimensional spectra to detect ion binding to macromolecules is a well established procedure.[299] In that case the $\pm 3/2 \leftrightarrow \pm 1/2$ and the $\pm 1/2 \leftrightarrow \mp 1/2$ coherences have a 6:4 intensity ratio but if the magnetization is passed through a double-quantum filter the two components appear in antiphase and with equal intensity.[300] The filtered signal then appears as the difference of two lorentzian lines which are of unequal width if the rotational correlation time is long but will cancel exactly for free ions with short correlation times. This has been used to distinguish intracellular sodium ions[301,302] and to study sodium in lyotropic liquid crystals.[303]

C. Multiple-quantum experiments

The only real difference between a multiple-quantum filtered experiment and a multiple-quantum experiment is that the first has a fixed period for the multiple-quantum state whereas the second increments the period as an evolution time. The multiple-quantum coherence cannot be observed directly[304] so it must be converted into single-quantum coherence for detection, hence all of these experiments are essentially two-dimensional. There are certain advantages in correlating the ordinary NMR frequencies with multiple-quantum frequencies in the second dimension because overlap between peaks in the first dimension may be removed in the second, but the efficiency of excitation varies with coupling constants.[305] The two-

dimensional filtering experiment has the advantage in this sense because the excitation sequence comprises the variable evolution period and eliminates the dependence on J. Summing over several experiments with variable excitation periods achieves a similar effect, but it is very time consuming.[306]

Zero- and double-quantum spectra have attracted most attention and other applications have been discussed in a recent review.[307] Homonuclear zero-quantum coherence has frequencies lower than the maximum range of shifts for the nucleus, that is of the order of kilohertz, and is therefore quite insensitive to inhomogeneity in the static magnetic field. This creates the possibility of obtaining high resolution in the second dimension even in the presence of severe B_0 inhomogeneity, and this may have applications to tissue samples.[308-310] Phase cycling in these experiments can be simplified because the poor B_0 homogeneity destroys all higher order coherence, but there are problems in the efficient generation of zero-quantum coherence[311,312] and in separating it from longitudinal magnetization because that also has order zero.[313]

A method has been proposed for generating pure homonuclear zero-quantum coherence selectively in the linear coupled spin system H–H–^{13}C for use in long range ^{1}H–^{13}C correlation.[314] The relaxation behaviour of multiple quantum coherence is of some interest and an unusual case has been found in which scalar coupling to a rapidly relaxing quadrupolar nucleus causes the heteronuclear double-quantum state to relax more slowly than the zero-quantum in $SiHCl_3$ since J_{SiCl} and J_{HCl} are of opposite sign.[315]

Double-quantum COSY spectra correlate normal NMR frequencies with the sums of frequencies such that, for example, NH–αCH cross-peaks are shifted away from the frequency of solvent water in the second dimension and peaks may be revealed which are not accessible even in the double-quantum filtered COSY spectrum.[151,316,317] Peaks representing remote connectivities may also appear, but with shifted phase.[318] This makes the technique attractive for cross-checking assignments in protein studies and the multiplet patterns obtained have been described in detail.[319,320] Most of the modifications applicable to the COSY experiment have also been adapted for double-quantum COSY, including constant time experiments,[321] scaling,[322] difference spectra[323] and filtering.[324,325] The maximum spectral area occupied by such spectra is naturally lozenge-shaped and the experiment can be made more efficient by limiting the spectral width in the second dimension to half of the maximum without causing overlap through folding. Pure absorption lineshapes can then be generated and the "true" frequencies restored by digital unwrapping. If the spectrum is skewed by refocusing,[326,327] then it is no longer possible to generate pure phases. The experiment is subject to violations of the same kind as double-quantum filtered COSY, and the

appearance of "forbidden" peaks in AX_3 spin systems has been used to distinguish the more rigid parts of proteins.[328]

The double-quantum COSY experiment is particularly useful for the observation of couplings between directly bonded carbon-13 nuclei because the double-quantum state can be excited efficiently since the range of coupling constants is small, and the strong singlets arising from isolated carbon-13 nuclei are naturally suppressed. A number of spectra have been assigned and structures elucidated by this means[132,329-334] and the possibility of applying the experiment in the solid state has been demonstrated.[335] The method is also useful for identifying sites of double labelling in synthetic and biosynthetic studies[336-340] and has even been extended to triple-quantum COSY to pick out a group of three ^{13}C labels.[341] The one-dimensional double-quantum filtered experiment is also useful for measuring coupling constants without interference from singlets.[342]

D. Filtering spectra by means of heteronuclear couplings

The popularity of biological NMR has led to a demand for resolving power even beyond that of multiple-quantum filtered two-dimensional spectra. This is easily obtained in the presence of dilute spin-1/2 heteronuclei by taking the difference between the normal spectrum and one obtained with inversion of the heteronucleus just before detection. The effect has been tested with ^{113}Cd in a Cd^{2+}-EDTA complex and put to work in metallothionein.[343,344] Similar effects may be achieved using the BIRD sequence or heteronuclear zero-quantum coherence.[345-348]

E. Incoherent coherence transfer

Whereas the methods discussed above all involve scalar couplings which allow the transfer of coherence between spins by means of pulse, the three-pulse experiment simply leaves longitudinal magnetization for a period to undergo exchange via the incoherent processes of dipolar cross-relaxation or chemical exchange. This may be more familiar if it is described as exchange between spin populations, but we should seek to maintain a coherent nomenclature and populations are as respectable a zero-order coherence as any other. The existence of two incoherent exchange mechanisms confuses both the terminology and the spectra since the effects of chemical or conformational exchange may be observed alongside those of cross-relaxation. For our purposes the identical experiment will therefore be called EXSY or NOESY according to the dominant mechanism for transfer, though most technical points apply to the two equally and this should be borne in mind when searching the literature.[349]

Distinguishing the two effects is straightforward in small molecules in non-viscous solvents since the nuclear Overhauser enhancement is positive and produces cross-peaks of opposite sign to the transfer of saturation. Both effects are negative in macromolecules, in which case a difference in temperature dependence may help sort them out[350] or a rotating frame experiment may prove useful. The same problem applies to selective saturation or inversion experiments and the dynamic effects observed by selective inversion are described by identical equations to those used in the two-dimensional case.[94] The advantage of observing all possible effects simultaneously in a two-dimensional experiment, be it NOESY or EXSY, is offset by the loss of intensity with respect to the steady state produced by selective saturation,[94] so experiments applied to simple molecules may be assumed to be for demonstration purposes only.

Unlike COSY, there is no advantage in using mixing pulses of less than 90° since it cannot affect the relative intensities of the diagonal and cross-peaks. Various methods have been tried for reducing diagonal peaks,[107,351-353] but the diagonal may actually be useful in providing references for intensity.[354] Indeed, if the 90° pulses are imperfect, longitudinal spin order (also referred to as "zz" magnetization from the PROP $I_{kz}I_{lz}$) may be generated in coupled spin systems which will create antiphase cross-peaks similar to those observed in COSY[74] or those generated by residual transverse zero-quantum coherence. The intrusive zero-quantum coherence may be attenuated by summing over sequences with varied mixing times or by varying the position of a refocusing pulse within the mixing period,[355] but the longitudinal spin order is unaffected by such tactics. Deliberate use of 45° pulses allows the exchange of two-spin order to be monitored in systems with resolved couplings and the dependence on the mixing time can then be used to distinguish the effects of cross-relaxation and chemical exchange.[356] Integrating over cross-peaks in pure absorption spectra is recommended for quantitative measurements,[357-359] and, since the COSY type cross-peaks have zero integrals, "zz" magnetization may safely be ignored.

F. EXSY studies of chemical exchange

Many experiments are susceptible to purely qualitative interpretation, but EXSY and, to a lesser extent, NOESY are becoming established as sources of quantitative data. Willem has reviewed the technique and its applications to stereochemical problems.[360] The essential difficulty with the extraction of rate constants is the need to know relaxation times. This information is available in principle from the intensities of the diagonal peaks, but these often exhibit severe overlap and may be difficult to measure. Prefacing the experiment with an inversion-recovery sequence weights the cross-peaks with T_1

information so that comparison with a normal EXSY experiment makes reference to the diagonal peaks unnecessary.[361] It has also been shown that the total intensity of signals on individual cross-sections can be used to obtain relative relaxation rates without the need to measure the absolute intensities of signals at zero mixing time.[362] A variety of procedures for analysing data from systems exhibiting multisite exchange have been considered. Data may be fitted to obtain rates and amplitudes from multiexponential decays as the first step[363] or fitted directly to obtain the exchange rates and T_1 values of individual nuclei,[364] in which case the fit can be constrained to reflect the physically possible exchange processes.[365] Analysis of EXSY data has been used in the study of the mechanism of rearrangements[366-370] and the assignment of subspectra from exchanging species,[371,372] but selective one-dimensional methods still find use[373] though two-dimensional methods have the advantage of avoiding the need for selectivity in crowded spectra.[374,375] Laser pulses have also been used in conjunction with EXSY to generate photo-CIDNP and pick out aromatic groups on the surface of proteins by a difference method.[376-378] The normal mixing period has also been replaced by a laser pulse for the study of a photocyclization.[379]

The ACCORDION experiment was proposed to avoid the need for several EXSY experiments performed with different mixing times. Incrementing the mixing period in concert with the evolution period modifies the lineshapes of the cross-peaks, though good resolution and high sensitivity are needed to obtain any information from them. A selective experiment would be expected to be more efficient under such circumstances and this has been demonstrated for phosphorus undergoing two-site exchange.[380] Even so, the method has been used to extract approximate rate constants[381] and in qualitative studies.[382]

G. NOESY studies of dipolar cross-relaxation

It is actually easier to obtain good NOESY spectra from macromolecules than it is for COSY since the components of the cross-peak multiplets reinforce each other, and the technique has become standard for the assignment of protons in peptide backbones. Unfortunately, the key NH protons exchange with solvent water and these experiments must be performed in 90% H_2O;[383-385] some aspects of this problem are discussed in Section IV.B. The increasing natural linewidths and spectral crowding place an upper limit in the region of 15 kD on the size of systems to be assigned comprehensively, but some primary assignments have been obtained from the flexible *N*-terminal regions of an assembly of approximately 3.6 MD[386] and per-deuteriated amino acids have been used to avoid interference from aromatic protons in a protein of 18 kD.[387] NOESY has also become popular in studies

of oligosaccharides,[388-391] and oligonucleotides and their complexes[392-402] and these areas have been reviewed.[403,404]

Although the theory of Overhauser enhancements in multispin systems is well established, the growing interest in defining conformations of macromolecules in solution[405-413] has led to a great deal of discussion about the extraction of internuclear distances from NOESY spectra. The interpretation of cross-peaks is generally qualitative, typically being used to establish relative configurations or place a 4 Å constraint on separations to be used in distance geometry reconstructions. Computed structures are increasingly common in the literature and often appear to carry the conviction of similar diagrams obtained from X-ray diffraction patterns, but solution conformations are generally dynamic and the conformation of peptide side chains is only poorly defined by NMR. The dynamic problem is more severe in short peptides, and it should be noted that NH_i–NH_{i+1} nOe's are normally observed as a result of averaging over many conformations in the "random coil" and do not necessarily represent any kind of structural feature.

Quantitative measurements are usually made from build-up rates in a series of spectra obtained with different mixing times, though a knowledge of the rotational correlation time from a rigid system may make it possible to use the ratio of intensity between the diagonal and cross-peaks in a single experiment.[414] Careful measurements made with small rigid systems seem to give good agreement with crystallographic data,[415-417] but it is clearly important to test the assumption of rigidity by T_1 measurements. The two-spin approximation is then commonly used to fit data[418-423] and comparison with three-spin simulations[424] or analysis of data allowing for spin diffusion[425-427] suggests that distances may be overestimated by up to 20%, which is acceptable for establishing gross conformational features. Some information has also been obtained about the structure of aggregates from intermolecular cross-relaxation between phospholipids in micelles and with their counterions.[428,429]

HOESY,[430] the heteronuclear analogue for NOESY, has found applications in the assignment of non-protonated nuclei, including ^{31}P, ^{19}F, ^{13}C and ^{6}Li[431-434] which have been reviewed recently.[435] Some apparently negative nOe's have been observed in small molecules which result from the heteronuclear analogue of the three-spin effect in relaying the Overhauser enhancement from ^{1}H to ^{1}H to ^{13}C.[436-438]

H. Rotating frame experiments

Just as the COSY and NOESY/EXSY experiments use pulses or incoherent exchange mechanisms to transfer longitudinal magnetization, schemes have been devised for the interchange of transverse magnetization. Since exchange

of magnetization through scalar coupling in the rotating frame requires that the Zeeman term be suppressed during an extended mixing period, the two experiments become essentially indistinguishable except insofar as exchange through scalar couplings is oscillatory and that through dipole–dipole relaxation or chemical exchange reaches an equilibrium. Little has been added to the understanding of these experiments since Braunschweiler and Ernst introduced "isotropic mixing", called TOCSY,[439] and Bothner-By and coworkers devised its counterpart for incoherent exchange and called it CAMELSPIN,[440] but a number of minor modifications have been proposed under aliases such as HOHAHA and ROESY as the potential advantages of these experiments have become more widely realized.

The TOCSY experiment offers the ultimate extension of relayed COSY spectra insofar as cross-peaks are observed throughout each spin system with the added advantage that there is net magnetization transfer so that all components of a multiplet are positive, but it shares the disadvantage that the peak intensities vary with the mixing time and coupling constants so they may disappear altogether. The major advantage of the CAMELSPIN experiment over the conventional NOE is that the effects are positive for all rotational correlation times so there is no possibility of the effect vanishing for molecules of intermediate size, such as the small peptides, which are beginning to attract a great deal of interest. Conversely, a comparison of the transverse and longitudinal cross-relaxation rates can provide an estimate of τ_c.[441]

Since both TOCSY and CAMELSPIN effects can be generated in a mixing period during which a simple spin locking field is applied, it is not surprising that considerable effort has gone into testing modulation schemes which may separate the two. Both isotropic mixing and chemical exchange represent saturation transfer and generate cross-peaks of the same sign as the diagonal peaks, while the rotating frame nOe is an enhancement which is of opposite sign.[440,442] Competition between these effects is particularly serious when methylene protons are used to provide a yardstick for estimating relative internuclear distances from nOe's, though the oscillatory nature of the TOCSY effect[443–446] should help to distinguish it in studies which use a series of mixing times. The problem is compounded further by the complement of the three-spin effect in ordinary nOe experiments, in which the direct enhancement is positive and may be relayed to the next-nearest neighbour to produce a negative effect.[447,448] It is also possible to observe two-step transfers in which the mechanism alternates between scalar and dipolar couplings.[449]

The essence of increasing the TOCSY effect lies in ensuring that the modulation is broadband and so the composite pulse decoupling schemes would seem to be obvious candidates, despite the fact that the component pulses are not designed to invert transverse magnetization. Variants in which

the magnetization is rotated to the z-axis at the beginning of a mixing period during which the WALTZ-16 sequence is applied seem to have cleaner phase characteristics,[450,451] as well as having the advantages that the low power spin locking field may have a different frequency to the main transmitter and reference. On the other hand, there is general agreement that a low power spin locking field will allow the observation of nOe's and minimize the effects of scalar couplings.[452] Kessler *et al.*[453,454] claim that replacing the continuous field with a series of short pulses will further reduce the TOCSY effect if the effective flip angle of the pulses differs from 180°. Bax[455] insists that this is incorrect, but only offers a simplistic account of the theory and assumes that flip angles in the region of 30° can be treated as "very much less than 180°", so the matter has yet to be resolved.

A theoretical framework for understanding the TOCSY effect has been developed by Waugh[456] and used to evaluate the performance of different modulation schemes. MLEV-16 is expected to be inefficient if the field strength is lower than about three times the shift difference between coupled spins, and WALTZ-16 should perform less well with high powers but be more tolerant of reduced field strengths. A simple periodic phase inversion of the spin locking field has also been proposed[457] and evaluated.[458] Several other modulation schemes have been advanced,[459-461] including MLEV-16 cycles separated by simple 180° pulses and with the mixing period bracketed by short periods of continuous spin locking to destroy residual off-axis magnetization. However, these "purging" pulses have been found to be unnecessary in applications to proteins using a 20 kHz field for the MLEV-16 sequence.[462]

Cross-sections from a two-dimensional TOCSY spectrum should ideally show the subspectrum from a complete spin system, and this can be achieved in a one-dimensional difference experiment by using a selective 180° pulse.[463] The TOCSY effect has also been employed to restore magnetization to parts of the spin sytem "bleached" by water presaturation in COSY experiments,[464] and a variety of heteronuclear and relayed rotating frame experiments have been proposed.[465-467]

VI. HETERONUCLEAR EXPERIMENTS

A. Polarization transfer techniques in one dimension

Just as the multiple-quantum excitation in a filtered COSY experiment is broadband with respect to coupling constants by virtue of the incremented evolution period (Section V.B) but runs into difficulties when the preparation period is fixed (section V.C), borrowing the heteronuclear polarization

transfer step from shift correlation experiments as in the "INEPT" experiment leads to enhancements which depend strongly on J values and multiplicities. The "DEPT" experiment is unusual insofar as it was first developed as a one-dimensional experiment at a time when most activity was concentrated in developing two-dimensional experiments and it has since made the reverse journey to become the preferred method for polarization transfer in two-dimensional experiments as well as for the editing spectra according to the number of coupled protons. The two techniques are actually quite closely related in spin space.[468] Considerable effort has been put into determining the optimum delays to use with INEPT or DEPT with exotic combinations of quadrupolar nuclei and equivalent spins.[469–474] Attempts have also been made to broaden the effective range of couplings[199] and to take account of the effects of homonuclear couplings.[475]

The principal application of DEPT and INEPT remains the separation of ^{13}C subspectra according to the number of attached protons[476,477], and the enhancement of signals from nuclei of low magnetogyric ratio also proves useful.[478] The dependence on multiplicity has been coupled with homonuclear J modulation both to select specific patterns of homonuclear coupling[479] and to edit J-resolved spectra.[480] Long-range couplings and two-step transfers can also be used to identify non-protonated neighbours of specific CH groups.[481,482]

With their close practical relationship to heteronuclear shift correlation experiments, DEPT, INEPT, and a variety of other polarization transfer sequences have been used to calibrate proton decoupling field strengths for pulsing in two-dimensional experiments.[483–488] While this will remain important for spectrometers designed with little more than broadband decoupling in mind, the development of symmetrical radio-frequency architecture in response to the needs of modern methodology means that it is becoming more usual to calibrate pulses for heteronuclear experiments simply by observing the proton signal following a single pulse in the traditional manner.

B. Heteronuclear shift correlation

This heteronuclear analogue of the COSY experiment is perhaps best understood as a selective variant of COSY. In its most basic form, the 90° mixing pulse is applied simultaneously to both heteronuclei with no attempt to remove splittings from the cross-peaks in either dimension. This has been dubbed "FUCOUP" in print,[489] but such terms are better avoided, at least in oral presentations. A reversion to the original proposal of exciting the heteronucleus and detecting protons has even been reported,[490,491] but this shares the disadvantages of the heteronuclear multiple-quantum experiments discussed in the next section without taking full advantage of the larger proton population differences.

In the usual form of the experiment, proton magnetization evolves at its Larmor frequency and the effect of heteronuclear coupling is cancelled by refocusing. A fixed additional period is required to generate antiphase terms which are transferred and then left to come back into phase before the protons are decoupled and the heteronuclear signal is detected. Similar principles have been applied to the COSY experiment itself. The standard techniques for generating pure absorption lineshapes by incorporating signals from proton coherence evolving with order $+1$ and -1 can also be used to increase the sensitivity,[105] and the recycle time of the experiment is determined by the relaxation rates of the higher frequency nuclide. Using proton T_1 values to optimize experiments with heteronuclei of low natural abundance is actually conservative since the relevant satellites have the additional relaxation mechanism of dipolar coupling to the heteronucleus.[492] Shift correlation spectra can therefore be obtained with sensitivity approaching that of a normal proton-decoupled one-dimensional spectrum but with the enhanced resolution of signals spread out in the second dimension and separated according to the number of attached protons,[105,493] and the explicit incorporation of specific assignments from the proton spectrum. This has led to renewed interest in ^{13}C studies of proteins and a huge increase in the number of assigned lines[494-497] and the routine use of the method in multinuclear NMR.[498-523]

Long-range proton–carbon-13 couplings in particular have obvious value for obtaining structural information, but the sensitivity of the shift correlation experiment is reduced by transverse relaxation during the extended polarization transfer sequence. For small couplings, the fixed delay $1/(2J)$ is usually longer than the maximum evolution period so that the effective period of proton evolution can be controlled by shifting a refocusing pulse in a "constant time" modification of the experiment called "COLOC".[524,525] In addition to minimizing the loss of signal, this improves resolution and enhances peak heights by suppressing the effects of homonuclear couplings in the second dimension. The technique is best applied to quaternary carbons since the long-range transfer is complicated by the presence of one-bond couplings[526-529] and has proved its utility in systems of moderate complexity such as small peptides.[530-537]

C. Heteronuclear shift correlation with proton detection

The idea behind "inverse" or proton detected experiments is rather simple:[538] the heteronuclear multiple-quantum state created in, for example, a DEPT experiment has the magnitude of the proton population differences and evolves at frequencies which are the sums and differences of the frequencies of both heteronuclei, from which the proton frequency is easily cancelled by switching zero- and double-quantum states.[539] The excitation can then be

reversed to allow detection at the proton frequency, which means picking up a voltage increased by the larger proton magnetic moment and also by the higher frequency. This yields a sensitivity enhancement of $(\gamma_H/\gamma_X)^2$ with respect to the X-nucleus detected DEPT signal or a normal shift correlation experiment and $(\gamma_H/\gamma_X)^3$ with respect to direct detection of the X-nucleus without enhancement.[540] This is reduced by an increase in noise proportional to the square root of the frequency, although the full $(\gamma_H/\gamma_X)^3$ enhancement has been claimed in experiments with ^{15}N.[541]

The advantages of using heteronuclear multiple-quantum coherence in shift correlation experiments would therefore seem to be overwhelming.[542] There are three significant drawbacks, of which the need to buy a heteronuclear probe with an efficient proton coil and usually a smaller sample diameter is the least significant. The X-nucleus often has a much larger spectral dispersion than protons so that the two-dimensional experiment is less efficient in the inverse mode, and it is desirable to restrict the second dimension to a small range of frequencies such as that of ^{15}N in amides. Finally, the proton spectrum may be dominated by signals from uncoupled nuclei if the heteronucleus has a low natural abundance or if the solvent is protonated. At the very least, therefore, the phase cycling must be good enough to suppress singlets of similar magnitude to those encountered in double-quantum filtered carbon-13 spectra, and the difficulties of water suppression discussed in Section IV.B apply to most inverse experiments with biological samples.

Various modifications have been suggested to improve the suppression of signals from protons without heteronuclear couplings, including extended delays to take advantage of the shorter T_2 values of protons bonded to ^{14}N,[543] using the BIRD sequence for selective inversion of protons bonded to ^{12}C for T_1 nulling,[544-546] and selective rotation of unmodulated proton magnetization back to the z-axis before detection.[547] Difference methods can also be used to distinguish the effects of short- and long-range coupling.[548,549] The suppression of water signals is a more serious problem with biological samples and most of the standard methods have been tried, including the Redfield "214" pulse,[550-552] "Jump-return" pulses,[553,554] and spin-lock periods to allow the water signal to decay.[555]

The experiment has obvious applications to the selective observation of signals from protons around an isotopic label and several experiments have made use of ^{113}Cd couplings in model compounds and proteins.[556-558] Further progress in correlating ^{15}N chemical shifts with structure[559] is to be expected, and a considerable database has been obtained from amide nitrogens in BPTI.[560] Proton detection has also been used to assign many of the α-carbons in this small protein.[561] The method has also been applied to ^{31}P in oligonucleotides[562-564] and to ^{57}Fe in iron complexes.[565]

D. Relayed coherence transfer

Almost any pulse experiment can be modified by the addition of a fixed sequence such as DEPT or INEPT to transfer the magnetization to some third nucleus before detection. Many have already been illustrated in addition to the original COSY-relay sequence, including NOESY,[566-569] double-quantum COSY,[570] proton detected heteronuclear multiple-quantum shift correlation,[571] and even the inversion-recovery sequence.[572] This may be useful to pick out structural units[573-580] or to employ the additional resolution or sensitivity of a heteronucleus.[581,582] Related experiments can be used to determine the relative signs of coupling constants in three-spin systems.[583,584] The major difficulty with such "relayed" experiments is that the fixed delays in the coherence transfer step must be optimized for particular coupling constants, as in DEPT or INEPT. These are simple to calculate, at least for weakly coupled systems, but the coefficients for coherence transfer vary dramatically in the presence of additional homonuclear couplings.[585-588] This permits selection of particular spin systems by multiple relay steps,[589-591] but this approach may eventually succumb to the spread of equipment suited to TOCSY experiments. Nonetheless, the basic RELAY experiment in which a COSY-type evolution period is followed by a single transfer to a third spin has been used regularly as an aid in the assignment of proton spectra.[592-597]

REFERENCES

1. W. McFarlane and D.S. Rycroft, in *Annual Reports on NMR Spectroscopy*, Vol. 16, Academic Press, London, 1985.
2. D.L. Turner, *Specialist Periodical Report on Nuclear Magnetic Resonance*, Vol. 17, Ch. 6, Royal Society of Chemistry, London, 1988.
3. D.L. Turner, *Prog. Nucl. Magn. Reson. Spectrosc.*, 1985, **17**, 281.
4. A.D. Bain, *J. Magn. Reson.*, 1988, **77**, 125.
5. R.R. Ernst, A. Wokaun and G. Bodenhausen, *Principles of Nuclear Magnetic Resonance in One and Two Dimensions*, Clarendon Press, Oxford, 1987.
6. G. Bodenhausen, H. Kogler and R.R. Ernst, *J. Magn. Reson.*, 1984, **58**, 370.
7. M.H. Levitt, G. Bodenhausen and R.R. Ernst, *J. Magn. Reson.*, 1984, **58**, 462.
8. N. Müller, G. Bodenhausen and R.R. Ernst, *J. Magn. Reson.*, 1987, **75**, 297.
9. R.R. Ernst, *Q. Rev. Biophys.*, 1987, **19**, 183.
10. O.W. Sørensen, G.W. Eich, M.H. Levitt, G. Bodenhausen and R.R. Ernst, *Prog. Nucl. Magn. Reson. Spectrosc.*, 1983, **16**, 163.
11. G. Bodenhausen, *Prog. Nucl. Magn. Reson. Spectrosc.*, 1983, **14**, 137.
12. K. Wüthrich, *NMR of Proteins and Nucleic Acids*, Wiley, New York, 1986.
13. J.L. Markley, D.H. Croll, R. Krishnamoorthi, G. Ortiz-Polo, W.M. Westler, W.C. Bogard and M. Laskowski, *J. Cell. Biochem.*, 1986, **30**, 291.
14. A. Bax and L. Lerner, *Science*, 1986, **232**, 960.
15. W. Braun, *Q. Rev. Biophys.*, 1986, **19**, 115.
16. R. Benn and A. Rufinska, *Angew. Chem. Int. Engl.*, 1986, **25**, 861.

17. G.A. Morris, *Magn. Reson. Chem.*, 1986, **24**, 371.
18. M.H. Levitt in *Two Dimensional NMR and Related Techniques* (W.S. Brey, ed.), Academic Press, London, 1987.
19. A. Bax, in *Topics in Carbon-13 NMR*, Vol. 4 (G.C. Levy, ed.), Wiley, New York, 1985.
20. R.K. Harris, *Nuclear Magnetic Resonance Spectroscopy*, Longman UK, 1986.
21. D. Shaw, *Fourier Transform NMR Spectroscopy*, 2nd edn, Elsevier, Amsterdam, 1984.
22. J.K.M. Sanders and B.K. Hunter, *Modern NMR Spectroscopy*, Oxford, 1987.
23. A.E. Derome, *Modern NMR Techniques for Chemistry Research*, Pergamon Press, Oxford, 1987.
24. R. Freeman, *Nuclear Magnetic Resonance*, Longman UK, 1987.
25. R.S. Milner and D.W. Turner, *J. Chem. Soc. Chem. Commun.*, 1965, **31**, 00.
26. C.J. Turner, *Prog. Nucl. Magn. Reson. Spectrosc.*, 1984, **16**, 311.
27. K.J. Packer and K.M. Wright, *Mol. Phys.*, 1983, **50**, 797.
28. F.J.M. Van de Ven and C.W. Hilbers, *J. Magn. Reson.*, 1983, **54**, 512.
29. P.K. Wang and C.P. Slichter, *Bull. Magn. Reson.*, 1986, **8**, 3.
30. M.A. Howarth, L-Y. Lian, G.E. Hawkes and K.D. Sales, *J. Magn. Reson.*, 1986, **68**, 433.
31. V. Blechta and J. Schraml, *J. Magn. Reson.*, 1986, **69**, 293.
32. L.R. Brown and J. Bremer, *J. Magn. Reson.*, 1986, **68**, 217.
33. R. Bazzo, J. Boyd, I.D. Campbell and N. Soffe, *J. Magn. Reson.*, 1987, **73**, 369.
34. D.R. Muhandiram and R.E.D. McClung, *J. Magn. Reson.*, 1988, **76**, 121.
35. L.E. Kay and R.E.D. McClung, *J. Magn. Reson.*, 1988, **77**, 258.
36. J. Keeler, D. Neuhaus and M.P. Williamson, *J. Magn. Reson.*, 1987, **73**, 45.
37. T.T. Nakashima and R.E.D. McClung, *J. Magn. Reson.*, 1986, **70**, 187.
38. J.P. Grivet, *J. Magn. Reson.*, 1985, **62**, 328.
39. J.M. Bulsing and D.M. Doddrell, *J. Magn. Reson.*, 1985, **61**, 197.
40. G.J. Bowden and W.D. Hutchison, *J. Magn. Reson.*, 1987, **72**, 61.
41. G.J. Bowden and W.D. Hutchison, *J. Magn. Reson.*, 1986, **67**, 403.
42. G.J. Bowden, W.D. Hutchison and J. Khachan, *J. Magn. Reson.*, 1986, **67**, 415.
43. G.J. Bowden and W.D. Hutchison, *J. Magn. Reson.*, 1986, **70**, 361.
44. B.C. Sanctuary, *Mol. Phys.*, 1983, **49**, 785.
45. B.C. Sanctuary and H.B.R. Cole, *J. Magn. Reson.*, 1987, **71**, 106.
46. A.D. Bain, *Prog. Nucl. Magn. Reson. Spectrosc.*, 1988, **20**, 295.
47. I. Bock and P. Rosch, *J. Magn. Reson.*, 1987, **73**, 177.
48. D.L. Turner, *J. Magn. Reson.*, 1982, **46**, 213.
49. A.G. Avent, J.W. Emsley and D.L. Turner, *J. Magn. Reson.*, 1983, **52**, 57.
50. B.K. John and R.E.D. McClung, *J. Magn. Reson.*, 1984, **58**, 47.
51. M.A. Thomas and A. Kumar, *J. Magn. Reson.*, 1984, **56**, 479.
52. H. Widmer and K. Wüthrich, *J. Magn. Reson.*, 1987, **74**, 316.
53. J.R. Garbow, D.P. Weitekamp and A. Pines, *J. Chem. Phys.*, 1983, **79**, 5301.
54. J.B. Murdoch, W.S. Warren, D.P. Weitekamp and A. Pines, *J. Magn. Reson.*, 1984, **60**, 205.
55. H. Widmer and K. Wüthrich, *J. Magn. Reson.*, 1986, **70**, 270.
56. P. Piveteau, M.A. Delsuc and J-Y. Lallemand, *J. Magn. Reson.*, 1986, **70**, 290.
57. L.E. Kay, J.N. Scarsdale, D.R. Hare and J.H. Prestegaard, *J. Magn. Reson.*, 1986, **68**, 515.
58. T. Allman and A.D. Bain, *J. Magn. Reson.*, 1986, **68**, 533.
59. J.C.J. Barna and E.D. Laue, *J. Magn. Reson.*, 1987, **75**, 384.
60. J.C.J. Barna and E.D. Laue, M.R. Mayger, J. Skilling and S.J.P Worrall, *J. Magn. Reson.*, 1987, **73**, 69.
61. M.A. Delsuc, F.Ni and G.C. Levy, *J. Magn. Reson.*, 1987, **73**, 548.

62. S. J. Davies, C. Bauer, P. J. Hore and R. Freeman, *J. Magn. Reson.*, 1988, **76**, 476.
63. H. Gesmar and J. J. Led, *J. Magn. Reson.*, 1988, **76**, 183.
64. M. Shinnar and S. M. Eleff, *J. Magn. Reson.*, 1988, **76**, 200.
65. M. A. Delsuc and G. C. Levy, *J. Magn. Reson.*, 1988, **76**, 306.
66. B. A. Johnson, J. A. Malikayil and I. M. Armitage, *J. Magn. Reson.*, 1988, **76**, 352.
67. P. Barone, L. Guidani, E. Massaro and V. Viti, *J. Magn. Reson.*, 1988, **77**, 23.
68. H. Barkhuisen, R. DeBeer, W. M. J. Bovee and D. van Ormondt, *J. Magn. Reson.*, 1985, **61**, 465.
69. H. Barkhuisen, R. DeBeer and D. van Ormondt, *J. Magn. Reson.*, 1987, **73**, 553.
70. G. A. Pearson, *J. Magn. Reson.*, 1985, **64**, 487.
71. B. U. Meier, G. Bodenhausen and R. R. Ernst, *J. Magn. Reson.*, 1984, **60**, 161.
72. P. Pfändler and G. Bodenhausen, *J. Magn. Reson.*, 1986, **70**, 71.
73. C. Griesinger, O. W. Sørensen and R. R. Ernst, *J. Am. Chem. Soc.*, 1985, **107**, 6394.
74. G. Bodenhausen, G. Wagner, M. Rance, O. W. Sørensen, K. Wüthrich and R. R. Ernst, *J. Magn. Reson.*, 1984, **59**, 542.
75. H. Oschkinat, A. Pastore, P. Pfändler and G. Bodenhausen, *J. Magn. Reson.*, 1986, **69**, 559.
76. P. Pfändler and G. Bodenhausen, *J. Am. Chem. Soc.*, 1987, **72**, 475.
77. E. R. P. Zuiderweg, *J. Magn. Reson.*, 1987, **71**, 283.
78. C. Griesinger, O. W. Sørensen and R. R. Ernst, *J. Magn. Reson.*, 1987, **75**, 474.
79. H. Grahn, F. Delaglio, M. A. Delsuc and G. C. Levy, *J. Magn. Reson.*, 1988, **77**, 294.
80. M. Novic, U. Eggenberger and G. Bodenhausen, *J. Magn. Reson.*, 1988, **77**, 394.
81. S. Glaser and H. R. Kalbitzer, *J. Magn. Reson.*, 1987, **74**, 450.
82. B. U. Meier, Z. L. Madi and R. R. Ernst, *J. Magn. Reson.*, 1987, **74**, 565.
83. A. Bax, R. A. Byrd and A. Aszalos, *J. Am. Chem. Soc.*, 1984, **106**, 7632.
84. H. Oschkinat, G. M. Clore, M. Nilges and A. M. Gronenborn, *J. Magn. Reson.*, 1987, **75**, 534.
85. J. Golik, G. Dubay, G. Groenewold, H. Kawaguchi, M. Konishi, B. Krishnan, H. Okhuma, K. Saitoh and T. W. Doyle. *J. Am. Chem. Soc.*, 1987, **109**, 3462.
86. K. V. R. Chary. S. Srivastava, R. V. Hosur, K. B. Roy and G. Govil, *Eur. J. Biochem.*, 1986, **158**, 323.
87. M. Bruch and J. A. K. Bonesteel, *Macromolecules*, 1986, **19**, 1622.
88. D. Loganathan, G. K. Trivedi and K. V. R. Chary, *J. Org. Chem.*, 1986, **51**, 3366.
89. F. J. M. Van de Ven and C. W. Hilbers, *J. Mol. Biol.*, 1986, **192**, 389.
90. M. P. Williamson, M. J. Hall and B. K. Handa, *Eur. J. Biochem.*, 1986, **158**, 527.
91. S. Szalma and I. Pelczer, *J. Magn. Reson.*, 1988, **76**, 416.
92. M. Billeter, V. J. Basus and I. D. Kuntz, *J. Magn. Reson.*, 1988, **76**, 400.
93. D. L. Turner, *J. Magn. Reson.*, 1984, **58**, 500.
94. D. L. Turner, *J. Magn. Reson.*, 1985, **61**, 28.
95. M. B. Comisarow, *J. Magn. Reson.*, 1984, **58**, 209.
96. A. F. Mehlkopf, D. Korbee, T. A. Tiggelman and R. Freeman, *J. Magn. Reson.*, 1984, **58**, 315.
97. R. W. Dykstra and A. J. Wand, *J. Magn. Reson.*, 1987, **75**, 158.
98. D. A. Lande, R. W. K. Lee, and C. L. Wilkins, *J. Magn. Reson.*, 1984, **60**, 453.
99. H. Santos and D. L. Turner, *J. Magn. Reson.*, 1986, **68**, 345.
100. E. R. P. Zuiderweg, K. Hallenga and E. T. Olejniczak, *J. Magn. Reson.*, 1986, **70**, 336.
101. P. H. Bolton, *J. Magn. Reson.*, 1986, **68**, 180.
102. R. E. Klevit, *J. Magn. Reson.*, 1985, **62**, 551.
103. S. Glaser and H. R. Kalbitzer, *J. Magn. Reson.*, 1986, **68**, 350.
104. G. Otting, H. Widmer, G. Wagner and K. Wüthrich, *J. Magn. Reson.*, 1986, **66**, 187.
105. D. L. Turner, *J. Magn. Reson.*, 1986, **70**, 465.

106. I.L. Barsukov and A.S. Arseniev, *J. Magn. Reson.*, 1987, **73**, 148.
107. H. Santos, D.L. Turner and A.V. Xavier, *J. Magn. Reson.*, 1983, **55**, 463.
108. A.D. Bain, *J. Magn. Reson.*, 1984, **56**, 418.
109. J. Cavanagh and J. Keeler, *J. Magn. Reson.*, 1988, **77**, 356.
110. P. Barker and R. Freeman, *J. Magn. Reson.*, 1985, **64**, 334.
111. C.J.R. Counsell, M.H. Levitt and R.R. Ernst, *J. Magn. Reson.*, 1985, **64**, 470.
112. D. Piveteau, M. Delsuc and J. Lallemand, *J. Magn. Reson.*, 1985, **63**, 255.
113. M. Decorps, J.P. Albrand, P. Blondet, F. Devreux and M.F. Foray, *J. Magn. Reson.*, 1986, **66**, 364.
114. E. Guittet, D. Piveteau, M. Delsuc and J. Lallemand, *J. Magn. Reson.*, 1985, **62**, 336.
115. L.D. Field and M.L. Terry, *J. Magn. Reson.*, 1986, **69**, 176.
116. J. Boyd, R. Porteous, C. Redfield and N. Soffe, *J. Magn. Reson.*, 1985, **63**, 392.
117. J.P. Lee and M.B. Comisarow, *J. Magn. Reson.*, 1987, **72**, 139.
118. L. Lerner and A. Bax, *J. Magn. Reson.*, 1986, **69**, 375.
119. K. Nagayama, *J. Magn. Reson.*, 1986, **69**, 508.
120. N. Chandrakumar and K. Nagayama, *J. Magn. Reson.*, 1986, **69**, 535.
121. M. Ohuchi, M.H. Osono, K. Furihata and H. Seto, *J. Magn. Reson.*, 1987, **72**, 279.
122. M.A. Delsuc, *J. Magn. Reson.*, 1988, **77**, 119.
123. D.J. States, R.A. Haberkorn and D.J. Ruben, *J. Magn. Reson.*, 1982, **48**, 286.
124. D. Marion and K. Wüthrich, *Biochem. Biophys. Res. Commun.*, 1983, **113**, 967.
125. J. Keeler and D. Neuhaus, *J. Magn. Reson.*, 1985, **63**, 454.
126. S. Macura and L.R. Brown, *J. Magn. Reson.*, 1985, **62**, 328.
127. E.R.P Zuiderweg, *J. Magn. Reson.*, 1986, **66**, 153.
128. A.Z. Gurevich, I.L. Barsukov, A.S. Arseniev and V.F. Bystrov, *J. Magn. Reson.*, 1984, **56**, 471.
129. C.A.G. Haasnoot, F.J.M. Van de Ven and C.W. Hilbers, *J. Magn. Reson.*, 1984, **56**, 343.
130. D.J. Meyerhoff and R. Nunlist, *J. Magn. Reson.*, 1988, **76**, 316.
131. K.E. Köver, *J. Magn. Reson.*, 1984, **59**, 485.
132. D.L. Turner, *J. Magn. Reson.*, 1983, **53**, 259.
133. C. Griesinger, O.W. Sørensen and R.R. Ernst, *J. Magn. Reson.*, 1987, **73**, 574.
134. C. Griesinger, O.W. Sørensen and R.R. Ernst, *J. Am. Chem. Soc.*, 1987, **109**, 7227.
135. S. Davies, J. Friedrich and R. Freeman. *J. Magn. Reson.*, 1988, **76**, 555.
136. H. Kessler, H. Oschkinat, C. Griesinger and W. Bermel, *J. Magn. Reson.*, 1986, **70**, 106.
137. R. Bruschweiler, J.C. Madsen, C. Griesinger, O.W. Sørensen and R.R. Ernst, *J. Magn. Reson.*, 1987, **73**, 380.
138. J. Cavanagh, J.P. Waltho and J. Keeler, *J. Magn. Reson.*, 1987, **74**, 386.
139. C. Bauer, R. Freeman, T. Frenkiel, J. Keeler and A.J. Shaka, *J. Magn. Reson.*, 1984, **58**, 442.
140. C. Bauer and R. Freeman, *J. Magn. Reson.*, 1985, **61**, 376.
141. S. Davies, J. Friedrich and R. Freeman, *J. Magn. Reson.*, 1987, **75**, 540.
142. R. Brandes and D.R. Kearns, *J. Magn. Reson.*, 1985, **64**, 506.
143. F. Loaiza, M.A. McCoy, S.L. Hammes and W.S. Warren, *J. Magn. Reson.*, 1988, **77**, 175.
144. J. Friedrich, S. Davies and R. Freeman, *J. Magn. Reson.*, 1987, **75**, 390.
145. C.L. Dumoulin, *J. Magn. Reson.*, 1985, **64**, 38.
146. J.D. Bell, J.C.C. Brown and P.J. Sadler, *Biochem. Soc. Trans.*, 1986, **14**, 1263.
147. D.L. Rabenstein and S. Fan, *Anal. Chem.*, 1986, **58**, 3178.
148. D.L. Rabenstein, G.S. Srivatsa and R.W.K. Lee, *J. Magn. Reson.*, 1987, **71**, 175.
149. P.A. Mirau, *J. Magn. Reson.*, 1987, **73**, 123.

150. L-F. Kao and V. J. Hruby, *J. Magn. Reson.*, 1986, **70**, 394.
151. G. Otting and K. Wüthrich, *J. Magn. Reson.*, 1986, **66**, 359.
152. S. Davies, C. Bauer, P. B. Barker and R. Freeman, *J. Magn. Reson.*, 1985, **64**, 155.
153. J. M. Bulsing and D. M. Doddrell, *J. Magn. Reson.*, 1986, **68**, 52.
154. J. H. Prestegard and J. N. Scarsdale, *J. Magn. Reson.*, 1985, **62**, 136.
155. E. Guittet, M. A. Delsuc and J. Y. Lallemand, *J. Am. Chem. Soc.*, 1984, **106**, 4278.
156. R. Boelens, R. M. Scheek, K. Dijkstra and R. Kaptein, *J. Magn. Reson.*, 1985, **62**, 378.
157. D. Piveteau, M. A. Delsuc, E. Guittet and J. Y. Lallemand, *J. Magn. Reson.*, 1987, **71**, 347.
158. E. Quignard, B. Bun and G. V. Fazakerly, *J. Magn. Reson.*, 1986, **67**, 342.
159. M. McCoy and W. S. Warren, *Chem. Phys. Lett.*, 1987, **133**, 165.
160. J. H. Gutow, M. McCoy, F. Spano and W. S. Warren, *Phys. Rev. Lett.*, 1985, **55**, 1090.
161. P. Plateau and M. Gueron, *J. Am. Chem. Soc.*, 1982, **104**, 7310.
162. A. G. Redfield, *NATO ASI Ser.A*, 1986, **107** (NMR Life Sci.), 1.
163. D. L. Turner, *J. Magn. Reson.*, 1983, **54**, 146.
164. Z. Starcuk and V. Sklenar, *J. Magn. Reson.*, 1985, **61**, 567.
165. G. A. Morris, K. I. Smith and J. C. Waterton, *J. Magn. Reson.*, 1986, **68**, 526.
166. C. Wang and A. Pardi, *J. Magn. Reson.*, 1987, **71**, 154.
167. Z. Starcuk and V. Sklenar, *J. Magn. Reson.*, 1986, **66**, 391.
168. M. P. Hall and P. J. Hore, *J. Magn. Reson.*, 1986, **70**, 350.
169. R. Freeman and W. Xili, *J. Magn. Reson.*, 1987, **75**, 184.
170. G. J. Galloway, L. J. Haseler, M. F. Marshman, D. H. Williams and D. M. Doddrell, *J. Magn. Reson.*, 1987, **74**, 184.
171. M. H. Levitt and M. F. Roberts, *J. Magn. Reson.*, 1987, **71**, 567.
172. M. H. Levitt, J. L. Sudmeier and W. W. Bachovchin, *J. Am. Chem. Soc.*, 1987, **109**, 6540.
173. P. J. Hore, *J. Magn. Reson.*, 1983, **55**, 283.
174. V. Sklenar, R. Tschudin and A. Bax, *J. Magn. Reson.*, 1987, **75**, 352.
175. V. Sklenar and A. Bax, *J. Magn. Reson.*, 1987, **75**, 373.
176. V. Sklenar and A. Bax, *J. Magn. Reson.*, 1987, **74**, 469.
177. A. Bax, V. Sklenar, G. M. Clore and A. M. Gronenborn, *J. Am. Chem. Soc.*, 1987, **109**, 6511.
178. M. von Kienlin, M. Decorps, J. P. Albrand, M. F. Foray and P. Blondet, *J. Magn. Reson.*, 1988, **76**, 169.
179. R. W. Dykstra, *J. Magn. Reson.*, 1987, **72**, 162.
180. A. Bax, *J. Magn. Reson.*, 1985, **65**, 142.
181. H. Santos, D. L. Turner and A. V. Xavier, *J. Magn. Reson.*, 1984, **58**, 344.
182. C. M. Dobson, L-Y. Lian, C. Redfield and K. D. Topping, *J. Magn. Reson.*, 1986, **69**, 201.
183. V. J. Basus, *J. Magn. Reson.*, 1984, **60**, 132.
184. J. L. Fox, P. A. Tipton, W. W. Cleland and A. S. Mildvan, *J. Am. Chem. Soc.*, 1987, **109**, 2127.
185. J. R. Garbow, D. P. Weitekamp and A. Pines, *Chem. Phys. Lett.*, 1982, **93**, 504.
186. A. Bax, *J. Magn. Reson.*, 1983, **52**, 330.
187. A. Bax, *J. Magn. Reson.*, 1983, **53**, 517.
188. J. A. Wilde and P. H. Bolton, *J. Magn. Reson.*, 1984, **59**, 343.
189. V. Rutar, *J. Magn. Reson.*, 1984, **58**, 132.
190. V. Rutar, *J. Magn. Reson.*, 1984, **58**, 306.
191. V. Rutar, W. Guo and T. C. Wong, *J. Magn. Reson.*, 1986, **69**, 100.
192. T. C. Wong, V. Rutar and J-S. Wang, *J. Am. Chem. Soc.*, 1984, **106**, 7046.
193. T. C. Wong and V. Rutar, *J. Am. Chem. Soc.*, 1984, **106**, 7380.

194. V. Rutar and T.C. Wong, *J. Magn. Reson.*, 1985, **64**, 527.
195. J. Lambert and M. Klessinger, *J. Magn. Reson.*, 1987, **73**, 323.
196. V. Rutar and T.C. Wong, *J. Magn. Reson.*, 1987, **73**, 275.
197. M. Perpick-Dumont, R.G. Enriquez, S. McLean, F.V. Puzzuoli and W.F. Reynolds, *J. Magn. Reson.*, 1987, **75**, 414.
198. S. Wimperis and R. Freeman, *J. Magn. Reson.*, 1985, **62**, 147.
199. S. Wimperis and G. Bodenhausen, *J. Magn. Reson.*, 1986, **69**, 264.
200. M.H. Levitt and R. Freeman, *J. Magn. Reson.*, 1979, **33**, 473.
201. M.H. Levitt, *Prog. Nucl. Magn. Reson. Spectrosc.*, 1986, **18**, 61.
202. S. Brownstein and J. Bornais, *J. Magn. Reson.*, 1985, **64**, 330.
203. A.J. Shaka, P.B. Barker and R. Freeman, *J. Magn. Reson.*, 1986, **67**, 580.
204. T. Fujiwara and K. Nagayama, *J. Magn. Reson.*, 1988, **77**, 53.
205. S.L. Patt, *J. Magn. Reson.*, 1982, **49**, 161.
206. G.A. Morris and M.J. Toohey, *J. Magn. Reson.*, 1985, **63**, 629.
207. R. Goc and D. Fiat, *J. Magn. Reson.*, 1986, **70**, 295.
208. D.J. Lurie, *J. Magn. Reson.*, 1986, **70**, 11.
209. K.V. Schenker and W. von Philipsborn, *J. Magn. Reson.*, 1986, **66**, 219.
210. B. Blümich and H.W. Spiess, *J. Magn. Reson.*, 1985, **61**, 356.
211. C. Counsell, M.H. Levitt and R.R. Ernst, *J. Magn. Reson.*, 1985, **63**, 133.
212. R. Tycko and A. Pines, *Chem. Phys. Lett.*, 1984, **111**, 463.
213. R. Tycko, H.M. Cho, E. Schneider and A. Pines, *J. Magn. Reson.*, 1985, **61**, 90.
214. S. Wimperis and G. Bodenhausen, *J. Magn. Reson.*, 1987, **71**, 355.
215. A.J. Shaka and A. Pines, *J. Magn. Reson.*, 1987, **71**, 495.
216. T.M. Barbara, R. Tycko and D.P. Weitekamp, *J. Magn. Reson.*, 1985, **62**, 54.
217. W.S. Warren, J.B. Murdoch and A. Pines, *J. Magn. Reson.*, 1984, **60**, 236.
218. A.J. Shaka and J. Keeler, *Prog. Nucl. Magn. Reson. Spectrosc.*, 1987, **19**, 47.
219. M.H. Levitt, G. Bodenhausen and R.R. Ernst, *J. Magn. Reson.*, 1983, **53**, 443.
220. G.A. Morris, G.L. Nayler, A.J. Shaka, J. Keeler and R. Freeman, *J. Magn. Reson.*, 1984, **58**, 155.
221. A.J. Shaka, J. Keeler, R. Freeman, G.A. Morris and G.L. Nayler, *J. Magn. Reson.*, 1984, **58**, 161.
222. J.S. Waugh, *J. Magn. Reson.*, 1982, **50**, 30.
223. A. Allerhand, R.E. Addleman and D. Osman, *J. Am. Chem. Soc.*, 1985, **107**, 5809.
224. A. Allerhand and M. Dohrenwend, *J. Am. Chem. Soc.*, 1985, **107**, 6684.
225. A.J. Shaka, P.B. Barker, C.J. Bauer and R. Freeman, *J. Magn. Reson.*, 1986, **67**, 396.
226. A.J. Shaka, J. Keeler and R. Freeman, *J. Magn. Reson.*, 1983, **53**, 313.
227. A.J. Shaka, C.J. Lee and A. Pines, *J. Magn. Reson.*, 1988, **77**, 274.
228. B.M. Fung, *J. Magn. Reson.*, 1984, **60**, 424.
229. A.J. Shaka, P.B. Barker and R. Freeman, *J. Magn. Reson.*, 1987, **71**, 520.
230. P.B. Barker, A.J. Shaka and R. Freeman, *J. Magn. Reson.*, 1984, **65**, 535.
231. D. Suter, K.V. Schenker and A. Pines, *J. Magn. Reson.*, 1987, **73**, 90.
232. K.V. Schenker, D. Suter and A. Pines, *J. Magn. Reson.*, 1987, **73**, 99.
233. M.A. Weiss, J.L. Eliason and D.J. States, *Proc. Natl Acad. Sci. USA*, 1984, **81**, 6019.
234. A. Sheth, M. Ravikumar and R.V. Hosur, *J. Magn. Reson.*, 1986, **70**, 213.
235. R.V. Hosur, M. Ravikumar and A. Sheth, *J. Magn. Reson.*, 1985, **65**, 375.
236. A. Kumar, R.V. Hosur and K. Chandrasekhar, *J. Magn. Reson.*, 1984, **60**, 143.
237. A. Kumar, R.V. Hosur, K. Chandrasekhar and N. Murali, *J. Magn. Reson.*, 1985, **63**, 107.
238. R.V. Hosur, K.V.R. Chary, A. Kumar and G. Govil, *J. Magn. Reson.*, 1985, **62**, 123.
239. K. Chandrasekhar and A. Kumar, *J. Magn. Reson.*, 1987, **73**, 417.

240. M. Rance, G. Wanger, O.W. Sørensen, K. Wüthrich and R.R. Ernst, *J. Magn. Reson.*, 1984, **59**, 250.
241. T.T. Nakashima and D.L. Rabenstein, *J. Magn. Reson.*, 1986, **66**, 157.
242. O.W. Sørensen, C. Griesinger and R.R. Ernst, *J. Am. Chem. Soc.*, 1985, **107**, 7778.
243. J. Cavanagh and J. Keeler, *J. Magn. Reson.*, 1987, **71**, 561.
244. L. Müller, *J. Magn. Reson.*, 1987, **72**, 191.
245. G. Wider, S. Macura, A. Kumar, R.R. Ernst and K. Wüthrich, *J. Magn. Reson.*, 1984, **56**, 207.
246. A.B. Manger, O.A. Stuart, J.A. Ferretti and J.V. Silverton, *J. Am. Chem. Soc.*, 1985, **107**, 7154.
247. J. Pawlak, M.S. Tempesta, J. Golik, M.G. Zagorski, M. Shee, K. Nakashima, T.I. Washita, M.L. Gross and K.B. Tomer, *J. Am. Chem. Soc.*, 1987, **109**, 114.
248. G.C. King and P.E. Wright, *Biochemistry*, 1986, **25**, 2364.
249. J.E. Bishop, H. Rapoport, A.V. Klotz, C.F. Chan, A.N. Glazer, P. Füglistaller and H. Zuber, *J. Am. Chem. Soc.*, 1987, **109**, 875.
250. A. Bax, L.G. Marzilli and A.F. Summers, *J. Am. Chem. Soc.*, 1987, **109**, 566.
251. A. Pardi, R. Walker, H. Rapoport, G. Wider and K. Wüthrich, *J. Am. Chem. Soc.*, 1983, **105**, 1652.
252. R.V. Hosur, M. Ravikumar, K.V.R. Chary, A. Sheth, G. Govil and Z.K. Tan, *FEBS Lett.*, 1986, **205**, 71.
253. S. Desilets and M.St. Jacques, *J. Am. Chem. Soc.*, 1987, **109**, 1641.
254. P. Dionne and M.St. Jacques, *J. Am. Chem. Soc.*, 1987, **109**, 2616.
255. R.R. Birge, L.P. Murray, R. Zidovetski and H.M. Knapp, *J. Am. Chem. Soc.*, 1987, **109**, 2090.
256. U. Simonis, F.A. Walker, P.L. Lee, B.J. Hanquet, D.J. Meyerhoff and W.R. Scheidt, *J. Am. Chem. Soc.*, 1987, **109**, 2659.
257. C. Kruk, A.W.H. Jans, J. Cornelisse and J. Lugtenburg, *Magn. Reson. Chem.* 1985, **23**, 710.
258. A.L. Balch, Y.W. Chan, R. Olmstead and M.W. Renner, *J. Am. Chem. Soc.*, 1985, **107**, 2393.
259. A. Rajca and L.M. Tolbert, *J. Am. Chem. Soc.*, 1987, **109**, 1782.
260. V.W. Miner, P.M. Tyrell and J.H. Prestegard, *J. Magn. Reson.*, 1983, **55**, 438.
261. D. Moskau and H. Günther, *Angew. Chem.*, 1987, **99**, 151.
262. C.T. Brewer, R.G. Swisher, E. Sinn and R.N. Grimes, *J. Am. Chem. Soc.*, 1985, **107**, 3558.
263. E.W. Corcoran and G. Sneddon, *J. Am. Chem. Soc.*, 1985, **107**, 7446.
264. O.W. Howarth, M.J. Jasztal, J.G. Taylor and M.G.H. Wallbridge, *Polyhedron*, 1985, **4**, 1461.
265. D.G. Meina, J.H. Morris, and D. Reed, *Polyhedron*, 1986, **5**, 1639.
266. X.L.R. Fontaine and J.D. Kennedy, *J. Chem. Soc. Chem. Commun.*, 1986, 779.
267. A.W.H. Jans, E.M. Osselton, C.P. Eyken, B. Griewel and J. Cornalisse, *J. Magn. Reson.*, 1986, **70**, 169.
268. C.T.G. Knight, R.J. Kirkpatrick and E. Oldfield, *J. Am. Chem. Soc.*, 1986, **108**, 169.
269. C.T.G. Knight, R.J. Kirkpatrick and E. Oldfield, *J. Am. Chem. Soc.*, 1987, **109**, 1632.
270. S. Guesmi, N.J. Taylor, P.H. Dixneuf and A.J. Carty, *Organometallics*, 1986, **5**, 1964.
271. P.J. Domaille, *J. Am. Chem. Soc.*, 1984, **106**, 7677.
272. N. Murali and A. Kumar, *Chem. Phys. Lett.*, 1986, **128**, 58.
273. M.H. Levitt, C. Radloff and R.R. Ernst, *Chem. Phys. Lett*, 1985, **114**, 435.
274. O.W Sørensen, C. Griesinger and R.R. Ernst, *Chem. Phys. Lett.*, 1987, **135**, 313.
275. C. Griesinger, C. Gemperle, O.W. Sørensen and R.R. Ernst, *Mol. Phys.*, 1987, **62**, 295.

276. J. Keeler and F. Sanchez-Ferrando, *J. Magn. Reson.*, 1987, **75**, 96.
277. G. Jaccard, S. Wimperis and G. Bodenhausen, *Chem. Phys. Lett.*, 1987, **138**, 601.
278. T.E. Bull, *J. Magn. Reson.*, 1987, **72**, 397.
279. S. Wimperis and G. Bodenhausen, *Chem. Phys. Lett.*, 1987, **140**, 41.
280. M. Ravikumar and A. Sheth, *Chem. Phys. Lett.*, 1986, **126**, 352.
281. J. Courtieu, N.T. Lai and L. Werbelow, *Chem. Phys. Lett.*, 1987, **140**, 565.
282. D.S. Williamson, D.L. Nagel, R.S. Markin and S.M. Cohen, *J. Magn. Reson.*, 1987, **71**, 163.
283. D.S. Williamson, P. Cremonesi, E. Cavalieri, D.L. Nagel, R.S. Markin and S.M. Cohen, *J. Org. Chem.*, 1986, **51**, 5210.
284. R. Ramchandran, P. Darba and L.R. Brown, *J. Magn. Reson.*, 1987, **73**, 349.
285. N. Müller, R.R. Ernst and K. Wüthrich, *J. Am. Chem. Soc.*, 1986, **108**, 6482.
286. J. Boyd and C. Redfield, *J. Magn. Reson.*, 1986, **68**, 67.
287. B.T. Farmer and L.R. Brown, *J. Magn. Reson.*, 1987, **71**, 365.
288. P.H. Bolton, *J. Magn. Reson.*, 1983, **51**, 134.
290. G.A. Morris and K.I. Smith, *J. Magn. Reson.*, 1985, **65**, 506.
291. A. Otter and G. Kotovych, *J. Magn. Reson.*, 1986, **69**, 187.
292. L.E. Kay, P. Jones and J.H. Prestegard, *J. Magn. Reson.*, 1987, **72**, 392.
293. N. Müller, G. Bodenhausen, K. Wüthrich and R.R. Ernst, *J. Magn. Reson.*, 1985, **65**, 531.
294. M. Rance and P.E. Wright, *Chem. Phys. Lett.*, 1986, **124**, 572.
295. M. Rance and P.E. Wright, *J. Magn. Reson.*, 1986, **66**, 372.
296. A.S. Arseniev, A.G. Sobol and V.F. Bystrov, *J. Magn. Reson.*, 1986, **70**, 427.
297. J.K. Saunders and J.D. Stevens, *Magn. Reson. Chem.*, 1986, **24**, 1023.
298. N. Müller, *Chem. Phys. Lett.*, 1986, **131**, 218.
299. A. Delville, P. Laszlo and R.T. Schyns, *Biophys. Chem.*, 1986, **24**, 121.
300. G. Jaccard, W. Wimperis and G. Bodenhausen, *J. Chem. Phys.*, 1986, **85**, 6282.
301. J. Pekar and J.S. Leigh, *J. Magn. Reson.*, 1986, **69**, 582.
302. J. Pekar, P.F. Renshaw and J.S. Leigh, *J. Magn. Reson.*, 1987, **72**, 159.
303. W.D. Rooney, T.M. Barbara and C.S. Springer, *J. Am. Chem. Soc.*, 1987, **109**, 674.
304. M. Bloom and M.A. LeGros, *Can. J. Phys.*, 1986, **64**, 1522.
305. O.W. Sørensen, M.H. Levitt and R.R. Ernst, *J. Magn. Reson.*, 1983, **55**, 104.
306. M. Rance, O.W. Sørensen, W. Leupin, H. Kogler, K. Wüthrich and R.R. Ernst, *J. Magn. Reson.*, 1985, **61**, 67.
307. M. Munowitz and A. Pines, *Science*, 1986, **233**, 525.
308. L.D. Hall an T.J. Norwood, *J. Magn. Reson.*, 1986, **69**, 397.
309. L.D. Hall and T.J. Norwood, *J. Magn. Reson.*, 1986, **69**, 585.
310. L.D. Hall and T.J. Norwood, *J. Magn. Reson.*, 1988, **76**, 241.
311. L. Müller, *J. Magn. Reson.*, 1984, **59**, 326.
312. L. Müller and A. Pardi, *J. Am. Chem. Soc.*, 1985, **107**, 3484.
313. P.H. Bolton, *J. Magn. Reson.*, 1984, **60**, 342.
314. D.L. Turner, *J. Magn. Reson.*, 1985, **65**, 169.
315. J. Kowalewski and K.M. Larsson, *Chem. Phys. Lett.*, 1985, **119**, 157.
316. J. Boyd, C.M. Dobson and C. Redfield, *J. Magn. Reson.*, 1985, **62**, 543.
317. S.C. Brown, P.L. Weber and L. Müller, *J. Magn. Reson.*, 1988, **77**, 166.
318. C. Dalvit, P.E. Rance and P.E. Wright, *J. Magn. Reson.*, 1986, **69**, 344.
319. J. Boyd, C.M. Dobson and C. Redfield, *J. Magn. Reson.*, 1983, **55**, 170.
320. L. Braunschweiler, G. Bodenhausen and R.R. Ernst, *Mol. Phys.*, 1983, **48**, 535.
321. J.A. Wilde and P.H. Bolton, *J. Magn. Reson.*, 1986, **67**, 570.

322. A. Majumdar and R.V. Hosur, *Chem. Phys. Lett.*, 1987, **138**, 431.
323. P.H. Bolton, *J. Am. Chem. Soc.*, 1984, **106**, 4299.
324. M. Novic, H. Oschkinat, P. Pfändler and G. Bodenhausen, *J. Magn. Reson.*, 1987, **73**, 493.
325. H.Oschkinat and G. Bodenhausen, *J. Magn. Reson.*, 1987, **73**, 565.
326. D.L. Turner, *J. Magn. Reson.*, 1982, **49**, 175.
327. M. Ikura and K. Hikichi, *J. Am. Chem. Soc.*, 1984, **106**, 4275.
328. L.E. Kay, T.A. Holak and J.H. Prestegard, *J. Magn. Reson.*, 1988, **76**, 30.
329. T. Kikuchi, S. Kadota, S. Matsuda and H. Suehara, *Tetrahedron Lett.*, 1984, **25**, 2565.
330. J.M. Bulsing, E.D. Laue, F.J. Leeper, J. Staunton, D.H. Davies, G.A.F. Ritchie, A. Davies, A.B. Davies and R.P. Mabelis, *J. Chem. Soc. Chem. Commun.*, 1984, 1301.
331. D.M. Roll, C.W.J. Chang, P.J. Schener, G.A. Gray, J.N. Shoolery, G.K. Matsumoto, G.D. Van Duyne and J. Clardy, *J. Am. Chem. Soc.*, 1985, **107**, 2916.
332. R.N. Moore, G. Bigam, J.K. Chan, A.M. Hogg, T. Nakashima and J.C. Vederas, *J. Am. Chem. Soc.*, 1985, **107**, 3694.
333. Z. Spavold, J.A. Robinson and D.L. Turner, *Tetrahedron Lett.*, 1986, **27**, 3299.
334. A.A. Ajaz, J.A. Robinson and D.L. Turner, *J. Chem. Soc. Perkin Trans. 1*, 1987, 27.
335. T.A. Early, B.K. John and L.F. Johnson, *J. Magn. Reson.*, 1987, **75**, 134.
336. M. Ubukata, J. Uzawa and K. Isono, *J. Am. Chem. Soc.*, 1984, **106**, 2213.
337. P.J. Keller, Q.L. Van, A. Bacher and H.G. Floss, *Tetrahedron Lett.*, 1983, **39**, 3471.
338. G.A. Olah, G.K.S. Prakash and V.V. Krishnamurthy, *J. Am. Chem. Soc.*, 1984, **106**, 7073.
339. G. Müller, J. Schmiedl, E. Schneider, R. Sedlmeier, and G. Wörner, A.I. Scott, H.J. Williams, P.J. Santander, N.J. Stolowich, P.E. Fagerness, N.E. Mackenzie and H.-P. Kriemler, *J. Am. Chem. Soc.*, 1986, **108**, 7875.
340. D.E. Cane and C.-C. Yang, *J. Am. Chem. Soc.*, 1987, **109**, 1255.
341. J.M. Beale, C.E. Cottrell, P.J. Keller and H.G. Floss, *J. Magn. Reson.*, 1987, **72**, 574.
342. V.V. Krishnamurthy, G.K.S. Prakash, P.S. Iyer and G.A. Olah, *J. Am. Chem. Soc.*, 1984, **106**, 7068.
343. E. Wörgotter, G. Wagner and K. Wüthrich, *J. Am. Chem. Soc.*, 1986, **108**, 6162.
344. E. Wörgotter, G. Wagner, M. Vasak, J.H.R. Kägi and K. Wüthrich, *J. Am. Chem. Soc.*, 1987, **109**, 2388.
345. G. Otting, H. Senn, G. Wagner and K. Wüthrich, *J. Magn. Reson.*, 1986, **70**, 500.
346. J.A. Wilde, P.H. Bolton, N.J. Stolowich and J.A. Gerlt, *J. Magn. Reson.*, 1986, **68**, 168.
347. M. Rance, P.E. Wright, B.A. Messerle and L.D. Field, *J. Am. Chem. Soc.*, 1987, **109**, 1591.
348. A. Bax and M.A. Weiss, *J. Magn. Reson.*, 1987, **71**, 571.
349. M.P. Williamson and D. Neuhaus, *J. Magn. Reson.*, 1987, **72**, 369.
350. J. Boyd, G.R. Moore and G. Williams, *J. Magn. Reson.*, 1984, **58**, 511.
351. K. Nagayama, Y. Kobayashi and Y. Kyogoku, *J. Magn. Reson.*, 1983, **51**, 84.
352. W. Denk, G. Wagner, M. Rance and K. Wuthrich, *J. Magn. Reson.*, 1985, **62**, 350.
353. G.S. Harbison, J. Feigon, D.J. Ruben, J. Herzfeld and R.G. Griffin, *J. Am. Chem. Soc.*, 1985, **107**, 5567.
354. S. Macura, B.T. Farmer and L.R. Brown, *J. Magn. Reson.*, 1986, **70**, 493.
355. M. Rance, G. Bodenhausen, G. Wagner, K. Wüthrich and R.R. Ernst, *J. Magn. Reson.*, 1985, **62**, 497.
356. G. Wagner, G. Bodenhausen, N. Müller, M. Rance, O.W. Sørensen, R.R. Ernst and K. Wüthrich, *J. Am. Chem. Soc.*, 1985, **107**, 6440.
357. E.T. Olejniczak, J.C. Hoch, C.M. Dobson and F.M. Poulsen, *J. Magn. Reson.*, 1985, **64**, 199.

358. E.R. Johnson, M.J. Dellwo and J. Hendrix, *J. Magn. Reson.*, 1986, **66**, 399.
359. T.A. Holak, J.N. Scarsdale and J.H. Prestegard, *J. Magn. Reson.*, 1987, **74**, 546.
360. R. Willem, *Prog. Nucl. Magn. Reson. Spectrosc.*, 1988, **20**, 1.
361. J. Bremer, G.L. Mendz and W.J. Moore, *J. Am. Chem. Soc.*, 1984, **106**, 4691.
362. E.W. Abel, T.P.J. Coston, K.G. Orrell, V. Sik and D. Stephenson, *J. Magn. Reson.*, 1986, **70**, 34.
363. H. Gesmer and J.J. Led, *J. Magn. Reson.*, 1986, **68**, 95.
364. M. Grassi, B.E. Mann, B.T. Pickup and C.M. Spencer, *J. Magn. Reson.*, 1986, **69**, 92.
365. D.R. Muhandiram and R.E.D. McClung, *J. Magn. Reson.*, 1987, **71**, 187.
366. R. Willem, M. Gielen, H. Pepermans, J. Brocas, D. Fastenakel and P. Finnochiario, *J. Am. Chem. Soc.*, 1985, **107**, 1146.
367. R. Willem, M. Gielen, H. Pepermans, K. Hallenga, A. Racca and P. Finnochiario, *J. Am. Chem. Soc.*, 1985, **107**, 1153.
368. G.E. Hawkes, L.-Y. Lian, E.W. Randall and K.D. Sales, *J. Magn. Reson.*, 1985, **65**, 173.
369. G.E. Hawkes, L.-Y. Lian, E.W. Randall, K.D. Sales and S. Aime, *J. Chem. Soc. Dalton Trans.*, 1985, 225.
370. R. Ramachandran, C.T.G. Knight, R.J. Kirkpatrick and E. Oldfield, *J. Magn. Reson.*, 1985, **65**, 136.
371. H. Santos, D.L. Turner, A.V. Xavier and J. LeGall, *J. Magn. Reson.*, 1984, **59**, 177.
372. R. Willem, A. Jans, C. Hoogzand, M. Gielen, G. van Binst and H. Pepermans, *J. Am. Chem. Soc.*, 1985, **107**, 28.
373. M.H. Chang, B.B. Masek and D.A. Dougherty, *J. Am. Chem. Soc.*, 1985, **107**, 1124.
374. P.B. Garlick and C.J. Turner, *J. Magn. Reson.*, 1983, **51**, 536.
375. C.L. Perrin and R.K. Gipe, *J. Am. Chem. Soc.*, 1984, **106**, 4036.
376. R.M. Scheek, S. Stob, R. Boelens, K. Dijkstra and R. Kaptein, *J. Am. Chem. Soc.*, 1985, **107**, 705.
377. A. De Marco, L. Zetta, A.M. Petros, M. Llinas, R. Boelens and R. Kaptein, *Biochemistry*, 1986, **25**, 7918.
378. R. Boelens, A. Podoplelov and R. Kaptein, *J. Magn. Reson.*, 1986, **69**, 116.
379. J. Kemmink, G.W. Vuister, R. Boelens, K. Dijkstra and R. Kaptein, *J. Am. Chem. Soc.*, 1986, **108**, 5631.
380. J. Boyd, K.M. Brindle, I.D. Campbell and G.K. Radda, *J. Magn. Reson.*, 1984, **60**, 149.
381. G.L. Mendz, G. Robinson and P.W. Kuchel, *J. Am. Chem. Soc.*, 1986, **108**, 169.
382. J-P. Charland, M.T.P. Phan Viet, M. St. Jacques and A.L. Beauchamp, *J. Am. Chem. Soc.*, 1985, **107**, 8202.
383. G. Wider, K. Hosur and K. Wüthrich, *J. Magn. Reson.*, 1983, **52**, 130.
384. A.L. Schwartz and J.D. Cutnell, *J. Magn. Reson.*, 1983, **53**, 398.
385. D. Wemmer and N.R. Kallenbach, *Biochemistry*, 1983, **22**, 1901.
386. G. Vriend, M.A. Hemminga, C.A.G. Haasnoot and C.W. Hilbers, *J. Magn. Reson.*, 1985, **64**, 501.
387. D.A. Torchia, S.W. Sparks and A. Bax, *J. Am. Chem. Soc.*, 1987, **109**, 2320.
388. Z-Y. Yan, B.N.N. Rao and C.A. Bush, *J. Am. Chem. Soc.*, 1987, **109**, 7663.
389. E. Berman and P. Bendel, *FEBS Lett.*, 1986, **204**, 257.
390. S. Gasa, M. Nakamura, A. Makita, M. Ikura and K. Hikichi, *Eur. J. Biochem.*, 1986, **155**, 603.
391. S.W. Homans, R.A. Dwek, J. Boyd, M. Mahmoudian, W.G. Richards and T.W. Rademacher, *Biochemistry*, 1986, **25**, 6342.
392. R.M. Scheek, N. Russo, R. Boelens and R. Kaptein, *J. Am. Chem. Soc.*, 1983, **105**, 2914.
393. M.A. Weiss, D.J. Patel, R.T. Sauer and M. Karplus, *J. Am. Chem. Soc.*, 1984, **106**, 4269.

394. R.E. Klevit, D.E. Wemmer and B.R. Reid, *Biochemistry*, 1986, **25**, 3296.
395. D.J. Patel and L. Shapiro, *Biopolymers*, 1986, **25**, 707.
396. D.J. Patel, L. Shapiro, S.A. Kozlowski, B.L. Gaffney and R.A. Jones, *J. Mol. Biol.*, 1986, **188**, 677.
397. S. Ikuta, R. Chattopadhyaya, H. Ito, R.E. Dickerson and D.R. Kearns, *Biochemistry*, 1986, **25**, 4840.
398. L.J. Rinkel, M.R. Sanderson, G.A. Van der Marel, J.H. Van Boom and C. Altona, *Eur. J. Biochem.*, 1986, **159**, 85.
399. W. Leupin, W.J. Chazin, S. Hyberts, W.A. Denny and K. Wüthrich, *Biochemistry*, 1986, **25**, 5902.
400. G.M. Clore, A.M. Gronenborn, G. Carson and E.F. Meyer, *J. Mol. Biol.*, 1986, **190**, 259.
401. G.M. Clore, M. Nilges, D.K. Sukumaran, A. Brünger, M. Karplus and A.M. Gronenborn, *EMBO J.*, 1985, **5**, 2729.
402. J. Kemmink, R. Boelens, T.M.G. Koning, R. Kaptein, G.A. Van der Marel and J.H. Van Book, *Eur. J. Biochem.*, 1987, **162**, 37.
403. D.J. Patel, L. Shapiro and D. Hare, *Ann. Rev. Biophys. Chem.*, 1987, **16**, 423.
404. R.V. Hosur, *Curr. Sci.*, 1986, **55**, 597.
405. L.M. Gierasch, I.L. Karle, A.L. Rockwell and K. Yenal, *J. Am. Chem. Soc.*, 1985, **107**, 3321.
406. P.W. Jeffs, L. Müller, C. DeBrosse, S.L. Heald and R. Fisher, *J. Am. Chem. Soc.*, 1986, **108**, 3063.
407. A. Cuer and G. Dauphin, *J. Chem. Soc. Perkin Trans. 2*, 1986, 295.
408. G.T. Montelione, P. Hughes, J. Clardy and H.A. Scheraga, *J. Am. Chem. Soc.*, 1986, **108**, 6765.
409. S. Heald, L. Müller and P.W. Jeffs, *J. Magn. Reson.*, 1987, **72**, 120.
410. A.S. Arseniev, A.L. Lomize, I.L. Barsukov and V.F. Bystrov, *Biol. Membranes*, 1986, **3**, 1077.
411. D.C. Dalgarno, M.W. Harding, A. Lazarides, R.E. Handschumacher and I.M. Armitage, *Biochemistry*, 1986, **25**, 6778.
412. D.E. Wemmer, N.V. Kumar, R.M. Metrione, M. Lazdunski, G. Drobny and N.R. Kallenbach, *Biochemistry*, 1986, **25**, 6842.
413. A. Motta, D. Picone, T. Tancredi and P.A. Temussi, *J. Magn. Reson.*, 1987, **75**, 364.
414. G. Esposito and A. Pastore, *J. Magn. Reson.*, 1988, **76**, 331.
415. G.B. Young and T.L. James, *J. Am. Chem. Soc.*, 1984, **106**, 7986.
416. M.D. Bruch, J.H. Noggle and L.M. Gierasch, *J. Am. Chem. Soc.*, 1985, **107**, 1400.
417. D. Gondol and G. VanBinst, *Biopolymers*, 1986, **25**, 977.
418. M. Feigel, *J. Am. Chem. Soc.*, 1986, **108**, 181.
419. T. Ohkubo, Y. Kyogoku, Y. Nishiuchi, S. Sakakibara, W. Braun and N. Go, *Pept. Chem.*, 1986, 259.
420. T.A. Holak and J.H. Prestegard, *Biochemistry*, 1986, **25**, 5766.
421. P.A. Mirau and F.A. Bovey, *Polym. Mater. Sci. Engng.*, 1986, **54**, 480.
422. P.A. Mirau and F.A. Bovey, *J. Am. Chem. Soc.*, 1986, **108**, 5130.
423. J.N. Scarsdale, R.K. Yu and J.H. Prestegard, *J. Am. Chem. Soc.*, 1986, **108**, 6778.
424. G.M. Clore and A.M. Gronenborn, *J. Magn. Reson.*, 1985, **61**, 158.
425. E.T. Olejniczak, R.T. Gampe and S.W. Fesik, *J. Magn. Reson.*, 1986, **67**, 243.
426. S.W. Fesik, T.J. O'Donnell, R.T. Gampe and E.T. Olejniczak, *J. Am. Chem. Soc.*, 1986, **108**, 3165.
427. T.L. James, G.B. Young, M.S. Broido, J.W. Keepers, N. Jamin and G. Zon, *J. Biosci.*, 1986, **8**, 553.

428. J.F. Ellena, W.C. Hutton and D.F. Cafiso, *J. Am. Chem. Soc.*, 1985, **107**, 1530.
429. R.E. Stark, R.W. Storrs, S.E. Levine, S. Yee and M.S. Broido, *Biochim. Biophys. Acta*, 1986, **860**, 399.
430. C. Yu and G.C. Levy, *J. Am. Chem. Soc.*, 1984, **106**, 6533.
431. W. Bauer, T. Clark and P.v.R. Schleyer, *J. Am. Chem. Soc.*, 1987, **109**, 970.
432. N. Niccolai, C. Rossi, V. Brizzi and W.A Gibbons, *J. Am. Chem. Soc.*, 1984, **106**, 5732.
433. K.E. Köver and G. Batta, *J. Am. Chem. Soc.*, 1985, **107**, 5829.
434. W.J. Metzler, P. Leighton and P. Lu, *J. Magn. Reson.*, 1988, **76**, 534.
435. K.E. Köver and G. Batta, *Prog. Nucl. Magn. Reson. Spectrosc.*, 1987, **19**, 223.
436. K.E. Köver and G. Batta, *J. Magn. Reson.*, 1986, **69**, 344.
437. K.E. Köver and G. Batta, *J. Magn. Reson.*, 1986, **69**, 519.
438. K.E. Köver, G. Batta and Z. Madi, *J. Magn. Reson.*, 1986, **69**, 538.
439. L. Braunschweiler and R.R. Ernst, *J. Magn. Reson.*, 1983, **53**, 521.
440. A.A. Bothner-By, R.L. Stevens, J.T. Lee, C.D. Warren and R.W. Jeanloz, *J. Am. Chem. Soc.*, 1984, **106**, 811.
441. D.G. Davis, *J. Am. Chem. Soc.*, 1987, **109**, 3471.
442. D.G. Davis and A. Bax, *J. Magn. Reson.*, 1985, **64**, 533.
443. N. Chandrakumar and S. Subramanian, *J. Magn. Reson.*, 1985, **62**, 346.
444. N. Chandrakumar, *J. Magn. Reson.*, 1986, **67**, 457.
445. N. Chandrakumar, G.V. Visalakshi, D. Ramaswamy and S. Subramanian, *J. Magn. Reson.*, 1986, **67**, 307.
446. N. Chandrakumar, *J. Magn. Reson.*, 1987, **71**, 322.
447. B.T. Farmer, S. Macura and L.R. Brown, *J. Magn. Reson.*, 1987, **72**, 347.
448. A. Bax, V. Sklenar and M.F. Summers, *J. Magn. Reson.*, 1986, **70**, 327.
449. D. Neuhaus and J. Keeler, *J. Magn. Reson.*, 1986, **68**, 568.
450. M. Rance, *J. Magn. Reson.*, 1987, **74**, 557.
451. R. Bazzo and I.D. Campbell, *J. Magn. Reson.*, 1988, **76**, 358.
452. B.T. Farmer and L.R. Brown, *J. Magn. Reson.*, 1987, **72**, 197.
453. H. Kessler, C. Griesinger, R. Kerssebaum, K. Wagner and R.R. Ernst, *J. Am. Chem. Soc.*, 1987, **109**, 607.
454. C. Griesinger and R.R. Ernst, *J. Magn. Reson.*, 1987, **75**, 261.
455. A. Bax. *J. Magn. Reson.*, 1988, **77**, 134.
456. J.S. Waugh, *J. Magn. Reson.*, 1986, **68**, 189.
457. D.G. Davis and A. Bax, *J. Am. Chem. Soc.*, 1985, **107**, 2820.
458. R. Bazzo and J. Boyd, *J. Magn. Reson.*, 1987, **75**, 452.
459. D.G. Davis and A. Bax, *J. Am. Chem. Soc.*, 1985, **107**, 7197.
460. M.W. Edwards and A. Bax, *J. Am. Chem. Soc.*, 1986, **108**, 918.
461. A. Bax and D.G. Davis, *J. Magn. Reson.*, 1985, **65**, 355.
462. P.L. Weber, L.C. Sieker, T.S. Anantha Samy, B.R. Reid and G.P. Drobny, *J. Am. Chem. Soc.*, 1987, **109**, 5842.
463. S. Subramanian and A. Bax, *J. Magn. Reson.*, 1987, **71**, 325.
464. G. Otting and K. Wüthrich, *J. Magn. Reson.*, 1987, **75**, 546.
465. N. Chandrakumar and K. Nagayama, *Chem. Phys. Lett.*, 1987, **133**, 288.
466. A. Bax, D.G. Davis and S. Sarkar, *J. Magn. Reson.*, 1985, **63**, 230.
467. H. Kessler, G. Gemmecker and B. Haase, *J. Magn. Reson.*, 1988, **77**, 401.
468. N. Lee, H.B.R. Cole and B.C. Sanctuary, *J. Magn. Reson.*, 1988, **76**, 209.
469. D.T. Pegg and M.R. Bendall, *J. Magn. Reson.*, 1984, **58**, 14.
470. T.T. Nakashima, R.E.D. McClung and B.K. John, *J. Magn. Reson.*, 1984, **58**, 27.
471. N. Chandrakumar, *J. Magn. Reson.*, 1984, **60**, 28.
472. J.R. Wesener, P. Schmitt and H. Günther, *Org. Magn. Reson.*, 1984, **22**, 468.

473. D.P. Burum, *J. Magn. Reson.*, 1984, **59**, 430.
474. O.W. Sørensen, J.C. Madsen, N.C. Nielsen, H. Bildsøe and H.J. Jakobsen, *J. Magn. Reson.*, 1988, **77**, 170.
475. K.V. Schenker and W. von Philipsborn, *J. Magn. Reson.*, 1985, **61**, 197.
476. U.B. Sørensen, H. Bildsøe, H.J. Jakobsen and O.W. Sørensen, *J. Magn. Reson.*, 1985, **65**, 222.
477. J.C. Madsen, H. Bildsøe, H.J. Jakobsen and O.W. Sørensen, *J. Magn. Reson.*, 1986, **67**, 243.
478. G.C. Van Stein, G. van Koten, K. Vrieze, C. Brevard and A.L. Spek, *J. Am. Chem. Soc.*, 1984, **106**, 4486.
479. H.J. Jakobsen, U.B. Sørensen, H. Bildsøe and O.W. Sørensen, *J. Magn. Reson.*, 1985, **63**, 601.
480. B. Coxon, *J. Magn. Reson.*, 1986, **66**, 230.
481. H. Kessler, W. Bermel and C. Griesinger, *J. Magn. Reson.*, 1985, **62**, 551.
482. K.S. Lee and G.A. Morris, *J. Magn. Reson.*, 1986, **70**, 332.
483. J.M. Bernassau, *J. Magn. Reson.*, 1985, **62**, 533.
484. N. Chandrakumar, *J. Magn. Reson.*, 1985, **63**, 174.
485. V. Sklenar, K. Nejezchleb and Z. Starcuk, *J. Magn. Reson.*, 1986, **69**, 144.
486. N.C. Nielsen, H. Bildsøe, H.J. Jakobsen and O.W. Sørensen, *J. Magn. Reson.*, 1986, **66**, 456.
487. O.W. Sørensen, N.C. Nielsen, H. Bildsøe and H.J. Jakobsen, *J. Magn. Reson.*, 1986, **70**, 54.
488. N.C. Nielsen, H. Bildsøe, H.J. Jakobsen and O.W. Sørensen, *J. Am. Chem. Soc.*, 1987, **109**, 901.
489. R.L. Halterman, N.H. Nguyen and K.P.C. Vollhardt, *J. Am. Chem. Soc.*, 1985, **107**, 1379.
490. D. Neuhaus, J. Keeler and R. Freeman, *J. Magn. Reson.*, 1985, **61**, 553.
491. D. Williamson and A. Bax, *J. Magn. Reson.*, 1987, **75**, 174.
492. C. Rossi and N. Niccolai, *Chem. Phys. Lett.*, 1987, **142**, 418.
493. T.T. Nakashima, B.K. John and R.E.D. McClung, *J. Magn. Reson.*, 1984, **59**, 124.
494. W.M. Westler, G. Ortiz-Polo and J.L. Markley, *J. Magn. Reson.*, 1984, **58**, 354.
495. H. Santos and D.L. Turner, *FEBS Lett.*, 1985, **184**, 240.
496. H. Santos and D.L. Turner, *FEBS Lett.*, 1986, **194**, 73.
497. S. Coffin, M. Limm and D. Cowburn, *J. Magn. Reson.*, 1984, **59**, 268.
498. N.S. Bhacca, M.F. Balandrin, A.D. Kinghorn, T.A. Frenkiel, R. Freeman and G.A. Morris, *J. Am. Chem. Soc.*, 1983, **105**, 2538.
499. D.A. Aikens, S.C. Bunce, O.F. Onasch, H.M. Schwartz and C. Hurwitz, *J. Chem. Soc. Chem. Commun.*, 1983, 43.
500. P. Schmitt and H. Günther, *Angew. Chem.*, 1983, **22**, 499.
501. H. Bleich, S. Gould, P. Pitner and J. Wilde, *J. Magn. Reson.*, 1983, **56**, 515.
502. R. Nardin and M. Vincendon, *J. Magn. Reson.*, 1985, **61**, 338.
503. J.R. Everett and J.W. Tyler, *J. Chem. Soc. Perkin Trans. 1*, 1985, 2599.
504. G.A. Olah, G.K.S. Prakash, J.G. Shih, V.V. Krishnamoorthi, G.D. Mateescu, G. Liang, G. Sipos, V. Buss, T.M. Gund and P.v.R. Schleyer, *J. Am. Chem. Soc.*, 1985, **107**, 2764.
505. R.J. Smith, D.H. Williams, J.C.J. Barne, I.R. McDermott, K.D. Haegele, F. Pirion, J. Wagner and W. Higgins, *J. Am. Chem. Soc.*, 1985, **107**, 2849.
506. T.C. Wong, *J. Magn. Reson.*, 1985, **63**, 179.
507. V. Rutar and T.C. Wong, *J. Magn. Reson.*, 1987, **71**, 75.
508. J.R. Wesener and H. Günther, *J. Am. Chem. Soc.*, 1985, **107**, 1537.

509. L.A. Trimble, P.B. Reese and J.C. Vederas, *J. Am. Chem. Soc.*, 1985, **107**, 2175.
510. M.J. Smith, J.N. Shoolery, B. Schwyn, I. Holden and J.B. Neilands, *J. Am. Chem. Soc.*,1985, **107**, 1739.
511. T.M. Zabriskie, J.A. Klocke, C.M. Ireland, A.H. Marcus, T.F. Molinski, D.J. Faulkner, C. Xu and J.C. Clardy, *J. Am. Chem. Soc.*, 1986, **108**, 3123.
512. D.M. Roll, J.E. Biskupiak, C.L. Mayne and C.M. Ireland, *J. Am. Chem. Soc.*,1986, **108**, 6680.
513. L.A. Paquette, L. Waykole, H. Jendralla and C.E. Cottrell, *J. Am. Chem. Soc.*, 1986, **108**, 3739.
514. P.H. Harrison, H. Noguchi and J.C. Vederas, *J. Am. Chem. Soc.*, 1986, **108**, 3833.
515. Y. Sata and S.J. Gould, *J. Am. Chem. Soc.*, 1986, **108**, 4625.
516. M.G. Reinecke, W.H Watson, D.C Chang and W.M. Yan, *Heterocycles*, 1986, **24**, 49.
517. D.E. Cane, T-C. Liang, P.B. Taylor, C. Chang and C.-C. Yang, *J. Am. Chem. Soc.*, 1986, **108**, 4957.
518. C.W. Funke, J.S. DeGraaf, E. Buurnen, H. Thalen and P. Vrijhof, *J. Chem. Soc. Perkin Trans. 2*, 1986, 735.
519. J-L. Cornillou, J.E. Anderson, C. Swistak and K.M. Kadish, *J. Am. Chem. Soc.*, 1986, **108**, 7633.
520. M.S. Lee, D.J. Repeta, K. Nakashini and M.G. Zagorski, *J. Am. Chem. Soc.*, 1986, **108**, 7855.
521. T. Nishida, G.A. Morris, I. Forsblom, I. Wahlberg and C.R. Enzell, *J. Chem. Soc. Chem. Commun.*, 1986, 998.
522. T. Nishida, C.R. Enzell and G.A. Morris, *Magn. Reson. Chem.*, 1986, **24**, 179.
523. E. Giralt and M. Feliz, *Magn. Reson. Chem.*, 1986, **24**, 123.
524. H. Kessler, C. Griesinger and J. Lautz, *Angew. Chem. Int. Ed. Engl.*, 1984, **23**, 444.
525. H. Kessler, C. Griesinger, J. Zarbock and H.R. Loosli, *J. Magn. Reson.*, 1984, **57**, 331.
526. H. Kessler, W. Bermel and C. Griesinger, *J. Am. Chem. Soc.*, 1985, **107**, 1083.
527. A.S. Zekster, M.J. Quast, G.S. Linz, G.E. Martin, J.D. McKenney, M.D. Johnston and R.N. Castle, *Magn. Reson. Chem.*, 1986, **24**, 1083.
528. M.J. Quast, A.S. Zekster, G.E. Martin and R.N. Castle, *J. Magn. Reson.*, 1987, **71**, 554.
529. A.S. Zekster, B.K. John, R.N. Castle and G.E. Martin, *J. Magn. Reson.*, 1987, **72**, 556.
530. H. Kessler, W. Bermel, C. Griesinger and C. Kolar, *Angew. Chem.*, 1986, **98**, 352.
531. J. Wernly and J. Lauterwein, *J. Magn. Reson.*, 1986, **66**, 355.
532. M.D. Lee, T.S. Dunne, M.M. Siegel, C.C. Chang, G.O. Morton and D.B. Borders, *J. Am. Chem. Soc.*, 1987, **109**, 3464.
533. M.D. Lee, T.S. Dunne, C.C. Chang, G.A. Ellestad, M.M. Siegel, G.O. Morton, W.J. McGahren and D.B. Borders, *J. Am. Chem. Soc.*, 1987, **109**, 3466.
534. L. Müller and P.W. Jeffs, *J. Magn. Reson.*, 1987, **73**, 405.
535. H. Kessler, C. Griesinger and K. Wagner, *J. Am. Chem. Soc.*, 1987, **109**, 6927.
536. A. Otter, P.G. Scott and G. Kotovych, *J. Am. Chem. Soc.*, 1987, **109**, 6995.
537. H. Kessler, J.W. Bats, C. Griesinger, S. Koll, M. Will and K. Wagner, *J. Am. Chem. Soc.*, 1988, **110**, 1033.
538. L. Müller, *J. Am. Chem. Soc.*, 1979, **101**, 4481.
539. M.R. Bendall, D.T. Pegg, D.M. Doddrell and D.M. Thomas, *J. Magn. Reson.*, 1982, **46**, 43.
540. M.R. Bendall, D.T. Pegg and D.M. Doddrell, *J. Magn. Reson.*, 1983, **52**, 81.
541. D.H. Live, D.G. Davis, W.C. Agosta and D. Cowburn, *J. Am. Chem. Soc.*, 1984, **106**, 6104.
542. R.H. Griffey and A.G. Redfield, *Q. Rev. Biophys.*, 1987, **19**, 51.
543. L. Müller, R.A. Schiksmis and S.J. Opella, *J. Magn. Reson.*, 1986, **66**, 379.

544. A. Bax and S. Subramanian, *J. Magn. Reson.*, 1986, **67**, 565.
545. S.K. Sarkar, J.D. Glickson and A. Bax, *J. Am. Chem. Soc.*, 1986, **108**, 6814.
546. M.F. Summers, L.G. Marzilli and A. Bax, *J. Am. Chem. Soc.*, 1986, **108**, 4285.
547. D. Brühwiler and G. Wagner, *J. Magn. Reson.*, 1986, **69**, 546.
548. A. Bax and M.F. Summers, *J. Am. Chem. Soc.*, 1986, **108**, 2093.
549. A. Bax, A. Aszalos, Z. Dinya and K. Sudo, *J. Am. Chem. Soc.*, 1986, **108**, 8056.
550. A. Bax, R.H. Griffey and B.L. Hawkins, *J. Am. Chem. Soc.*, 1983, **105**, 7188.
551. A. Bax, R.H. Griffey and B.L. Hawkins, *J. Magn. Reson.*, 1983, **55**, 301.
552. V. Sklenar and A. Bax, *J. Magn. Reson.*,1987, **71**, 365.
553. R.H. Griffey, A.G. Redfield, R.E. Loomis and F.W. Dahlquist, *Biochemistry*, 1985, **24**, 817.
554. R.H. Griffey, A.G. Redfield, L.P. McIntosh, T.G. Oas and F.W. Dahlquist, *J. Am. Chem. Soc.*, 1986, **108**, 6816.
555. G. Otting and K. Wüthrich, *J. Magn. Reson.*, 1988, **76**, 569.
556. D.H. Live, I.M. Armitage, D.C. Dalgarno and D. Cowburn, *J. Am. Chem. Soc.*, 1985, **107**, 1775.
557. D.H. Live, C.L. Kojiro, D. Cowburn and J.L. Markley, *J. Am. Chem. Soc.*, 1985, **107**, 3043.
558. M.H. Frey, G. Wagner, M. Vasak, O.W. Sørensen, D. Neuhaus, E. Wörgotter, J.H. Kägi, R.R. Ernst and K. Wüthrich, *J. Am. Chem. Soc.*, 1985, **107**, 6847.
559. G. Ortiz-Polo, R. Krishnamoorthi and J.L. Markley, *J. Magn. Reson.*, 1986, **68**, 303.
560. J. Glushka and D. Cowburn, *J. Am. Chem. Soc.*, 1987, **109**, 7879.
561. G. Wagner and D. Brühweiler, *Biochemistry*, 1986, **25**, 5839.
562. R.A. Byrd, M.F. Summers and G. Zon, *J. Am. Chem. Soc.*, 1986, **108**, 504.
563. V. Sklenar, A. Bax and G. Zon, *J. Am. Chem. Soc.*, 1987, **109**, 2221.
564. V. Sklenar, H. Miyashiro, G. Zon, T. Miles and A. Bax, *FEBS Lett.*, 1986, **208**, 94.
565. R. Benn and C. Brevard, *J. Am. Chem. Soc.*, 1986, **108**, 5622.
566. J.L. Dimicoli, A. Volk and J. Mispelter, *J. Magn. Reson.*, 1985, **63**, 605.
567. F.J.M. Van de Ven, C.A.G. Haasnoot and C.W. Hilbers, *J. Magn. Reson.*, 1985, **61**, 181.
568. S. Macura, J. Bremer and L.R. Brown, *J. Magn. Reson.*, 1985, **63**, 484.
569. M.A. Weiss, A.G. Redfield and R.H. Griffey, *Proc. Natl Acad. Sci. USA*, 1986, **83**, 1325.
570. S. Macura, N.G. Kumar and L.R. Brown, *J. Magn. Reson.*, 1984, **60**, 28.
571. P.H. Bolton, *J. Magn. Reson.*, 1985, **62**, 143.
572. L.E. Kay, T.L. Jue, B. Bangerter and P.C. Demon, *J. Magn. Reson.*, 1987, **73**, 558.
573. M.A. Delsuc, E. Guittet, N. Trotin and J.Y. Lallemand, *J. Magn. Reson.*, 1984, **56**, 163.
574. H. Kessler, M. Bernd, H. Kogler, J. Zarbock, O.W. Sorensen, G. Bodenhausen and R.R. Ernst, *J. Am. Chem. Soc.*, 1983, **105**, 6944.
575. O.W. Sørensen and R.R. Ernst, *J. Magn. Reson.*, 1983, **55**, 338.
576. A. Bax, *J. Magn. Reson.*, 1983, **53**, 149.
577. P.H. Bolton, *J. Magn. Reson.*, 1985, **63**, 225.
578. L.D. Field and B.A. Messerle, *J. Magn. Reson.*, 1985, **62**, 453.
579. J. Santoro, M. Rico and F.J. Bermejo, *J. Magn. Reson.*, 1986, **67**, 1.
580. T.A. Holak and J.H. Prestegard, *J. Magn. Reson.*, 1987, **73**, 530.
581. S.W. Sparks and P.D. Ellis, *J. Magn. Reson.*, 1985, **62**, 1.
582. P.J. Keller and K.E. Vogele, *J. Magn. Reson.*, 1986, **68**, 389.
583. J. Lambert, K. Wilhelm and M. Klessinger, *J. Magn. Reson.*, 1985, **63**, 189.
584. O.W. Sørensen and R.R. Ernst, *J. Magn. Reson.*, 1985, **63**, 219.
585. A. Bax and G. Drobny, *J. Magn. Reson.*, 1985, **61**, 306.

586. W.J. Chazin and K. Wüthrich, *J. Magn. Reson.*, 1987, **72**, 358.
587. S.K. Sarkar and A. Bax, *J. Magn. Reson.*, 1985, **63**, 512.
588. T.C. Wong and V. Rutar, *J. Magn. Reson.*, 1985, **63**, 524.
589. G. Wagner, *J. Magn. Reson.*, 1983, **55**, 151.
590. L.D. Field and B.A. Messerle, *J. Magn. Reson.*, 1986, **66**, 483.
591. P.L. Weber and L. Müller, *J. Magn. Reson.*, 1987, **73**, 184.
592. N.J. Namuri, M. Hassan and M. Goodman, *J. Am. Chem. Soc.*, 1985, **107**, 4008.
593. S.R. Johns, J.A. Lamberton, H. Snares and R.I. Willing, *Aust. J. Chem.*, 1985, **38**, 1091.
594. B. Bodo, S. Rebuffat, M. El Hajji and D. Davoust, *J. Am. Chem. Soc.*, 1985, **107**, 6011.
595. G.A. Morris and M.S. Richards, *Magn. Reson. Chem.*, 1985, **23**, 676.
596. G.S. Linz, M. Alam, A.J. Weinheimer, G.E. Martin and E.L. Ezell, *J. Heterocycl. Chem.*, 1986, **23**, 529.
597. S. Hyberts, M. Rance, W.A. Denny and W. Leupin, *J. Mol. Biol.*, 1986, **190**, 439.

High-Resolution Solid-State NMR Studies of Synthetic and Biological Macromolecules

HAZIME SAITÔ

Biophysics Division, National Cancer Center Research Institute, Tsukiji 5-chome, Chuo-ku, Tokyo 104, Japan

and

ISAO ANDO

Department of Polymer Chemistry, Tokyo Institute of Technology, Ookayama, Meguro-ku, Tokyo 152, Japan

ANNUAL REPORTS ON NMR SPECTROSCOPY
VOLUME 21 ISBN 0-12-505321-5

I. INTRODUCTION

The first successful recording of high-resolution solid-state NMR spectra of rare spins such as ^{13}C nuclei in complex molecules was reported[1] in 1976, using a combination of cross-polarization (CP)[2] and magic angle spinning (MAS).[3] Since then, this methodology (CP-MAS NMR) has proved to be the most powerful means available to characterize the primary and secondary structures of macromolecules, as well as being an efficient probe for analysing their dynamic features in solids.[4-14]

In general, the ^{13}C NMR spectral features recorded in the solid state are more complicated than those observed in solution. In the solid state, the observed peak is either split into many lines or displaced (up to 8–10 ppm), while in solution such characteristic features are usually obscured by averaging due to rapid molecular reorientation. Unfortunately the complexity of the spectra, in spite of the mass of information contained, makes interpretation by NMR data alone very difficult in many instances. Inevitably, spectral assignment of NMR peaks from nuclei of natural abundance has been mainly based on knowledge obtained from other physical means such as X-ray diffraction or optical spectroscopy. More importantly, however, accumulation of empirical relationships between the displacement of peaks and secondary structures and/or intermolecular interactions of the molecular systems under consideration is vital in order to gain a unified view of the underlying general principles determining characteristc displacements of peaks in ^{13}C NMR spectroscopy.

In the present chapter, high-resolution solid-state NMR studies of synthetic polymers and naturally occurring biological macromolecules are reviewed with emphasis placed on revealing their conformations. A survey of high-resolution solid-state NMR studies of both types of macromolecular system has the advantage of being able to cover topics of conformation and dynamics of polymers in general. A proportion of the studies reviewed have been devoted to the analysis of secondary structures in biological macromolecules such as peptides, proteins, polysaccharides, etc., while the majority of the studies reviewed have been performed for the analysis of phase structure, the various modes of molecular motions, and their influence on the mechanical properties of synthetic polymers.

The scope of this chapter is restricted mainly to studies of ^{13}C nuclei, although some studies using other rare spin-1/2 nuclei such as ^{31}P or ^{15}N are reviewed where appropriate. This is because the use of ^{13}C NMR is most suitable for organic macromolecules and the majority of studies on these subjects have been caried out by means of ^{13}C NMR spectroscopy. We do not therefore discuss applications of high-resolution solid-state NMR studies of other spin-1/2 nuclei such as ^{29}Si, ^{119}Cd, etc., or those of quadrupolar nuclei such as ^{2}H, ^{14}N, ^{23}Na, etc.

II. EXPERIMENTAL ASPECTS OF SOLID-STATE NMR TECHNIQUES

A. Standard NMR techniques

High-resolution solid-state NMR spectra of rare spins are usually recorded by the standard technique of cross-polarization (CP) between observing the rare spin S and the abundant spin I (usually ^1H) with the pulse sequence illustrated in Fig. 1(A), combined with magic angle spinning (MAS). In the case of synthetic polymers at temperatures above their glass transition

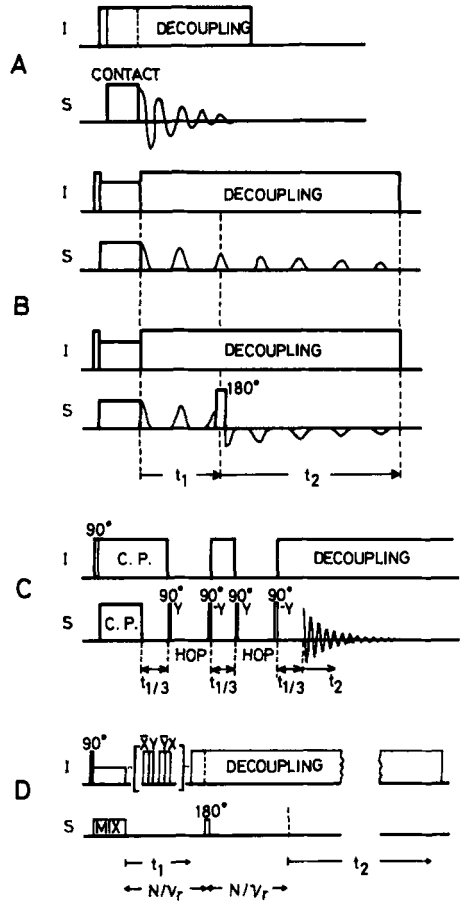

FIG. 1. Pulse sequences of conventional CP (A) and two-dimensional CP methods for the recovery of chemical shielding anisotropy (B, ref. 22; and C, ref. 24) and heteronuclear dipolar interaction (D, ref. 30).

temperatures, however, spectra of better S/N ratio are not always achieved by this pulse sequence alone because time-averaged dipolar interactions due to molecular motion make magnetization transfer by cross-polarization inefficient. Instead, simple dipolar decoupling combined with MAS turns out to be a suitable alternative means. The basic principles and practical applications of this standard method have been well documented in textbooks and in a number of excellent review articles.[4-14]

If the spinning rate ν_r is less than the width of chemical shielding anisotropy (CSA), $\Delta\sigma = (|\sigma_{11} - \sigma_{33}|)$, then the resulting spinning sidebands (rotational echo) flank the centreband, as illustrated in Fig. 2.[15,16] The presence of such spinning sidebands is prominent in quaternary or carbonyl carbons, whose CSA values are as large as 10 kHz if the NMR spectra are recorded by

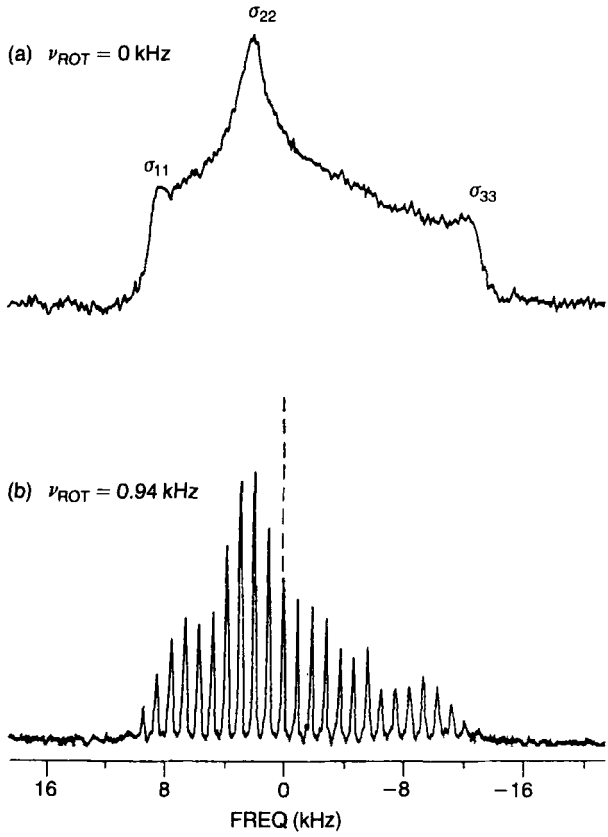

FIG. 2. Typical example of a powder pattern spectrum with chemical shift anisotropy (a) and its splitting into spinning sidebands by slow MAS spinning (b). (Proton decoupled ^{31}P spectra of barium diethylphosphate, ref. 16).

a high-frequency spectrometer employing a superconducting magnet. To suppress these undesirable sidebands, a pulse sequence named TOSS (total suppression of spinning sidebands)[17] is now routinely used. The use of high-frequency spectrometers at 7 T is thus prevailing, in spite of the previous belief that low-frequency measurements were preferable in the solid state. Moreover, ^{13}C NMR spectra of nitrogen-containing compounds can be much simplified at high frequency, because peak splittings by ^{13}C–^{14}N dipolar interactions[18] can be ignored at frequencies higher than 75 MHz (7 T). The chemical shift is intrinsically independent of the strength of the magnetic field employed. However, VanderHart recently proposed the existence of field-dependent ^{13}C chemical shifts (0.72 and 0.36 ppm for a methylene and methine, respectively) in protonated carbons in the solid state between 1.4 and 4.7 T, although changes of chemical shifts beyond 3.5 T are small.[19] He showed that such shifts result from a second-order energy perturbation involving the non-secular "C" and "D" terms of the dipolar Hamiltonian. He therefore proposed a "correction" of chemical shifts measured at 1.4 T based on this scheme.

A variable-temperature (VT) CP-MAS study offers an indispensable means to study molecular motion, reactive chemical intermediates and slow chemical exchange.[8] A VT CP-MAS probe is now commercially available which makes use of a ceramic cylindrical-type rotor. The range for temperature variation is about $+150$ to -120°C. It is important to consider the problems of temperature measurement and control.[20] However, there are several factors which contribute to the uncertainty in sample temperature, including radio frequency sample heating, mismatches in the drive- and bearing-gas channel, sample temperature equilibration times, and Joule–Thomson cooling and heating. Techniques are reported that allow the uncertainity in sample temperature to be reduced to approximately 1 K. Several compounds exhibiting solid–solid phase transitions have been examined for the purpose of temperature calibration in MAS experiments.[21]

B. Recovery of chemical shielding anisotropy and dipolar interactions

High-resolution solid-state NMR for powdered samples is made possible by suppressing valuable information from the heteronuclear dipolar interaction by RF decoupling, and by removing CSA by magic angle spinning. If the molecule is rigid, the dipolar interactions contain information about internuclear distances and directions, and CSA is strongly related to the molecular electronic state of a functional group under consideration. Alternatively, if the rigid lattice tensors of these interactions are known as reference, molecular motions which take place on a 10^{-4} s timescale can be studied in view of partial time-averaging in these parameters. For this reason, a

number of procedures mainly using two-dimensional (2D) NMR methods have been developed to recover the above-mentioned interactions from CP-MAS NMR spectra.

1. CSA

The simplest means to recover this interaction is either by recording solid-state ^{13}C NMR spectra of powder patterns with principal values σ_{11}, σ_{22} and σ_{33} (Fig. 2(a)) without MAS,[2] or by analysing patterns of spinning sidebands (rotational spin-echo)[15,16] by slowing the spinning frequency to less than the width of the CSA (Fig. 2(b)). This latter approach is very simple but is not always applicable to complex molecular systems which give rise to many spectral lines, unless peak selectivity can be achieved by isotope labelling.

Instead, the following two types of 2D NMR method have been developed to separate the CSA or resulting rotational spin-echo from the isotropic chemical shifts. Aue *et al.*[22,23] proposed an approach in which data acquisition for the t_2 period is initiated at the peak of a rotational echo and the increment t_1 is the period of one spin evolution (Fig. 1(B)). However, fast spinning speeds of 15 kHz are required for application to ^{13}C NMR, although a new version of chemical shift scaling has been developed to circumvent this problem. Instead, an alternative 2D method is to "hop" the spinning axis mechanically from the magic angle by 120°[24] (Fig. 1(C)) or by about 10°[25] before the detection period. Application of CSA patterns for the analysis of molecular motions in collagen has been previously reviewed.[26]

The CSA powder pattern illustrated in Fig. 2(a) arises from a completely random orientation of molecules with respect to a certain axis such as the direction of the magnetic field. If the molecules were either in a single crystal or orientated with respect to a certain axis in a rotor, then the CSA patterns would consist either of discrete sharp lines or of a lineshape more intense in some regions and less intense in others, respectively. Thus, the extent of molecular orientation can easily be analysed by examination of CSA pattern recorded by high-resolution NMR utilizing either of the two types of 2D experiment mentioned above.[27,28]

2. Dipolar interactions

In a similar manner, separation of CSA and heteronuclear dipolar interactions is accomplished by allowing the evolution of the dipolar Hamiltonian prior to a proton-decoupled detection of a rotational spin-echo arising from the above-mentioned chemical shifts.[29-31] In particular, high-power proton decoupling, either by a WAHUHA[32] or a MREV-8[33] pulse-sequence, is

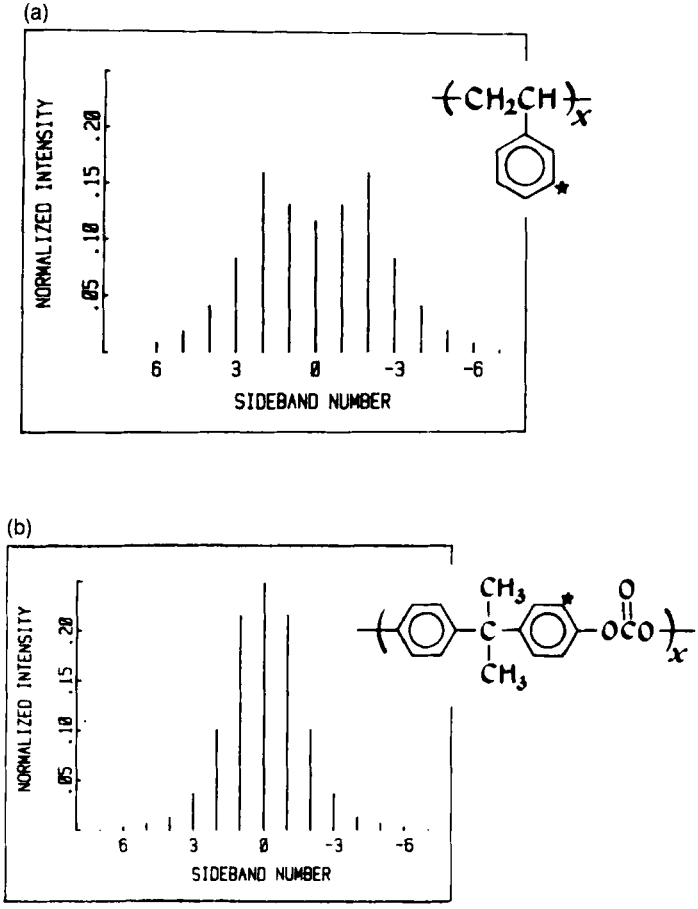

FIG. 3. Dipolar Pake patterns for ^{13}C-^{1}H fragments of (a) polystyrene and (b) polycarbonate. (Ref. 31.)

inserted to isolate the heteronuclear spin pair from ^{1}H–^{1}H couplings, and a 180° pulse at the peak of the nth rotational echo may be used to refocus chemical shifts (Fig. 1(D)). The characteristic dipolar Pake patterns thus obtained are broken up into separate spinning sidebands, as illustrated in Figs 3(a) and (b) for polystyrene and polycarbonate,[31] respectively. For static samples such as polystyrene, the peak separation of the Pake doublet is given by

$$D = \gamma_I \gamma_S h / r^3 \tag{1}$$

where r is the distance between spin I (^{1}H) and spin S (^{13}C). Griffin *et al.*[34]

showed that bond distances, accurate to within 0.005 Å, and mutual orientations of dipolar and CSA tensors, accurate to 3°, can be obtained by analysis of the ^{15}N–H dipolar tensor.

This dipolar Pake pattern may be modified in a similar manner as occurs with quadrupolar interactions,[35] when molecular motion partially averages the dipolar couplings (C_2 rotation, for instance, of the aromatic ring). Schaefer *et al.*[36] showed that the ratio of intensities of the second (n_2) to first dipolar rotational sidebands (n_1) is a sensitive measure of averaging of the C–H dipolar coupling by molecular motion. In fact, the ratio n_2/n_1 changes from about 1.5 for a system with little motion to 0.5 for a system with substantial motion. Thus, they showed that the dipolar Pake pattern of poly(BPA-formal) with a smaller n_2/n_1 ratio (Fig. 3(b)) is ascribable to the presence of 180° flips about the C_2 axis of the aromatic ring.

C. Spin exchange

Szeverenyi *et al.* have introduced a solid-state CP-MAS analogue of the 2D exchange (Fig. 4(A)) method used with solutions to study spin exchange, spin

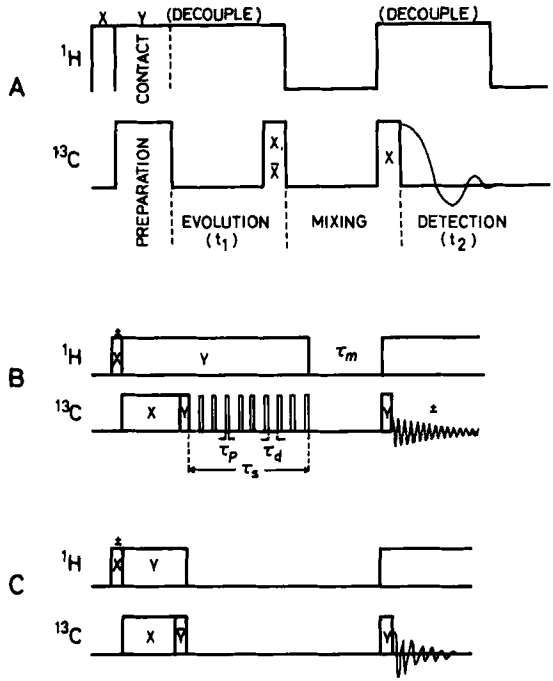

FIG. 4. Pulse sequences for (A) 2D spin exchange (ref. 37), (B) 1D exchange (ref. 44), and (C) T_1^C measurements (ref. 45).

diffusion, the effect of ^{14}N relaxation and intrinsic T_2 effects.[37,38] In this experiment, a 90° pulse at t_1 converts the ^{13}C magnetization obtained by cross-polarization into the z-component, which is allowed to become mixed, by spin exchange or spin diffusion during the mixing time, without proton decoupling. Frey and Opella used this method to detect carbons of amino-acid residues that are near to each other in space even when they are on separate residues in peptides.[39] This method has also been utilized to examine interchain ^{13}C spin exchange in static crystalline polyethylene,[40] because MAS modifies the rate of spin exchange by averaging dipolar interactions during the mixing time.[41] Further, for detection of slow molecular orientation,[42] or ultraslow molecular motion in crystalline polyoxymethylene,[43] Veeman *et al.* made use of the off-diagonal sideband intensities of the 2D spectrum from slow MAS.

Caravatti *et al.* have explored a 1D approach to the study of spin exchange utilizing a selective pulse experiment,[44] as illustrated in Fig. 4(B). This pulse sequence is analogous to that for the measurement of spin–lattice relaxation times in the solid state[45] (Fig. 4(C)), except for the insertion of the DANTE sequence[46] prior to the mixing time to invert the labelled magnetization selectively. Figure 5 shows a typical example of this sort of experiment applied to a single crystal of 1,5-dimethylnaphthalene.[44] In the chosen crystal orientation, the two methyl peaks A and B are well resolved due to the presence of two non-equivalent molecules per unit cell. In a non-selective T_1 experiment (Fig. 5(a)), the two methyl groups decay with the time constant $R_1 = 1/T_1 = (0.45 \pm 0.02)\ s^{-1}$. The decay of the low frequency methyl peak B becomes biexponential when the high frequency methyl peak A is initially inverted by the selective inversion (Fig. 5(b)). The relaxation rates are given by

$$R_A = R_1 + R_{AB} + 10R_{A\phi} = (1.0 \pm 0.1)\ s^{-1}$$
$$R_B = R_1 + R_{AB} = (0.58 \pm 0.02)\ s^{-1}$$

where R_{AB} ($= 0.13 \pm 0.04\ s^{-1}$) is the spin diffusion rate between the two methyl groups and $R_{A\phi}$ ($= 0.06 \pm 0.016\ s^{-1}$) is the mean diffusion rate between 10 aromatic sites.

In general, carbon spin diffusion is much less efficient (lower rate) than spin diffusion amongst protons because of the smaller gyromagnetic ratio and substantially lower natural abundance of the latter. The use of a ^{13}C-enriched sample circumvents this problem. Linder *et al.*[47] have applied this technique to probe the miscibility of polymer blends, using selectively ^{13}C-enriched poly(ethylene terephthalate) (PET) and bisphenol A polycarbonate (BPAPC). They showed that the PET/BPAPC blends are homogeneously mixed at a distance of 4–6 Å, on the basis of the interchain rate of spin diffusion, 0.5–0.8 s^{-1}. In a similar manner, Roy[48] *et al.* studied the local

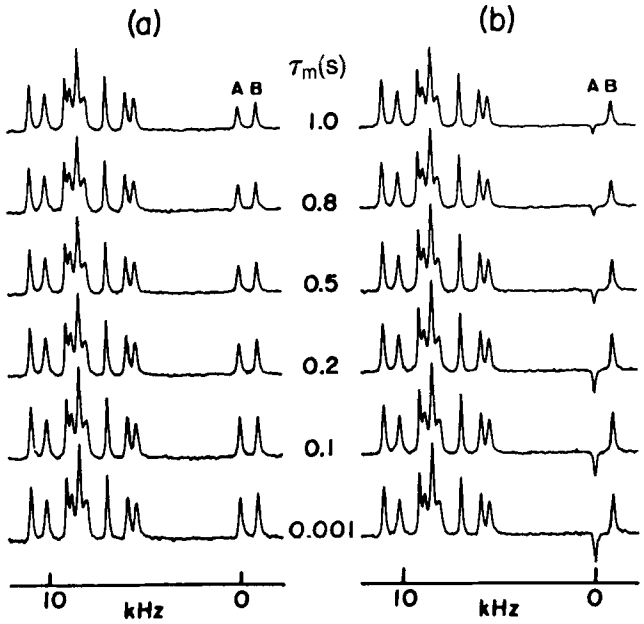

FIG. 5. (a) Measurement of the decay of the longitudinal ^{13}C magnetization for a single crystal of 1,5-dimethylnaphthalene, and (b) decay after selective inversion of one of the two magnetically non-equivalent methyl resonances, A. (Ref. 44.)

intermolecular structure of antiplasticized glass consisting of BPAPC and the antiplasticizer di-*n*-butyl phthalate (DBP) selectively labelled with ^{13}C. At a low DBP ratio selective spin diffusion was observed between the two components, indicating the presence of specific interactions. VanderHart[49] has extensively analysed the ^{13}C spin diffusion rate at natural abundance for both polyethylene and cellulose.

III. SIGNIFICANCE OF NMR PARAMETERS

A. Chemical shifts

1. Conformation-dependent ^{13}C chemical shifts

Chemical shifts are the most important parameters in high-resolution solid-state NMR: they are not merely the fingerprints of the primary chemical structure of the molecules under consideration but are, in favourable cases, useful as a means of probing the secondary structure or molecular con-

formation.[50,51] This view is substantiated by the fact that chemical shifts are determined by the electronic structures of molecules which are naturally influenced by their secondary structure. Previous experimental data for a variety of molecular systems, including paraffins, polysaccharides, polypeptides, and several types of ionophores, have shown that the maximal displacements of peaks upon conformational changes are in most instances as large as 8 ppm, but can be up to 12 ppm in some cases.[50,51] This type of conformation-dependent ^{13}C chemical shift is in many instances related to the nearby torsion angles of skeletal bonds.

Furthermore, another type of conformation-dependent displacement of ^{13}C NMR peaks has been recognized. In particular, the frozen conformation in the solid state induces a non-equivalent chemical environment, as manifested by the additional splitting of ^{13}C NMR signals for nominally equivalent carbons observed in solution. Schaefer *et al.*[4,52] showed that the protonated benzene carbons of poly(phenylene oxide) adjacent to etheric oxygen give rise to a doublet in the solid but a singlet in solution. The origin of this type of splitting has not yet been clarified. Garroway *et al.*[53] interpreted the splittings of two *ortho* carbons in epoxy polymers in terms of steric effects. In contrast, Saitô *et al.*[54] pointed out the contribution of electron density non-equivalence between the two *ortho* and two *meta* carbons in *para*-substituted methoxybenzenes. As an additional source of peak displacement, it is worthwhile pointing out that the ^{13}C chemical shifts of methyl groups are displaced to low frequency by short interatomic contact:[55-57] deformation of C—C—H angles by 1-3° from the tetrahedral angle is probably responsible. The effect of bond distortion by crystalline packing on the displacements of ^{13}C chemical shifts has been previously demonstrated,[58,59] as described in more detail in Section IV.

The magnitude of these peak displacements, however, seems to be small compared with the total spread of peaks (200 ppm), but should be sufficiently large to be a convenient intrinsic probe of conformational characterization. In some instances, however, such conformation dependence is obscured for samples of highly disordered states because the ^{13}C NMR peaks are broadened and the peak positions are less sensitive to various types of preparations. In Sections IV and V, applications of high-resolution solid-state NMR to conformational elucidation are reviewed in more detail.

2. *Theoretical interpretations of ^{13}C chemical shifts*

Nuclear shielding can be expressed as a second-rank tensor. In principle, non-spinning CP measurements in the solid state can yield values for the individual components of the shielding tensor σ as expressed by

$$\sigma = \begin{pmatrix} \sigma_{11} & 0 & 0 \\ 0 & \sigma_{22} & 0 \\ 0 & 0 & \sigma_{33} \end{pmatrix} \tag{2}$$

where the σ_{ii} are the principal tensor components taken in accordance with the convention $\sigma_{11} < \sigma_{22} < \sigma_{33}$. The rapid isotropic molecular motion in liquid or solution and the magic angle spinning in solid-state CP-MAS experiments ensure that the isotropic nuclear shielding, σ_{iso}, is given by one-third of the trace of σ as

$$\sigma_{iso} = (\sigma_{11} + \sigma_{22} + \sigma_{33})/3 \tag{3}$$

The shielding constant σ_A of a nucleus A, is expressed as the sum of the diamagnetic contribution, σ^d, the paramagnetic contribution, σ^p, and another contribution, σ', as follows[60]

$$\sigma_A = \sigma_A{}^d + \sigma_A{}^p + \sigma' \tag{4}$$

where σ' is the contribution from the neighbouring atoms bonded to the atom A. Usually the effect of σ' on the ^{13}C chemical shift is known to be very small, contributing less than a few ppm, and can be considered negligible. Thus, σ can be estimated from the sum of σ^d and σ^p. Further, it is known that of these two terms, σ^p predominates in the contribution to the relative ^{13}C chemical shift. For the shielding constant (σ) an associated negative sign means deshielding, while a negative sign associated with the observed chemical shift (δ) means shielding. Chemical shift δ_A is expressed as $\delta_A = \sigma_0 - \sigma_A$, where σ_0 is the shielding constant of a reference compound such as TMS.

Calculated chemical shifts, in principle, are obtained as the nine elements of the chemical shielding tensor as expressed by $\sigma_{\alpha\beta}$ where $\alpha\beta = x, y, z$ in cyclic order. The three principal values of the shielding tensor can be obtained by finding its eigenvalues. In general, the paramagnetic shielding contribution is anisotropic but the diamagnetic shielding contribution is isotropic. Thus, the paramagnetic shielding term governs the CSA. The calculated principal values may be compared with those available from solid-state samples. Accordingly, more detailed information is available as to the electronic state of polymer samples based on high-resolution solid-state NMR, in particular ^{13}C NMR.

A number of theories of nuclear shielding[60] have been proposed since Ramsey's work appeared. According to Ramsey's expression, it is clear that σ^d arises from the ground state electronic functions. As such it is the molecular counterpart of the Lamb formula for atomic shielding. This term does not contribute significantly to the relative ^{13}C chemical shift. On the other hand, as described above, the chemical shift of a ^{13}C nucleus is governed predominantly by σ^p. It is noteworthy that the diamagnetic and paramagnetic

contributions act in opposite directions, as indicated by the negative sign for σ^p. In the estimation of σ^p, one often encounters difficulties in evaluating the energies in the excited states of molecules. At present, there are two methods commonly used to estimate σ^p. One is the sum-over-states (SOS) method and the other is the finite perturbation theory (FPT).

The SOS method is derived from the second-order perturbation method and so contains a summation of terms including the transition energies from the ground states to the excited states. The FPT method has the advantage of permitting the calculation of the paramagnetic term without the use of the explicit wavefunctions for excited states, which cannot be obtained accurately by an ordinary SCF-MO method. Since the paramagnetic term requires the presence of electrons with orbital angular momentum, it will not be operative for s valence electrons.

The ^{13}C chemical shifts for polymer systems have been studied in order to obtain useful information about the conformation of crystalline and non-crystalline structures in the solid state. These chemical shifts arise from changes in the electronic structure due to changes in the dihedral angles of the skeletal bonds and the existence of intermolecular interactions. There are two approaches used to obtain the information about the electronic structure of polymers which is needed in the calculation of the chemical shift. One method is to use dimers, trimers, etc. as representative fragments of the polymer under consideration. For example, an attempt at calculating the ^{13}C chemical shift of a dipeptide fragment of poly(L-alanine) was made using the FPT INDO method.[61] The ^{13}C chemical shifts of the C_β carbons of alanine residues in various polypeptides vary significantly, depending on the conformation, which may be a right-handed α-helix, β-sheet or other conformation, as shown in Table 1. Such sizeable displacements of the ^{13}C chemical shifts can be characterized by variations of the electronic structure of the local conformation as defined by the dihedral angles (ϕ and ψ). As proof of this view, the shielding of a dipeptide fragment has been calculated by using the FPT INDO method. The calculated contour map for the C_β carbon is shown in Fig. 6. From this map, we can estimate the ^{13}C shielding for any specified conformation. In Table 1, the calculated ^{13}C shielding and the observed ^{13}C chemical shifts of the L-alanine C_β carbon in the polypeptides are shown for various conformations. Clearly, the calculated shieldings parallel the experimental data. Such calculations are very useful as a means of analysing the structure of polymers.

Sometimes the estimation of the electronic structures of polymer chains requires us to include the long-range interactions and intermolecular interactions in the calculations. To do so, it is necessary to use a sophisticated theoretical method which can take account of the characteristics of polymers. The tight-binding MO theory[62,63] from the field of solid-state physics is used,

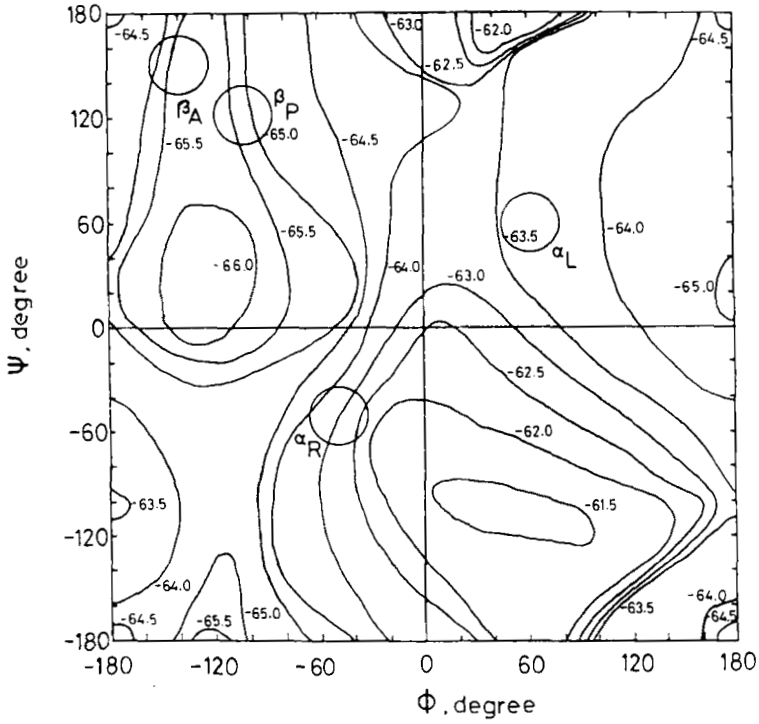

FIG. 6. The calculated ^{13}C chemical shift contour map for the C_β in *N*-acetyl-*N'*-methyl-L-alanine amide. The chemical shifts were calculated at 15° intervals in ϕ and ψ. (Ref. 61.)

in the sense in which it is used in the LCAO approximation in molecular quantum chemistry, to describe the electronic structures of infinite polymers with periodic structure. In a polymer chain with linearly bonded monomer units, the potential energy of an electron varies periodically along the chain. In such a system the wavefunction for electrons at position r can be given by Bloch's theorem as follows:

$$\Psi_n(k) = \frac{1}{\sqrt{N}} \sum_{\nu}^{\ell} \sum_{j}^{N} \exp(ikj) C_{\nu n}(k)\, \phi_\nu(r - ja) \tag{5}$$

where n is the band index, ν is an orbital index in the jth cell, N is the total number of cells, ℓ is the number of atomic orbitals in the cell, a is the unit vector of transitional symmetry, and k is the wavenumber. $\phi_\nu(r-ja)$ represents the νth atomic orbital in the jth cell and $C_{\nu n}(k)$ the expansion coefficient. The formulae needed to calculate the ^{13}C shielding of polymers using the tight-binding MO theory incorporated with the sum-over-states

TABLE 1

Comparison of the ^{13}C chemical shifts of Ala C_β signals of various polypeptides having different conformations with those of theoretical calculations[a] (ref. 206).

Conformation	Dihedral angles[b] (ϕ and ψ)	C_β ^{13}C chemical shifts (ppm)	
		Observed[c]	Calculated[d]
Right-handed α-helix	$-48°$ and $-57°$	14.9	−63.0
Left-handed α-helix	48° and 57°	14.9	−63.7
Antiparallel β-sheet	$-142°$ and 145°	19.9	−65.7
3_1-helix	$-80°$ and 150°	17.5	−64.7

[a]Calculated for *N*-acetyl-*N'*-methyl-L-alanine amide.
[b]Data from G. N. Ramachandran and V. Sasisekharan, *Adv. Protein Chem*, 1968, **23**, 283–438.
[c]Chemical shifts referred to Me_4Si.
[d]Chemical shifts expressed by the nuclear shielding constants.

method have been derived.[64–67] This theoretical approach has been successfully applied to polymers[68–70] such as polyethylene, polyacetylene, polyoxymethylene and various polypeptides.

B. Relaxation parameters

As in conventional high-resolution NMR in the liquid state, spin relaxation times are very important parameters in the solid state for obtaining spectra under optimum conditions. In some instances the interpretation of the data in terms of molecular motions involved in the solid state is dependent on a knowledge of spin-relaxation times. In general, the following eight relaxation parameters should be taken into account in recording ^{13}C NMR spectra by cross-polarization (CP) methods: T_1^H, $T_{1\rho}^H$, T_1^C, $T_{1\rho}^C$ (for other nuclei such as ^{15}N, ^{31}P, ^{29}Si, etc., the superscript C stands for the respective nuclei), T_{1D}, T_{CH}, T_{CH}^{ADRF} and T_2^C. Here, T_1^X and $T_{1\rho}^X$ are the spin–lattice relaxation times in the laboratory and rotating frame, respectively, for nucleus X (H or C), and T_{1D} is the proton dipolar spin–lattice relaxation time. In addition, T_{CH} and T_{CH}^{ADRF} are cross-relaxation times under the Hartmann–Hahn condition and under a carbon radio-frequency field alone, respectively.[4,8,11,14,71] In this connection, it has been shown from the analysis of the dynamics of cross-polarization that optimum sensitivity is achieved only when the following conditions are satisfied:[8] the radio-frequency fields for proton and carbon nuclei $\gg$ proton and carbon natural linewidths, and $T_1^C > T_1^H \geq T_{1\rho}^H >$ contact time $> T_{CH}$.

1. T_1^H and $T_{1\rho}^H$

The proton spin–lattice relaxation times of the laboratory frame (T_1^H) and rotating frame ($T_{1\rho}^H$) are less informative for the detection of molecular motions in the solid state, because the relaxation times of protons in different chemical environments are averaged to give single values due to efficient spin diffusion processes.[72,73] Nevertheless, carbon-resolved proton spin–lattice relaxation times of the rotating frame ($T_{1\rho}^H$), as obtained by ^{13}C NMR measurements, have turned out to be a very useful means for evaluating the compatibility of solid polymeric blends.[74] This is possible because in most cases neither the carbon–proton cross-relaxation nor the proton homonuclear couplings among the protons are affected by the MAS and the final evolution of the ^{13}C follows the $T_{1\rho}^H$ decay.[75] In fact, through spin diffusion, $T_{1\rho}^H$ values of a multicomponent system are strongly dependent on the short (1 nm) spatial proximity, or mixing, of the various components. As a result, a single $T_{1\rho}^H$ value is obtained from a multicomponent system when $T_{1\rho}^H$ values of polymers of homogeneous mixing are measured by this method. However, different $T_{1\rho}^H$ values are observable for multicomponent systems when polymer blends are not homogeneously mixed. As mentioned above, the carbon-resolved $T_{1\rho}^H$ values are easily obtained from the exponential decrease in ^{13}C NMR peak intensity of longer contact time in a plot of ^{13}C NMR peak intensity against contact time. In a similar manner, miscibility of two polymers can be evaluated by observation of ^{13}C signals from deuteriated components due to intermolecular cross-polarization.[76]

Spin diffusion of ^{13}C nuclei is much less efficient than that of protons because the dipolar interaction between two ^{13}C nuclei is about 1/16 of the dipolar coupling of two protons and the distances between nuclei of naturally occurring ^{13}C isotope are, on average, too great. Therefore, it is possible to use ^{13}C spin–lattice relaxation times of the laboratory frame (T_1^C values) and rotating frame ($T_{1\rho}^C$ values) of individual carbons to examine the presence of rapid and slow molecular motions whose correlation times are of the order of 10^{-10}–10^{-6} s and 10^{-4}–10^{-2} s, respectively. This is because the minimum values of T_1^C and $T_{1\rho}^C$ correspond with the correlation times comparable to the inverses of the Larmor frequencies of the laboratory frame, ω_0 ($=\gamma H_0 \sim 50$ MHz), and the rotating frame, ω_{1H} ($=\gamma H_1^C \sim 30$ kHz), respectively (see Fig. 7).

2. T_1^C

The T_1^C measurements by means of the CP sequence[45] (CP version of inversion recovery sequence) as shown in Fig. 4(C) are preferable for solid samples with longer T_1^C values, although a conventional inversion recovery sequence can be used for obtaining very short T_1^C values. It is expected from the trend

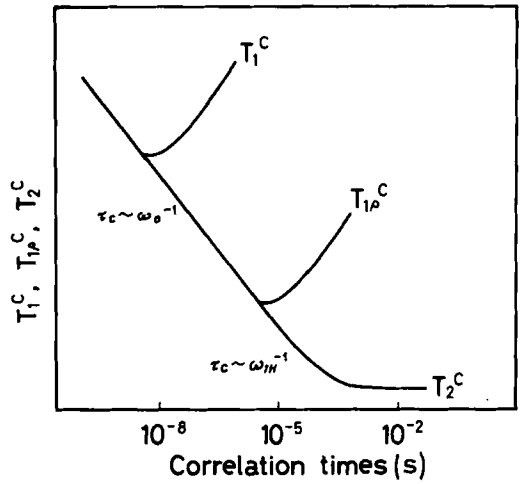

FIG. 7. A plot of T_1^C, $T_{1\rho}{}^C$ and T_2^C against correlation times, τ.

of Fig. 7 that the T_1^C of a crystalline component is much longer than that of the amorphous portions. In fact, this is the case for polyethylene, since the T_1^C of the crystalline component approaches 1000 s and the T_1^C of the non-crystalline component is 175 ± 25 ms.[77] The presence of rapid internal molecular motion in the latter component causes the spin–lattice relaxation times to be much shorter owing to its liquid-like property as compared with that of the former. On the other hand, the T_1^C values of the crystalline and non-crystalline components of poly(oxymethylene) are 15 s and 75 ms at 45 MHz, respectively, which are much shorter compared with the case of the polyethylene mentioned above.[78] The data indicate that restricted molecular motions do take place in the crystalline regions with correlation times comparable with those of the amorphous regions (10^{-8}–10^{-9} s). In many instances, however, the ^{13}C spin-lattice relaxation times of the laboratory frame, in samples with rigid backbones as found in crystalline or semi-crystalline polymers, are mainly due to dipolar couplings to protons undergoing rapid internal rotation, as in methyl groups or others. The T_1^C values of isotactic polypropylene and some solid amino-acids have been quantitatively explained by this treatment.[79,80] We find that even the T_1^C values of non-crystalline polysaccharides are determined primarily by dipolar couplings to protons at the C-6 hydroxymethyl group, which undergoes rapid internal reorientation.[81] This is clearly disappointing, because the potential for better information on backbone motion from the high resolution of the CP-MAS experiment cannot be realized.[79]

3. $T_{1\rho}^{C}$

The $T_{1\rho}^{C}$, the time for loss of carbon magnetization in the rotating frame, is determined as a function of the time that the proton H_1 field is turned off, as shown in Fig. 8(A). The interpretation of $T_{1\rho}^{C}$ data, however, is complicated, because both spin-spin and spin-lattice processes can contribute to $T_{1\rho}^{C}$ relaxation. If a static spin-spin process (mutual spin flip between C and H as the reverse process of the cross-polarization) is the dominant process, the value of $T_{1\rho}^{C}$ cannot be a measure of molecular motion. Therefore, it is crucially important to evaluate such spin-spin contributions in order to be able to use $T_{1\rho}^{C}$ as a means of characterizing molecular motion of mid-kHz region.[52,71,82,83] Schaefer *et al.*[52,82,83] and VanderHart and Garroway[71] showed that the percentage spin-spin contribution to $T_{1\rho}^{C}$ is determined by the ratio of $T_{1\rho}^{C}$ to T_{CH}^{ADRF}, where T_{CH}^{ADRF} is the rate of CP transfer using adiabatic demagnetization in the rotating frame (Fig. 8(B)). In other words, the $T_{1\rho}^{C}$ is dominated by the spin-lattice relaxation if the proton H_1 field is much larger than the local dipolar field, H_L. Thus, the $T_{1\rho}^{C}$ values of glassy or amorphous polymers were shown to be dominated by spin-lattice effects, while a crystalline polymer relaxes through a spin-spin mechanism.[52,82,83] For glassy polymers, Schaefer *et al.*[52] showed that the ratio of averaged T_{CH} to averaged $T_{1\rho}^{C}$ for protonated carbons in the main chain of each polymer is found to have a direct correlation with toughness or impact strength. The ratio can be thought of as a measure of the number of chain segments of a dynamically heterogeneous polymeric solid capable of dissipating the energy of an impact (10–100 kHz component) relative to the number of more rigid segments unable to respond to the impact.[52]

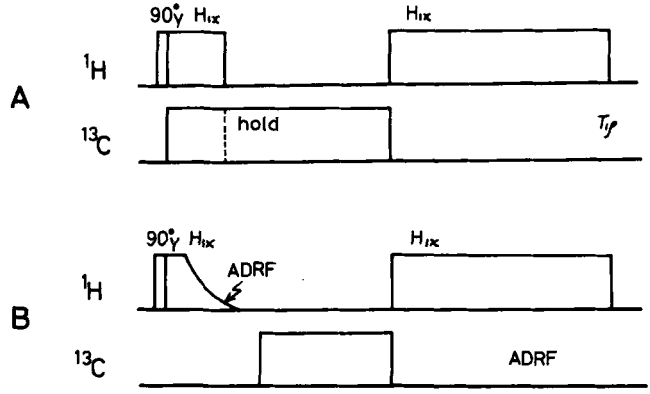

FIG. 8. Pulse sequences for measurements of (A) $T_{1\rho}^{C}$ and (B) T_{CH}^{ADRF}. (Ref. 83.)

4. T_2^C

It is generally accepted that molecular motion causes line narrowing as a result of averaging of dipolar interactions. However, molecular motion in a solid can cause line broadening by providing relaxation pathways for the transverse ^{13}C magnetization, T_2^C.[58,84] In particular, molecular motion at the Larmor frequency of the rotating frame, ω_{1H}, corresponding to the amplitude of the proton decoupling field, may produce linewidths of up to 4 kHz for protonated carbons.[58] At the same time, for non-protonated carbons with large CSA values (150–200 ppm), motions at the sample spinning frequency may cause broadening varying from a few hundred hertz to 1 kHz, depending on B_0. This was nicely demonstrated by Lyerla and Yannoni[9] as a progressive broadening of methyl resonances in isotactic polypropylene as a result of lowering temperature. In addition, Laupretre *et al.* showed that the ^{13}C NMR signals of the cyclohexyl side group in poly(cyclohexyl methacrylate) are so broadened that the resolution in the right-hand part of spectrum disappeared due to the above-mentioned modulation of the CH dipolar coupling by slow motion.[85]

C. Comparison of NMR and X-ray diffraction data

In principle, the secondary structures of polymers, including geometrical factors such as bond distance r and bond (I–S) angle with respect to the applied magnetic field θ, can be accurately determined by analysis of the dipole–dipole interaction given by

$$D = \gamma_I \gamma_S h r^{-3} (3\cos^2\theta - 1) \tag{6}$$

or by a similar formula for the quadrupolar interaction for nuclei involving ^2H or ^{14}N (θ angles only), if single crystal or uniaxially oriented samples were used. Chemical shielding tensors are also utilized for this purpose, if their principal values and axes are known in advance. Detailed strategies for this sort of structural determination from NMR as applied to proteins and nucleic acids have been reviewed by Opella *et al.*[86] and by Shindo,[87–89] respectively.

An alternative and simpler approach for structural elucidation is the use of an empirical relationship between the isotropic chemical shifts, namely conformation-dependent ^{13}C shifts, and the torsion angles of the related backbone structure. The major advantage of this approach is that any solid sample of crystalline or non-crystalline (amorphous) nature can be used for conformational characterization. In fact two or more crystalline samples, judged to be polymorphic in structure from X-ray diffraction studies, can be readily distinguished by their specific displacements of ^{13}C chemical shifts (up to 8 ppm). This has been shown in studies of a series of polypeptides and

fibrous proteins,[50] cellulose,[90] and chitosans.[91] Conformational elucidation by means of conformation-dependent ^{13}C chemical shifts becomes straightforward with the aid of X-ray diffraction.

By contrast, it has been demonstrated that individual molecular chains of amorphous samples of biological macromolecules such as polypeptides and polysaccharides do not always assume a disordered conformation. For instance, the conformation of the random coil form of silk fibroin is very similar to that of silk I;[92] laminaran, a low molecular-weight (1-3)-β-D-glucan, adopts a triple helix conformation similar to that of annealed curdlan,[81] in spite of substantial differences in the quality of their X-ray diffraction patterns. A distinction between non-crystalline samples and crystalline ones is that the torsion angles characteristic of secondary structures are statistically deviated from those of ideal crystalline compounds, as manifested by the line broadening in the former. For this reason, it is emphasized that displacements of the ^{13}C chemical shifts of non-crystalline samples are more informative than expected, although conformational elucidation itself should be made independently from solution NMR study or other spectroscopic means. It is worth noting that the conformation of a lyophilized sample can be a replica of that encountered in solution, if the solution conformation is ordered and solvent molecules do not play an important role in maintaining the conformation. Otherwise, a disordered form could be obtained from samples of ordered state. Further, it should be taken into account that X-ray diffraction cannot provide any information about the non-crystalline portion present in crystalline or semicrystalline samples. Accordingly, there is a tendency for X-ray diffraction patterns to give rise to oversimplified pictures as to the secondary structures of polymers when compared with the data obtained from the rather complicated peak splittings of ^{13}C NMR of cellulose[90] or paramylon, a (1-3)-β-D-glucan.[81]

No information about molecular orientation can be obtained from isotropically averaged ^{13}C NMR spectra under MAS. Nevertheless, the extent of molecular orientation may be evaluated by examination of the extent of CSA profile deviation from the powder pattern, obtained either by spin hopping or analysis of spinning sidebands.[27,28] This technique has been applied to highly oriented polyethylene,[27] wood[28] and polyethylene terephthalate.[93] In particular, Maciel *et al.* showed on the basis of the CSA pattern that there is no net molecular orientational order of lignin or cellulose of *Eucalyptus polyanthemus* wood over a macroscopic volume of about 0.9 cm^3, although these molecules are highly ordered, over a dimension of say 100 Å, as viewed from X-ray diffraction.[28] Thus, care should be exercised in interpreting the results obtained for the region under consideration by the two techniques, especially for heterogeneous samples such as wood.

IV. SYNTHETIC POLYMERS

A number of high-resolution ^{13}C CP-MAS NMR works on synthetic polymers have been published since the first ^{13}C CP-MAS NMR experiments were reported by Schaefer *et al.*[1,52] Several excellent review articles have been published[4-13,51,94-97]. More recently, a comprehensive monograph of high-resolution NMR of polymers in the solid state has appeared.[14] The present section on synthetic polymers is therefore an attempt to review this field from a somewhat different viewpoint so that overlap with the reviews cited above will be avoided. More emphasis is made here on the structures and dynamics of some polymers which are popular and fundamental in polymer science. The remaining polymers will only be reviewed briefly.

A. Paraffins and polyethylene

Polyethylene consists only of methylene units, and so is the most simple and fundamental molecule in polymer chemistry. Nevertheless, the structure of polyethylene in the solid state is very complicated and depends strongly on the crystallization process. Therefore *n*-paraffins and cyclic paraffins lend themselves for use as model molecules.

1. Paraffins

n-Paraffins crystallize into various unit cells including orthorhombic, monoclinic and pseudohexagonal forms with all-*trans* zig-zag conformation.[98] ^{13}C NMR chemical shift data provide information about the conformation of an *n*-paraffin chain and the effects of molecular packing on the conformation. As shown in Fig. 9, VanderHart[59] reported that the influence of molecular packing on isotropic ^{13}C chemical shifts of *n*-paraffins with a variety of chain lengths may be probed experimentally. It is shown that the chemical shift of the interior methylene carbons in the triclinic form, which takes the all-*trans* conformation, appears at a higher frequency by about 1 ppm than it does in other crystal forms. In Table 2 the ^{13}C chemical shift data in the solid state are listed compared with those of the liquid paraffins. The liquid state ^{13}C chemical shift values appear at lower frequency by about 3 ppm than those in the solid state. Such displacements arise from fast exchange between *trans*(T) and *gauche*(G) conformations in an *n*-paraffin chain. It is known that the methylene carbon appears at low frequency by 4–6 ppm (the γ-effect) if any carbon atom three bonds away is in a *gauche*, rather than a *trans*, conformation. Earl and VanderHart[77] showed that the observed chemical shift can be expressed by

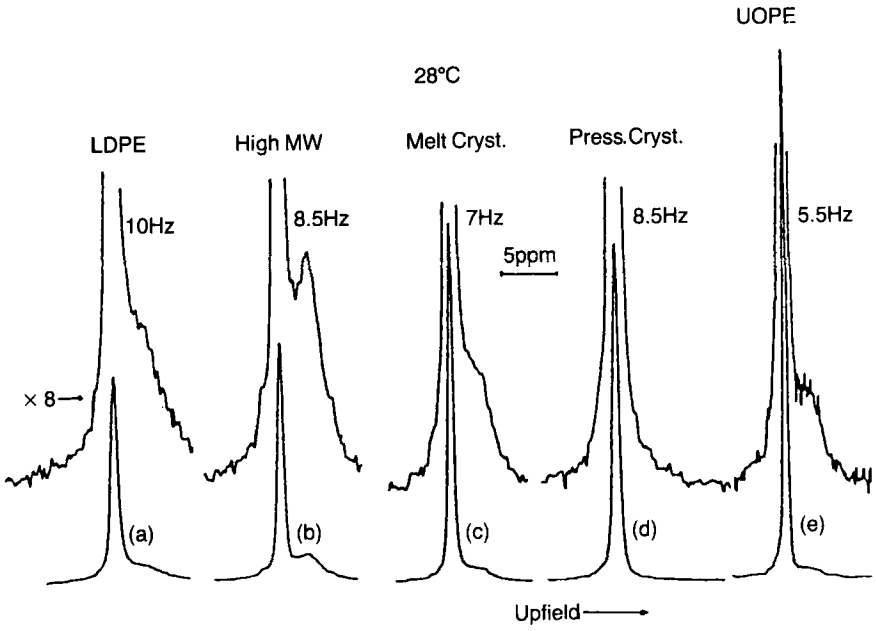

FIG. 9. ^{13}C CP-MAS NMR spectra of five polyethylenes taken at 28°C. (a) Low density sample; (b) high molecular weight sample; (c) melt crystallized sample; (d) sample crystallized under high pressure; and (e) ultraoriented sample. (Ref. 77.)

TABLE 2

Solid-state ^{13}C isotropic chemical shift values[a] for selected *n*-alkanes (ref. 59).

Alkane	Crystal habit	Shifts			
		CH_3	α-CH_2	β-CH_2	int-CH_2
C-19	Pseudohexagonal	14.81	24.99	34.91	33.66
C-20	Triclinic	16.02	26.55	36.35	34.92
C-23	Orthorhombic	15.06	25.59	35.06	33.62
C-32	Monoclinic	15.25	25.53	35.08	33.66
LPE	Orthorhombic				33.60
C-19	(Liquid)	14.05	22.62	31.89	29.65
C-20	(Liquid)	14.05	22.62	31.89	29.65

[a]Values are referred to TMS which was present in a sealed capillary concentric with the sample. Under MASS this referencing ought to be equivalent to internal referencing. Uncertainties in the chemical shift values in this table are ±0.2 ppm.

$$\delta_{obs} = \delta_0 - 2\gamma f_g \tag{7}$$

where f_g is the equilibrium fraction of *gauche* bonds, δ_0 the chemical shift for the all-*trans* conformation, and the value of γ is attributed entirely to the *trans* to *gauche* change (Tonelli[100] proposed $\gamma = -5.3$ ppm). In *n*-paraffins, the energy difference between the *trans* and *gauche* conformations is about 600 cal mol^{-1} (corresponding to $f_g = 0.357$)[102] and so the ^{13}C chemical shift in the liquid or solution state is smaller by about 3 ppm than that in the solid state.[101] Such situations may be relevant to the understanding of the behaviour of ^{13}C CP-MAS NMR for polyethylene samples containing non-crystalline components.

Okazaki and McDowell[103, 104] measured ^{13}C CP-MAS NMR spectra of the urea inclusion complexes of *n*-paraffin and substituted paraffins. Changes

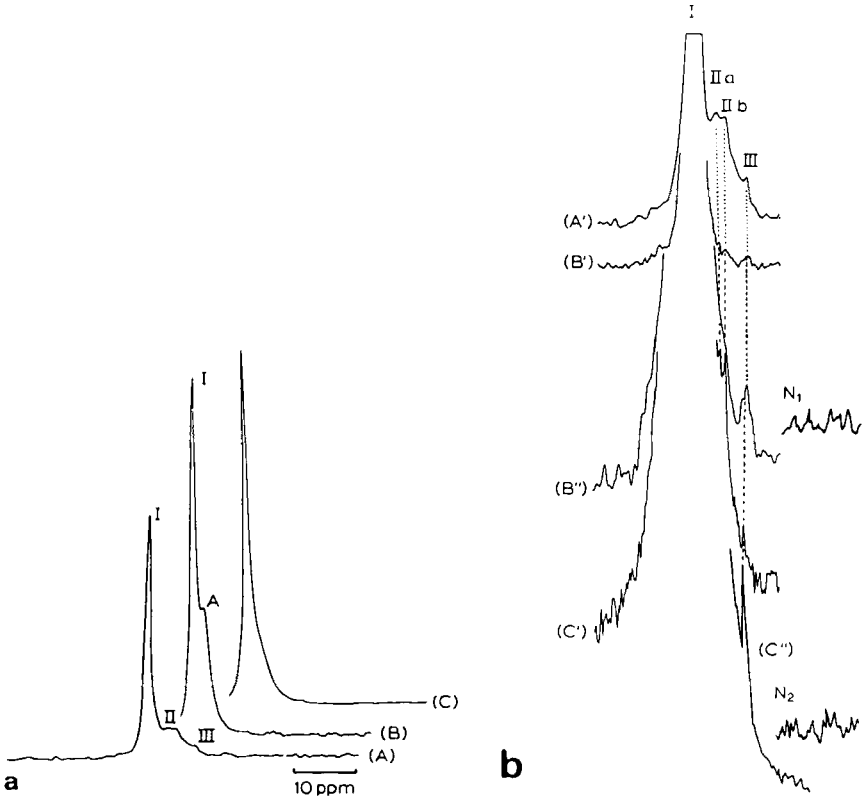

FIG. 10. ^{13}C CP-MAS NMR spectra of cyclic paraffin $C_{64}H_{128}$ (A and A'), melt-quenched polyethylene (B, B' and B'') and polyethylene single crystals (C, C' and C''). (Ref. 99.)

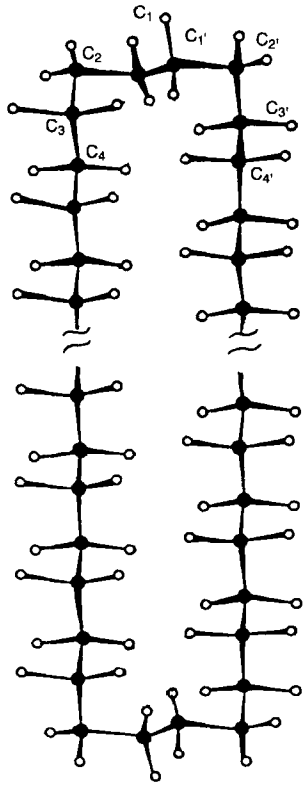

FIG. 11. Schematic drawing of the conformation of a cyclic paraffin. (Ref. 105.)

of the chemical shift values in inclusion complex formation from those of solution NMR spectra can be explained by the assumption that the long chain molecules in urea inclusion complexes have the all-*trans* conformation.

Ando *et al.*[105] reported ^{13}C CP-MAS NMR spectra of a series of cyclic paraffins at room temperature in the solid state. $C_{24}H_{48}$ produces a sharp single peak. The linewidth of the ^{13}C signal of cyclic paraffins increases with increase in the carbon number. Cyclic paraffins having more than 36 carbon atoms show low frequency peaks on the main peak. The main peak and smaller peaks are designated by I, II and III, respectively. In the expanded spectrum of $C_{64}H_{128}$, these small peaks can be identified as shown in Fig. 10. Cantow *et al.*[106, 107] independently measured the ^{13}C CP-MAS NMR spectrum of $C_{24}H_{48}$ at low temperature where the molecular motion is frozen, and obtained a good resolved signal consisting of peaks I, II and III.

These peak can be more effectively interpreted following Ando *et al.*[105] The sharp single signals observed for $C_{24}H_{48}$–$C_{32}H_{64}$ suggest that they have a definite molecular structure which is evident without the freezing of molecular motion due to a rapid transition between *trans* and *gauche* conformations. This was justified by a ^1H NMR relaxation study. Further, the three peaks I, II and III were assigned by means of the *r*-effect concept. This has been justified by both experiment and theory, and has been successfully used to predict the chemical shift of each stereosequence of polymers. From this point of view, it is shown that peaks I, II and III can be assigned to the methylene carbons arising from the *trans* zig-zag structure region and folded structure region, respectively. As shown in Fig. 11, the cyclic paraffins crystallize in a conformation characterized by two parallel all-*trans*, planar zig-zag strands connected by two GGTGG loops.[108, 109] If this conformation is fixed in the solid state, we would expect loop carbons C_3, C_3', C_4, C_4' to resonate by the γ-effect to low frequency, and loop carbons C_1, C_1' by 2γ-effects to low frequency from the all-*trans* carbon and loop carbons C_2, C_2', whose next-nearest neighbour bonds are also both *trans*. Thus, for $C_{36}H_{72}$ we would expect 24 carbons with 0γ values, 8 carbons with 1γ values, and 4 carbons with 2γ values leading to a 6 : 2 : 1 ratio of peaks, each separated by a γ-effect. Similarly, for $C_{40}H_{80}$ the ratio is 7 : 2 : 1, for $C_{48}H_{96}$ 9 : 2 : 1, and for $C_{64}H_{128}$ 13 : 2: 1. If -4 to -6 ppm is used as γ, the peaks I, II and III may appear at 34, 28–30 and 22–26 ppm, respectively. These predictions agree fairly well with the experimental results. On the other hand, Möller *et al.*[106] measured the ^{13}C CP-MAS NMR spectra of $C_{12}H_{24}$, $C_{24}H_{48}$ and $C_{36}H_{72}$ at temperatures below their melting points. Complete freezing of the molecular motion for the cyclic paraffin provides better-resolved peaks. The features of these spectra are similar to those reported by Ando *et al.*[105] Möller *et al.*[106] assigned resolved peaks on the basis of the γ-effect concept and Anet's assignment[110] for cyclic $C_{12}H_{24}$ in solution at low temperature. It has been shown that the carbons other than C_2 and C_2' can be assigned on the basis of the γ-effect, while for C_2 and C_2' carbons whose next-nearest bonds are also *trans*, another contribution to the ^{13}C chemical shift is of importance. This is the vicinal *gauche* effect, and results in a low frequency shift of about 6 ppm compared with that of the all-*trans* carbons. Their assignment agrees with that of Ando *et al.*[105] except for the C_2 and C_2' carbons. Yamanobe *et al.*[101] showed that these solid-state ^{13}C chemical shift data become reference data to obtain information about the conformation of molecules in solution. They reported that, from a comparison of solid-state and solution-state ^{13}C chemical shift data, it appears that the compact conformation of short chain length cyclic paraffins in the solid state, which consists of two parallel straight chains bridged at both ends, is retained in solution; in long chain length cyclic paraffins the conformation in solution

deviates from that in the solid state. The intramolecular motion is also clarified by the relaxation study.[111]

Ando *et al.*[112,113] reported that the influence of molecular packing on the isotropic ^{13}C chemical shift of cyclic paraffins with a variety of chain lengths may be probed experimentally. It was shown that the signal for the triclinic form appears at higher frequency by about 1 ppm than that for the orthorhombic form, as was also the case for *n*-paraffins.

2. *Polyethylene*

^{13}C CP-MAS NMR experiments to obtain information about polyethylene chain conformation in the crystalline and non-crystalline states, which is one of the most important problems in polymer science, were first carried out by VanderHart *et al.*[77] It was shown that the ^{13}C resonance lines of the crystalline and non-crystalline components in the polyethylene sample are readily distinguishable by their peak separation from one another. This produces a low frequency shoulder on the crystalline resonance line as shown in Figs 9[77] and 10[99]. However, in the case of samples of polyethylene single crystals, the non-crystalline resonance line does not appear. Two peaks have been resolved in a low crystallinity sample, the non-crystalline peak (peak A) being displaced by 2.32 ppm to low frequency from the crystalline peak (peak I) (Fig. 10, B–B″). As discussed by VanderHart *et al.*[77] peak I may be ascribed to the *trans* zig-zag region and peak A arises from the methylene carbons in the non-crystalline region undergoing rapid transitions between the *trans* and *gauche* conformations. The chemical shift of peak A can be expressed by equation (7). At room temperature, the *gauche* fraction f_g in long *n*-paraffins or polyethylene chains in the liquid and/or solution states becomes 0.35 (corresponding to the energy difference between the T and G states, $\Delta E = 600$ cal mol^{-1}), and 5.3 ppm is used as the value of γ. Thus, each carbon experiences about 3.8 ppm low frequency shift from its solid state position. This is close to the observed value of 3.0 ppm. Therefore, the assignment of peak A to the non-crystalline state may be supported. On the other hand, the intensity fraction of the methylene carbons in the non-crystalline state can be estimated to be approximately 0.28 from the intensity of peak A. This value is very close to the value of 0.296 determined from the density of the sample. These experimental results lead to a picture for the structure of the polyethylene sample with both crystalline and non-crystalline regions. The partition of the end group and side chains between the crystalline and non-crystalline regions in polyethylene was determined from ^{13}C CP-MAS NMR spectra.[114] Polyethylene samples sometimes contain side chains and this affects the crystallization. Since Earl and VanderHart's work,[77] some research groups[115–117] have observed the high-resolution NMR

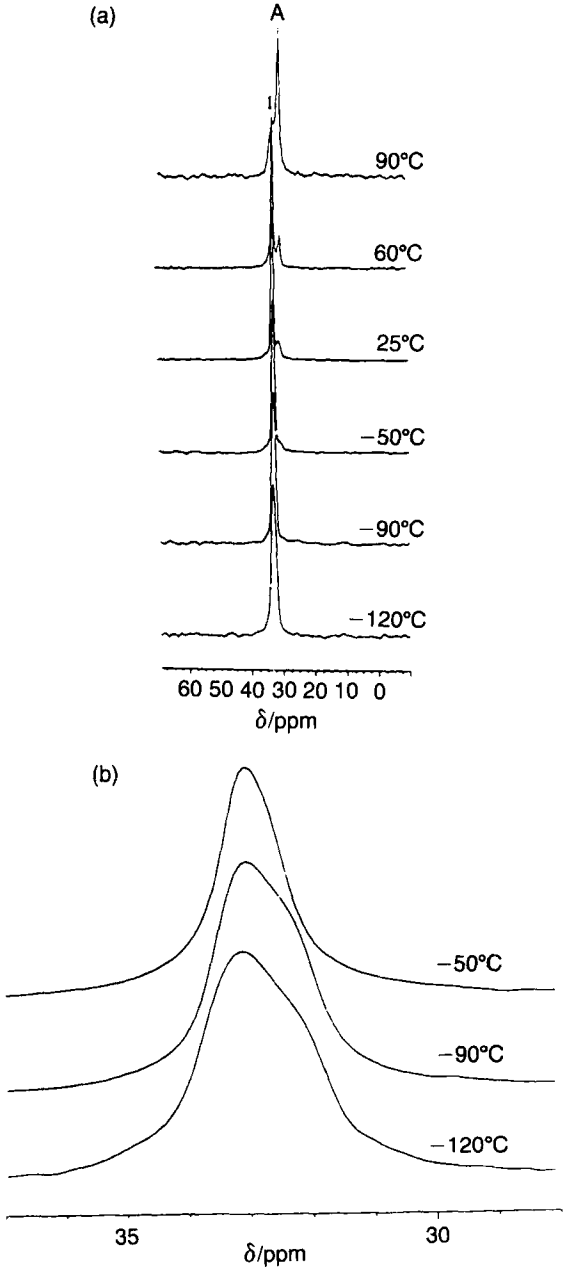

FIG. 12. (a) ^{13}C CP-MAS NMR spectra of melt-quenched polyethylene measured as function of temperature, and (b) expanded spectra at temperatures ranging from −50 to −120°C. (Ref. 122.)

spectra of polyethylene samples with different crystalline structures. The component phases in the polyethylene samples were characterized in terms of their T_1 and T_2.[118,119]

VanderHart *et al.*[120,121] measured ^{13}C NMR spectra of samples of drawn ultrahigh molecular weight polyethylene film. They showed the existence of the monoclinic form as well as the orthorhombic form from the sharp peak that occurred at about 34 ppm. This peak was shifted about 1.5 ppm to high frequency from the orthorhombic peaks, I (see Fig. 12). The occurrence of orientation in the non-crystalline regions may be evidence of internal stress, which also stabilizes the metastable monoclinic crystalline phase in the drawn sample.

Most of the ^{13}C CP-MAS NMR experiments have been carried out only at room temperature, but VT CP-MAS NMR experiments also provide useful information. ^{13}C CP-MAS NMR spectra of melt-crystallized polyethylene samples were measured in the temperature range of $-120°$ to 90°C, as shown in Fig. 12. The spectra at temperatures from $-50°$ to $-120°C$ are expanded as shown in Fig. 12(b).[122] Polyethylene samples at room temperature have a small low frequency peak on the main peak A whose peak intensity is enhanced as temperature is increased. This indicates that the fraction of non-crystalline components present increases as temperature is increased. Another interesting feature is the progressive broadening of peak A as the temperature is decreased. At about $-50°C$, the peak is broadened to the point of disappearing from the spectrum, where this temperature is near the glass temperature, below which the molecular motion is frozen. As pointed out in Section III.B.4, such broadening arises when the reorientation rate of the methylene carbons in the non-crystalline region is close to the average dipolar interaction with the methylene protons. This means that the methylene carbons in the non-crystalline components are undergoing a transition between the *trans* and *gauche* conformations at a frequency of about 60 kHz. Further, at temperatures below $-90°C$, the peak narrows and reappears in the spectra shown in Fig. 12(b) due to the freezing of the molecular motion. The chemical shifts for peak I are independent of temperature, but those for peak A vary with temperature. At $-120°C$, the chemical shifts for peaks I and A are about 33 and 32 ppm, respectively, where the molecular motion is frozen. As described above, the methylene carbons in the crystalline component are in the orthorhombic form, from which peak I arises, and peak A arises from the methylene carbons with *trans* conformation in the non-crystalline components due to the freezing of molecular motion. Therefore, the difference in chemical shift (about 1 ppm) between the peaks I and A for the methylene carbons can be ascribed to going from the orthorhombic form to the non-crystalline state. In the spectra at $-120°C$, the signal, in principle, must appear at low frequency by about 5 ppm relative

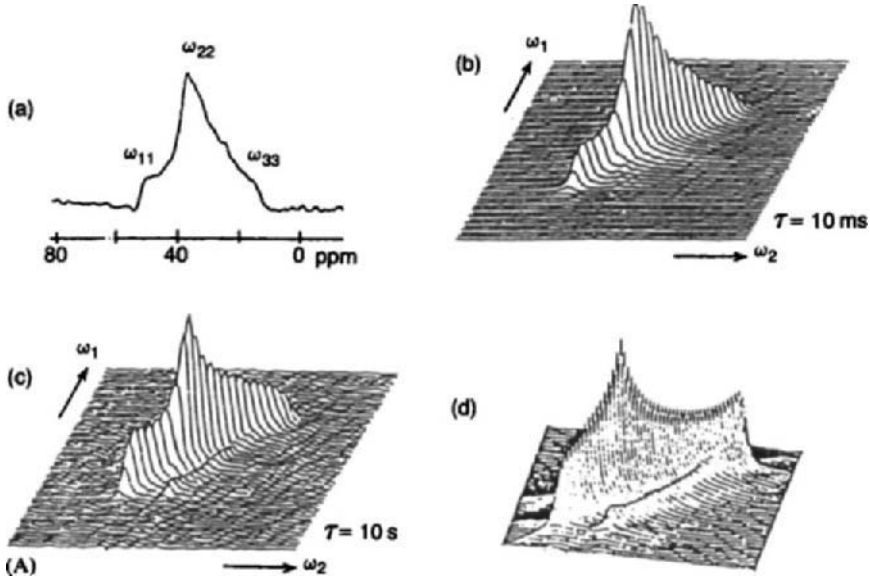

FIG. 13. (A) ^{13}C exchange NMR of the methylene resonance in the crystalline region of polyethylene at room temperature. (a) Normal spectrum. (b,c) Stacked plots of the 2DECSA spectra after exchange times t of 10 ms and 10 s. (d) Simulated 2DECSA spectrum for exchange between shielding tensor orientations that are rotated by 0°, 90°, 180°, and 270° around the σ_{33} axis.

to peak I, which comes from the methylene carbons for *gauche* conformation in the non-crystalline state. It is difficult, however, to identify its peak due to the very weak intensity.

Several types of two-dimensional NMR have been applied to a powdered solid to recover CSA (see Section II.B.1).[40,123,124] The 2D exchange spectra (ECSA) of static polyethylene (Fig. 13)[40] show that the signal from the non-crystalline fraction is strongly suppressed by the relatively short cross-polarization. The spectra obtained after exchange times of 10 ms and 10 s are strikingly different (see Section II.D). A pronounced ridge appears on both sides of the diagonal for the longer exchange. In Fig. 13(A), the posterior ridge is hidden behind the diagonal peaks. The ridges are the manifestation of spin exchange. The ridges begin at the intersection of ω_{11} and ω_{33} and converge toward ω_{33}, indicating that the exchange leaves the direction of σ_{33} unaltered whereas σ_{11} and σ_{22} are interchanged (Fig. 13(B)). This corresponds with two possible tensor reorientations: (1) a rotation by 90° around the σ_{33} axis; or (2) a rotation by 180° around the axis bisecting the σ_{11} and σ_{22} directions. Reorientations (1) and (2) give the same two-dimensional exchange spectrum.

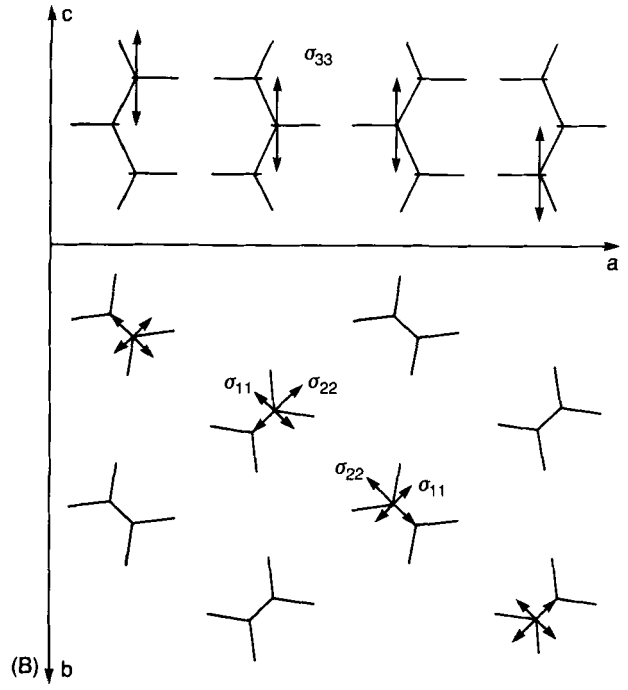

FIG. 13. (B) Crystalline structure of polyethylene and the orientation of the ^{13}C methylene shielding tensor. The orientation of the shielding tensor is shown for the four different methylene groups in the unit cell. (Ref. 40.)

The simulated spectrum (Fig. 13(A) (a)–(d)) indeed reproduces the measured one accurately. Simulations with rotation angles deviating more than 10° never matched with the measured spectrum. The crystalline structure of polyethylene and orientation of the ^{13}C shielding tensor are known and are shown in Fig. 13(B). The molecular chain axes are parallel, but two orientations of the molecular planes are approximately perpendicular to each other. The physical process responsible for the observed exchange can be discussed; interchain spin exchange is the most plausible explanation.

In polypeptides such as poly(L-glutamate) with long *n*-alkyl side chains, the side chains form a crystalline phase composed of paraffin-like crystallites and the melting of side chain crystallites imparts a thermotropic liquid-crystalline nature to the right-handed α-helical main chains. The side chains in the melt behave as a liquid paraffin. ^{13}C CP-MAS NMR experiments provide useful information about the conformation and dynamic aspects of the *n*-alkyl side chain and main chain.[125] ^{13}C CP-MAS NMR spectra of poly(γ-*n*-octadecyl L-glutamate) as a function of temperature are shown in

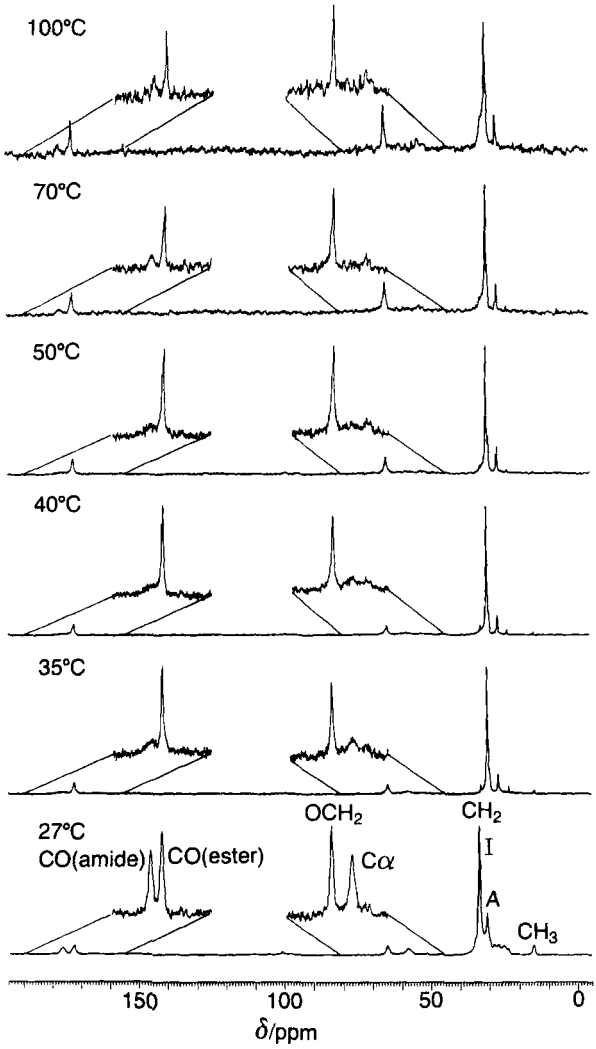

FIG. 14. ^{13}C CP-MAS NMR spectra of poly(γ-*n*-octadecyl-L-glutamate) as a function of temperature. The main chain carbons are expanded. (Ref. 125.)

Fig. 14. The main peak and small peak for the interior methylene carbons are designated by I and A, respectively. Peak I is ascribed to the all-*trans* zig-zag conformation in the crystalline state, while peak A arises from the CH_2 carbons in the non-crystalline state on the basis of the ^{13}C chemical shift for melt-crystallized polyethylene. The *n*-alkyl CH_2 peaks are found to change observably as the temperature is increased. Peak I disappears above 35°C

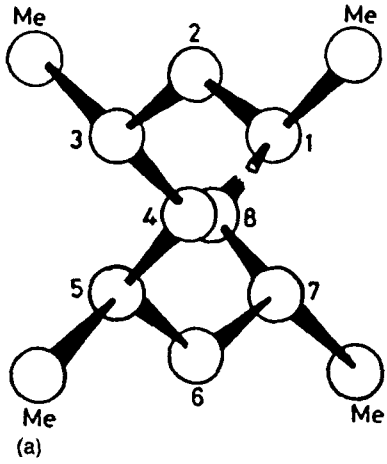

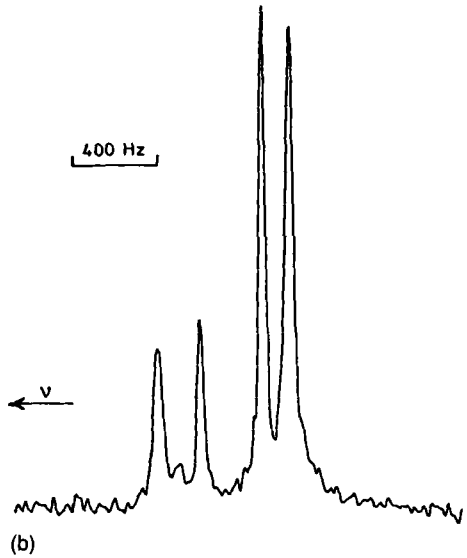

FIG. 15. (a) A view of the conformation of syndiotactic polypropylene looking down the helical axis. The backbone methine and methylene carbons are numbered sequentially for clarity with the methyl carbons labelled Me. The two non-equivalent sites for the methylene carbons are clear, being typified by atoms 2 and 6, and 4 and 8 respectively. (b) ^{13}C CP-MAS NMR spectrum of syndiotactic polypropylene. (Ref. 126.)

and the intensity of peak A increases noticeably. This phenomenon is associated with the melting of side chain crystallites. When the temperature is further increased, peak A moves gradually from 30.6 to 30.2 ppm. A progressive broadening of the main chain amide CO and C_α carbon peaks is observed. This observation is similar to that seen in polypropylene, as described above (Section III.B.4).

B. Polypropylene and polyolefins

It is known from X-ray diffraction that syndiotactic and isotactic polypropylenes take the $(GGTTG'G')_n$ and the $(TG)_n$ (3_1 helix) conformation. Bunn and co-workers showed that the ^{13}C CP-MAS NMR signal of the methylene carbons for the syndiotactic polymers[126] clearly splits into two peaks as shown in Fig. 15(b). This indicates that there are two kinds of magnetically equivalent methylene carbons, as shown in Fig. 15(a). The above results give confirmation of the helical structure of syndiotactic polypropylene as reported by X-ray diffraction work.

Isotactic polypropylene takes a 3_1 helical conformation in the solid state and can be made to adopt the various crystalline modifications by using the appropriate treatment. The arrangement of the helical polymers in the crystalline region of the α-form is obtained by X-ray diffraction. If its view provides a projection along the helix axis with corners of the triangles representing the positions of the methyl groups in the 3_1 helical conformation and the sense of the individual helices it is evident from the structure that two distinct environments exist and these are identified. The β-form of isotactic polypropylene takes helices with the 3_1 helical conformation as in the α-form, but it differs in the way the helices are packed together in the crystalline regions. It is expected from the structure that these interchain interactions may well be less in the β-form. Figure 16 shows ^{13}C CP-MAS NMR spectra of isotactic polypropylene samples[127] with both the α- and β-forms. As expected from the structure, the spectrum of the α-form sample shows resolved splitting for the methyl and methylene carbons. The methine carbon resonance indicates the presence of an asymmetric lineshape consistent with the existence of an unresolved splitting of the order of 3 Hz with an intensity distribution in the same sense as those seen for methyl and methylene carbon resonances. On the other hand, the spectrum of the β-form sample consists of the unresolved methyl, methine and methylene resonances.

The ^{13}C CP-MAS NMR spectra of isotactic polypropylene at temperatures from 17 to 300 K have been measured.[9] A progressive broadening of the methyl resonance is observed as the temperature is lowered. At about 110 K, the resonance broadens to the point of disappearing from the spectrum. At temperatures below 77 K, the methyl resonance narrows and reappears in the

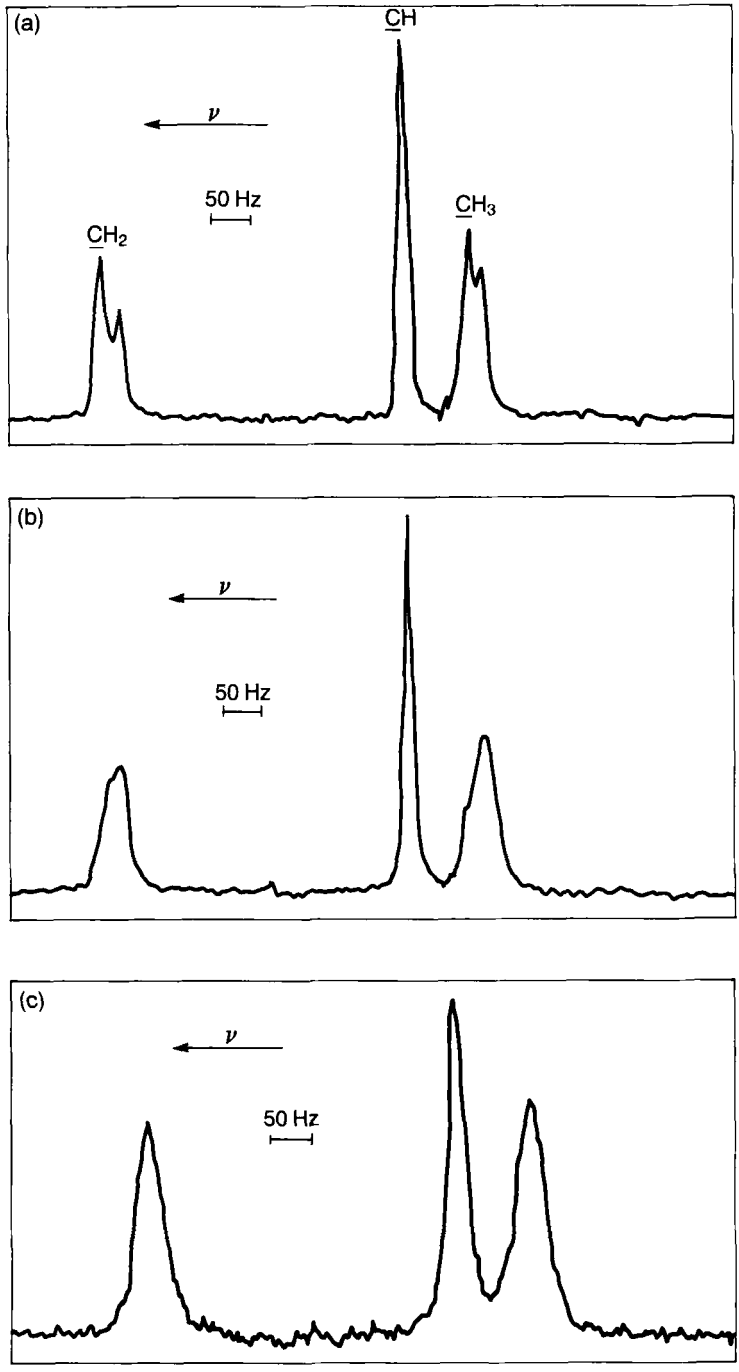

FIG. 16. ^{13}C CP-MAS NMR spectra of various forms of isotactic polypropylene. (a) The anealed α-form, (b) the quenched α-form and (c) the β-form. (Ref. 127.)

spectrum. This broadening arises because the reorientation rate of the methyl group about the C_3 axis becomes insufficient to compensate for the average dipolar interaction with the methyl protons. This has already been discussed in Section III.B.4.

Like most isotactic vinyl polymers, isotactic poly(1-butene) adopts a 3_1 helical conformation at room temperature. The chains have dihedral angles of 60° for *gauche* and 180° for *trans* conformations and are packed in a trigonal unit cell (form I). However, at about 90°C and above this polymer is known to prefer a tetragonal form, called form II, in which the chain conformation is an 11_3 helix with alternating *gauche* and *trans* angles of 77° and 160°, respectively. There is a third polymorph, form III. This form is orthorhombic and has a 4_1 helical conformation with *gauche* and *trans* angles of 83° and 159°. The ^{13}C CP-MAS NMR spectrum gives splittings of the main chain and side chain methylene resonances as studied by Belfiore *et al.*[128] and Cudby *et al.*[129] This splitting probably arises from features of the crystal structure, as was the case with isotactic polypropylene.

Gronski and co-workers[130–132] have carried out a conformational analysis of threodiisotactic poly(1,2-dimethyltetramethylene) in the glassy state by VT CP-MAS experiments. They found that at 220 K different conformational diads were resolved and assigned.

C. Conducting polymers

Since Shirakawa's discovery[133,134] that both the *cis* and *trans* polyacetylenes can be synthesized in the form of crystalline films, and that their electrical

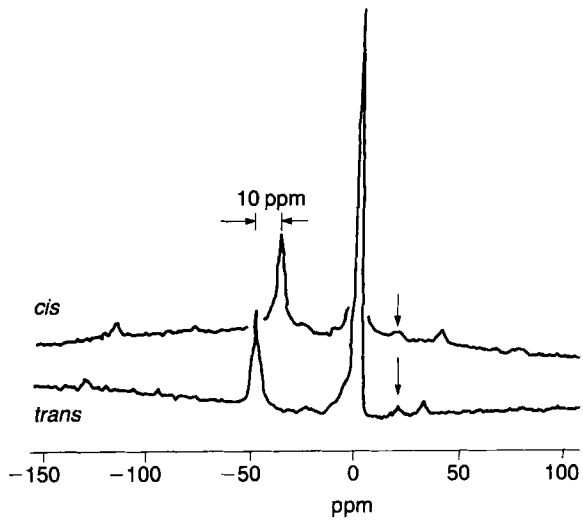

FIG. 17. ^{13}C CP-MAS NMR spectra of *cis*- and *trans*-polyacetylenes. (Ref. 135.)

conductivity is remarkably increased by doping with small quantities of electron-attracting species such as iodine, AsF_5, etc., a number of papers on conducting polymers have been published. The ^{13}C CP-MAS NMR technique has provided a special advantage in such studies since chemical shifts are highly diagnostic of chemical structure.

Maricq *et al.*[135] measured ^{13}C CP-MAS NMR spectra of *cis* and *trans* polyacetylene films as shown in Fig. 17. The main feature in each spectrum is a single line arising from the polyene carbons (apart from the strong ^{13}C resonance of the Derlin rotor). The *cis* shifts differ by about 10 ppm. Each spectrum shows a weaker line at low frequency which can be ascribed to saturated carbon defects such as would occur in chain terminations, cross-links or hydrogenated double bonds. Terao *et al.*[136] show that the existence of 3.4 mol% methylene moieties as defects in the chains can be observed in *trans* polyacetylene.

The *cis* polyacetylene film is thermally unstable and is converted to the *trans* form on heating.[137] The isomerization of *cis* to *trans* polyacetylene in time was studied by ^{13}C CP-MAS NMR through the heating process. In the initial period, the spectrum provides only a sharp resonance (128.5 ppm) corresponding to the *cis* isomer. In the intermediate period two peaks can be observed with chemical shift values of 128 and 137 ppm, respectively, for the *cis* and *trans* isomers. In the final period, only a sharp resonance can be observed at 137 ppm. This means that the *cis* polyacetylene is converted to the *trans* isomer. Terao *et al.*[136] showed by careful analysis of partially *cis*-to-*trans* isomerized polyacetylene that there are characteristic differences between the peaks of *trans* and *cis* parts; the *trans* peak positions are shifted to low frequency by 1.0 and 0.7 ppm, respectively, with respect to that of a pure *trans* chain. The low frequency shifts demonstrate that the structure of the *trans* parts in partially isomerized polyacetylene is different from that of pure polyacetylene.

^{13}C CP-MAS NMR spectra of polyacetylene have been measured as a function of doping. Peo *et al.*[138,139] found that *cis* polyacetylene shows no substantial change in its ^{13}C spectrum up to a doping level of about 7 mol%, at which level a rather abrupt change to a broad line occurs. They attributed this change to a Knight shift and correlated the result with the sudden increase in Pauli susceptibility observed at about 7 mol% doping. On the other hand, Clarke and Scott[140] found that the doping of *cis* polyacetylene led, even at low doping levels, to a new signal characteristic of the doped regions of the polymer. Comparisons with appropriate model compounds suggest that the observed shift of the ^{13}C signal on doping is primarily a chemical shift rather than a Knight shift. In order to understand the mechanism of electrical conductivity, it is important to determine whether the observed shift is a Knight shift or a chemical shift. In this connection, Terao *et al.*[141] reported that a spectrum of polyacetylene doped with AsF_5 shows a high frequency shift,

while doping with potassium produces a low frequency shift. Such experimental findings suggest that the shift is due to the change of π electron density on doping and so is due to a chemical shift. An NMR study on doped polyacetylene is very interesting in relation to the electrical conductivity. However, no ^{13}C CP-MAS NMR spectrum of polyacetylene at high concentration doping has been reported.

Terao *et al.*[136] and Mehring *et al.*[142] measured ^{13}C powder patterns of *trans* polyacetylene and the orientation of the chemical shielding tensor was determined. The tensor element σ_{33} is found to be perpendicular to the molecular plane, and the σ_{11} makes an angle of 40° with respect to the single C—C bond and 80° with respect to the double bond. Yamanobe and Ando have calculated the ^{13}C shielding tensor of an infinite polyacetylene chain using the tight-binding MO theory within the CNDO/2[65] and INDO/S[69] frameworks. The experimentally determined orientation of the principal values of the shielding tensor is supported theoretically.

Linear conjugated polymers composed of aromatic or heterocyclic nuclei also attract attention as conducting polymers. The ^{13}C CP-MAS NMR spectra of poly(*p*-phenylene), poly(*m*-phenylene), poly(*p*-phenylene sulphide), poly(2,5-thienylene), poly(2,5-selenienylene), poly(pyrrolyene), etc. have been measured.[143-146] As an example, in the spectrum of poly(pyrrolyene) three peaks can be distinguished. The major peaks are shifted by about 123 and 105 ppm to high frequency from TMS. These peaks correspond well with the α and β carbons of the pyrrole monomer, which occur at 117 and 108 ppm downfield relative to TMS. The two peaks confirm the presence of the pyrrole moiety in the polymer, and the high frequency shift of the α carbons relative to monomeric pyrrole is consistent with α—α' linkages. The shoulder at about 135 ppm may indicate the presence of some non-α—α' linkages, e.g. α—β linkages, although the possibility that these carbons correspond to chain end groups cannot be eliminated.

D. Insoluble polymers

The main advantages of a direct solid-state investigation are that this approach eliminates structural uncertainties associated with the dissolution process and provides an opportunity to study insoluble polymers under non-destructive conditions. It has proved particularly useful in the case of cure polymer resins which are totally intractable materials, and for which the reactions occurring during the curing process may differ from the behaviour observed in the early stage of resin formation. ^{13}C CP-MAS NMR has been successfully applied to different cured polymers such as phenolic polymers[147-152], urea-formaldehyde polymers[153], furfuryl alcohol polymers[154, 155], resol-type phenol-formaldehyde polymers[156], epoxy polymers[53, 157-161]

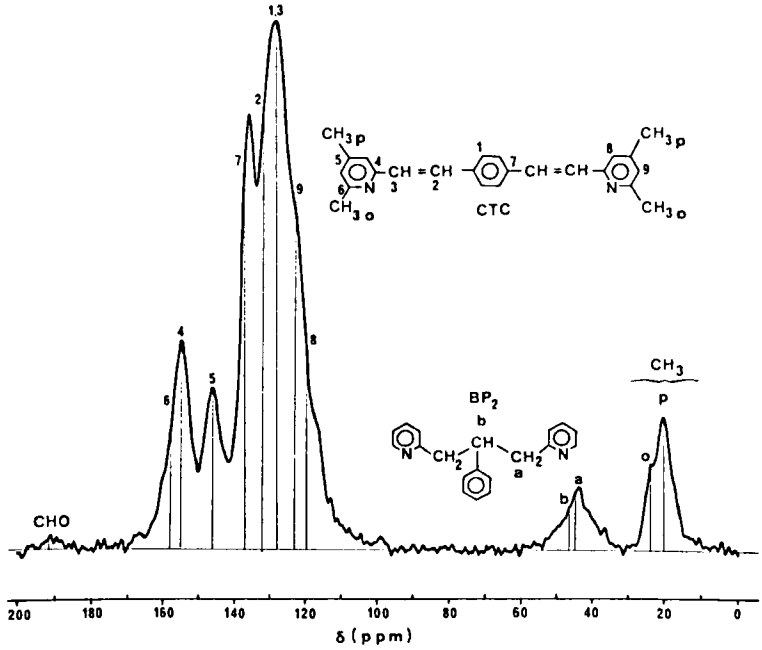

FIG. 18. ^{13}C CP-MAS NMR spectrum of a cured PSP sample with peak assignments. Stick spectra are drawn from ^{13}C NMR spectra of the model compounds CTC and BP_2 in solution. (Ref. 165.)

and polyimides,[162,163] and fibre reinforced composites.[164] As an example, the determination of the chemical structure and the characterization of the chemical reactions involved in the case of polystyrylpyridine system will be discussed.

Polystyrylpyridine resins are thermosetting matrices used in composite materials, which are stable at high temperatures. The ^{13}C CP-MAS NMR spectrum of a typical sample is shown in Fig. 18, together with stick spectra of the model compounds BP_2 and CTC.[165] The solid-state spectrum consists of several lines which are identified by comparison with the solution-state spectra of the model compounds and prepolymers and assigned from right to left, in order of decreasing magnetic field, as a composite line produced by the *p* and *o*-collidine methyl carbons, a composite line corresponding to the CH and CH_2 of the cross-linking points, a broad line from the aromatic and ethylene carbons, and a line from the aldehyde carbons. The two peaks furthest to the left correspond to the three quaternary carbons of the pyridine ring. The spectral resolution is good enough to distinguish the separate contributions of the *o*- and *p*-methyl collidine carbons. The decreasing amounts of aldehyde and methyl groups and the appearance of network linkages were

studied as a function of both the temperature and duration of the curing treatment. The results are interpreted quantitatively in terms of two chemical mechanisms: first, the addition of a methyl group from the collidine molecule to the aldehyde function of terephthalic aldehyde followed by elimination of water; and second, a cross-linking reaction consisting of the addition of a collidine methyl group to the double bonds formed in the first process.

E. Polyethers

Polyoxymethylene, the simplest polyether, sometimes consists of two components with very different relaxation behaviours. These components are attributed to crystalline and non-crystalline regions. In ^{13}C CP and ^{13}C CP-MAS NMR measurements of polyoxymethylene, two overlapped peaks were obtained.[166,167] In order to separate clearly the overlapped peaks, the CP-MAS NMR spectra as a function of the recovery time in a ^{13}C spin–lattice relaxation experiment were measured. According to their relaxation times, the two peaks were assigned to the crystalline and non-crystalline regions respectively, from low frequency. A two-dimensional exchange NMR spectrum of crystalline polyoxymethylene was also obtained.[167] In this spectrum, the cross-peaks were very weak after a 0.5 s mixing time but became more pronounced at a mixing time of 2 s. This showed that the observed motion must be slower than about 1 Hz. The motion may be associated with the α relaxation.

Polyoxymethylene exists in two crystallographic forms;[168,169] one is the trigonal form with a 9_5 helical (all *gauche*) conformation, and the other is the orthorhombic form with 2_1 helical conformation. The crystal modification of the former is very stable, but that of the latter is remarkably unstable and hence easily converted to the former by heating. Kurosu *et al.*[170] measured ^{13}C CP-MAS NMR spectra of trigonal and orthorhombic polyoxymethylene samples in the solid state. It was found that the ^{13}C resonance lines of these structures had different chemical shifts; the position of the orthorhombic form appeared to low frequency by about 2 ppm from that for the trigonal form. Also, the corresponding shielding tensors were measured. The experimental results were reasonably well explained by a theoretical calculation for infinite polyoxymethylene chains based on a tight-binding MO theory within the CNDO/2 framework.[68,171] The interchain effect on the ^{13}C chemical shift was also discussed.

Tabeta and Saitô[172] measured ^{13}C CP-MAS NMR spectra of ethyelene oxide oligomers, cryptands and crown ethers complexed with metal ions. It was found that peak intensities of these complexes were significantly enhanced by the presence of metal ions which act toward conformational fixation of flexible ligand molecules. The ^{13}C chemical shifts of ethylene

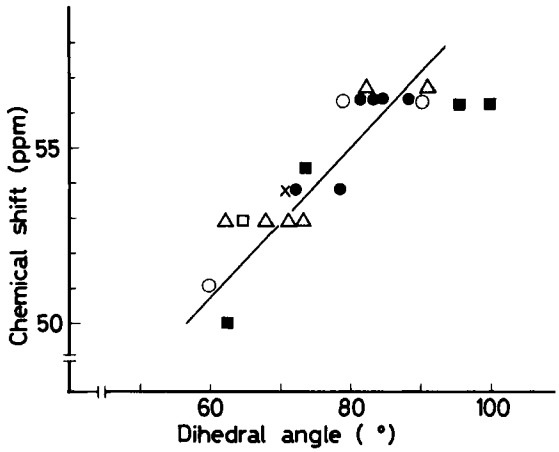

FIG. 19. A plot of C-3(cryptand[2.2.2]) and C-4 plus C-5(cryptand[2.2.1]) ^{13}C chemical shifts of cryptands[2.2.2] and [2.2.1] against the N—C-3([2.2.2]) and N—C-4 and N—C-5([2.2.1]) torsion angles. □, K-[2.2.2]; Δ, Ba-[2.2.2]; ○, Ca-[2.2.2]; X, Tl-[2.2.2]; ●, Na-[2.2.1]; ■, K-[2.2.1]. (Ref. 172.)

oxide oligomers complexed with $HgCl_2$ or $CdCl_2$ as open chain analogues of crown ethers were successfully related with a pair of torsion angles of nearby single bonds. ^{13}C chemical shifts of cyclic ionophores were displaced up to 6 ppm together with conformation changes of ligand molecules. Tabeta and Saitô also analysed the ^{3}C chemical shift behaviour of metal-complexed cryptands as a function of the torsion angles, as shown in Fig. 19.

Poly(oxetane) and poly(3,3-dimethyloxetane) have two different crystalline modifications, with TTGG and TTTG conformations. Perez and VanderHart[173] measured ^{13}C CP-MAS NMR spectra of these samples. The corresponding ^{13}C chemical shifts for each sample, both non-crystalline and crystalline, were determined. Single resonances for the methylene carbons attached to the oxygens are observed for the crystal forms having TTGG conformation. Two resonances are observed for these carbons in each of the crystals having TTTG conformation. The equivalence of these carbons in the TTGG conformation and their non-equivalence, within the same monomer unit, in the TTTG conformation, is a property of the isolated chain. The observed NMR non-equivalence in the TTTG crystalline forms has the same origin.

F. Other polymers

All polymers, whether crystalline or non-crystalline, exhibit a glass transition at a particular temperature, T_g.[174] Changes in mechanical properties and

other properties may occur at this same temperature. Such behaviour stems from the abrupt onset of extensive molecular motion at the transition temperature. The motions are inhibited in the glassy state, in which the viscosity is so high that the specific volume cannot reach its equilibrium value in a practical timespan. An understanding of the relationship between the structure and motion properties of glassy polymers is important for the design of materials with specific properties, as well as for advancing our knowledge of the amorphous state.

In glassy polymers there is much heterogeneity in the local molecular environment, and motion is characterized by a distribution of correlation times. This may result in significant changes in resonance lineshape as a function of temperature. This comes from the fact that the carbons in differing environments undergo severe broadening at different temperatures. The CP-MAS NMR experiments allow relaxation data to be obtained on each resolved cabon of the polymers, and these data provide information about local motion such as segmental modes.

The T_1 data of poly(methyl methacrylate)[175,176] as a function of plasticizer type and content show that the effects of plasticizer on poly(methyl methacrylate) backbone produce motions which are still slow compared to the resonance frequency. The methyl side group dominates the backbone relaxation and little can be learned about main chain motion.

Gobbi *et al.*[177] and Parmer *et al.*[178] studied intermolecular mixing in polymer blends through CP experiments. Polymer blends are of particular interest because of their engineering significance as a means of modifying the physical properties of the mixture relative to the starting components and because of their scientific value as a means of studying compatibility of similar and dissimilar polymers. The two groups of workers used blends of deuteriated polystyrene-d_8 and poly(vinyl methyl ether), which have been well characterized to be compatible. In ^{13}C CP-MAS NMR the dipolar interactions between the abundant proton spins and the rare ^{13}C spins are utilized to polarize the latter by the Hartmann–Hahn technique through spin polarization transfer. This brings about significant gains in ^{13}C signal intensity and a reduction in data acquisition time. The efficiency of this cross-polarization depends on the strength of the proton–carbon magnetic dipolar coupling, and thus on the proximity of the protons to the ^{13}C nuclei.[179] Figure 20(a) shows a ^{13}C CP-MAS NMR spectrum for polystyrene-d_8 obtained with a CP contact time of 3 ms. The sample contains 2% of protonated polystyrene, giving a weak resonance at 127 ppm from the aromatic proton impurities. A spectrum for protonated polystyrene is shown in Fig. 20(c) (2 ms CP time) for comparison. The methylene carbons, aromatic carbons $C_{2\text{-}6}$ and aromatic carbon C_1 resonances appear at 39, 127 and 145 ppm, respectively. Figure 20(b) is a spectrum for poly(vinyl methyl

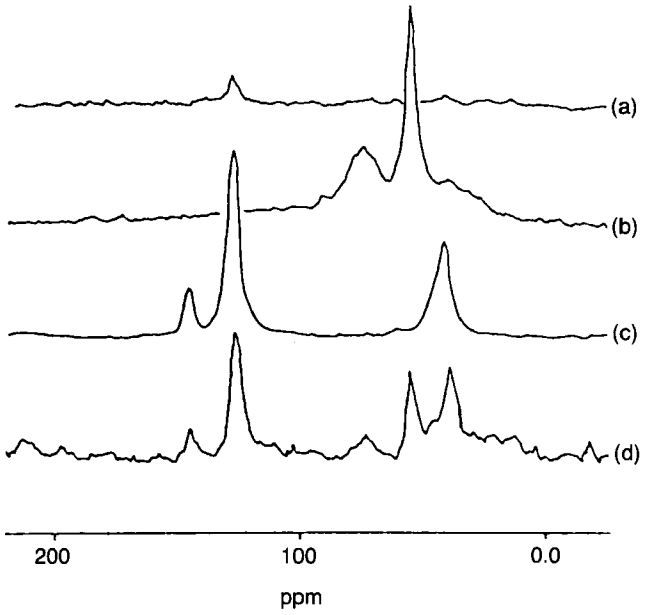

FIG. 20. ^{13}C CP-MAS NMR spectra of (a) PS-d_8, (c) protonated PS and (d) a 65PS-d_8/35PVME blend, respectively. (b) ^{13}C CP-MAS NMR spectrum of PVME. (Ref. 179.)

ether) obtained by using direct carbon polarization. The methylene carbon, methine carbon and methyl carbon resonances appear at 45, 75 and 55 ppm, respectively. Motional freedom in poly(vinyl methyl ether), a viscous liquid at room temperature, renders polarization by the Hartmann-Hahn method ineffective. The ^{13}C CP-MAS NMR spectrum of a blend of polystyrene-d_8 and poly(vinyl methyl ether) (their weight ratio = 65:35) is shown in Fig. 20(d). The normalized intensities of the resonances for the polystyrene-d_8 in the blend are 12 times that of pure polystyrene-d_8. This experiment demonstrates the occurrence of significant intermolecular cross-polarization of the carbon spins of polystyrene-d_8 by the proton spins of poly(vinyl methyl ether). This is possible when the proton-carbon internuclear distances are observable by CP conditions, indicating restriction of its main chain motions in the blend. Therefore, it can be said that there is molecular-scale mixing for this blend. Polystyrene/poly(methyl methacrylate) and poly(methyl methacrylate)/ poly(vinyl chloride) blend systems have also been examined by the same method.

The molecular dynamics of some amorphous piezoelectric polymers such as copoly(vinylidene cyanide/vinyl acetate) and copoly(vinylidene cyanide/methyl methacrylate) have been studied through T_1 data obtained from ^{13}C CP-MAS NMR experiments.[180] The piezoelectric origin of these

polymers is discussed on the basis of the information obtained about the molecular motion.

The structure and dynamics of polyesters and polycarbonates have been studied extensively in early ^{13}C CP-MAS NMR studies[14] and have been reviewed in detail. Many studies on polyesters[180-185] and polycarbonates[185-189] as polymer materials have been carried out.

Poly(vinyl alcohol) has both intramolecular and intermolecular hydrogen bonds. This leads to interesting spectral behaviour in CP-MAS NMR.[190]

V. BIOLOGICAL MACROMOLECULES

High-resolution solid-state ^{13}C NMR spectroscopy has been extensively used to analyse the conformation, dynamics and molecular ordering of a variety of biological macromolecular systems. A number of review articles has been already published to this end.[18, 50, 51, 86-90, 191-200]

A. Polypeptides, proteins and peptides

1. Isotropic chemical shifts

Polypeptides, proteins, and peptides consist of repeating sequences of peptide bonds (Fig. 21) with twenty different kinds of substituent at the C_α carbon. The secondary structure of this class of compounds is classified as α-helix, β-sheet, 3_{10}-helix, and so on, by means of a set of torsion angles (ϕ, ψ). It is thus expected that ^{13}C NMR signals will be sensitive to the different conformations. As an illustrative example, Fig. 22 shows 75.46 MHz ^{13}C NMR spectra of poly(L-alanine) with various molecular weights.[201] The two existing

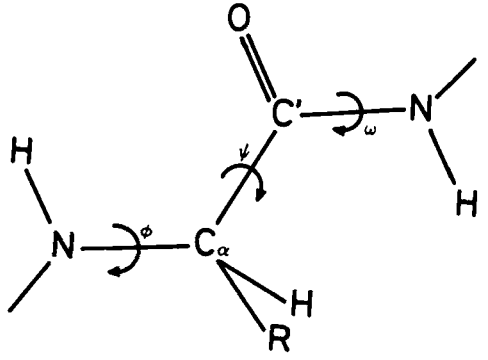

FIG. 21. Definition of the torsion angles in peptides.

FIG. 22. 75.46 MHz ^{13}C CP-MAS NMR spectra of poly(L-alanine) with various molecular weights: PLA-1, 16; PLA-5, 65; PLA-50, 700; PLA-200, 2800. (Ref. 201.)

kinds of conformations, the α-helix and β-sheet forms, are readily distinguished from the peak positions of the ^{13}C NMR signals: the C_α, C_β and C=O ^{13}C NMR signals of these compounds occur either at the peak position of the α-helix or β-sheet forms. Further examination of high-resolution solid-state ^{13}C NMR spectra of a number of polypeptides, whose secondary structures are known from IR or X-ray diffraction studies and others, showed that ^{13}C chemical shifts of the backbone C_α, C=O and side chain C_β signals are significantly displaced (up to 8 ppm), depending on the particular conformations, irrespective of there being a variety of neighbouring amino-acid residues.[201-223]

As summarized in Table 3, the C_α and C=O ^{13}C chemical shifts of the

TABLE 3

^{13}C chemical shifts characteristic of the α-helix and β-sheet forms (from TMS) (ref. 51).

Amino-acid residues in polypeptides	C-α			C-β			C=O		
	α-Helix	β-Sheet	Δ[a]	α-Helix	β-Sheet	Δ[a]	α-Helix	β-Sheet	Δ[a]
Ala	52.4	48.2	4.2	14.9	19.9	−5.0	176.4	171.8	4.6
	52.3	48.7	3.6	14.8	20.0	−5.2	176.2	171.6	4.6
	52.8	49.3	3.5	15.5	20.3	−4.8	176.8	172.2	4.6
Leu	55.7	50.5	5.2	39.5	43.3	−3.8	175.7	170.5	5.2
	55.8	51.2	4.6	43.7[b]	39.6	(4.1)	175.8	171.3	4.5
Glu(OBzl)	56.4	51.2	5.2	25.6	29.0	−3.4	175.6	171.0	4.6
	56.8	51.1	5.7	25.9	29.7	−3.8	175.4	172.2	3.2
Asp(OBzl)	53.4	49.2	4.2	33.8	38.1	−4.3	174.9	169.8	5.1
	53.6[c]			34.2[c]			174.9		
Val	65.5	58.4	7.1	28.7	32.4	−3.7	174.9	171.8	3.1
		58.2			32.4			171.5	
Ile	63.9	57.8	6.1	34.8	39.4	−4.6	174.9	172.7	2.2
		57.1			33.1			171.0	
Lys[d]	57.4			29.9			176.5		
Lys(Z)	57.6	51.4	6.2	29.3	28.5	−0.8	175.7	170.4	5.3
Arg[d]	57.1			28.9			176.8		
Phe	61.3	53.2	8.1	35.0	39.3	−4.3	175.2	169.0	6.2
Met	57.2	52.2	5.0	30.2	34.8	−4.6	175.1	170.6	4.5
Gly		43.2						168.4	
		44.3						169.2	
							171.6[e]	168.5	3.1

[a]Difference in the ^{13}C chemical shifts of the α-helix form relative to those of the β-sheet form.
[b]Mistyping or erroneous assignment. This assignment should be reversed.
[c]Erroneously assigned to the left-handed α-helix.
[d]Data taken from neutral aqueous solution.
[e]Averaged values from the data of polypeptides containing ^{13}C-labelled glycine residues.

α-helix form are displaced to high frequency with respect to those of the β-sheet form. The differences in the ^{13}C chemical shifts between the α-helix and β-sheet form, $\Delta_{\alpha\beta}$, do not vary strongly in a variety of amino-acid residues, although the absolute ^{13}C chemical shifts of the C_α and C_β are strongly affected by substituents at the C_α carbons. In addition, Table 4 demonstrates that a further three kinds of conformation, including left-handed α-helix, 3_1- or collagen-like triple helix and silk I form, can be distinguished by the characteristic displacement of the ^{13}C chemical shifts of the Ala residue.

At lower magnetic fields (<5 T), however, it has been shown that the C_α and C=O ^{13}C NMR signals are split into asymmetrical doublet patterns due to the ^{14}N quadrupolar effect on the ^{14}N–^{13}C dipolar interaction which is not completely suppressed by MAS. This is because the ^{14}N and ^{13}C spins are not quantized along the same axis.[18,224-227] The presence of the ^{13}C—^{14}N splitting

TABLE 4

Conformation-dependent ^{13}C chemical shifts of Ala residues in polypeptides of various conformations (ppm from TMS, ±0.5 ppm) (ref. 51).

			Antiparallel β-sheet				Collagen-like helix		Silk I
	α_R-Helix	α_L-Helix	$(Ala)_n$	$(Ala\text{-}Gly)_n$	$(Ala\text{-}Ala\text{-}Gly)_n$	$(Ala\text{-}Gly\text{-}Gly)_n$	3_1-Helix[a]	Triple-helix[b]	$(Ala\text{-}Gly)_nII$
C-α	52.4	49.1	48.2	48.5	49.1	48.7	48.7	48.3	50.5
C-β	14.9	14.9	19.9	20.0	20.4	21.6	17.4	17.6	16.6
C=O	176.4	172.9	171.8	171.9	171.1	171.2	172.1	173.1	177.1

[a] $(Ala\text{-}Gly\text{-}Gly)_nII$.
[b] $(Pro\text{-}Ala\text{-}Gly)_n$.

makes the spectral interpretation much more complicated in the case of complex polypeptides and proteins, although detailed analysis of this interaction provides geometrical information about the $^{14}N—^{13}C$ bonds. The above-mentioned ^{14}N quadrupolar effect turns out to be virtually non-existent at the higher magnetic field of 7 T, to yield effectively single lines for the C_α and C=O carbons. Hence, recording ^{13}C NMR spectra of solid polypeptides and proteins at higher magnetic fields is strongly recommended for the sake of simplified spectral interpretation.

It would seem reasonable to expect that the displacements of the ^{13}C chemical shifts (at higher magnetic fields) could be used as an intrinsic probe of local environment of a given amino-acid residue, if the conformation-dependent displacements of peaks were known in advance. This would apply

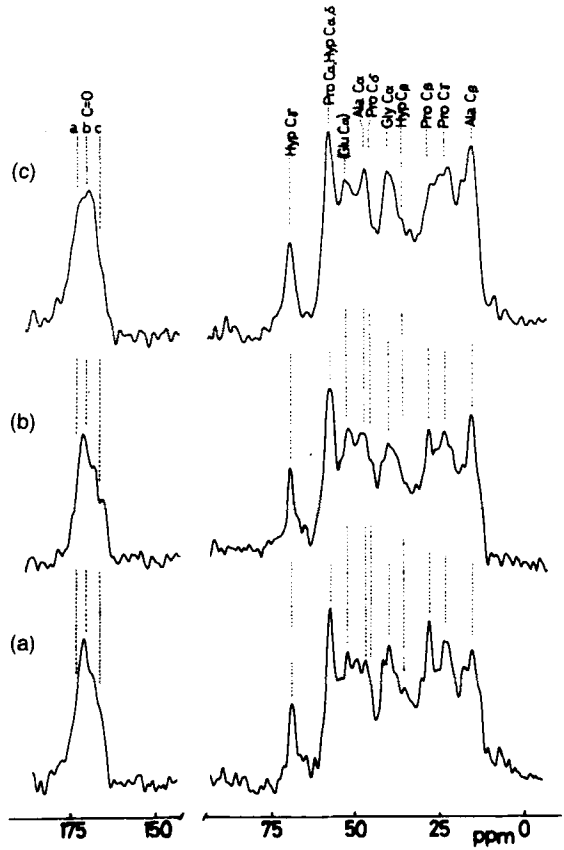

FIG. 23. 75.46 MHz ^{13}C CP-MAS NMR spectra of collagens from (a) bovine tendon, (b) bovine skin and (c) atelo-collagen. (Ref. 206.)

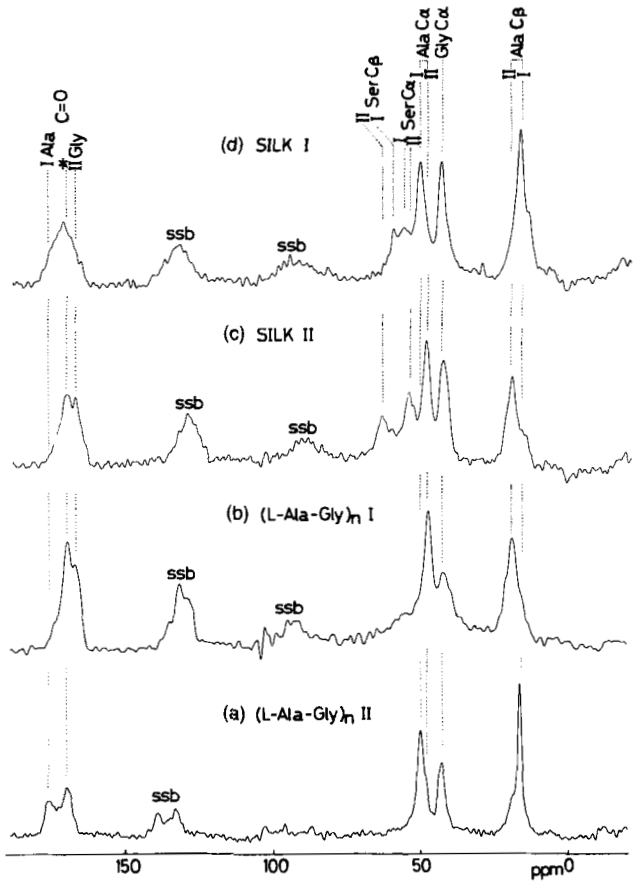

FIG. 24. 75.46 MHz ^{13}C CP-MAS NMR spectra of the crystalline fraction from *B. mori* silk fibroin and $(Ala-Gly)_n$ in the solid state. I and II stand for peaks from silk I and II, respectively. (Ref. 207.)

to amino-acid residues under consideration on the basis of high-resolution solid-state ^{13}C NMR studies of model homo- or sequential polypeptides. This approach has indeed been used to probe conformational elucidation of various types of fibrous proteins, namely, collagen,[206] silk fibroin,[92, 203, 207, 218] elastin,[221] and keratin.[222] In particular, several kinds of well-resolved peaks were observed for 75.46 MHz CP-MAS NMR spectra of collagen fibrils, as demonstrated in Fig. 23.[206] The assignment of peaks was made referring to the ^{13}C chemical shifts of appropriate model polypeptides, because individual triple chains of collagen are composed of a repeating pattern of $(Gly-X-Y)_n$, where X and Y are frequently occupied by prolyl,

4-hydroxyprolyl or alanyl residues. The similarity of the ^{13}C chemical shifts of respective amino-acid residues between collagen fibrils and model triple-helical polypeptides confirmed previous conclusions as to the tertiary structure of collagen analysed by X-ray diffraction studies.[206]

Saitô *et al.* showed that the ^{13}C NMR peaks of Ala, Gly and Ser residues of *Bombyx mori* fibroin are well separated in the dimorphs silk I and II (Fig. 24),[207] because the amino-acid composition is limited to the following four kinds of residues: Gly, 42.9%; Ala, 30.0%; Ser, 12.2%; Tyr, 4.8%. A later study showed that the Tyr C_α peak is superimposed on the Ser C_α peak and the Tyr C_β peak is suppressed, while side chain peaks are well resolved by TOSS experiments (H. Saito *et al.*, to be published). Consistent with expectations based on earlier X-ray diffraction and IR data, the ^{13}C chemical shifts of silk I and silk II are the same as those of $(Ala\text{–}Gly)_n$ II and I, respectively, within experimental error. However, none of the ^{13}C chemical shifts predicted from the crankshaft model of silk I, in which Ala and Gly residues are close to the β-sheet and α-helix conformations, respectively, were in agreement with those of silk I and $(Ala\text{–}Gly)_n$ II. In addition, "random-coil" and α-helix forms of silk fibroins are also identified by means of the conformation-dependent ^{13}C chemical shifts of the respective amino-acid residues on the basis of simple polypeptides.[92, 203, 207, 218]

High-resolution solid-state ^{13}C NMR spectra of globular proteins consist of a very broad envelope due to the overlap of many lines.[228, 229] Therefore, NMR study of globular protein at natural abundance is not always informative. To overcome this difficulty, selective isotope-labelling might be helpful. For instance, Huang *et al.*[230] recorded high-resolution solid-state ^{15}N NMR spectra of ^{15}N-enriched (at the imidazole N or N in His-57 of the catalytic triad) α-lytic protease, in order to compare directly enzyme structure in solution and in the solid state. The behaviour of the ^{15}N peak as a function of "pH" in the solid state closely parallels that observed in the solution state, except that in the powders proton exchange is slow on the NMR timescale whereas in solution it is fast. Mackenzie *et al.*[231] applied high-resolution solid-state ^{13}C and ^{15}N spectroscopy to analyse enzyme mechanism with respect to the direct observation of the hydrolysis of a slow substrate, amido-[^{13}C]- or amido-[^{13}C,^{15}N]Gly–Tyr, catalysed by an enzyme.

Shoji *et al.*[232] recorded 75.46 MHz ^{13}C CP-MAS NMR spectra of two cyclic dipeptides, cyclo(L-Ala-D-Ala) and cyclo(L-Ala-L-Ala). In the solid state, the presence of these two compounds is easily distinguished by specific displacements of the C_β and C=O ^{13}C NMR peaks (4–5 ppm), although these ^{13}C NMR peaks resonate at almost the same position, in solution, due to rapid conformational fluctuation. Opella and co-workers[193, 194, 233, 234] recorded the ^{13}C CP-MAS NMR spectra of cyclo(D-Phe^1–Pro^2–Gly^3–D-Ala^4–Pro^5) and cyclo(D–Phe–Gly–Ala–Gly–Pro) in the solid state at both 3.5

and 5.9 T. The asymmetric doublet pattern due to the ^{14}N–^{13}C dipolar interaction is still evident at 5.9 T, although less significant, for the C_α and C=O carbons adjacent to a nitrogen atom. This peptide has both β and γ turns stabilized by intramolecular hydrogen bonds. The authors showed that the difference in the chemical shift between C_β and C_γ, $\Delta_{\beta\gamma}$, of Pro serves as a convenient conformational marker of the presence of two different local conformations and is large (*c.* 4 ppm) for Pro in the β-turn (Pro^2) and small

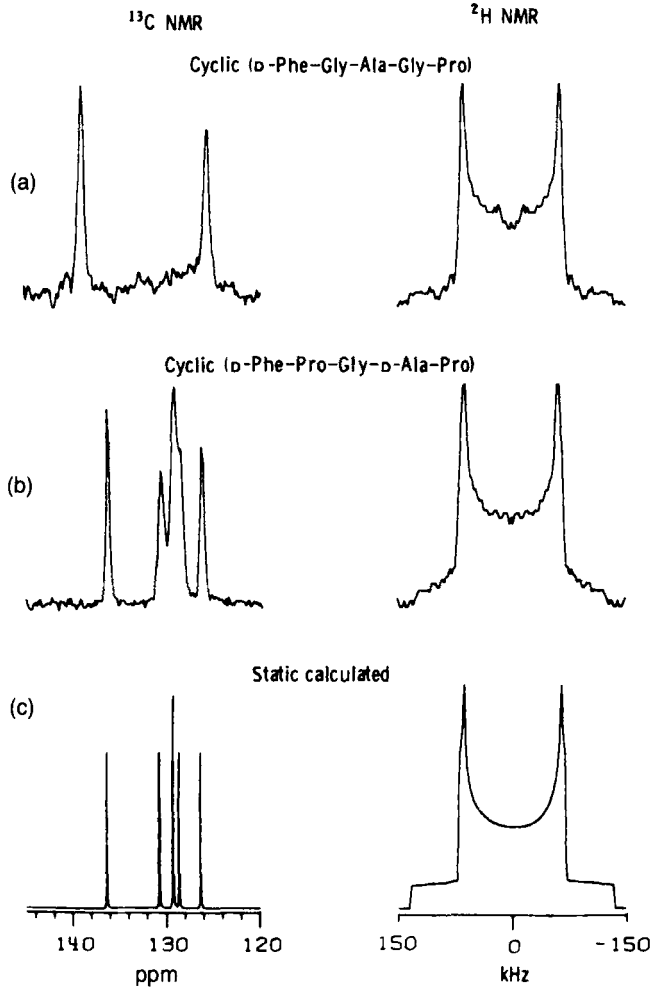

FIG. 25. ^{13}C (left) and ^{2}H (right) NMR spectra of aromatic rings in cyclic peptides. (a) Cyclic(D-Phe-Gly-Ala-Gly-Pro); (b) cyclic(D-Phe-Pro-Gly-D-Ala-Pro); (c) arbitrary ^{13}C chemical shift "stick" spectrum for a rigid ring and a calculated ^{2}H NMR powder pattern. (Ref. 234.)

(< 1 ppm) for Pro in a γ-turn (Pro[5]). Comparison of the ^{13}C chemical shifts between the solid and solution states showed that cyclo(D-Phe-Pro-Gly-D-Ala-Pro) exists in the same conformation in solution and in the solid state but that cyclo(D-Phe-Gly-Ala-Gly-Pro) appears to crystallize in two different forms under certain conditions and may exist in dynamic equilibrium between the two forms in solution. Further, they showed that prolines in type I and type II β-turns have different NMR parameters, notably C_β chemical shifts, as manifested by high-resolution solid-state ^{13}C NMR spectra of cyclo(Gly-L-Pro-Gly)$_2$.[233]

As illustrated in Fig. 25, the aromatic regions (Phe) (120–140 ppm) of the solid-state ^{13}C NMR of cyclo(D-Phe-Gly-Ala-Gly-Pro) have very unusual patterns: C_γ and C_ξ carbon resonances of Phe gives rise to a sharp single line, whereas C_α and C_β give a broad, ill-defined resonance between the C_γ and C_ξ peaks. This broad resonance peak was explained as being due to intramolecular reorientation of the Phe ring about the C_β—C_γ axis on a timescale of 10–100 Hz, resulting in intramolecular exchange broadening. Similar behaviour has been seen for phenylalanine hydrochloride.[235,236] In fact, ^2H NMR powder patterns of [$^2H_5$]Phe-labelled corresponding peptides show the ring to be rigid on the 10^6–10^7 timescale. Moreover, cross-peaks between the Phe C_δ and Pro C_γ resonances, and the Phe C_β and Pro C_β, C_γ and C_δ resonances were observed in the 2D ^{13}C—^{13}C spin exchange spectrum.[39] These cross-peaks indicate that spin exchange occurs through space due to the close spatial proximity of side chains from two different residues. In a similar manner, the conformational features of *N*-acetyl-*N'*-methylamide derivatives of seven isomeric monomethylprolines (AcProNHMe) were examined by means of the $\Delta_{\beta\gamma}$ values.[237] The three regions for the *trans* peptide bond isomers are referred to as α_R, C_7 and P_{II}, which have peptide ψ angles of *c.* $-60°$, 80° and 150°, respectively. In the solid state, $\theta(= \psi - 60)$ is in a narrow range (85 ± 11°), but $\Delta_{\beta\gamma}$ ranges from -4 to 17 ppm, owing to the methyl substituent. Sarkar *et al.*[238] studied three cyclic peptides, cyclo(Val-Pro-Gly)$_2$, cyclo(Phe-Pro-D-Ala)$_2$, and cyclo(Gly-Pro-D-Ala)$_2$, in the solid state. A comparison of $\Delta_{\beta\gamma}$ of Pro suggests that the Val-Pro and Phe-Pro peptide bonds are *cis* and that the Gly-Phe bonds are *trans*.

The *cis/trans* isomerism of the X-Pro bond in five classes of solid proline peptides was also characterized by $\Delta_{\beta\gamma}$ values.[239] At higher magnetic fields, ^{13}C NMR signals in biologically active peptides, Pro-Ala-Gly, gramicidin S and enkephalins, are well resolved.[240,241] In particular, two crystalline forms of [Leu[5]]enkephalin are readily distinguishable from the displacements of the ^{13}C chemical shifts.

Very little is known about the conformation-dependent ^{13}C chemical shifts of peptides containing α-disubstituted amino-acids in spite of their importance in naturally occurring channel-forming pentaibol antibiotics.[242] The

presence of α-aminoisobutyric acid (Aib) or C_α-methylalanine in peptides favours the formation of the 3_{10}-helix ($\phi = \pm 60°$, $\psi = \pm 30°$).

Recently, Saitô *et al.* showed that the formation of the 3_{10}-helix in two series of fully protected oligopeptides, Z-$(Aib)_n$-OMe (n = 3–8) and Z-$(Aib)_n$-L-Leu-$(Aib)_2$-OMe (n = 0–5), is readily monitored by a characteristic splitting of the C_β signals as large as 4–6 ppm, compared with a splitting of 2–3 ppm in the case of the monomers or dimers which are incapable of adopting this conformation.[57] It was shown on the basis of X-ray diffraction studies that a limited deformation of the $C_\beta{}^D$ and $C_\beta{}^L$ atoms results in a displacement of the ^{13}C NMR peaks as large as 6 ppm. This finding is consistent with the observed displacements of peaks about methyl ^{13}C peaks of tetranactin and nonactin: methyl peaks are displaced to low frequency by about 6 ppm when methyl groups are in shorter (< 3.8 Å) intermolecular contact.[56]

2. *Chemical shielding anisotropy and dipolar tensors*

In parallel with the above-mentioned analysis of high-resolution solid-state NMR spectra by magic angle spinning, a number of studies based on CSA or

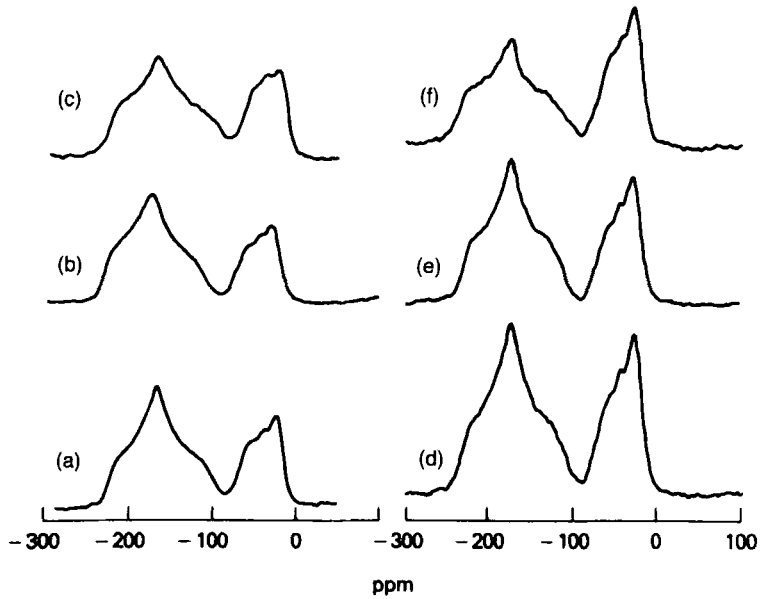

FIG. 26. Comparison of the 62.98 MHz ^{13}C NMR spectra of [1-^{13}C]glycine-labelled collagen from different tissues at 22°C. Proton enhanced and decoupled spectra of: (a) rat tail tendon; (b) demineralized rat calvaria; (c) mineralized rat calvaria. 90° – t proton-decoupled spectra of; (d) rat tail tendon; (e) demineralized rat calvaria; (f) mineralized rat calvaria. (Ref. 244.)

dipolar interactions has been carried out to analyse the orientation and dynamics of peptides and proteins, both in the solid state and encapsulated in lipids. Torchia *et al.* studied ^{13}C NMR powder patterns of ^{13}C-labelled collagen fibrils to gain insight into backbone and side chain motions.[26,197,243-245] Figure 26 illustrates the ^{13}C NMR spectra of [1-^{13}C]glycine-labelled collagen from different tissues, with (left) and without (right) cross-polarization, at 22°C: reconstituted (uncross-linked) chick calvaria collagen fibrils, rat tail tendon (cross-linked), and rat calvaria (cross-linked and mineralized) collagen.[244] The lineshapes observed by both methods turned out to be identical. The linewidth $\Delta(=|\sigma_{33}-\sigma_{11}|)$ for the uncross-linked collagen fibril is 108 ppm, whereas the maximum value of 140 ppm is observed for the cross-linked and mineralized collagen fibrils. The latter value is close to the static values of Δ for polycrystalline glycylglycine and polyglycine, 150 and 142 ppm, respectively. Such differences in Δ values have been ascribed to differences in molecular mobility in the various samples at 22°C, because all samples have the same lineshape and equal Δ values at −35°C. The root-mean-square fluctuations of the azimuthal angles γ_{rms} due to reorientation about the helix axis are found to be 41°, 33° and 14°, on the basis of the observed linewidths Δ, for the uncross-linked, cross-linked, and mineralized collagens, respectively. Analysis of ^{13}C-enriched oriented silk fibroin was performed by Fujiwara *et al.*[246]

To study membrane proteins by NMR, it is more appropriate to use solid-state methods for samples severely broadened by residual dipolar interaction. Cornell *et al.*[247,248] studied ^{13}C NMR spectra of [1-^{13}C]Gly^2-, Ala^3- or Val^7-labelled and [1,2-$^{13}C_2$]Gly^2-labelled gramicidin A incorporated into a hydrated dispersion of perdeuteriated dimyristoylphosphatidylcholine (DMPC) (1:15). The dispersion was aligned on glass coverslips whose orientation to the magnetic field could be varied through 180°. At temperatures well below the gel–liquid crystalline phase transition it was found that gramicidin A adopts a rigid structure, as seen from the carbonyl resonance. Cornell and co-workers then determined the direction of the $^{13}C{=}O$ bonds and compared their results with the various conformational models proposed so far. Their result is consistent with the left-handed $\pi^{6,3}{}_{LD}$ single-helix proposed by Urry *et al.* Lewis *et al.*[249] studied [1-^{13}C]Leu-labelled bacteriorhodopsin (bR) incorporated into a DMPC bilayer. They showed that bR undergoes rotational diffusion about an axis perpendicular to the plane of the bilayer, resulting in a narrowing of the ^{13}C NMR powder lineshape of the bR peptide carbonyls. The range of Euler angles of Leu peptide groups relative to the diffusion axis was determined in order to obtain information about the secondary structure of this protein in membranes.

Further, Opella *et al.* analysed secondary structure,[86,250-255] interaction with DNA,[253] and orientation[253,255] and dynamics[251] of side chains in oriented

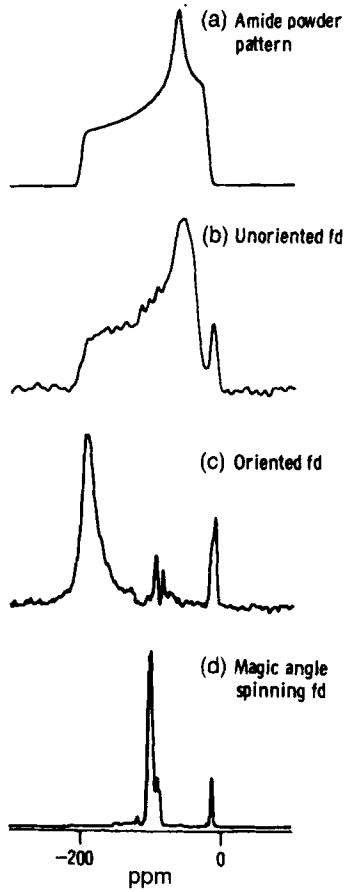

FIG. 27. ^{15}N NMR spectra of uniformly ^{15}N-labelled fd at 25.3 MHz. (a) Calculated powder pattern based on the spectrum of acetyl [^{15}N]glycine ($\sigma_{33} = -192$, $\sigma_{22} = -51$ and $\sigma_{33} = -10$ ppm) (b) unoriented fd solution; (c) magnetic field oriented fd solution; and (d) magic angle spinning sample fd gel. (Ref. 253.)

virus (bacteriophage) fd coat protein in solution by ^{13}C, ^{15}N and ^{31}P NMR techniques including analysis of ^{15}N—H dipolar splitting, CSA and spin exchange (see Section II.D). This uniaxial orientation of the fd coat protein is achieved through the interaction of the net diamagnetic anisotropy of the α-helical protein with the applied magnetic field.[253] The ^{15}N NMR spectrum of oriented uniformly ^{15}N-labelled fd coat protein (Fig. 27(c)) gives rise to nearly all of the ^{15}N amide signals at -185 ppm, which is approximately equal to σ_{33} (parallel to the N—H bond) of the ^{15}N shielding tensor (Fig. 27(a)). This means that nearly all of the amide groups of the coat

protein are arranged with their N—H bonds parallel to the applied magnetic field.[253] Cross and Opella analysed the orientation of DNA molecules in the virus by means of the ^{31}P anisotropy pattern.[254]

As described above, the interpretation of the oriented NMR spectra is critically dependent on an accurate knowledge of the principal values and direction cosines of the principal axes of CSA. Stark *et al.*[256] determined the ^{13}C shielding and ^{13}C—^{15}N dipolar tensors for the peptide bond by examination of single crystals of the dipeptide [1-^{13}C]glycyl[^{15}N]glycine HCl H_2O. They found that the σ_{22} component lies approximately along the carbonyl bonds and the most shielded component, σ_{33}, is perpendicular to the plane defined by the amide oxygen, carbonyl and nitrogen. These values cannot be determined without having a large single crystal and knowledge of the crystal structure. However, these principal values and the molecular orientations of the tensors can be extracted from powder samples if the nucleus under consideration is dipole-coupled to a second nearby nucleus, because the dipolar tensor is an axially symmetric tensor whose unique axis is known to lie along the internuclear vector.[257] Hence, the ^{13}C shielding tensors were determined from ^{15}N dipole-coupled chemical shift powder patterns for the glycine carbonyl carbon of a series of five peptides, *N*-acetyl[1-^{13}C]glycyl-X-amide, where X is [^{15}N]glycine, DL-[^{15}N]tyrosine, L-[^{15}N]phenylalanine and DL-[^{15}N]alanine. In a similar manner, the amide ^{15}N chemical shielding tensors of four peptides were determined from ^{13}C dipole-coupled ^{15}N powder patterns.[258] In addition, the ^{15}N and ^{13}C shielding tensors of L-[^{13}C]alanyl-L-[^{15}N]alanine were obtained from the dipole-coupled powder patterns.[259] The ^{15}N—^{13}C dipole-dipole coupling in amide linkage is at most 2.6 kHz, although this value is very informative. Opella *et al.*[260] proposed 1D or 2D triple resonance to separate and correlate ^{13}C shift and ^{15}N—^{13}C dipole-dipole couplings. They selectively observed ^{13}C NMR signals from a single ^{13}C—^{15}N pair, Phe-42 and Lys-43, from a double-labelled sample of the fd coat protein by ^{13}C-labelling at the carbonyl carbons and ^{15}N-labelling at the five lysine amide nitrogen.

Ando *et al.*[209] used ^{13}C NMR spectra to measure the principal values of the ^{13}C shielding tensors of Gly C=O of a variety of polypeptides (with antiparallel β-sheet, 3_1-helix, α-helix and ω-helix conformations) containing ^{13}C-enriched glycine as a minor component (<8%). They found that the magnitudes of the displacements of the signals upon change in conformation are larger for σ_{22} and σ_{33} than for the isotropic chemical shift values, while σ_{11} is almost unaffected by any conformational change.

B. Polynucleotides

There appears to be very few high-resolution ^{13}C NMR studies of poly-

nucleotides such as DNA[18] and RNA,[261] due to the complications of very broad linewidths of nucleotide resonances arising from overlaps of peaks from the $^{13}C—^{14}N$ dipolar interaction or the efficient $^{13}C—^{1}H$ dipolar relaxation mechanism. The only assignable peaks of DNA are found to be from the methyl and C-5 resonances of thymine (T) and the C-5 resonance of cytosine (C).[18]

Cross *et al.*[250] preferred to study biosynethetically ^{15}N-labelled DNA from *Escherichia coli* grown on a medium with $^{15}NH_4Cl$ as the sole nitrogen source because there are relatively few nitrogen atoms in DNA bases. They showed that resolved resonances for 13 of the 14 nitrogens are observed (Fig. 28). As shown in Figs 28(a) and (b), proton-bearing and non-proton-bearing nitrogen sites are easily distinguishable on the basis of the relative strengths of their $^{15}N—^{1}H$ dipolar couplings. Subsequently, the qualitative 2D correlation of the ^{15}N chemical shifts with the magnitude of the dipolar sidebands (see Section II.B) allows the nitrogen sites to be divided into those with substantial sidebands (—NH_2 and —NH) and those with no nearby hydrogens.[262] From the $^{15}N—^{1}H$ dipolar spectra, Cross *et al.* obtained the N—H bond length of G1 of B form DNA as 1.13 Å. This means that the hydrogen is localized on the hydrogen bond donor nitrogen sites (G1, T3) and not significantly shared with the acceptor nitrogen sites (C3, A1). Hemminga *et al.*[263] analysed the line broadening in MAS ^{31}P NMR spectra of tobacco mosaic virus (TMV) by selective saturation and T_2 measurements: about 90 Hz was ascribed to homogeneous effects, whereas the inhomogeneous contribution which depends upon the manner of sample preparation (either by lyophilization or pellet formation by ultracentrifugation followed by drying) is approximately 100 Hz. In addition, splittings of ^{31}P NMR signals into major and minor components by 3.7 ppm were interpreted in terms of differences in bond angles and torsion angles in phosphodiester bonds such as *gauche/gauche* or *gauche/trans* conformations.

Most other works on polynucleotides have been performed by ^{31}P NMR studies of either oriented[87-89,264-271] or non-oriented samples.[272-274] As described earlier (Section III.G), geometrical parameters related to DNA conformations can be obtained from analysis of ^{31}P NMR lineshapes of oriented fibres as referred to the principal values and axes of chemical shielding tensors.[87-89] At the same time, information as to anisotropic motion, if any, is directly available from the spectral analysis of oriented samples. Shindo *et al.*[87-89,264-270] and Nall *et al.*[271] extensively analysed ^{31}P NMR spectra of oriented fibres from a variety of synthetic polynucleotides and A, B, and C form DNA. They showed that the observed features of ^{31}P NMR spectra are significantly dependent on the relative humidity, as well as on the angle between the fibre axis and the applied magnetic field. As illustrated in Fig. 29, the A form of DNA at a relative

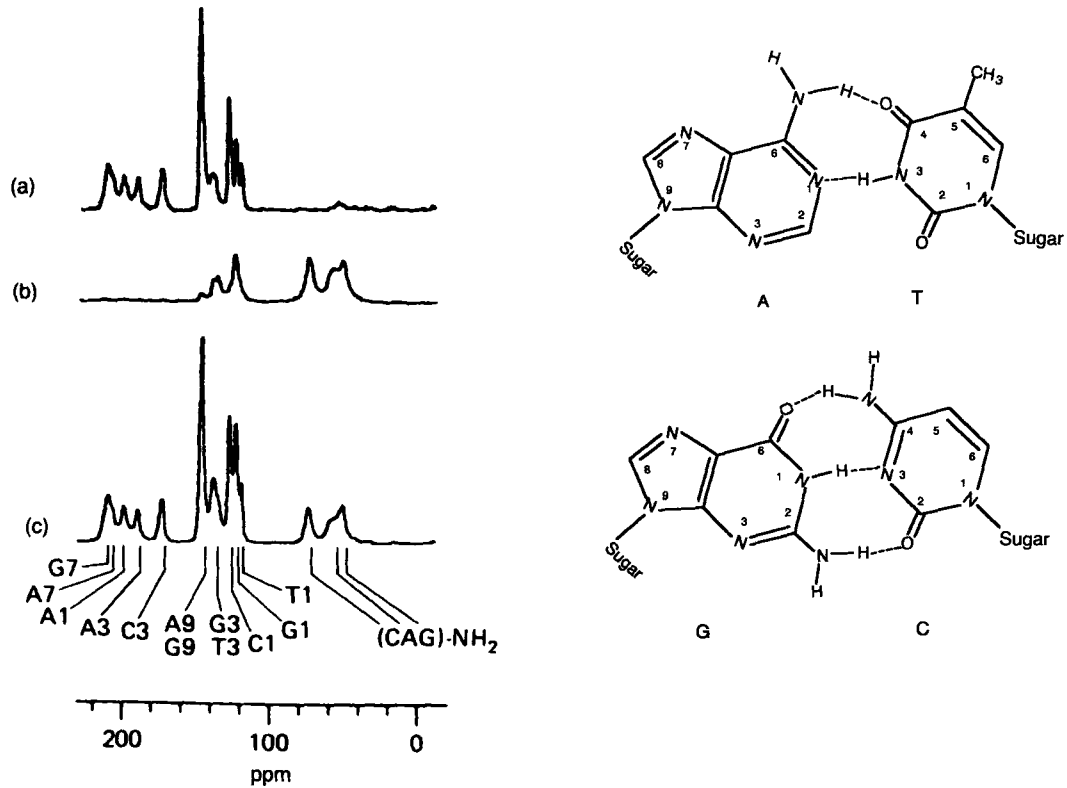

FIG. 28. ^{15}N NMR spectra of B-DNA and fd virus. (a) and (b) show non-protonated and protonated ^{15}N NMR spectra of B-DNA, respectively. (c) Complete ^{15}N NMR spectrum of B-DNA with a 4 ms mix time for 4000 transients. The structure on the right shows how the atoms are numbered. (Ref. 250.)

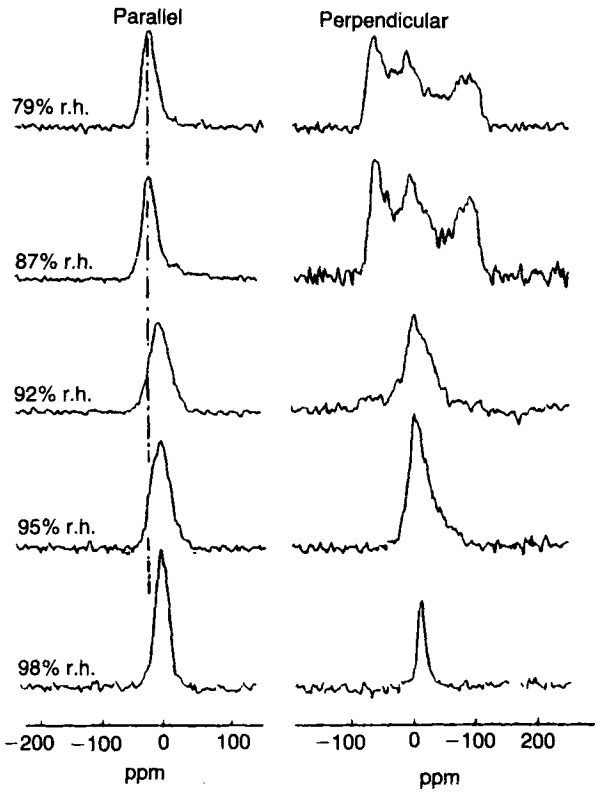

FIG. 29. Solid state ^{31}P NMR spectra of oriented DNA fibres at various relative humidities. (Ref. 267.)

humidity below 87% exhibits a singlet and a trimodal pattern for the parallel and perpendicular orientations, respectively. The analysis of the lineshapes of the A form of DNA[266,268,269,271] gave a single uniform backbone conformation comparable with that obtained by fibre or single crystal X-ray diffraction studies. However, the ^{31}P NMR spectrum of the B form of DNA is distinct from that of the A form of DNA in two respects: the low frequency displacement of the parallel spectrum and the single line in the perpendicular spectrum. The conformation of the B form of DNA[264–267,269,270] is very heterogeneous, depending on base sequences, which is consistent with the distribution of the torsion angles of the phosphodiester linkages. In addition, molecular motions occurring in the hydrated fibres were analysed in terms of three motional models: conformational fluctuations, restricted rotation about a tilted axis, and rotational diffusion about the helical axis.[270]

The presence of large amplitude motions of the phosphodiester groups at temperatures above 5°C in the hydrated solid B form of DNA was

demonstrated on the basis of the powder pattern ^{31}P NMR spectra.[272] No evidence of structural changes in DNA upon incorporation into the virus was given by ^{31}P shielding tensors of fd virus.[273]

C. Polysaccharides

Polysaccharides are some of the naturally occurring biological macromolecules most extensively studied by high-resolution solid-state ^{13}C NMR spectra. Nevertheless, their spectral interpretation, in some instances, is still a subject of dispute, as is the case for cellulose. Therefore, it appears that a comparative study of the various types of polysaccharides is urgently required to allow us to understand the general trend of displacements of the peaks. In particular, the diversity of the secondary structure of polysaccharides arises from the variety of anomeric forms, α or β, from the variety of constituent residues such as glucose, mannose, etc., from the different possible glycosidic linkages such as $1 \rightarrow 2$, $1 \rightarrow 3$, $1 \rightarrow 4$, etc., and from sources of isolation or physical treatment.

1. (1→4)-α-D-glucan[275-287]

The two main components of starch, amylopectin and amylose, are higher molecular weight (1→4)-α-D-glucans, either highly branched through (1→6)-α-linkages and linear or lightly branched, respectively. X-ray diffraction gives two different patterns, "A" and "B", from cereal starch and the starch found in tubers, respectively. As demonstrated in Fig. 30, these two forms are readily distinguishable from the ^{13}C CP-MAS NMR spectra: the C-1 peak of "A" starch is a triplet, while that of "B" starch is a doublet.[276-280] The presence of these multiplet patterns was interpreted in terms of the number of chains in the asymmetric unit:[276,277,279] the assigned $P2_1$ space-group for "A" starch has the 2_1 axis perpendicular to the six-residue per turn strands of the double helix, and has a two-fold axis in the helix direction. Therefore, maltotriose must be taken as the asymmetric unit. On the other hand, the assigned $P3_121$ space-group for "B" starch has the 3_1 axis down the strand, specifying the two D-glucose unit as the asymmetric unit. On drying of the starches, the ^{13}C NMR signals are substantially broadened, together with the appearance of signals from the non-crystalline region.[276-280,288] In particular, Gidley and Bociek[288] demonstrated that the C-1 peak of such an amorphous (1→4)-α-D-glucan shows a remarkably large chemical shift range (94–106 ppm), reflecting a wide diversity of local conformations. They showed that such peak positions are well correlated with the sum of contributions from allowed conformations, related to $|\phi| + |\psi|$ angles (Fig. 31). These results clearly indicate that water molecules play an important role in maintaining the secondary structure of "A" and "B" starches and amyloses.

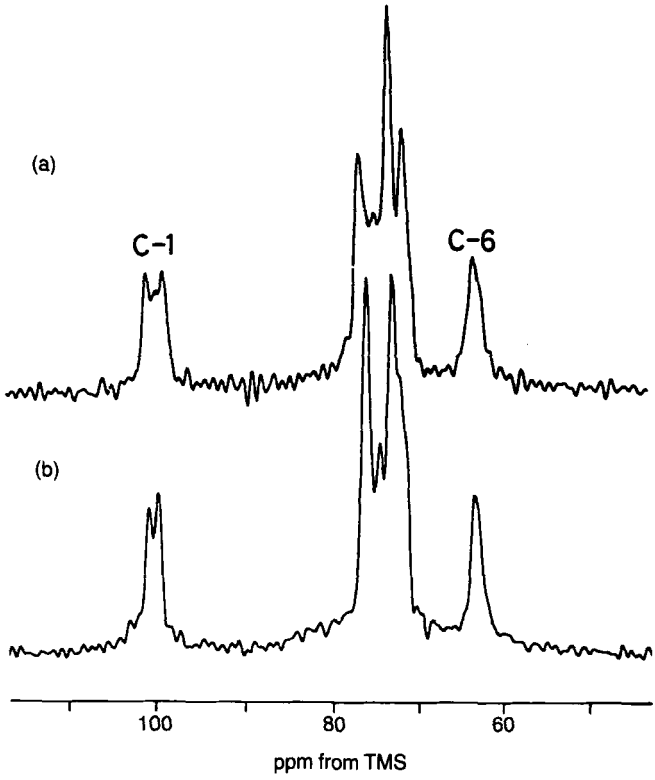

FIG. 30. ^{13}C CP-MAS NMR spectra of starches hydrated at 100% relative humidity. (a) Nageli amylodextrin (an "A" starch); (b) lintner starch (a "B" starch). (Ref. 279.)

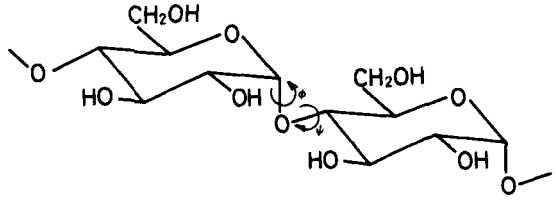

FIG. 31. Definition of torsion angles in amylose.

In contrast, the C-1 and C-4 signals of V-amylose, which adopts a single helix, gives rise to single lines: the C-4 peak, in particular, is substantially displaced downfield (*c.* 4–5 ppm) from that of the "A" or "B" forms.[275,280] These results, together with substantial displacements of peaks between the solid and solution states, suggest that the ^{13}C signals of carbons at the glycosidic linkages depend sensitively on the respective glycosidic torsion angles.[275] Nevertheless, the number of distinct conformations available is

limited to that of a few polymorphs, as far as macromolecular samples are concerned. In addition, it is very difficult, in many instances, to obtain accurate structural data from X-ray diffraction studies of fibre samples. Instead, it is useful to use a number of single-crystal X-ray diffraction data of cycloamyloses (α-, β- and γ-cyclodextrins) enclosing a variety of guest molecules as reference compounds to obtain a relationship between the C-1 or C-4 ^{13}C chemical shifts and the glycosidic torsion angles (ϕ, ψ) (see Fig. 31, for definitions). In fact, a few of the C-1 and C-4 ^{13}C signals are resolved when complexes with distorted conformations are examined. Several attempts have been made to relate the observed ^{13}C chemical shifts and the respective torsion angles.[281-287] Saitô *et al.* suggested a relationship between the C-1 and C-4 ^{13}C chemical shifts with ϕ and ψ angles, respectively.[281] Ripmeester showed that a better relationship is obtained by plotting the C-1 and C-4 signals with ψ angles.[284] In contrast, Veregin *et al.*[287] showed that the C-1 and C-4 chemical shifts are well correlated with the ψ and ϕ angles, respectively. In any case, it is true that the displacements of the carbons at the glycosidic linkages are related to the particular conformations of individual glucose residues. The splittings of the C-6 peaks are also related to the exocyclic C-4—C-5—C-6—O-6 torsion angles.[281,287]

2. *(1 → 3)-β-D-glucan*[81,289-299]

Linear (e.g. curdlan) or branched (e.g. lentinan) (1 → 3)-β-D-glucans of higher molecular weight form gels in aqueous media, when their aqueous suspensions are heated. Saitô *et al.*[297,298] demonstrated that several broad signals are visible from the gel samples despite their solid-like appearance. The ^{13}C chemical shifts of the C-1 and C-3 carbons at the glycosidic linkages of the gel state are displaced to high frequency by 2.8 and 3.2 ppm, respectively, compared with those of the random coil state in aqueous solution. Consistent with the argument described already for (1 → 4)-α-D-glucans, this observation supports the view that the C-1 and C-3 ^{13}C chemical shifts of (1 → 3)-β-D-glucans could vary significantly with the various conformational states. It has been shown that the two major conformations of (1 → 3)-β-D-glucans, curdlan-type (or helix) (Fig. 32(b)) and laminaran-type (or native) (Fig. 32(c)), are readily distinguishable from the characteristic peak positions of the C-3 carbon, 89.6 (± 0.5) ppm and 85.5 (± 0.5) ppm, respectively.[81,290-293,295,296] Thus, the amorphous state as suggested from X-ray diffraction studies does not necessarily mean assuming that there is a disordered conformation. In particular, linear glucans of higher molecular weight (curdlan, pachyman, etc.) and spray-dried branched glucans take the curdlan-type form, whereas laminaran (water-soluble fraction of lower molecular weight) and lyophilized branched glucans take the laminaran-type form.

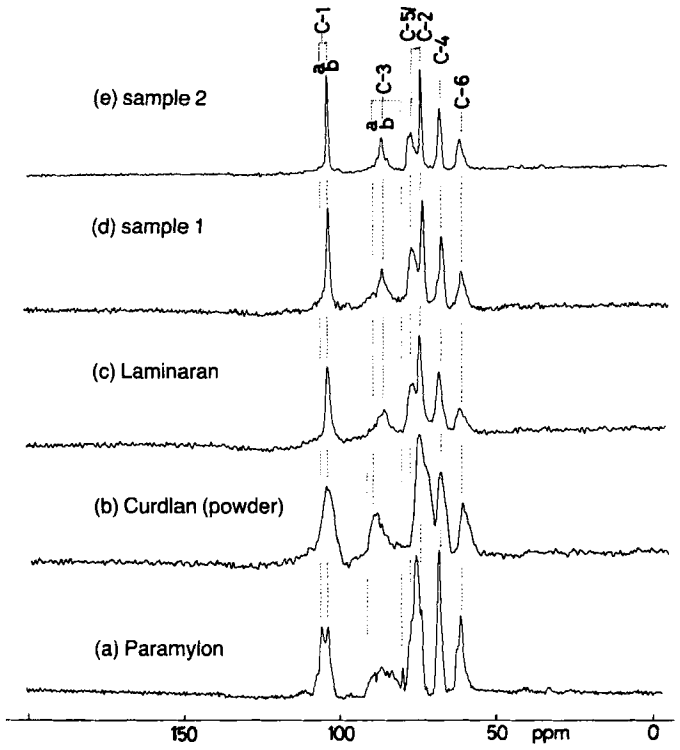

FIG. 32. 75.46 MHz ^{13}C CP-MAS NMR spectra of some linear (1 → 3)-β-D-glucans in the solid state: (a) paramylon; (b) curdlan powder; (c) laminaran, (d) sample 1 (annealed curdlan at 180°C; and (e) sample 2 (curdlan annealed at 150°C). (Ref. 81.)

It turned out that the laminaran-type form corresponds with the triple helix conformation,[81] as inferred from the peak positions being identical with those of annealed crystalline curdlan, whose secondary structure was previously analysed by X-ray diffraction (Fig. 32(d) and (e)), although individual ^{13}C NMR peaks are broadened, reflecting the non-crystalline nature (see Section III.C). However, no information is available from X-ray diffraction studies as to the conformation of the curdlan-type form. Nevertheless, it has been shown that the curdlan-type form is ascribed to a single change form, mainly because the intense high-resolution ^{13}C signals (70–80%) are visible from curdlan at the swelling temperature (54°C).[81,289-293] Thus, conversion from the single to triple helix form is conveniently monitored by observing the relative peak intensities obtained by varying the conditions of annealing and cooling.[81] The reverse conformational change from the triple helix to single chain may also be monitored by recording

spectra of samples lyophilized from DMSO solution.[293] In addition, the ^{13}C NMR spectra of crystalline paramylon showed a number of additional signals other than the peaks from the triple helical chain, in spite of the similarity in the X-ray diffraction pattern.[81] This is a consequence of the existence of additional conformations other than the triple helix which are not detected by X-ray diffraction. This sort of insensitivity of X-ray diffraction to a conformational change, however, is also seen for a number of cellulose samples, as described later.

In a gel sample of curdlan, Stipanovic and Giammatteo[299] reported that two types of the ^{13}C CP-MAS NMR peaks, "swollen" and "hydrated", are clearly resolved and the former peaks are converted to the latter by annealing the samples at a higher temperature (95–120°C). It is important to clarify whether or not this "swollen" form is related to the single helical region giving rise to conventional high-resolution ^{13}C NMR signals.

3. Cellulose, lignin and wood

Cellulose is a (1 → 4)-β-D-glucan and is the primary constituent of plant cell walls. Its most common polymorphs, cellulose I and II, are usually identified with the native and regenerated form, respectively. Atalla *et al.*[300] showed that these two polymorphs can easily be distinguished by examination of their ^{13}C NMR spectra. The C-1 peaks for both forms and the C-4 resonance of cellulose II show very definite splittings into two peaks with approximately equal intensities. In addition, both the C-4 and C-6 peaks contain a broad low frequency shoulder.[300,301] A number of studies[302-326] by ^{13}C NMR spectroscopy have been performed to obtain a better understanding of the structure of cellulose. Nevertheless, spectral interpretations differ greatly among investigators. This diversity may be related to the fact that many uncertainties still remain about the crystal structure of the celluloses as revealed by diffraction methods. The ^{13}C NMR data provide information complementary to the diffraction data, and serve to constrain the acceptable structural models to a smaller subset than would otherwise be admissible on the basis of diffractometric observation alone.[327]

The low frequency shoulders at C-4 and C-6 peaks (see Fig. 33) were initially ascribed to non-crystalline (amorphous) carbons.[301] In subsequent papers they were assigned to different morphological states[302,307] because the estimated crystallinity from the intensities of the broad and narrow C-4 resonances (55–60%) is far smaller than most other estimates of crystallinity (89–90%): the narrow peaks are due to anhydroglucoses buried in the elementary fibril and the broad shoulder peaks are due to the glucoses on the surface of the elementary fibril. Horii *et al.* and Teeaar and Lippmaa assigned these two types of peaks to ordered and disordered states,

respectively,[311,313-316,318] on the basis of their successful separation of the crystalline and non-crystalline components by the use of partially relaxed ^{13}C NMR spectra. They showed that the degree of crystallinity estimated from the ratio of the ^{13}C NMR spectra is in good agreement with that measured by X-ray diffraction. It was shown[315,316] that hydration of cellulose samples resulted in considerable narrowing of peaks from the crystalline portion, in parallel with the observation for (1 → 4)-α-D-glucans. Further, they showed that the displacements of the C-1, C-4 and C-6 signals were related to the torsion angles ϕ, ψ and χ (exocyclic torsion angle of the C-5—C-6 bond), respectively, in a similar manner to that observed for (1 → 4)-α-D-glucans described above.[311-313,316] Gagnaire *et al.*[319] reached the same conclusion from results of surface labelling experiments of accessible hydroxyl groups by OCD_3 and OTMS groups. The later studies by Atalla and VanderHart[303-306] suggested that the narrow component arises from the crystalline domain, and the broad component is associated with the surface of crystalline domains as well as with disordered regions.

The existence of two peaks for C-1 and C-4 was originally interpreted in terms of a non-equivalence of alternate glycosidic linkages within the same cellulose chain (i.e. a non-symmetrical cellobiose-like repeat unit rather than a two-fold helical conformation).[300] However, Dudley *et al.*[308] and Fyfe *et al.*[309] showed, from a study on a series of ^{13}C NMR spectra of cellulose oligomers, that the observed doublets in cellulose II are due to the presence of two independent chains in the unit cell. In contrast to cellulose II, it has been shown that the ^{13}C NMR spectrum of cellulose I from algae such as *Valonia ventricosa* or from bacteria such as *Acetobacter xylinum* exhibits triplet signals for both C-1 and C-4 peaks, as illustrated in Fig. 33.[303-306,310] In an earlier study, Earl and VanderHart suggested a unit cell containing four equivalent glucose units with two different types of glycosidic linkages.[302] Later, Atalla and VanderHart[303,305] proposed that native celluloses are composites of more than one crystalline form, I_α and I_β. They came to this conclusion because the multiplet intensities obtained by taking appropriate linear combinations of the spectra of the regenerated cellulose I and of the cellulose from *Acetobacter xylinum* are not constant and not in the ratios of small whole numbers as would be expected if they arose from different sites within a single unit cell. The alternative explanation is based on a comparison of NMR and X-ray diffraction data. Cael *et al.*[310] proposed a different interpretation as to the multiplet patterns of algal cellulose. The eight-chain unit cell model of cellulose I in *Valonia* algae derived from electron- and X-ray diffraction data predicts the existence of three distinct molecular chains with different chemical shifts, with a predicted intensity ratio of 4:2:2 or 2:1:1 (see Fig. 33(g)).

Chanzy *et al.*[320] examined, on the basis of ^{13}C NMR and electron-

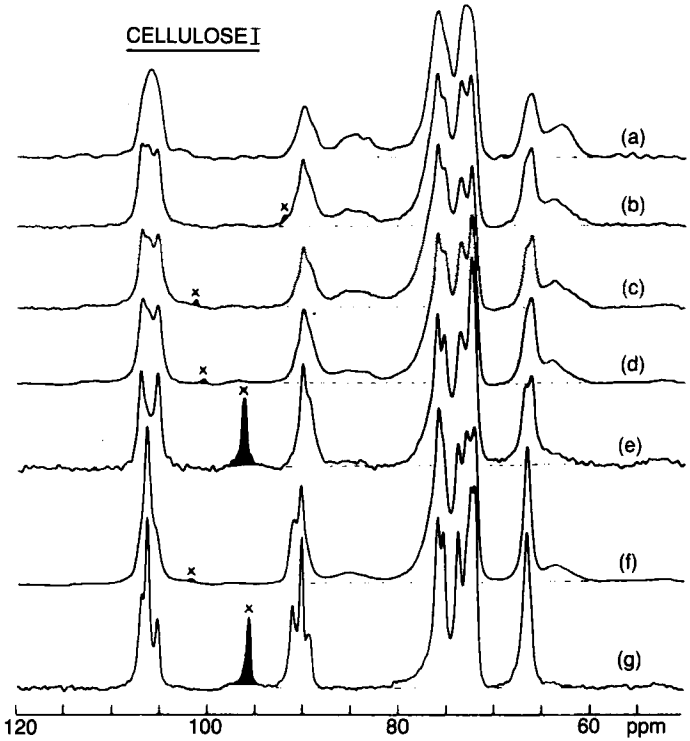

FIG. 33. ^{13}C CP-MAS NMR spectra of various cellulose I materials: (a) Norway spruce kraft pulp; (b) ramie; (c) cotton linters; (d) hydrocellulose made from cotton linters; (e) a low-DP generated cellulose I; (f) *Acetobacter xylinum* cellulose; and (g) *Valonia ventricosa* cellulose. (Ref. 305.)

diffraction methods, a cyclic transformation of highly crystalline cellulose I (*Valonia*) into cellulose III and back to cellulose I, hoping to gain an insight into the interpretation of cellulose I spectra. The ^{13}C NMR spectrum of cellulose III_I (treatment with ethylenediamine followed by washing in methanol) showed only six clearly resolved peaks. In addition, the C-6 peak of cellulose III_I is displaced to high frequency by 3.1 ppm as compared with that of cellulose I. Changing cellulose III_I into cellulose I_{III}, achieved by a high-temperature water treatment, gave a ^{13}C NMR spectrum identical with that of cotton cellulose. The transformation of native cellulose Ib (cotton-ramie type) to Ib (bacterial-valonia type) was also studied by Hirai *et al.*[317] Philipp *et al.*[321] and Hayashi *et al.*[323] examined the transformation of celluloses between the cellulose I and cellulose II families by X-ray, IR and ^{13}C NMR methods. Cellulose derivatives such as cellulose nitrates and

acetates could also be analysed conveniently by means of high-resolution solid-state ^{13}C NMR spectroscopy.[324,328-330]

To a first approximation, wood is a mixture (or possibly a copolymer) of cellulose, lignin and hemicellulose.[331] The principal repeat units of lignin are a variety of phenylpropane, most significantly derivatives of syringyl- [**1**] and guaiacylpropane [**2**]. Many of the characteristic ^{13}C NMR peaks of

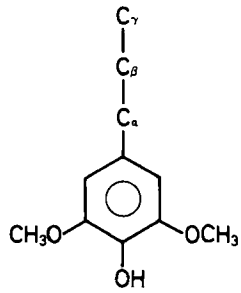

[**1**]

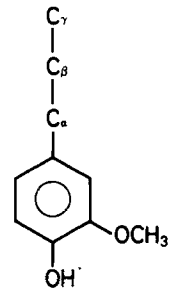

[**2**]

lignins[332-336] from various sources in the solid state are well separated from peaks of cellulose and hemicellulose. These peaks have been extensively analysed and assigned to the individual carbons, although several peaks are displaced from those previously published for the solution state. Hemicellulose, another component of wood, is a heteropolymer of several types of sugars. Many of the spectral features are similar to those of cellulose, although the hemicellulose signals tend to be broader, reflecting their heteropolymeric nature.[28,331,335] It is possible to analyse ^{13}C CP-MAS NMR spectra of whole wood samples to reveal lignin–carbohydrate interactions, lignin contents and structural changes occurring during different kinds of processing.[28,335,337-341] For example, Kolodziejski *et al.*[335] showed that grinding the wood has no effect on the ^{13}C NMR spectrum, but ball milling converts "crystalline" cellulose to the amorphous form. In addition, they provided indirect evidence for a lignin–carbohydrate complex in that all lignin fractions exhibit carbohydrate signals, and vice versa. Subsequently, Gerasimovicz *et al.*[342] used ^{13}C CP-MAS NMR techniques to examine relaxation profiles such as proton spin–lattice relaxation (T_1^H) and proton rotating-frame spin–lattice relaxation times ($T_{1\rho}^H$) to examine lignin–carbohydrate interactions. They found that proton spin diffusion is constant for all components, providing evidence for the existence of naturally occurring lignin–carbohydrate structures. As in isolated carbohydrates, water in wood and lignocellulosic materials markedly affect ^{13}C NMR spectra.[343,344]

4. Chitin, chitosan and other polysaccharides

Chitin [3] is a (1→4)-β-D-2-acetamido-2-deoxyglucan which is found in insect cuticles, shells of crustaceans and the cell walls of bacteria and fungi. Chitosan [4] is its deacetylated form as designated by (1→4)-β-

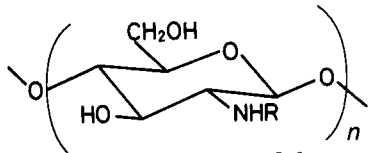

R=CH_3CO [3]
R=H [4]

D-2-amino-2-deoxyglucan. As expected from the similarity of their backbone structures, the fibre repeat of both polymers is identical with that of cellulose. Nevertheless, the ^{13}C NMR spectrum of chitin is much simpler than that of cellulose: the individual carbons give rise to single lines[91,345-347] (Fig. 34). Again, the ^{13}C CP-MAS NMR spectrum of the regenerated form of chitin, *N*-acetylchitosan, is the same as that of naturally occurring chitin, implying conformational similarity between the two compounds, although the ^{13}C NMR peaks of the former are much broader than those of the latter.[346,347]

The ^{13}C NMR spectral patterns of chitosans, on the other hand, are markedly different for the three preparations studied (Fig. 34). Chitosans from crab shell, shrimp shell and the annealed form at higher temperatures (220°C) produce different spectra, suggesting the presence of three polymorphs.[91,345-347] The C-1 and/or C-4 peaks of the polymorphs "tendon-chitosan" (crab shell) and "L-2" (shrimp shell) were split into doublets, whereas those of the "annealed" polymorph gave single lines. It is interesting to note that the non-equivalence of two chains in the unit cells of "tendon-chitosan" and "L-2" was made to disappear by the removal of water molecules in the annealing process ("annealed") or in the formation of metal complexes. Furthermore, it was found that the ^{13}C NMR technique could be applied to analyse conformational changes taking place due to the formation of salts and metal complexes.

Stipanovic *et al.* recorded ^{13}C NMR spectra of (1→6)-β-D-glucan (pustulan) in both the solid and the gel states.[348] They found that partially crystalline pustulan displays a resonance near 82 ppm that is absent in solution. This peak was also obtained in gels, suggesting that the gelation mechanism may involve a microcrystalline junction zone. Winter *et al.*[349] studied ^{13}C NMR and X-ray diffraction data of dermatan sulphate in the solid state in order to establish the ring conformation of the L-iduronate moiety. A $^1C_4$ ring conformation predominates in ^{13}C NMR data, whereas a

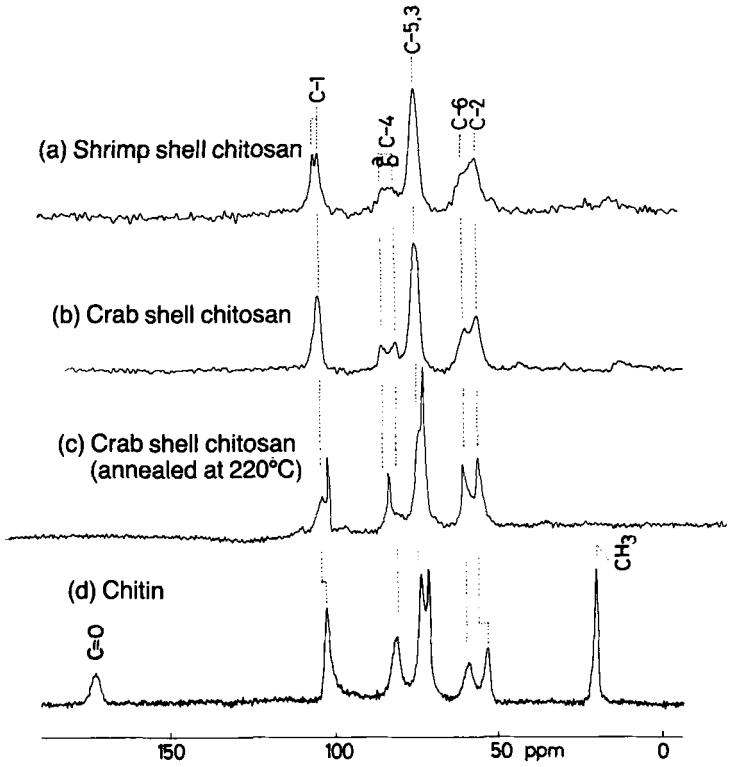

FIG. 34. 75.46 MHz ^{13}C CP-MAS NMR spectra of three preparations of chitosan (a–c) and of chitin (d) in the solid state. The broad component of signals in (c) was due to an unchanged fraction of (b). (Ref. 346.)

$^4C_1$ form was found from fibre diffraction studies. To provide a satisfactory interpretation these authors suggested that a distorted $^1C_4$ may emerge.

Schaefer *et al.*[350] analysed the cross-linking between the protein and chitin of insect cuticle by means of double labelling experiments with L-[1,3-^{15}N]histidine and [*ring*-^{13}C]dopamine using the technique of double cross-polarization.

D. Biomembranes and membrane-bound substances

In biological membranes or lipid bilayers, lipid molecules are known to undergo rapid conformational fluctuation as well as anisotropic rotation about an axis parallel to the bilayer normal, as has been revealed by a variety of physical means including ^2H NMR of selectively or uniformly ^2H-labelled lipids, ^{31}P NMR of head groups, and ^1H or ^{13}C NMR of sonicated

vesicles.[192,351-358] The observation of conventional high-resolution NMR spectra is hampered in these systems, except for sonicated vesicles, by the incomplete averaging of nuclear interactions such as dipolar, quadrupolar or chemical shielding anisotropy tensors. That is the reason why studies by ^{2}H or ^{31}P NMR spectroscopy are more suited than are others to the analysis of the organization, dynamics and polymorphs of lipid bilayers.

However, Harberkorn *et al.*[359] showed that high-resolution ^{13}C NMR spectra can be obtained from unsonicated multibilayer dispersions in the liquid crystalline state by MAS alone, because MAS can completely average residual dipolar interactions. More recently, Oldfield *et al.*[360,361] demonstrated that the resolution of ^{1}H and ^{13}C MAS NMR spectra of pure egg lecithin bilayers is essentially identical with that of sonicated samples. However, they showed that many of the cholesterol carbons in egg lecithin–cholesterol (1:1) which are not observable in the sonicated dispersion are made visible by the MAS experiment.[360] Yeagle and Frye[362] measured the spin–lattice relaxation times of individual carbons in unsonicated phospholipid bilayers by MAS. Sefcik *et al.*[363] studied the lipid bilayer dynamics of multilamellar dispersions of 1,2-dilauryl-1-*sn*-glycero-3-phosphocholine (DLPC), recombinant membranes containing DLPC and rhodopsin (66:1), and native retinal rod disk membranes. They noticed that rhodopsin reduces the rate of ultrahigh-frequency lipid motions as demonstrated by the rotating-frame ^{13}C relaxation times ($T_{1\rho}^{C}$) of membranes dominated by contributions from cooperative molecular or segmental fluctuations between 1 and 100 kHz.

Early works on the use of powder-pattern ^{13}C NMR to study biomembranes and lipid bilayers by cross-polarization were carried out by Waugh *et al.*[364,365] Subsequently, Cornell[366,367] showed that the powder-pattern ^{13}C NMR spectrum from the carbonyl groups consists of broad and narrow axially symmetric components which are assigned to the 1 and 2 positions, respectively, for liquid crystalline dimyristoylphosphatidylcholine (DMPC) and dipalmitoylphosphatidylcholine (DPPC). Cornell *et al.* also examined the interaction of lipids with cholesterol or gramicidin A:[368,369] these substances restrict the amplitude of the motion of lipid molecules, as shown by a decrease of T_{CH} and $T_{1\rho}^{H}$ values,[368] and alter the broad component (1 carbonyl, $\Delta\sigma = -29$ ppm) as a result of specific conformational change at this site.[369]

Witterbort *et al.*[370] recorded the temperature dependence of powder-pattern ^{13}C NMR spectra of ^{13}C-labelled 2-[1-^{13}C]DPPC as the *sn*-2 chain (narrow component) by a simple Hahn echo method. Cross-polarization was unnecessary in the hydrated system because of sufficiently short ^{13}C T_1 values. In the low temperature $L_{\beta'}$ gel phase, the *sn*-2 carbonyl exhibited an axially symmetric spectrum of 112 ppm breadth which collapsed to an

isotropic-like peak ($\Delta\sigma = -7$ ppm) in the liquid crystalline L_α phase. In the intermediate P_β phase, two peaks from the L_β and L_α ^{13}C NMR peaks were observed. These authors also demonstrated that this method is very useful, as a complementary technique to ^2H or ^{31}P powder-pattern NMR, for delineating phase equilibria in pure and mixed phospholipid bilayers[371-373] and the interaction with cholesterol or anaesthetic steroids.[374,375]

In the case of membrane proteins, it is impossible to record conventional high-resolution NMR spectra unless the membrane lipids are replaced by detergent to become "solubilized" in micelles, due to severe line-broadening caused by incomplete averaging of the dipolar interaction. These problems can be overcome by employing high-resolution solid-state NMR techniques. The application of these techniques to membrane proteins was reviewed in Section V.A. In this section we deal with solid-state ^{13}C NMR studies of ^{15}N- or ^{13}C-labelled retinal chromophores (Fig. 35(a)) in bacteriorhodopsin (bR) and bovine rhodopsin, in either lyophilized or hydrated forms.[375-383] Griffin *et al.*[377-382] and Mollenvanger *et al.*[383] measured the principal values of the ^{15}N and ^{13}C chemical shielding tensors of bR and rhodopsin and compared them with those of pertinent model compounds obtained from the rotating echo pattern of spinning sidebands.[16] Griffin *et al.*[379,381] showed that dark-adapted bR is composed of a mixture of all-*trans*,15-anti and 13-*cis*,15-syn isomers in the ratio 4:6. These isomers are identified as bR_{568} and bR_{548}, respectively, from the ^{13}C NMR peak-splitting (Fig. 35(a)). Griffin *et al.* demonstrated that the conformation of a 6s bond in hydrated bR is s-*trans* on the basis of a substantial high frequency signal displacement of ^{13}C-5-labelled bR, as compared with those of the ^{13}C-5 carbons of 6-s-*cis* (triclinic) and 6-s-*trans* (monoclinic) retinoic acid (Fig. 35(b)). This is in contrast to the 6-s-*cis* conformation that is energetically favoured for retinoids in solution. The additional 27 ppm high frequency in σ_{22} of the C-5 tensor was ascribed to the existence of a negatively charged protein residue near the C-5 atom (tensor components σ_{22} and σ_{33} lie in the plane of C=C double bond). In contrast, the isotropic chemical shift and principal values of the chemical shielding tensor of the ^{13}C-5 label in bovine rhodopsin indicated that the retinal chromophore is in the twisted 6-s-*cis* conformation in rhodopsin, rather than in the planar 6-s-*trans* conformation as in bR.[382,383]

V. CONCLUDING REMARKS

It is now clear that high-resolution solid-state NMR is an indispensable technique for routine analysis as well as for the study of the conformations and dynamics of various types of macromolecular systems. As described in the text, many experimental data have been accumulated so far. Nevertheless, it

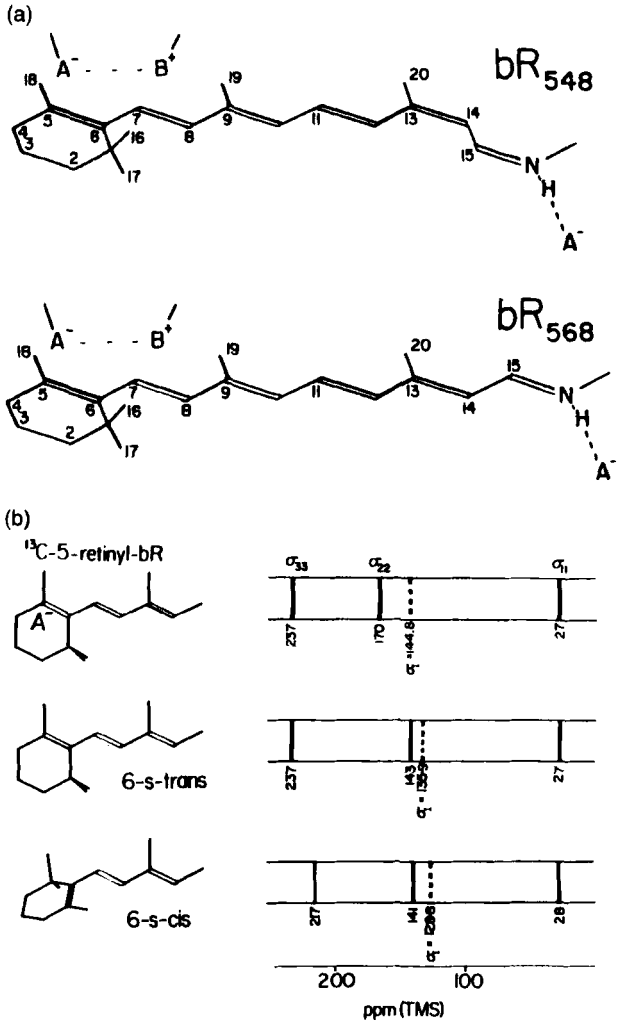

FIG. 35. (a) Structure of the retinal chromophores in bR_{548} and bR_{568} and (b) chemical shielding tensor elements of hydrated ^{13}C-5-labelled bR compared with those of ^{13}C-5 carbons in 6-s-*cis*-(triclinic) and 6-s-*trans*-(monoclinic) retinoic acid. (Ref. 381.)

appears that the mechanism of the displacement of peaks is still not well understood and further extensive work is required in this area. Another important future role for high-resolution solid-state NMR might be an extension to NMR imaging as a tool for materials research, for example in medical applications, although this is not included in the present chapter.

REFERENCES

1. J. Schaefer and E.O. Stejskal, *J. Am. Chem. Soc.*, 1976, **98**, 101.
2. A. Pines, M.G. Gibby and J.S. Waugh, *J. Chem. Phys.*, 1973, **59**, 569.
3. E.R. Andrew, *Prog. Nucl. Magn. Reson. Spectrosc.*, 1971, **8**, 1.
4. J. Schaefer and E.O. Stejskal, in *Topics in Carbon-13 NMR Spectroscopy*, Vol. 3 (G.C. Levy, ed.), Wiley-Interscience, New York, 1979, p. 284.
5. D.A. Torchia and D.L. VanderHart, in *Topics in Carbon-13 NMR Spectroscopy*, Vol. 3 (G.C. Levy, ed.), Wiley-Interscience, New York, 1979, p. 171.
6. J.R. Lyerla, in *Contemporary Topics in Polymer Science*, Vol. 3 (M. Shen, ed.), Plenum Publishing Corporation, New York, 1979, p. 143.
7. R.E. Wasylishen and C.A. Fyfe, *Ann. Rev. NMR Spectrosc.*, 1982, **12**, 1.
8. C.S. Yannoni, *Acc. Chem. Res.*, 1982, **15**, 201; J.R. Lyerla, C.S. Yannoni and C.A. Fyfe, *Acc. Chem. Res.*, 1982, **15**, 208.
9. J.R. Lyerla and C.S. Yannoni, *IBM J. Res. Dev.*, 1983, **27**, 302.
10. C.A. Fyfe, *Solid State NMR for Chemists*, C.F.C. Press, Guelph, Canada, 1983.
11. M. Mehring, *Principles of High Resolution NMR in Solids*, 2nd edn, Springer, Berlin, 1983.
12. B.C. Gerstein, *Anal. Chem.*, 1983, **55**, 781A, 899A.
13. B.C. Gerstein, *Topics in Carbon-13 NMR Spectroscopy*, Vol. 4 (G.C. Levy, ed.), Wiley-Interscience, New York, 1984, p. 123.
14. R.A. Komoroski, *High Resolution NMR Spectroscopy of Synthetic Polymers in Bulk* (R.A. Komoroski, ed.), VCH Publishers, Deerfield Beach, Florida, USA, 1986.
15. M. Maricq and J.S. Waugh, *J. Chem. Phys.*, 1979, **70**, 3300.
16. J. Herzfeld and A.E. Berger, *J. Chem. Phys.*, 1980, **73**, 6021.
17. W.T. Dixon, *J. Magn. Reson.*, 1981, **44**, 220.
18. S.J. Opella, J.G. Hexem, M.H. Frey and T.A. Cross, *Phil. Trans. R. Soc. Lond.*, 1981, **A299**, 665.
19. D.L. VanderHart, *J. Chem. Phys.*, 1986, **84**, 1196.
20. J.F. Haw, G.C. Campbell, and R.C. Crosby, *Anal. Chem.*, 1986, **58**, 3172.
21. J.F. Haw, R.A. Crook, and R.C. Crosby, *J. Magn. Reson.*, 1986, **66**, 551.
22. W.P. Aue, D.J. Ruben, and R.G. Griffin, *J. Magn. Reson.*, 1981, **43**, 472.
23. W.P. Aue, D.J. Ruben, and R.G. Griffin, *J. Chem. Phys.*, 1984, **80**, 1729.
24. A. Bax, N.M. Szeverenyi, and G.E. Maciel, *J. Magn. Reson.*, 1983, **52**, 147.
25. T. Terao, T. Fujii, T. Onodera, and A. Saika, *Chem. Phys. Lett.*, 1984, **107**, 145.
26. D.A. Torchia, *Methods Enzymol*, 1984, **82**, 174.
27. G.S. Harbison and H.W. Spiess, *Chem. Phys. Lett.*, 1986, **124**, 128.
28. G.R. Hatfield, M. Sardashti and G.E. Maciel, *Anal. Chem.*, 1987, **59**, 1659.
29. M.G. Munowitz, R.G. Griffin, G. Bodenhausen and T.H. Huang, *J. Am. Chem. Soc.*, 1981, **103**, 2529.
30. M.G. Munowitz and R.G. Griffin, *J. Chem. Phys.*, 1982, **76**, 2848; M.G. Munowitz, T.H. Huang, C.M. Dobson and R.G. Griffin, *J. Magn. Reson.*, 1984, **57**, 56.
31. J. Schaefer, R.A. McKay, E.O. Stejskal and W.T. Dixon, *J. Magn. Reson.*, 1983, **52**, 123.
32. J.S. Waugh, L.M. Huber and U. Haeberlen, *Phys. Rev. Lett.*, 1968, **20**, 180.
33. P. Mansfield, *J. Phys.*, 1971, **C4**, 1444; W.K. Rhim, D.D. Elleman and R.W. Vaughan, *J. Chem. Phys.*, 1973, **71**, 444.
34. J.E. Roberts, G.S. Harbison, M.G. Munowitz, J. Herzfeld and R.G. Griffin, *J. Am. Chem. Soc.*, 1987, **109**, 4163.

35. H.W. Spiess, *Colloid Polymer Sci.*, 1983, **261**, 193.
36. J. Schaefer, E.O. Stejskal, R.A. McKay and W.T. Dixon, *Macromolecules*, 1984, **17**, 1479.
37. N.M. Szeverenyi, M.J. Sullivan and G.E. Maciel, *J. Magn. Reson.*, 1982, **47**, 462.
38. N.M. Szeverenyi, A. Bax and G.E. Maciel, *J. Am. Chem. Soc.*, 1983, **105**, 2579.
39. M.H. Frey and S.J. Opella, *J. Am. Chem. Soc.*, 1984, **106**, 4942.
40. H.J. Edzes and J.P.C. Bernards, *J. Am. Chem. Soc.*, 1984, **106**, 1515.
41. C.E. Bronniman, N.M. Szeverenyi, and G.E. Maciel, *J. Chem. Phys.*, 1983, **79**, 3694.
42. A.F. De Jong, A.P.M. Kentgens, and W.S. Veeman, *Chem. Phys. Lett.*, 1984, **109**, 337.
43. A.P.M. Kentgens, E. deBoer, and W.S. Veeman, *J. Chem. Phys.*, 1987, **87**, 6859.
44. P. Caravatti, G. Bodenhausen, and R.R. Ernst, *J. Magn. Reson.*, 1983, **55**, 88.
45. D.A. Torchia, *J. Magn. Reson.*, 1978, **30**, 613.
46. G. Bodenhausen, R. Freeman and C.A. Morris, *J. Magn. Reson.*, 1976, **23**, 171.
47. M. Linder, P.M. Henrichs, J.M. Hewitt and D.J. Massa, *J. Chem. Phys.*, 1985, **82**, 1585.
48. A.K. Roy, P.T. Inglefield, J.H. Shibata and A.A. Jones, *Macromolecules*, 1987, **20**, 1437.
49. D.L. VanderHart, *J. Magn. Reson.*, 1987, **72**, 13.
50. H. Saitô, R. Tabeta, A. Shoji, T. Ozaki, I. Ando and T. Asakura, *Magnetc Resonance in Biology and Medicine* (G. Govil, C.L. Ketherapal and A. Saran, eds), Tata McGraw-Hill, New Delhi, 1985, pp. 195–215.
51. H. Saitô, *Magn. Reson. Chem.*, 1986, **24**, 835.
52. J. Schaefer, E.O. Stejskal and R. Buchdall, *Macromolecules*, 1977, **10**, 384.
53. A.N. Garroway, W.M. Ritchey and W.B. Moniz, *Macromolecules*, 1982, **15**, 1051.
54. H. Saitô, M. Yokoi, M. Aida, M. Kodama, T. Oda and Y. Sato, *Magn. Reson. Chem.*, 1988, **26**, 155.
55. R. Tebeta and H. Saitô, *Biochemistry*, 1985, **24**, 7696.
56. H. Saitô, R. Tabeta and M. Yokoi, *Magn. Reson. Chem.*, 1988, **26**, 775.
57. H. Saitô, R. Tabeta, F. Formaggio, M. Crisma and C. Toniolo, *Biopolymers*, 1988, **27**, 1607.
58. D.L. VanderHart, W.L. Earl and A.N. Garroway, *J. Magn. Reson.*, 1981, **44**, 361.
59. D.L. VanderHart, *J. Magn. Reson.*, 1981, **44**, 117.
60. I. Ando and G.A. Webb, *Theory of NMR Parameters*, Academic Press, London, 1983.
61. I. Ando, H. Saitô, R. Tabeta, A. Shoji and T. Ozaki, *Macromolecules*, 1984, **17**, 457.
62. J.-M. Andre and J. Ladik (eds), *Electronic Structure of Polymers and Molecular Crystals*, Plenum Press, New York, 1974.
63. J. Ladik, J.-M. Andre and M. Seel (eds), *Quantum Chemistry of Polymers - Solid State Aspects*, Reidel, Dordrecht, 1984.
64. T. Yamanobe, R. Chujo and I. Ando, *Mol. Phys.*, 1985, **50**, 3154.
65. T. Yamanobe and I. Ando, *J. Chem. Phys.*, 1985, **83**, 3154.
66. T. Yamanobe, I. Ando, H. Saitô, R. Tabeta, A. Shoji and T. Ozaki, *Bull. Chem. Soc. Jpn*, 1985, **58**, 23.
67. T. Yamanobe, I. Ando, H. Saitô, R. Tabeta, A. Shoji and T. Ozaki, *Chem. Phys.*, 1985, **99**, 259.
68. H. Kurosu, T. Yamanobe, T. Komoto and I. Ando, *Chem. Phys.*, 1987, **116**, 391.
69. T. Yamanobe, I. Ando and G.A. Webb, *J. Mol. Struc.*, 1987, **151**, 191.
70. H. Kurosu, T. Yamanobe and I. Ando, *J. Chem. Phys.*, 1989, **90** (in press).
71. D.L. VanderHart and A.N. Garroway, *J. Chem. Phys.*, 1979, **71**, 2773.
72. D.C. Douglass and C.P. Jones, *J. Chem. Phys.*, 1966, **45**, 956.
73. V.J. McBrierty, *Faraday Discuss. Chem. Soc.*, 1979, **68**, 78.

74. J. Schaefer, M.D. Sefcik, E.O. Stejskal and R.A. McKay, *Polymer Prep. Am. Chem. Soc. Div. Polymer Chem.*, 1979 **20**, 247.
75. E.O. Stejskal, J. Schaefer, M.D. Sefcik and R.A. McKay, *Macromolecules*, 1981, **14**, 275.
76. J. Schaefer, M.D. Sefcik, E.O. Stejskal and R.A. McKay, *Macromolecules*, 1981, **14**, 188.
77. W.L. Earl and D.L. VanderHart, *Macromolecules*, 1979, **12**, 762.
78. E.M. Menger, W.S. Veeman and E. de Boer, *Macromolecules*, 1982, **15**, 1406.
79. J.R. Lyerla, in *High Resolution NMR Spectroscropy of Synthetic Polymers in Bulk* (R.A. Komoroski, ed.), VCH Publishers, Deerfield Beach, Florida, 1986, pp. 121–152.
80. A. Naito, S. Ganapathy, K. Akasaka and C.A. McDowell, *J. Magn. Reson.*, 1983, **54**, 226.
81. H. Saitô, R. Tabeta, M. Yokoi and T. Erata, *Bull. Chem. Soc. Jpn*, 1987, **60**, 4259.
82. E.O. Stejskal, J. Schaefer and T.R. Steger, *Faraday Soc. Symp.*, 1979, **13**, 56.
83. J. Schaefer, E.O. Stejskal, T.R. Steger, M.D. Sefcik and R.A McKay, *Macromolecules*, 1980, **13**, 1121.
84. W.P. Rothwell and J.S. Waugh, *J. Chem. Phys.*, 1981, **74**, 2721.
85. F. Laupretre, L. Monnerie and J. Virlet, *Macromolecules*, 1984, **17**, 1397.
86. S.J. Opella, P.L. Stewart and K.G. Valentine, *Q. Rev. Biophys.*, 1987, **19**, 7.
87. H. Shindo, in *Phosphorus-31 NMR* (D.G. Gorenstein, ed.), Academic Press, Orlando, Florida, 1984, p. 401.
88. H. Shindo, in *Magnetic Resonance in Biology* (J.S. Cohen, ed.), John Wiley & Sons, New York, 1983, p. 95.
89. H. Shindo, *Adv. Biophys.*, 1985, **20**, 39.
90. R.H. Atalla (ed.), *The Structure of Cellulose*, ACS Symp. Ser. No. 340, American Chemical Society, Washington, D.C., 1987.
91. H. Saitô, R. Tabeta and K. Ogawa, *Macromolecules*, 1987, **20**, 2424.
92. T. Asakura, A. Kuzuhara, R. Tabeta and H. Saito, *Macromolecules*, 1985, **18**, 1841.
93. S. Harbison, V.-D. Vogt and H.W. Spiess, *J. Chem. Phys.*, 1987, **86**, 1206.
94. D. Bauer, *Prog. Org. Coat.*, 1986, **14**, 45.
95. R.A. Komoroski, J.P. Shockcor and J.L. Savoca, *Sagamore Army Mater. Res. Con.*, 1987, **32**, 55.
96. H.W. Spiess, *Phys. B1*, 1987, **43**, 233.
97. W.S. Veeman, A.P.M. Kentgens and R. Janssen, *Fresenius Z. Anal. Chem.*, 1987, **327**, 63.
98. M.G. Broadhurst, *J. Res. Natl. Bur. Stand.*, 1962, **A66**, 241.
99. I. Ando, T. Sorita, T. Yamanobe, T. Komoto, H. Sato, K. Deguchi and M. Imanari, *Polymer*, 1985, **26**, 1864.
100. H.E. Tonelli and F.C. Schilling, *Acc. Chem. Res.*, 1981, **14**, 233.
101. T. Yamanobe, T. Sorita, I. Ando and H. Sato, *Makromol. Chem.*, 1985, 1 862 071.
102. N.J. Sheppard and G.J. Szasz, *J. Chem. Phys.*, 1962, **17**, 86.
103. M. Okazaki and C.A. McDowell, *Chem. Phys. Lett.*, 1983, **102**, 20.
104. M. Okazaki and C.A. McDowell, *J. Mol. Struc.*, 1984, **118**, 149.
105. I. Ando, T. Yamanobe, T. Sorita, T. Komoto, H. Sato, K. Deguchi and M. Imanari, *Macromolecules*, 1984, **17**, 1955.
106. M. Möller, W. Gronski, H.-J. Cantow and H. Höcker, *J. Am. Chem. Soc.*, 1984, 1 065 093.
107. M.-J. Cantow, D. Emeis, W. Gronski, A. Hasenhidle, D. Lansberg, M. Möller and Y. Shahab, *Makromol. Chem. Suppl.*, 1984, **7**, 63.
108. B.A. Newman and M.K. Kay, *J. Appl. Phys.*, 1967, **38**, 4105.

109. P. Groth, *Acta. Chem. Scand.*, 1979, **A33**, 199.
110. F.A.L. Anet and A.K. Cheng, *J. Am. Chem. Soc.*, 1975, **97**, 2420.
111. M. Takenaka, T. Yamanobe, T. Komoto, I. Ando, H. Sato and K. Sato, *J. Polymer Sci., Polymer Phys.*, 1987, **25**, 2165.
112. T. Sorita, T. Yamanobe, T. Komoto, I. Ando, H. Sato, K. Deguchi and M. Imanari, *Makromol. Chem., Rapid Commun.*, 1985, **5**, 657.
113. M. Takenaka, T. Yamanobe, T. Komoto, I. Ando and H. Sato, *Solid State Commun.*, 1987, **61**, 563.
114. D.L. VanderHart and E. Perez, *Macromolecules*, 1986, **19**, 1902.
115. M. Möller, H.-J. Cantow, J.K. Kruger and H. Höcker, *Polymer Bull.*, 1981, **5**, 125.
116. D.E. Axelson, L. Manderkern, R. Popli and P. Mathieu, *J. Polymer Sci., Polymer Phys.*, 1983, **21**, 2319.
117. R. Kitamaru, F. Horii and F. Murayama, *Polymer Bull.*, 1982, **7**, 583.
118. D.E. Axelson, *J. Polymer Sci., Polymer Phys.*, 1982, **20**, 1427.
119. R. Kitamaru, F. Horii and K. Murayama, *Macromolecules*, 1986, **19**, 636.
120. D.L. VanderHart and F. Khoury, *Polymer*, 1984, **25**, 1589.
121. D.L. VanderHart, *J. Magn. Reson.*, 1987, **72**, 13.
122. I. Ando, T. Yamanobe, S. Akiyama, T. Komoto, H. Sato, T. Fujito, K. Deguchi and M. Imanari, *Solid State Commun.*, 1987, **62**, 785.
123. D.L. VanderHart, *J. Chem. Phys.*, 1976, **64**, 830.
124. S.J. Opella and J.S. Waugh, *J. Chem. Phys.*, 1977, **66**, 4919.
125. T. Yamanobe, M. Tsukahara, T. Komoto, J. Watanabe, I. Ando, I. Uematsu, K. Deguchi, T. Fujito and M. Imanari, *Macromolecules*, 1988, **21**, 48.
126. A. Bunn, M.E.A. Cudby, R.K. Harris, K.J. Packer and B.J. Say, *J. Chem. Soc., Chem. Commun.*, 1981, 15.
127. A. Bunn, M.E.A. Cudby, R.K. Harris, K.J. Packer and B.J. Say, *Polymer*, 1982, **23**, 694.
128. L.A. Belfiore, F.C. Schilling, A.E. Tonelli, A.J. Lovinger and F.A. Bovey, *Macromecules*, 1984, **17**, 2561.
129. M.E.A. Cudby, R.K. Harris, K. Metcalfe, K.J. Packer, P.W.R. Smith and A. Bunn, *Polymer*, 1985, **26**, 169.
130. W. Gronski, A. Hasenhindl, H. Limbach, M. Moller, H.-J. Cantow, *Polymer Bull.*, 1981, **6**, 93.
131. M. Möller and H.-J. Cantow, *Polymer Bull.*, 1981, **5**, 119.
132. M. Möller and H.-J. Cantow, *Macromolecules*, 1984, **17**, 733.
133. T. Ito, H. Shirakawa and S. Ikeda, *J. Polymer Sci., Polymer Phys.*, 1974, **12**, 11.
134. H. Shirakawa, E.J. Loius, A.G. MacDiarmid, C.K. Chiang and A.J. Heeger, *J. Chem. Soc., Chem. Commun.*, 1977, 578.
135. M.M. Maricq, J.S. Waugh, A.G. MacDiarmid, H. Shirakawa and A.J. Heeger, *J. Am. Chem. Soc.*, 1978, **100**, 7729.
136. T. Terao, S. Maeda, T. Yamabe, K. Akagi and H. Shirakawa, *Chem. Phys. Lett.*, 1984, **103**, 347.
137. H.W. Gibson, J.M. Pochan and S. Kaplan, *J. Am. Chem. Soc.*, 1981, **103**, 4619.
138. M. Peo, H. Forster, K. Menke, J. Höcker, J.A. Gardner, S. Roth and K. Dransfeld, *Solid State Commun.*, 1981, **38**, 467.
139. M. Peo, H. Forster, K. Menke, J. Höcker, J.A. Gardner, S. Roth and K. Dransfeld, *Mol. Cryst. Liq. Cryst.*, 1981, **77**, 103.
140. T.C. Clarke and J.C. Scott, *Solid State Commun.*, 1982, **41**, 389.
141. T. Terao, S. Maeda, T. Yamabe, K. Akagi and H. Shirakawa, *Solid State Commun.*, 1984, **49**, 829.

142. M. Mehring, H. Weber, W. Muller and G. Wegner, *Solid State Commun.*, 1983, **45**, 1079.
143. C.E. Brown, M.B. Jones and P. Kovacic, *J. Polymer Sci., Polymer Lett.*, 1980, **18**, 653.
144. C.E. Brown, I. Khoury, M.D. Bezoari and P. Kovacic, *J. Polymer Sci., Polymer Chem.*, 1982, **20**, 1697.
145. T.C. Clarke, J.C. Scott and G.B. Street, *IBM J. Res. Dev.*, 1983, **27**, 313.
146. F. Devreux, G. Bidan, A.A. Syed and C. Isintavis, *J. Phys.*, 1985, **46**, 1595.
147. C.A. Fyfe, A. Rudin and W.J. Tchir, *Macromolecules*, 1982, **15**, 1218.
148. R.L. Bryson, G.R. Hatfield, T.A. Early, A.R. Palmer and G.E. Maciel, *Macromolecules*, 1983, **16**, 1669.
149. C.A. Fyfe, M.S. KcKinnon, A. Rudin and W.J. Tchir, *Macromolecules*, 1983, **16**, 1216.
150. C.A. Fyfe, M.S. McKinnon, A. Rudin and W.J. Tchir, *J. Polymer Sci., Polymer Lett.*, 1983, **23**, 249.
151. S. So and A. Rudin, *J. Polymer Sci., Polymer Lett.*, 1985, **23**, 403.
152. G. Hatfield and G.E. Maciel, *Macromolecules*, 1987, **20**, 608.
153. G.E. Maciel, N.M. Szeverenyi, T.A. Early and G.E. Myers, *Macromolecules*, 1985, **16**, 598.
154. G.E. Maciel, I.-S. Chuang and G.E. Myers, *Macromolecules*, 1982, **15**, 1218.
155. I.-S. Chuang, G.E. Maciel and G.E. Myers, *Macromolecules*, 1984, **174**, 1087.
156. G.E. Maciel, I.-S. Chuang and L. Gollob, *Macromolecules*, 1984, **17**, 1081.
157. R.K. Harris, K.J. Packer and B.J. Say, *Makromol. Chem., Suppl.*, 1981, **4**, 117.
158. A.N. Garroway, D.L. VanderHart and W.L. Earl, *Phil. Trans. R. Soc. Lond.*, 1981, **A299**, 609.
159. A. Cholli, W.M. Ritchey and J. Koenig, *Am. Chem. Soc. Org. Coat., Appl. Polymer Sci. Proc.*, 1983, **48**, 450.
160. M.F. Grenier-Loustalot, F. Cazaux, J. Berecoechea and P. Grenier, *Eur. Polymer J.*, 1984, **20**, 1137.
161. J. Ancelle, A.J. Attias, B. Bloch, C. Cavalli, B. Jasse, F. Laupretre and L. Monnerie, *Crosslinked Epoxies, Proc. D*, 1987, 213.
162. M.D. Sefcik, E.O. Stejskal, R.A. McKay and J. Schaefer, *Macromolecules*, 1979, **12**, 423.
163. A.C. Wong, A.N. Garroway and W.M. Ritchey, *Macromolecules*, 1981, **14**, 832.
164. A.M. Zaper, A. Cholli and J.L. Koenig, *Polymer Sci. Technol.*, 1985, **27**, 299.
165. F. Laupretre, L. Monnerie and B. Bloch, *Anal. Chim. Acta*, 1986, **189**, 117.
166. W.S. Veeman, E.M. Menger, W. Ritchey and E. de Boer, *Macromolecules*, 1979, **12**, 924.
167. A.P.M. Kentgens, A.F. de Jong, E. de Boer and W.S. Veeman, *Macromolecules*, 1985, **18**, 1045.
168. G. Carazzolo and M. Mammi, *J. Polymer Sci.*, 1963, **A1**, 965.
169. M. Kobayashi, Y. Ihto, H. Tadokoro, M. Shimomura and M. Iguchi, *Polymer Commun.*, 1983, **24**, 38.
170. H. Kurosu, T. Komoto and I. Ando, *J. Mol. Struc.*, 1988, **176**, 279.
171. H. Kurosu, T. Yamanobe and I. Ando, *J. Chem. Phys.*, 1988, **89**, 5216.
172. R. Tabeta and H. Saitô, *Bull. Chem. Soc.*, 1985, **58**, 3215.
173. E. Perez and D.L. VanderHart, *Polymer*, 1987, **28**, 733.
174. F.A. Bovey and F.H. Winslow (eds), *Macromolecules. An Introduction to Polymer Science*, Academic Press, New York, 1979.
175. H.T. Edzes and W.S. Veeman, *Polymer Bull.*, 1981, **5**, 255.
176. J. Schaefer, E.O. Stejskal and R. Buchdall, *Macromolecules*, 1975, **8**, 291.
177. G.C. Gobbi, R. Silvestri, T.P. Russell, J.R. Lyerla and W.W. Fleming, *J. Polymer Sci., Polymer Lett.*, 1987, **25**, 61.
178. J.F. Parmer, L.C. Dickinson, J.C.W. Chien and Roger. S. Porter, *Macromolecules*, 1987, **20**, 2308.

179. B.C. Gerstein and C.R. Dybowski, *Transient Techniques in NMR of Solids*, Academic Press, New York, 1985.
180. Y.S. Jo, Y. Maruyama, Y. Inoue, R. Chujo, S. Tasaka and S. Miyata, *Polymer J.*, 1987, **19**, 769.
181. L.A. Belfiore, *Polymer*, 1986, **27**, 80.
182. G.L. Marshall, M.E.A. Cudy, K. Smith, T.H. Stevenson, K. Packer and R.K. Harris, *Polymer*, 1987, **28**, 1093.
183. G. VanderVelden, G. Kolfschoten-Smitsmans and A. Veermans, *Polymer Commun.*, 1987, **28**, 169.
184. P. Bergmark and P. Flodin, *Polymer*, 1987, **28**, 1657.
185. T. Uryu and T. Kato, *Chem. Lett.*, 1987, 211.
186. P.M. Henrichs, M. Linder, J.M. Hewitt, D. Massa and H. Isacson, *Macromolecules*, 1984, **17**, 2412.
187. A. Roy, A.A. Jones and P.T. Inglefield, *Macromolecules*, 1986, **19**, 1356.
188. L. Carton, R. Copperthwaite, G.J. Hutchings and E.C. Reynhardt, *J. Chem. Soc., Chem. Commun.*, 1986, 1008.
189. A.K. Roy, P.T. Inglefield, J.H. Shibata and A.A. Jones, *Macromolecules*, 1987, **20**, 1434.
190. T. Terao, S. Maeda and A. Saika, *Macromolecules*, 1983, **16**, 1535.
191. D.A. Torchia and D.L. VanderHart, in *Topics in Carbon-13 NMR Spectroscopy*, Vol. 3 (G.C. Levy, ed.), John Wiley & Sons, New York, 1979, p. 325.
192. R.G. Griffin, *Methods Enzymol*, 1981, **72**, 108.
193. L.M. Gierasch, S.J. Opella and M.H. Frey, in *Proc. 7th American Peptide Symposium* (D.H. Rich and E. Cross, eds), Pierce Chemical Co., Illinois, 1981, p. 267.
194. L.M. Gierasch, M.H. Frey, J.G. Hexem and S.J. Opella, *Am. Chem. Soc. Symp. Ser.*, No. 191, 1982, 233.
195. S.J. Opella, *Ann. Rev. Phys. Chem.*, 1982, **33**, 533.
196. K.N. Ganesh, *Curr. Sci.*, 1982, **51**, 866.
197. D.A. Torchia, *Ann. Rev. Biophys. Bioeng*, 1984, **13**, 125.
198. K.N. Ganesh, *Appl. Spectrosc. Rev.*, 1984, **20**, 107.
199. S.J. Opella and L.M. Gierasch, *The Peptides: Analysis, Synthesis, Biology*, Vol. 7 (S. Undernfriend and J. Meienhofer, eds), Academic Press, Orlando, 1985, p. 405.
200. S.J. Opella, *Methods Enzymol*, 1986, **131**, 327.
201. H. Saitô, R. Tabeta, A. Shoji, T. Ozaki and I. Ando, *Macromolecules*, 1983, **16**, 1050.
202. T. Taki, S. Yamashita, M. Satoh, A. Shibata, T. Yamashita, R. Tabeta and H. Saitô, *Chem. Lett.*, 1981, 1803.
203. H. Saitô, Y. Iwanaga, R. Tabeta, M. Narita and T. Asakura, *Chem. Lett.*, 1983, 427.
204. H. Saitô, R. Tabeta, I. Ando, T. Ozaki and A. Shoji, *Chem. Lett.*, 1983, 1437.
205. S. Ando, I. Ando, A. Shoji and T. Ozaki, *J. Am. Chem. Soc.*, 1988, **110**, 3380.
206. H. Saitô, R. Tabeta, A. Shoji, T. Ozaki, I. Ando and T. Miyata, *Biopolymers*, 1984, **23**, 2279.
207. H. Saitô, R. Tabeta, T. Asakura, Y. Iwanaga, A. Shoji, T. Ozaki and I. Ando, *Macromolecules*, 1984, **17**, 1405.
208. A. Shoji, T. Ozaki, H. Saitô, R. Tabeta and I. Ando, *Macromolecules*, 1984, **17**, 1472.
209. S. Ando, T. Yamanobe, I. Ando, A. Shoji, T. Ozaki, R. Tabeta and H. Saitô, *J. Am. Chem. Soc.*, 1985, **107**, 7648.
210. S. Tuzi, T. Komoto, I. Ando, H. Saitô, A. Shoji and T. Ozaki, *Biopolymers*, 1987, **26**, 1983.
211. H. Miyamoto, R. Takezaki, T. Komoto, I. Ando, H. Saitô, T. Ozaki and A. Shoji, *J. Mol. Struc.*, 1988, **172**, 395.
212. D. Muller and H.R. Kricheldorf, *Polymer Bull.*, 1981, **6**, 101.

213. H.R. Kricheldorf, D, Muller and H. Forster, *Polymer Bull.*, 1982, **8**, 487.
214. H.R. Kricheldorf, M. Mutter, F. Maser, D. Müller and H. Forster, *Biopolymers*, 1983, **22**, 1357.
215. H.R. Kricheldorf and D. Müller, *Macromolecules*, 1983, **16**, 615.
216. H.R. Kricheldorf and D. Müller, *Int. J. Biol. Macromol.*, 1983, **5**, 171.
217. H.R. Kricheldorf and D. Müller, *Polymer Bull.*, 1983, **10**, 513.
218. H.R. Kricheldorf, D. Müller, and K. Ziegler, *Polymer Bull.*, 1983, **9**, 284.
219. J. Stulz, D. Müller, W.E. Hull and K.R. Kricheldorf, *Macromol. Chem.*, 1983, **184**, 1311.
220. D. Müller, J. Stulz and H.R. Kricheldorf, *Int. J. Biol. Macromol.*, 1984, **6**, 81.
221. H.R. Kricheldorf and D. Müller, *Int. J. Biol. Macromol.*, 1984, **6**, 145.
222. H.R. Kricheldorf and D. Müller, *Coll. Polymer Sci.*, 1984, **262**, 856.
223. H. Pivcova, V. Saudek, P. Schmidt, D. Hlavata, J. Plestill and F. Laupretre, *Polymer*, 1987, **28**, 991.
224. J.G. Hexem, M.H. Frey and S.J. Opella, *J. Am. Chem. Soc.*, 1981, **103**, 224.
225. N. Zumbulyadis, P.M. Henrichs and R.H. Young, *J. Chem. Phys.*, 1981, **75**, 1603.
226. A. Naito, S. Ganapathy and C.A. McDowell, *J. Chem. Phys.*, 1981, **74**, 5393.
227. J.G. Hexem, M.H. Frey and S.J. Opella, *J. Chem. Phys.*, 1982, **77**, 3847.
228. O. Jardetzky and W.G. Wade-Jardetzky, *FEBS Lett.*, 1980, **110**, 133.
229. G.E. Maciel, M.P. Shatlock, R.A. Houtchens and W.S. Caughey, *J. Am. Chem. Soc.*, 1980, **102**, 6884.
230. T.-H. Huang, W.W. Bachovchin, R.G. Griffin and C.M. Dobson, *Biochemistry*, 1984, **23**, 5933.
231. N.E. Mackenzie, P.E. Fagerness and A.I. Scott, *J. Chem. Soc. Chem. Commun.*, 1985, 635.
232. A. Shoji, T. Ozaki, H. Saitô, R. Tabeta and I. Ando, *Makromol. Chem. Rapid Commun.*, 1984, **5**, 799.
233. L.G. Pease, M.H. Frey and S.J. Opella, *J. Am. Chem. Soc.*, 1981, **103**, 467.
234. M.H. Frey, S.J. Opella, A.L. Rockwell and L.M. Gierasch, *J. Am. Chem. Soc.*, 1985, **107**, 1946.
235. M.H. Frey, J.A. DiVerdi and S.J. Opella, *J. Am. Chem. Soc.*, 1985, **107**, 7311.
236. J. Schaefer, E.O. Stejskal, R.A. McKay and W.T. Dixon, *J. Magn. Reson.*, 1984, **57**, 85.
237. J.L. Flippen-Anderson, R. Gilardi, I.L. Karle, M.H. Frey, S.J. Opella, L.M. Gierasch, M. Goodman, V. Madison and N.G. Delaney, *J. Am. Chem. Soc.*, 1983, **105**, 6609.
238. S.K. Sarkar, D.A. Torchia, K.D. Kopple and D.L. VanderHart, *J. Am. Chem. Soc.*, 1984, **106**, 3328.
239. H.R. Kricheldorf, E.T.K. Haupt and D. Muller, *Magn. Reson. Chem.*, 1986, **24**, 41.
240. H. Saitô and R. Tabeta, *Chem. Lett.*, 1985, 83.
241. H. Saitô and R. Tabeta, *Peptide Chemistry 1987, Proceedings of Japan Symposium on Peptide Chemistry, Kobe, 1987*, (T. Shibata and S. Sakakibara, eds), Protein Research Foundation, Osaka, 1988, pp. 53–58.
242. C. Toniolo, G.M. Bonora, A. Bavoso, E. Benedetti, B. Di Blasio, V. Pavone and C. Pedone, *Biopolymers*, 1983, **22**, 205.
243. L.W. Jelinski and D.A. Torchia, *J. Mol. Biol.*, 1979, **133**, 45.
244. S.K. Sarkar, C.E. Sullivan and D.A. Torchia, *J. Biol. Chem.*, 1983, **258**, 9762.
245. S.K. Sarkar, C.E. Sullivan and D.A. Torchia, *Biochemistry*, 1985, **24**, 2348.
246. T. Fujiwara, Y. Kobayashi, Y. Kyogoku and K. Kataoka, *J. Mol. Biol.*, 1986, **187**, 137.
247. R. Smith and B.A. Cornell, *Biophys. J.*, 1986, **49**, 117.
248. B. Cornell, F. Separovic, A.J. Baldassi and R. Smith, *Biophys. J.*, 1988, **53**, 67.
249. B.A. Lewis, G.S. Harbison, J. Herzfeld and R.G. Griffin, *Biochemistry*, 1987, **24**, 4671.
250. T.A. Cross, J.A. Diverdi and S.J. Opella, *J. Am. Chem. Soc.*, 1982, **104**, 1759.
251. C.M. Gall, T.A. Cross, J.A. Diverdi and S.J. Opella, *Proc. Natl Acad. Sci. USA*, 1982, **79**, 101.

252. T.A. Cross, M.H. Frey and S.J. Opella, *J. Am. Chem. Soc.*, 1983, **105**, 7471.
253. A. Cross, P. Tsang and S.J. Opella, *Biochemistry*, 1983, **22**, 721.
254. T.A. Cross and S.J. Opella, *J. Am. Chem. Soc.*, 1983, **105**, 306.
255. T.A. Cross and S.J. Opella, *J. Mol. Biol.*, 1983, **182**, 367.
256. R.E. Stark, L.W. Jelinski, D.J. Ruben, D.A. Torchia and R.G. Griffin, *J. Magn. Reson.*, 1983, **55**, 266.
257. T.G. Oas, C.J. Hartzell, T.J. McMahon, G.P. Drobny and F.W. Dahlquist, *J. Am. Chem. Soc.*, 1987, **109**, 5956.
258. T.G. Oas, C.J. Hartzell, F.W. Dahlquist and G.P. Drobny, *J. Am. Chem. Soc.*, 1987, **109**, 5962.
259. C.J. Hartzell, M. Whitfield and G.P. Drobny, *J. Am. Chem. Soc.*, 1987, **109**, 5966.
260. D.M. Schneider, R. Tycko and S.J. Opella, *J. Magn. Reson.*, 1987, **73**, 568.
261. C.-J. Chang, L.E. Diaz, W.R. Woolfenden and D.M. Grant, *J. Org. Chem.*, 1982, **47**, 5318.
262. J.A. DiVerdi and S.J. Opella, *J. Am. Chem. Soc.*, 1982, **104**, 1761.
263. M.A. Hemminga, P.A. de Jager, J. Kruse and R.M.J. N. Lamerichs, *J. Magn. Reson.*, 1987, **71**, 446.
264. H. Shindo and S.B. Zimmerman, *Nature*, 1980, **283**, 690.
265. H. Shindo, J.B. Wooten, B.H. Pheiffer and S.B. Zimmerman, *Biochemistry*, 1980, **19**, 518.
266. H. Shindo, J.B. Wooten and S.B. Zimmerman, *Biochemistry*, 1981, **20**, 745.
267. H. Shindo, U. Matsumoto, H. Akutsu and T. Fujiwara, in *Nucleic Acids: The Vector of Life* (B. Pullman and J. Jortner, eds), D. Reidel, Dordrecht, 1983, pp. 169–182.
268. H. Shindo and U. Matsumoto, *J. Biol. Chem.*, 1984, **259**, 8682.
269. H. Shindo, T. Fujiwara, H. Akutsu, U. Matsumoto and Y. Kyogoku, *Biochemistry*, 1985, **24**, 887.
270. T. Fujiwara and H. Shindo, *Biochemistry*, 1985, **24**, 896.
271. B.T. Nall, W.P. Rothwell, J.S. Waugh and A. Rupprecht, *Biochemistry*, 1981, **20**, 1881.
272. J.A. DiVerdi and S.J. Opella, *J. Mol. Biol.*, 1981, **149**, 307.
273. J.A. DiVerdi and S.J. Opella, *Biochemistry*, 1981, **20**, 280.
274. T. Terao, S. Matsui and K. Akasaka, *J. Am. Chem. Soc.*, 1977, **99**, 6136.
275. H. Saitô and R. Tabeta, *Chem. Lett.*, 1981, 713.
276. R.H. Marchessault, M.G. Taylor, C.A. Fyfe and R.P. Veregin, *Carbohydrate Res.*, 1983, **144**, C1.
277. M.J. Gidley and S.M. Bociek, *J. Am. Chem. Soc.*, 1985, **107**, 7040.
278. F. Horii, A. Hirai and R. Kitamaru, *Macromolecules*, 1986, **19**, 930.
279. R.P. Veregin, C.A. Fyfe, R.H. Marchessault and M.G. Taylor, *Macromolecules*, 1986, **19**, 1030.
280. F. Horii, H. Yamamoto, A. Hirai and R. Kitamaru, *Carbohydrate Res.*, 1987, **160**, 29.
281. H. Saitô, G. Izumi, T. Mamizuka, S. Suzuki and R. Tabeta, *J. Chem. Soc. Chem. Commun.*, 1982, 1386.
282. Y. Inoue, T. Okuda and R. Chûjô, *Carbohydrate Res.*, 1985, **141**, 179.
283. M.J. Gidley and S.M. Bociek, *J. Chem. Soc. Chem. Commun.*, 1986, 1223.
284. J.A. Ripmeester, *J. Inclusion Phenom.*, 1986, **4**, 129.
285. J.M. Hewitt, M. Linder, S. Perez and A. Buleon, *Carbohydrate Res.*, 1986, **154**, 1.
286. I. Furo, I. Pocsik, K. Tompa, R. Teeaar and E. Lippmaa, *Carbohydrate Res.*, 1987, **166**, 27.
287. R.P. Veregin, C.A. Fyfe, R.H. Marchessault and M.G. Taylor, *Carbohydrate Res.*, 1987, **160**, 41.
288. M.J. Gidley and S.M. Bociek, *J. Am. Chem. Soc.*, 1988, **110**, 3820.
289. H. Saitô, *Am. Chem. Soc. Symp. Ser.*, No. 150, 1981, 125.
290. H. Saitô, R. Tabeta and T. Harada, *Chem. Lett.*, 1981, 571.

291. H. Saitô, R. Tabeta, T. Sasaki and Y. Yoshioka, *Bull. Chem. Soc. Jpn*, 1986, **59**, 2093.
292. H. Saitô, Y. Yoshioka, C. Hara, T. Kiho and S. Ukai, *Bull. Chem. Soc. Jpn*, 1987, **60**, 4267.
293. H. Saitô and M. Yokoi, *Bull. Chem. Soc. Jpn.*, 1989, **62**, (in press).
293a H. Saitô, M. Yokoi and Y. Yoshioka, submitted.
294. C.A. Fyfe, P.J. Stephenson, M.G. Taylor, T.L. Bluhm, Y. Deslandes and R.H. Marchessault, *Macromolecules*, 1984, **17**, 501.
295. N. Ohno, Y. Adachi, Z. Suzuki, S. Oikawa, K. Sato, Y. Suzuki, M. Ohsawa and T. Yadomae, *Chem. Pharm. Bull.*, 1986, **34**, 2555.
296. N. Ohno and T. Yadomae, *Carbohydrate Res.*, 1987, **159**, 293.
297. H. Saitô, T. Ohki and T. Sasaki, *Biochemistry*, 1977, **16**, 908.
298. H. Saitô, T. Miyata and T. Sasaki, *Macromolecules*, 1978, **11**, 1244.
299. A.J. Stipanovic and P.J. Giammatteo, in *Industrial Polysaccharides: Genetic Engineering, Structure/Property Relations and Applications* (M. Yalpani, ed.), Elsevier, Amsterdam, 1987, p. 281.
300. R.H. Atalla, J.C. Gast, D.W. Sindorf, V.J. Bartuska and G.E. Maciel, *J. Am. Chem. Soc.*, 1980, **102**, 3249.
301. W.L. Earl and D.L. VanderHart, *J. Am. Chem. Soc.*, 1980, **102**, 2351.
302. W.L. Earl and D.L. VanderHart, *Macromolecules*, 1981, **14**, 570.
303. R.H. Atalla and D.L. VanderHart, *Science*, 1984, **223**, 283.
304. J.R. Havens and D.L. VanderHart, *Macromolecules*, 1985, **18**, 1663.
305. D.L. VanderHart and R.H. Atalla, *Macromolecules*, 1984, **17**, 1465.
306. D.L. VanderHart and R.H. Atalla, *Am. Chem. Soc. Symp. Ser.*, No. 340, 1987, 88.
307. G.E. Maciel, W.L. Kolodziejski, M.S. Bertran and B.E. Dale, *Macromolecules*, 1982, **15**, 686.
308. R.L. Dudley, C.A. Fyfe, P.J. Stephenson, Y. Deslandes, G.K. Hamer and R.H. Marchessault, *J. Am. Chem. Soc.*, 1983, **105**, 2469.
309. C.A. Fyfe, P.J. Stephenson, R.P. Veregin, G.K. Hamer and R.H. Marchessault, *J. Carbohydrate Chem.*, 1984, **3**, 663.
310. J.J. Cael, D.L.W. Kwoh, S.S. Bhattacharjee and S.L. Patt, *Macromolecules* 1985, **18**, 821.
311. F. Horii, A. Hirai and R. Kitamaru, *Polymer Bull.*, 1982, **8**, 163.
312. F. Horii, A. Hirai and R. Kitamaru, *Polymer Bull.*, 1983, **10**, 357.
313. F. Horii, A. Hirai and R. Kitamaru, *Am. Chem. Soc. Symp. Ser.*, No. 260, 1984, 27.
314. F. Horii, A. Hirai and R. Kitamaru, *J. Carbohydrate Res.*, 1984, **3**, 641.
315. F. Horii, A. Hirai, R. Kitamaru and I. Sakurada, *Cellulose Chem. Technol.*, 1985, **19**, 513.
316. F. Horii, A. Hirai, and R. Kitamaru, *Am. Chem. Soc. Symp. Ser.*, No. 340, 1987, 119.
317. A. Hirai, F. Horii and R. Kitamaru, *Macromolecules*, 1987, **20**, 1442.
318. R. Teeaar and E. Lippmaa, *Polymer Bull.*, 1984, **12**, 315.
319. D. Gagnaire, J. Saint-Germain and M. Vincedon, *Polymer Bull.*, 1985, **13**, 365.
320. H. Chanzy, B. Henrissat, M. Vincedon, S.F. Tanner and P.S. Belton, *Carbohydrate Res.*, 1987, **160**, 1.
321. B. Philipp, J. Kunze and H.-P. Fink, *Am. Chem. Soc. Symp. Ser.*, No. 340, 1987, 178.
322. B. Henrissat, S. Perez, I. Tvaroska and W.T. Winter, *Am. Chem. Soc. Symp. Ser.*, No. 340, 1987, 38.
323. J. Hayashi, H. Kon, M. Takai, M. Hatano and T. Nozawa, *Am. Chem. Soc. Symp. Ser.*, No. 340, 1987, 138.
324. C.A. Fyfe, R.L. Dudley, P.J. Stephenson, Y, Deslandes, G.K. Hamer and R.H. Marchessault, *J. Macromol. Sci. Macromol. Chem. Phys.*, 1983, **C23**, 187.

325. D.I. Clark, A.H.K. Fowler and P.J. Stephenson, *J. Macromol. Sci. Macromol. Chem. Phys.*, 1983, **C23**, 217.
326. J.J. Lindberg and B. Hortling, *Adv. Polymer Sci.*, 1985, **66**, 1.
327. R.H. Atalla, *Am. Chem. Soc. Symp. Ser*, No. 340, 1987, 1.
328. P.M. Patterson, D.J. Patterson, J. Blackwell, J.L. Koenig, A.M. Jamieson, Y.P. Carignan and D.V. Turngren, *J. Polymer Sci., Polymer Phys.*, 1985, **23**, 483.
329. S. Doyle, R.A. Pathrick, R.K. Harris, J.M. Lane, K.J. Packer and F. Heatly, *Polymer*, 1986, **27**, 19.
330. M. Takai, K. Fukuda and J. Hayashi, *J. Polymer Sci. Part C, Polymer Lett.*, 1987, **25**, 121.
331. J.F. Haw, G.E. Maciel and H.A. Schroeder, *Anal. Chem.*, 1984, **56**, 1323.
332. V.J. Bartuska, G.E. Maciel, H.I. Bolker and B.I. Fleming, *Holzforschung*, 1980, **34**, 214.
333. G.E. Maciel, D.J. O'Donnell, J.J.H. Ackerman, B.L. Hawkins and V.J. Bartuska, *Makromol. Chem.*, 1981, **182**, 2297.
334. J. Schaefer, M.D. Sefcik, E.O. Stejskal, R.A. McKay and P.L. Hall, *Macromolecules*, 1981, **14**, 557.
335. W. Kolodziejski, J.S. Frye and G.E. Maciel, *Anal. Chem.*, 1982, **54**, 1419.
336. G.R. Hatfield, G.E. Maciel, O. Erbatur and G. Erbatur, *Anal. Chem.*, 1987, **59**, 172.
337. M.G. Taylor, Y. Deslandes, T. Bluhm, R.H. Marchessault, M. Vincedon and J. Saint-Germain, *Tappi*, 1983, **66**, 92.
338. J.M. Willis, N.R. Jagannathan and F.G. Herring, *J. Wood Chem. Technol.*, 1986, **6**, 249.
339. P.F. Barron, R.L. Frost, L. Doimo and M. Kennedy, *J. Macromol. Sci. Chem.*, 1985, **A22**, 303.
340. J.F. Haw, G.E. Maciel, and C.J. Biermann, *Holzforschung*, 1985, **39**, 99.
341. J.F. Haw, G.E. Maciel, J.C. Linden and V.G. Murphy, *Holzforschung*, 1985, **39**, 99.
342. W.V. Gerasimowicz, K.B. Hicks and P.E. Pfeffer, *Macromolecules*, 1984, **17**, 2597.
343. H. Sterk, W. Sattler and H. Esterbauer, *Carbohydrate Res.*, 1987, **164**, 85.
344. J.M. Willis and F.G. Herring, *Macromolecules*, 1987, **20**, 1554.
345. H. Saitô, R. Tabeta and K. Ogawa, in *Industrial Polysaccharides: Genetic Engineering, Structure/Property Relations and Applications*, (M. Yalpani, ed.), Elsevier, Amsterdam, 1987, p. 267.
346. H. Saitô, R. Tabeta and S. Hirano, *Chem. Lett.*, 1981, 1479.
347. H. Saitô, R. Tabeta and S. Hirano, in *Chitin and Chitosan. Proceeding of the Second International Conference on Chitin and Chitosan* (S. Hirano and S. Tokura, eds), Japanese Society of Chitin and Chitosan, Tottori 1982, pp. 71–76.
348. A.J. Stipanovic, P.J. Giammatteo and S.B. Robie, *Biopolymers*, 1985, **24**, 2333.
349. W.T. Winter, M.G. Taylor, E.S. Stevens, E.R. Morris and D.A. Rees, *Biochem. Biophys. Res. Commun.*, 1986, **137**, 87.
350. J. Schaefer, K.J. Kramer, J.R. Garbow, G.S. Jacob, E.O. Stejskal, T.L. Hopkins and R.D. Speirs, *Science*, 1987, **235**, 1200.
351. J. Seelig, *Q. Rev. Biophys.*, 1977, **10**, 353.
352. H.H. Mantsch, H. Saitô and I.C.P. Smith, *Prog. NMR Spectrosc.*, 1977, **11**, 211.
353. J. Seelig, *Biochim. Biophys. Acta*, 1978, **515**, 105.
354. P.R. Cullis and B. De kruijff, *Biochim. Biophys. Acta*, 1979, **559**, 399.
355. J. Seelig and A. Seelig, *Q. Rev. Biophys.*, 1980, **13**, 19.
356. R.E. Jacob and E. Oldfield, *Prog. NMR Spectrosc.*, 1981, **14**, 113.
357. J. Davis, *Biochim. Biophys. Acta*, 1983, **737**, 117.
358. I.C.P. Smith, *Biomembranes*, 1984, **12**, 133.

359. R.A. Harberkorn, J. Herzfield and R.G. Griffin, *J. Am. Chem. Soc.*, 1978, **100**, 1296.
360. E. Oldfield, J.L. Bowers and J. Forbes, *Biochemistry*, 1987, **26**, 6919.
361. J. Forbes, C. Husted and E. Oldfield, *J. Am. Chem. Soc.*, 1988, **110**, 1059.
362. P.L. Yeagle and T. Frye, *Biochim. Biophys. Acta*, 1987, **899**, 137.
363. M.D. Sefcik, J. Schaefer, E.O. Stejskal, R.A. McKay, J.F. Ellena, S.W. Dodd and M.F. Brown, *Biochem. Biophys. Res. Commun.*, 1983, **114**, 1048.
364. J. Urbina and J.S. Waugh, *Proc. Natl Acad. Sci. USA*, 1974, **71**, 5062.
365. S.J. Opella, J.P. Yesinowski and J.S. Waugh, *Proc. Natl Acad. Sci. USA*, 1976, **73**, 38112.
366. B.A. Cornell, *Chem. Phys. Lett.*, 1980, **72**, 462.
367. B.A. Cornell, *Chem. Phys. Lipids*, 1981, **28**, 69.
368. B.A. Cornell, M. Keniry, R.G. Hiller and R. Smith, *FEBS Lett.*, 1980, **115**, 134.
369. B.A. Cornell and M. Keniry, *Biochim. Biophys. Acta*, 1983, **732**, 705.
370. R.J. Witterbort, C.F. Schmidt and R.G. Griffin, *Biochemistry*, 1981, **20**, 4223.
371. R.J. Witterbort, A. Blume, T.-H. Huang, S.K. Das Gupta and R.G. Griffin, *Biochemistry*, 1982, **21**, 3487.
372. A. Blume, R.J. Witterbort, S.K. Das Gupta and R.G. Griffin, *Biochemistry*, 1982, **21**, 6243.
373. B.A. Lewis, S.K. Das Gupta and R.G. Griffin, *Biochemistry*, 1984, **23**, 1988.
374. A. Blume and R.G. Griffin, *Biochemistry*, 1982, **21**, 6230.
375. A. Makriyannis, D.J. Siminovitch, S.K. Das Gupta and R.G. Griffin, *Biochim. Biophys. Acta*, 1986, **859**, 49.
376. G.D. Mateescu, E.W. Abrahamson, J.W. Shriver, W. Copan, D. Muccio, M. Iqbal and V. Waterhous, in *Spectroscopy of Biological Molecules* (C. Sandorfy and T. Theophanides, eds), D. Reidel, Dordrecht, 1984, pp. 257–290.
377. G.S. Harbison, J. Herzfeld and R.G. Griffin, *Biochemistry*, 1983, **22**, 1.
378. G.S. Harbison, P.P.J. Mulder, H. Pardoen, J. Lugtenburg, J. Herzfeld and R.G. Griffin, *J. Am. Chem. Soc.*, 1985, **107**, 4809.
379. G.S. Harbison, S.O. Smith, J.A. Pardoen, C. Winkel, J. Lugtenburg, J. Herzfeld, R.A. Mathies and R.G. Griffin, *Proc. Natl Acad. Sci. USA*, 1984, **81**, 1706.
380. G.S. Harbison, S.O. Smith, J.A. Pardoen, P.P.J. Mulder, J. Lugtenburg, J. Herzfeld, R. Mathies and R.G. Griffin, *Biochemistry*, 1984, **23**, 2662.
381. G.S. Harbison, S.O. Smith, J.A. Pardoen, J.M. Couerin, J. Lugtenburg, J. Herzfeld, R.A. Mathies and R.G. Griffin, *Biochemistry*, 1985, **24**, 6955.
382. S.O. Smith, I. Palings, V. Copie, D.P. Raleigh, J. Courtin, J.A. Pardoen, J. Lugtenburg, R.A. Mathies and R.G. Griffin, *Biochemistry*, 1987, **26**, 1606.
383. L.O.P.J. Mollevanger, A.P.M. Kentgens, J.A. Pardoen, J.M.L. Courtin, W.S. Veeman, J. Lugtenburg and W.J. de Grip, *Eur. J. Biochem.*, 1987, **163**, 9.

Index